New Bipolar Organic Materials for Optoelectronic Applications

LINTON, KATHARINE,ELIZABETH

New Bipolar Organic Materials for Optoelectronic Applications

Katharine Elizabeth Linton
Collingwood College

Department of Chemistry
Durham University

A thesis submitted for the degree of Doctor of Philosophy at Durham University

July 2012

Declaration

The work described in this thesis was carried out in the Department of Chemistry at Durham University between July 2009 and June 2012. All the work was carried out by the author unless otherwise stated and has not been previously submitted for a degree at this or any other university.

Table of Contents

Abstract

New Bipolar Organic Materials for Optoelectronic Applications

Katharine Elizabeth Linton, Durham University, 2012

The literature surrounding organic small-molecule donor-acceptor systems is summarised for a range of optoelectronic applications (OLEDs, OPVs, OFETs etc.). There is a focus on the key building blocks: 1,3,4-oxadiazole (**OXD**), diphenylamine (**DPA**), carbazole (**Cbz**) and fluorene (**F**). The incorporation of such moieties into various donor-acceptor systems is discussed with further reference to selected alternative organic donor and acceptor systems.

The syntheses of novel bipolar molecules based on a donor-spacer-acceptor (**DPA**/**Cbz**-**F**-**OXD**) structure and the incorporation of these molecules into single-layer OLEDs is presented. It is demonstrated how the emission colour can be tuned from green to deep blue by systematic manipulation of the structure. A significant result is that high efficiency accompanied with pure, deep blue emission in single-layer OLEDs can be achieved with this structural motif. The incorporation of these materials as part of a simple two-component blend to produce white OLEDs is presented and the modification of the materials to improve electron-transport properties is discussed.

The synthesis of **DPA**-bridge-**OXD** wire systems is presented with the use of oligo-*p*-phenyleneethynylene units as a bridge of varying length to investigate the effect on charge transfer between the donor and acceptor. Photophysical studies demonstrate the change in absorption, emission and fluorescence lifetimes as the length scale of the molecules is altered. The synthesis of a series of planarised and twisted **DPA**-bridge-**OXD** systems based upon phenylene linkers is discussed.

Finally, a series of **DPA**-**F**-**OXD**-anchor molecules is presented for incorporation into DSSC devices. The synthesis of these materials is described and the suitability of various anchoring groups for DSSCs is analysed through photophysical and device studies.

Acknowledgements

Firstly, I would like to thank Professor Martin Bryce for inviting me to a PhD position in his group. I have had a wonderful time at Durham for the past three years and it has been a great experience working with all the members of the Bryce group past and present.

I would like to thank all the other chemists who have been involved in this work. The work described in chapters 2 and 3 was developed from previous studies by Dr. Kiran Kamtekar. The work from chapter 4 is developed from studies by Dr. Changsheng Wang. I would also like to thank Dr. Mark Fox for computational work and assistance with the cyclic voltammetry studies in chapters 2 and 3. I thank Dr. Lars-Olof Pålsson for his help with thin-film measurements in chapters 2 and 3 and for the time-resolved fluorescence studies in chapter 4. I would like to thank Miss Geri Rosser of Dr. Andrew Beeby's group for her advice and assistance with absorption and fluorescence measurements for the work in chapters 2, 3 and 4. I would finally like to thank the analytical staff at Durham University for all the help and advice they have provided.

I would like to thank the members of Professor Michael Petty's group in the Engineering Department of Durham University for both device studies and invaluable discussion. The device studies in chapter 2 and 3 were carried out by Miss Alison Fisher and Dr. Christopher Pearson. Miss Cristina Roldán-Carmona is acknowledged for device studies in chapter 3. I would also like to thank Dr. Dan Bright and Dr. Fernando Dias of Pofessor Andy Monkman's group at Durham University for their help with the time-resolved fluorescence spectroscopy in chapter 4.

For the work in chapter 5, I would like to offer my thanks to Dr. Mateusz Wielopolski of the École Polytechnique Fédérale de Lausanne (EPFL) in Professor Jacques Moser's laboratory for all his help with the thin-film studies and time-resolved measurements described in chapter 5. I would also like to thank Miss Magdalena Marszalek of Professor Michael Grätzel's group at the EPFL for device studies in chapter 5.

Publications and Presentations

The following papers are based on work described in this thesis:

- Alison L. Fisher, Katharine E. Linton, Kiran T. Kamtekar, Christopher Pearson, Martin R. Bryce and Michael C. Petty; **Efficient deep-blue electroluminescence form an ambipolar fluorescent emitter in a single-active-layer device,** *Chem. Mater.*, **2011**, *23*, 1640

- Katharine E. Linton, Alison L. Fisher, Christopher Pearson, Mark A. Fox, Lars-Olof Pålsson, Martin R. Bryce and Michael C. Petty; **Colour tuning of blue electroluminescence using bipolar carbazole-oxadiazole molecules in single-active-layer organic light emitting devices (OLEDs),** *J. Mater. Chem.*, **2012**, *22*, 1186

- Cristina Roldán-Carmona, Alison L. Fisher, Katharine E. Linton, Christopher Pearson, Marta Pérez-Morales, María T. Martín-Romero, Martin R. Bryce and Michael C. Petty; **White light emission from blended organic light emitting devices containing two active components**, *manuscript in preparation*

The following presentations were based on work described in this thesis:

- RSC Organic division Northeast regional symposium, York University, March 2012; poster presentation

- European Conference for Molecular Electronics (ECME), Barcelona, September 2011; poster presentation

- RSC Organic division Northeast regional symposium, Northumbria University, April 2011; poster presentation

- 43rd IUPAC World Polymer Congress Macro2010, Glasgow, July 2010; poster presentation

List of Abbreviations

A	Acceptor
ASAP	Atmospheric solids analysis probe
β	Attenuation factor
Cbz	Carbazole
CIE	Commission international d'eclairage
CT	Charge transfer
CV	Cyclic voltammetry
D	Donor
D-A	Donor-acceptor
D-B-A	Donor-bridge-acceptor
DCM	Dichloromethane
DFT	Density functional theory
DMF	*N*,*N*-Dimethylformamide
DMSO	Dimethyl sulfoxide
DPA	Diphenylamine
DSSC	Dye sensitised solar cell
EL	Electroluminescence
EQE	External quantum efficiency
ET	Electron transport
eV	Electron volts
exTTF	Extended tetrathiafulvalene
F	Fluorene
Fc	Ferrocene
HOMO	Highest occupied molecular orbital
HT	Hole transport
HTL	Hole transport layer
ICT	Intramolecular charge transfer
IP	Ionisation potential
IPCE	Internal power conversion efficiency
ISC	Intersystem crossing
ITO	Indium tin oxide
LE	Locally excited
LUMO	Lowest occupied molecular orbital

NDR	Negative-differential-resistance
NO	Nitric oxide
NTSC	National television standard committee
OFET	Organic field effect transistor
OLED	Organic light emitting diode
OLET	Organic light emitting transistor
OPV	Organic Photovoltaic
OXD	1,3,4-oxadiazole
PCE	Power conversion efficiency
PEDOT:PSS	Poly(3,4-ethylenedioxythiophene) poly(styrenesulfonate)
PET	Photoinduced electron transfer
PFO	Poly-9,9-di-*n*-octylfluorene
PHOLED	Phosphorescent organic light emitting diode
PL	Photoluminescence
PLQY	Photoluminescent quantum yield
PTC	Phase transfer catalyst
PVK	Poly vinyl carbazole
TCNQ	Tetracyanoquinodimethane
TFT	Thin film transistor
T_g	Glass transition temperature
TGA	Thermal gravimetric analysis
THF	Tetrahydrofuran
TICT	Twisted intramolecular charge transfer
TOF	Time of flight
TPA	Triphenylamine
WOLED	White organic light emitting device

Chapter 1: Organic Ambipolar Materials for Optoelectronic Applications

---

1.1 Introduction

In recent years interest in the development of organic materials for their use in electronic devices has been growing. There are many unique and valuable properties that organic compounds may provide which complement those found in traditional inorganic electronic components. The commercial potential for solution processible optoelectronic materials and flexible displays is huge. Much research has gone into the development of organic light emitting devices (OLEDs) and organic photovoltaic cells (OPVs), utilising molecular and polymeric conjugated materials in order to exploit their electroluminescent (EL), photoluminescent (PL) and charge transport characteristics for such devices. Additionally, conjugated linear molecules have been utilised for roles in molecular wires to develop more fundamental understanding of the charge transfer processes occurring in such donor-acceptor molecules.

When Moore predicted in 1965 that the number of transistors that could fit onto a chip would increase at a rate of approximately twofold a year, it could be extrapolated that eventually a size limit would be approached where individual molecular structures would become candidates as components in electronic devices.[1] In 1974 Aviram and Ratner proposed a molecular rectifier consisting of conjugated donor and acceptor segments joined by a non-conjugated bridge.[2] These observations, in combination with the first report of electroluminescence (EL) from organic crystals of anthracene in 1963 demonstrated the potential for organic materials to be exploited in molecular electronics.[3] It was not until 1987 that the development of thin films by vapour deposition by Tang and Van Slyke allowed the fabrication of the first working OLED.[4] Since these early advances a very large body of work in this field has developed.

There is huge scope for the application of organic materials in various electronic or optoelectronic devices. The potential advantages of organic materials over their inorganic counterparts are numerous. Organic materials may be solution processed, which allows low-cost and large-area production of devices through spin-coating and ink-jet printing techniques. Thin-films of organic materials allow flexible devices to be fabricated. Molecular design allows physical characteristics of materials to be finely tuned, altering colour, conductivity, absorption, emission and morphology, amongst others. This chapter will briefly explore the use of donor-acceptor (D-A) and donor-bridge-acceptor (D-B-A) structural motifs in different areas of organic materials chemistry. Specifically, small molecule systems will be explored with emphasis placed upon those containing the 1,3,4-oxadiazole (**OXD**, **1**) acceptor and carbazole (**Cbz**, **2**) and diphenylamine (**DPA**, **3**) donor moieties and the emissive fluorene (**F**, **4**) unit, figure 1.1. Subsequent chapters will discuss the design, synthesis and application of these types of molecules in various optoelectronic applications.

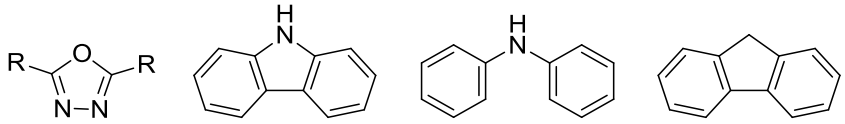

1 **2** **3** **4**

Figure 1.1 - Structures of 1,3,4-oxadiazole (OXD), 1, carbazole (Cbz), 2, diphenylamine (DPA), 3 and fluorene (F), 4

1.2: Applications of Bipolar Materials

A bipolar material is able to support both hole and electron transport; this can be achieved by combining both electron transport and hole transport portions within its structure. This can be advantageous for the simplification of many electronic and optoelectronic devices, by removing the need to synthesise multiple materials with different charge carrier characteristics. This is demonstrated particularly well in the case of OLEDs. At their most simple an OLED structure consists of an electroluminescent material sandwiched between two electrodes (figure 1.2). Electrons are injected through the cathode and holes through the anode. Migration of these charge carriers occurs through the EL material and recombination to form an exciton allows relaxation from the singlet state with the emission of light by fluorescence. If, for example, a compound does not support electron transport (has a low electron affinity) and does not favour the formation of anion radicals, then the cation radicals formed *via* hole injection are likely to migrate through the device without formation of an exciton. By incorporation of both electron and hole transport regions in a molecule, such as in

a donor-acceptor system, the efficiency of an OLED may be drastically increased. One of the most common strategies to improve OLED efficiency is to include extra electron and/or hole injection layer(s) into the device. This has been demonstrated in many instances and has been reviewed extensively and will be discussed in this chapter.[5-8] The disadvantage of this approach is the extra complexity in fabricating both the device and the synthesis of extra organic materials. To include all the desired features into one material is often preferable.

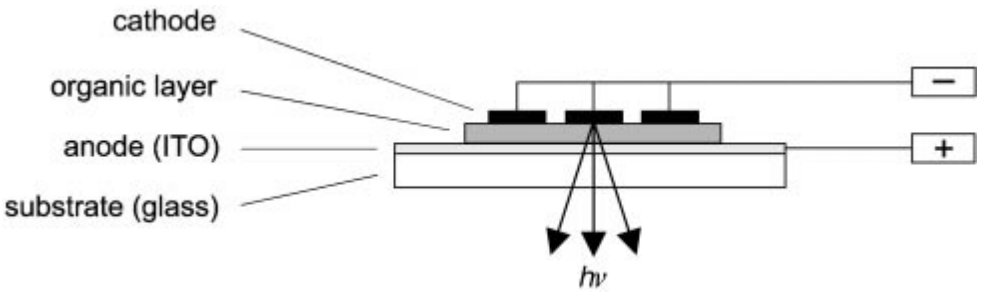

Figure 1.2 - Schematic structure of a simple OLED device[8]

There are various parameters that quantify the performance of an OLED.[8] The **external quantum efficiency (EQE, η_{ext})** defines the ratio of the number of observed emitted photons to the number of electrons injected; it is defined by equation 1.1 containing the internal quantum efficiency (η_{int}). The internal quantum efficiency is the ratio of number of photons emitted to electrons injected.

$$\eta_{ext} = 2n^2\eta_{int}$$

Equation 1.1: External quantum efficiency where n is the refractive index of the organic layer

The **power efficiency (η_{pow}, lm W^{-1})** is the ratio of output light power to the input electrical power.

The **luminous efficiency (η_{lum}, cd A^{-1})** is the power efficiency multiplied by the eye sensitivity curve *S* (defined by the Commision Internationale de L'Eclairage (CIE)), figure 1.3. This takes into account the sensitivity of the human eye to different wavelengths of light.

The **brightness** of a device in cd m^2 is also an indicator of the performance of an OLED device.

The **colour** of emitted light from an OLED is a very important parameter, often defined using the CIE coordinates, figure 1.3. When developing OLEDs as colour elements in displays it is important that colour purity is high and the CIE coordinates conform to the standards for displays, for example the National Television System Committee (NTSC).

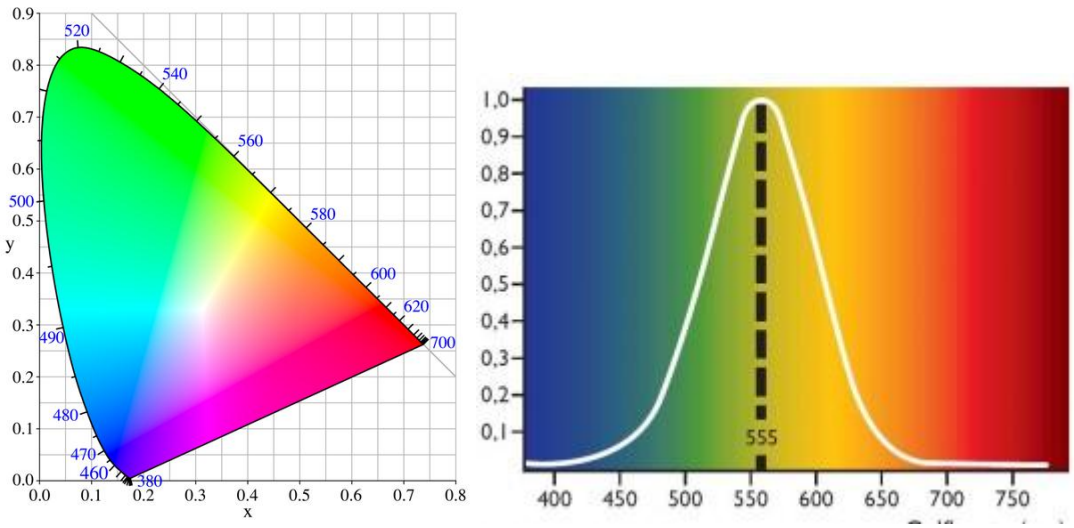

Figure 1.3 - The CIE diagram for the description of colour (left) and the human eye sensitivity curve (right)

Materials for use in OLEDs will be discussed in more detail later in this chapter and throughout chapters 2 and 3.

Fundamental studies in charge transfer processes in molecular D-A systems are of great interest for the development of molecular electronics and will be the subject of chapter 4. One of the most vigorously researched areas currently in organic materials is the creation of efficient and commercially viable organic photovoltaics (OPVs), which is the subject of chapter 5. There are many other organic materials that may benefit from the presence of both donor and acceptor characteristics within the same molecule or polymer; these include organic transistors, electrochromic materials and molecular switches, some of these are briefly discussed below.

Organic transistors (OFETs) and particularly organic light emitting field effect transistors (OLETs) are currently a popular field of research.[9,10] In order to create a working transistor it is essential to have high mobilities of either holes or electrons, or both in the case of ambipolar transistors. OLETs also require ambipolar charge transport in order to create a recombination zone (p-n junction) within the device, away from the electrodes, where light emission can occur. The simplest device design would utilise a single organic material able to support both hole and electron transport, rather than a blend or multilayer device structure. Tang *et al.* have developed an evaporated compound, **5** based on a D-A tetracenothiophene unit substituted with fluorine to improve electron transport, figure 1.4. This material showed

ambipolar transport, with electron mobilities in a nitrogen atmosphere of 0.37 $cm^2 V^{-1} s^{-1}$, but reduced hole mobilities of 0.065 $cm^2 V^{-1} s^{-1}$.[11] In ambient conditions, the hole mobility was increased but the electron mobility was reduced suggesting charge carrier trapping for n-type behaviour.

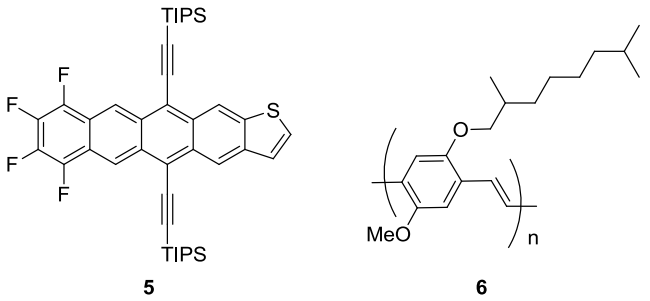

5 **6**

Figure 1.4 - Molecular structure of 5 and 6 used for ambipolar transport in transistor devices

An ambipolar OLET based on polymer **6**, with mobility values of $\mu_e = 10^{-3}$ $cm^2 V^{-1} s^{-1}$ and $\mu_h = 10^{-4}$ $cm^2 V^{-1} s^{-1}$ and an external quantum efficiency of 0.35 % for the device was demonstrated by Zaumseil *et al*.[12] They emphasised the importance of a trap-free dielectric-semiconductor interface in order to avoid exciton quenching as well as the correct organic material for ambipolar charge transport.

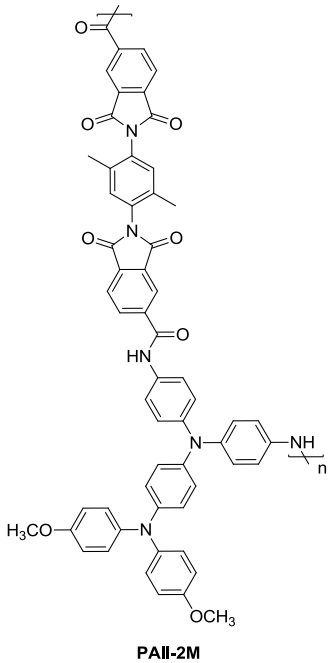

PAII-2M
7

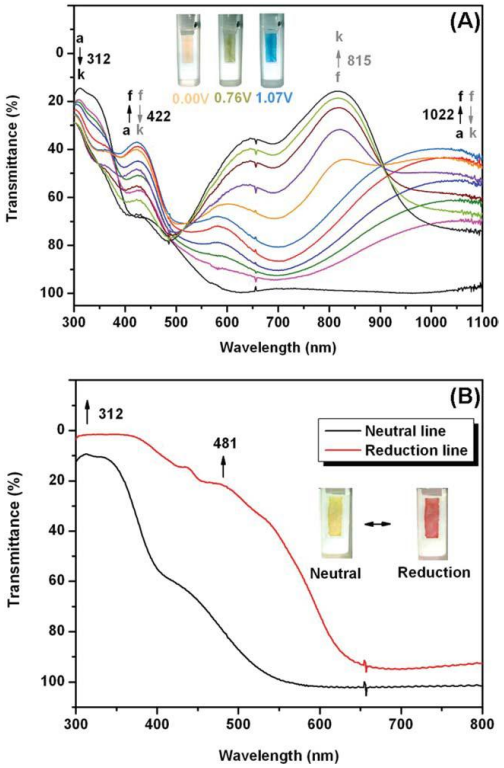

Figure 1.5 - The structure of ambipolar polymer 7 PAII-2M and graphs displaying its electrochromic behaviour under positive applied potentials (A) and negative potentials (B) and their associated colour changes[13]

Electrochromic materials display an optical change in their absorption or transmittance upon an electrochemical change to the compound. A recent study by Huang *et al.* discusses the advantages of using an ambipolar system in this context. Incorporating donor (arylamine) and acceptor (imide) units within a polymer gave easily accessible neutral oxidised and reduced states, each with an associated colour change, figure 1.5.[13]

1.3 Molecules suitable for electron or hole transport in organic materials

The following section discusses the syntheses of **OXD**, **Cbz**, **DPA** and **F** derivatives and their application as components of compounds for optoelectronic applications.

1.3.1 1,3,4-Oxadiazoles in ambipolar systems

1,3,4-Oxadiazole (**OXD**) derivatives have been very widely investigated as electron deficient candidates in a variety of different optoelectronic applications due to their excellent chemical and thermal stability and high photoluminescent quantum yields (PLQY). They have been exploited particularly as electron-transporting materials in OLEDs.

There are two common strategies for the synthesis of 1,3,4-oxadiazoles. The first reported synthesis of an oxadiazole by Hayes *et al.* in 1955 demonstrated that refluxing an amide precursor with phosphorus oxychloride yielded the oxadiazole in moderate to good yields.[14] The amide may be produced from the reaction of a hydrazide with an acid chloride, scheme 1.1.

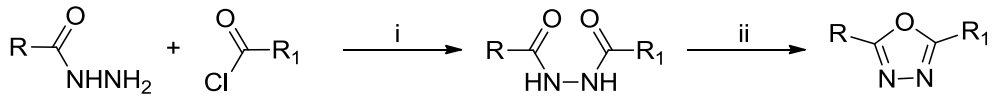

8 **9** **10** **11**

Reagents and conditions: i) pyridine, then precipitation with HCl (aq); ii) $POCl_3$

Scheme 1.1 - Formation of a 1,3,4-oxadiazole by dehydration of its parent amide.

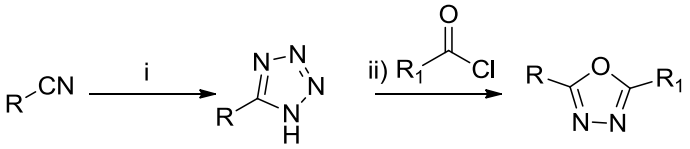

12 **13** **14**

Reagents and conditions: i) NaN_3, NH_4Cl, DMF, reflux; ii) pyridine, reflux

Scheme 1.2 - Formation of a 1,3,4-oxadiazole from a tetrazole.

Alternatively, as reported by Huisgen *et al.,* the oxadiazole may be prepared by the reaction of a tetrazole with an acid chloride under basic conditions.[15] The tetrazole may be formed by the reaction of a nitrile compound with sodium azide and ammonium chloride, scheme 1.2.

Both of these routes to **OXDs** allow easy functionalisation of the R and R_1 positions with a large variety of aryl groups. This offers great freedom in the synthetic modification of such systems, allowing fine tuning of the electronic and structural properties of the molecule, thereby increasing the utility of such materials.

The use of 1,3,4-oxadiazoles to improve electron transport properties has been reviewed comprehensively and is discussed further in chapter 3.[5,6] Lee *et al.* showed that compound **15** assists in ambipolar charge transport when used as a host in the emissive layer of an iridium based OLED, figure 1.6.[16] When $Ir(ppy)_3$, **18**, was doped into the **OXD** material **15** the device demonstrated improved characteristics when compared to the conventional carbazole host, CBP. Increased power efficiency, device stability and reduced driving voltage were attributed to the increased oxidation potential of **15** (5.9 eV compared to 6.3 eV for CBP) which gives a better match to the NPB (HOMO level 5.7 eV) hole transport layer (HTL) thus aiding hole injection into the emissive layer. The higher glass transition temperature (T_g) of **15** compared with CBP helped to improve device stability.[16] This study demonstrates that an electron transporting oxadiazole derivative in combination with a suitable hole transporter can result in balanced hole and electron transport.

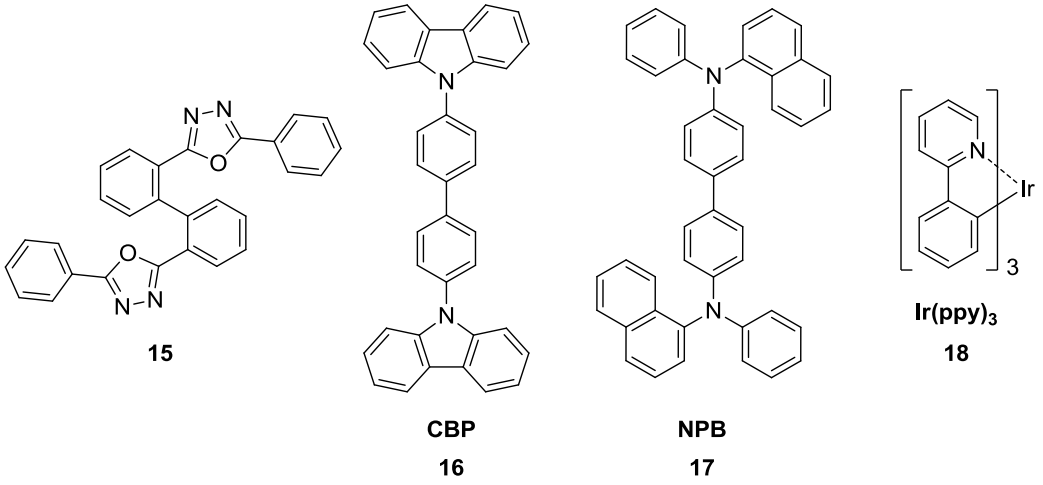

Figure 1.6 - Structures of electron transporting host 15, hole-transporting host CBP, hole-transporting material NPB and iridium complex $Ir(ppy)_3$

The electron-withdrawing nature of an oxadiazole means that it has potential as a unit within a transistor for promotion of electron conduction. It will lower the LUMO level of materials. Although there have been many instances of the incorporation of oxadiazole units in OLED materials, they have been used less often in transistor materials. Katz *et al.* attempted to design an electron-deficient oxadiazole containing molecule, **19**, for use in n-channel transistors, figure 1.7.[17] The material showed reasonable mobilities, up to 0.18 $cm^2 V^{-1} s^{-1}$, but for holes not electrons. The analogue **20**, on the other hand, did display n-channel behaviour and maximum electron mobilities of 0.02 $cm^2 V^{-1} s^{-1}$.[17] The low mobilities compared with other analogues in the study were attributed to the weak crystallinity of the material in thin films.

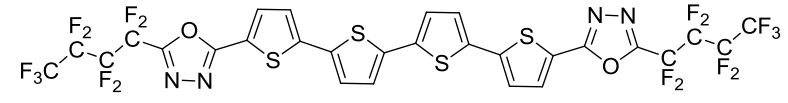

19

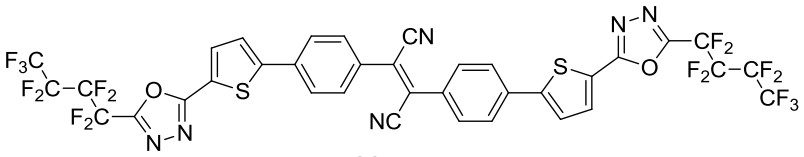

20

Figure 1.7 - Two oxadiazole containing transistor molecules showing both p- and n-type conduction.

1.3.2. Diphenylamine in ambipolar systems

Arylamines have long been known to be good hole transporting compounds with their incorporation into many materials for OLEDs and photovoltaic devices. Aromatic amines have low ionisation potentials and readily form cation radicals. Additionally they possess a low electron affinity and therefore help prevent negative charge carriers reaching the anode in OLEDs. Amines are often incorporated into devices as hole transporting layers to improve charge injection and transport between the electrodes and the semiconducting layer, for example N,N'-bis(naphthalen-1-yl)-N,N'-bis(phenyl)-benzidine, NPB **17**, is one such material.[18] Various arylamines may be synthesised readily *via* a palladium catalysed Buchwald-Hartwig cross-coupling reaction from readily available starting materials, for example the synthesis of the substituted diphenylamine **23**, scheme 1.3.[19]

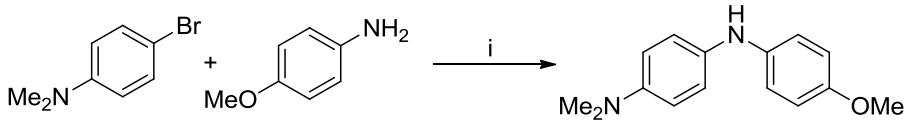

21 **22** **23**

Reagents and Conditions: i) $[Pd_2(dba)_3]$ (0.5 mol%), JohnPhos (2 mol%), NaO^tBu, toluene, 93%

Scheme 1.3 - Palladium catalysed amination of an aryl bromide[19]

Charge carrier mobility is a fundamental property that is required for all electro-optical applications. High charge carrier mobility of 10^{-2} cm^2 V^{-1} s^{-1} has been demonstrated in an amorphous low molecular weight arylamine, 1,1-bis(di-4-tolylaminophenyl)cyclohexane **24**, figure 1.8, by Borsenberger *et al*.[20]

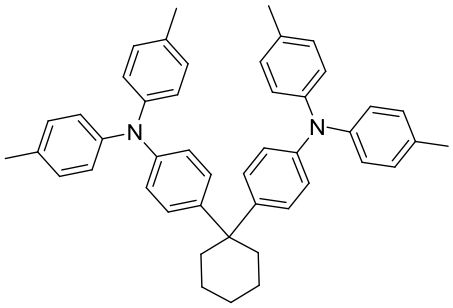

24

Figure 1.8 - Molecular structure of 1,1-bis(di-4-tolylaminophenyl)cyclohexane

Development of a donor-acceptor system, **25**, based on a star-shaped motif with a triphenylamine (**TPA**) core substituted with benzimidazole allowed a simple, solution processed OLED to be fabricated exhibiting good device characteristics with excellent thermal stability, figure 1.9. Fabrication of a single-layer device was possible due to the molecule supporting both hole and electron transport, negating the need for extra transport layers.[21]

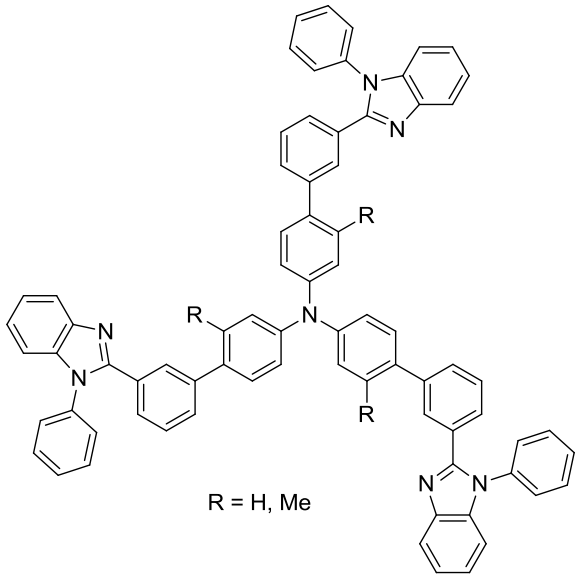

25

Figure 1.9 - Structure of star-shaped D-A arylamine-benzimidazole material

Arylamines have also been exploited for their electrochemical properties. Readily oxidised arylamines may be electrochemically stable when the positions *para* to the nitrogen are blocked. These oxidised states may be accompanied by a colour change and therefore have use as electrochromic materials. A polymer based on a TPD core was synthesised by Lim *et al.* and its electrochromic properties in thin films were investigated, figure 1.10.[22] Reversible switching was observed on oxidation between 0.7 and 1.2 V with an associated colour change from colourless to yellow then green-blue.[22]

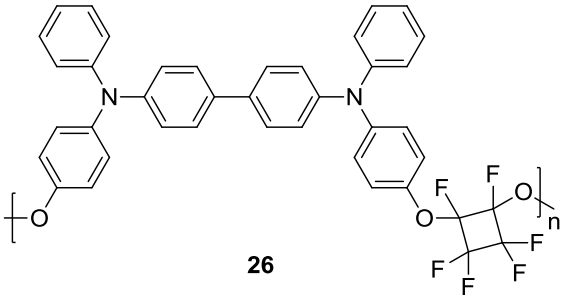

26

Figure 1.10 - Structure of electrochromic arlyamine polymer

Koene *et al.* investigated the effect of systematic structural changes to a variety of arylamines as hole-transporting compounds, figure 1.11.[23] They tuned the HOMO level of the material by altering the amine structure slightly, demonstrating synthetic control of energy levels in HT materials for OLEDs by easily matching up energy levels to the specific device. They also observed that some arylamine derivatives, particularly iminostilbenes **27**, gave consistently higher T_g values, an important parameter to consider for device stability.[23]

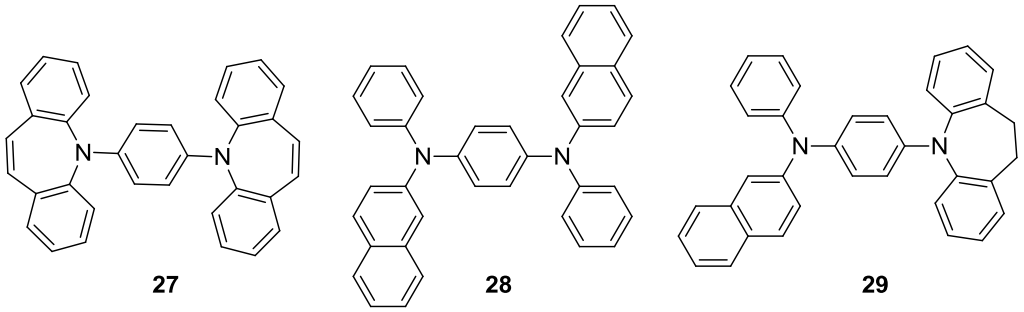

27 **28** **29**

Figure 1.11 - Structure of some arylamine host materials in a study by Koene *et al.*[23]

1.3.3 Carbazole in ambipolar systems

Carbazole is very commonly exploited in a variety of opto-electronic applications. This is because it is chemically stable, synthetic modifications at the 3- and 6-, 2- and 7- and also 9-positions are easily achieved, and **Cbz** exhibits a high oxidative potential, characteristic of a good hole-transporting material. The ability of **Cbz** to form stable amorphous glasses is an

advantage in device fabrication. Finally, for applications where the emission of light is desired, carbazole exhibits intense and efficient fluorescence, the colour of which is tuneable depending on the substituents appended to the carbazole.[24]

Synthesis of carbazole is classically achieved *via* the Borsche-Drechsel cyclisation described in scheme 1.4.[25,26] Carbazole itself may be easily functionalised further, either at the nitrogen or on the phenyl rings, primarily in the 3- and 6-positions. Reaction at the nitrogen occurs by simple substitution reactions or by Buchwald-Hartwig or Ullmann type cross-coupling reactions. Substitution onto the rings is achieved through a variety of reactions including Friedel-Crafts alkylations or halogenation reactions, shown in scheme 1.5. The 3- and 6-positions are the most reactive (i.e. more nucleophilic) as they are *para* to the nitrogen atom of the carbazole.

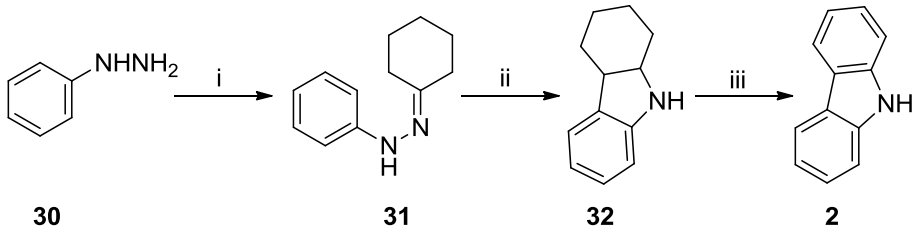

30 **31** **32** **2**

Reagents and Conditions: i) cyclohexanone; ii) HCl; iii) Pb_3O_4

Scheme 1.4 - The Borsche-Drechsel synthesis of carbazole

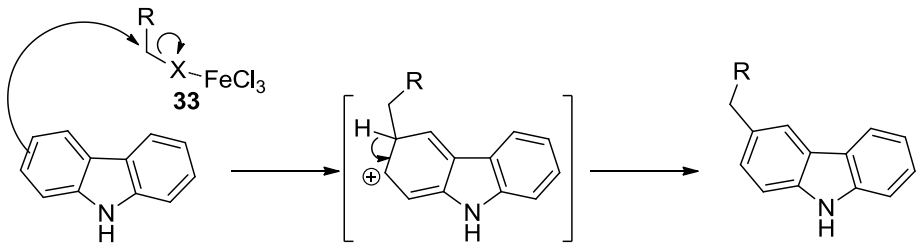

34 **35** **36**

Reagents and conditions: R-X, $FeCl_3$

Scheme 1.5 - Friedel-Crafts alkylation of carbazole

Functionalisation may also be achieved in the 2- and 7- positions by synthesis of carbazole *via* a copper mediated coupling reaction, followed by a cyclisation, scheme 1.6.[27]

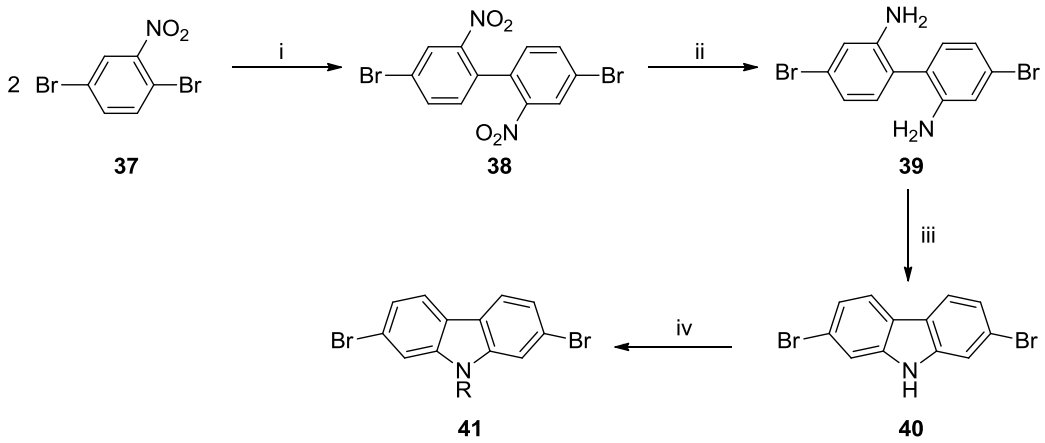

Reagents and conditions: i) Cu-powder, DMF, 120 ^{o}C, 3 h; ii) Sn/HCl, ethanol, 80 ^{o}C, 3h; iii) H_3PO_4, 24 h; iv) R-Br, KOH, acetone, PTC, reflux, 4 h

Scheme 1.6 - Synthesis of 2,7-disubstituted carbazole

One of the advantages of utilising carbazole or arylamine systems in devices is their ability to form stable amorphous glasses *via* spin-coating or vacuum deposition.[28] The stability of the glass is important. If the glass-transition temperature (T_g) of the material is low, then the device may degrade easily during operation. For example, TPD **42**, figure 1.12, is a well known hole-transporting material that forms amorphous glasses. However, it has a T_g of only 60 ^{o}C and is known to crystallise at 25 ^{o}C in the air after being deposited under vacuum.[29] This has implications for device stability and development, demonstrating the critical importance of morphological parameters as well as electronic characteristics when developing compounds for device applications.

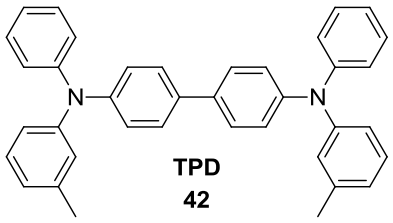

Figure 1.12 - Chemical structure of TPD

Often, the T_g of such compounds can be improved by altering the molecular structure, which in turn can help to improve device lifetimes. This may be achieved by increasing molecular weight, introducing rigid moieties and by encouraging intermolecular interactions such as dipolar interactions.[28]

The benefits of using a 2,7-disubstituted carbazole compared with the more commonly encountered 3,6-analogues have been investigated by Sonntag *et al.,* figure 1.13.[27] They observe that the 2,7-linked carbazole trimers **43** show stronger deep blue fluorescence than their 3,6-counterparts **44**, attributed to the increased conjugation in **43**. However, the electrochemical stability of the 2,7-carbazoles is much lower showing only irreversible oxidation waves in the cyclic voltammetry (CV), due to coupling reactions occurring at the reactive 3- and 6-positions.[27]

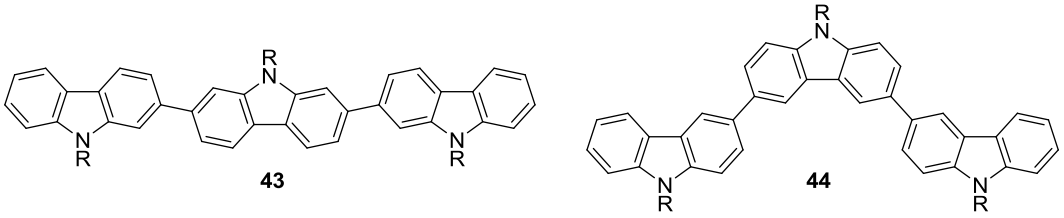

Figure 1.13 - Structures of 2,7 and 3,6-carbazole trimers

Much work has been done on the development of high triplet level materials for use as hosts for blue phosphorescent emitters. Phosphorescent emitters are usually dispersed within an organic host material to prevent concentration quenching of phosphorescence. In order to prevent back transfer of energy from guest to host the triplet energy of the host material must be higher than the guest emitter. This can be readily achieved for red and green phosphors, but achieving a sufficiently high triplet level so that the host is suitable for blue emitters is currently an area of intense research.[8,30-32] Another important requirement of this type of material is to maintain balanced charge carrier ability. Bredas and co-workers have recently discussed D-A-D systems utilising carbazole as the donor in high triplet level host compounds, figure 1.14.[32] Detailed DFT calculations indicate that the carbazole units within their systems are largely responsible for the cationic ionisation potential (IP) states; however, these are also influenced by the proximate acceptor groups. The anionic state, the electron affinity, while being largely determined by the electron deficient acceptor group is also influenced by the nearby carbazole groups.[32] There is clearly a finely balanced relationship in such ambipolar systems and careful molecular design is required to manipulate the electronic properties appropriately.

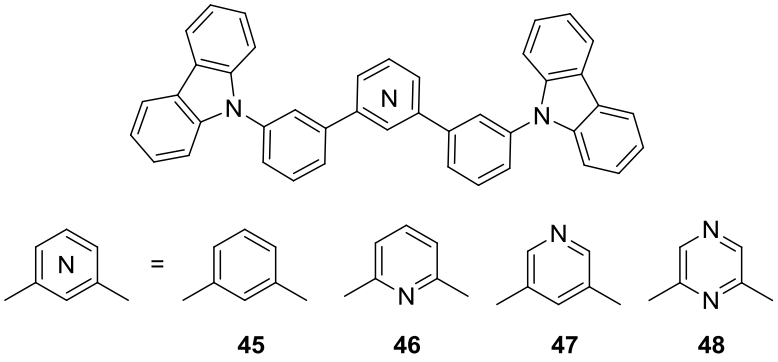

Figure 1.14 - Structure of Cbz hosts 45 – 48

A commonly used polymeric host material is poly(vinylcarbazole) (PVK) **49**, figure 1.15. It has a high triplet level, due to the non-conjugated linkers between carbazole molecules and has been widely used as a host for phosphorescent emitters,[33-36] although dimer formation can be a problem which may result in unwanted exciton quenching.[37] However, due to PVK's HOMO level at *ca*. -5.9 eV, there is a large barrier for the injection of holes which can result in high onset voltages, combined with the fact that the material is a hole-transporter means that ET materials should be incorporated into the device to improve performance.[38,39]

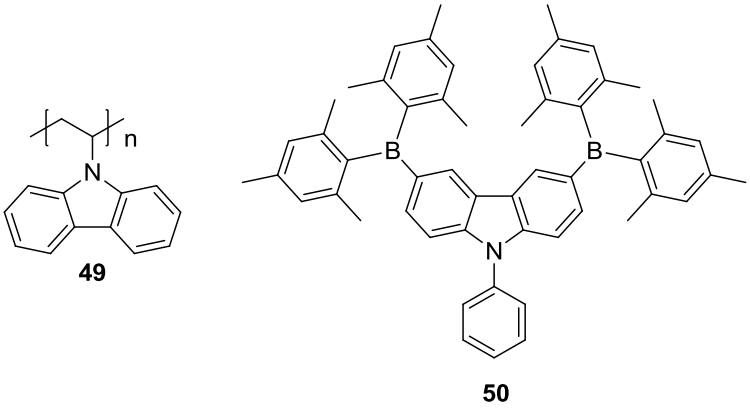

Figure 1.15 - Structure of poly(vinylcarbazole) (PVK) 49 and dimesitylboron based 50 host materials

Carbazole was functionalised with electron deficient dimesitylborane units to give **50**, figure 1.15.[40] The intrinsic high triplet energy and good hole transporting properties of carbazole, combined with the electron transport properties of the borane units, result in a molecule with a high triplet energy of 2.94 eV, capable of hosting OLEDs of all colours with excellent EQEs (20.7% for red, 20.0% for green, 16.5% for blue, and 15.7% for white).[40]

Electron-deficient benzimidazole units have been incorporated at the 3 and 6-positions of carbazole to improve electron transporting properties, Figure 1.16.[41] Comparable electron and

hole mobilities were recorded for **51**, resulting in efficient blue fluorescence in OLEDs (EQE: 3%; CIE: (0.16, 0.05)). In addition, the CV of **51** shows the single oxidation and reduction present in the compound, with no electropolymerisation observed on multiple scans, denoting good electrochemical stability.[41]

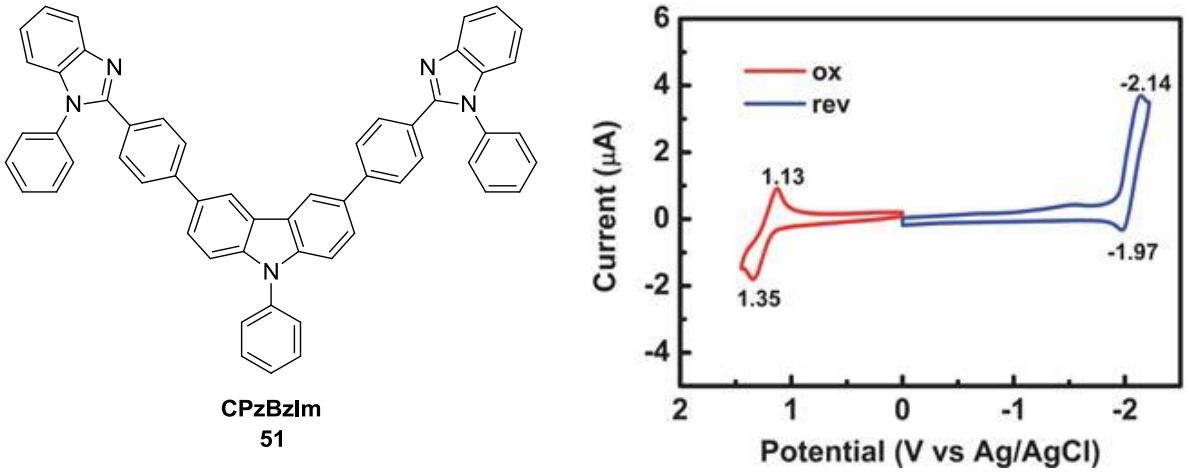

Figure 1.16 - Structure of CPzBzIm and its cyclic voltammogram in DCM solution and THF solution for the oxidative and reductive scans respectively[41]

Ladder carbazole derivatives were synthesised and characterised by Boudreault *et al*. with the aim of developing p-type semiconductors with high mobility and also good solubility for solution processing, figure 1.17.[42] The derivative **52** demonstrated high hole mobilities of 0.12 $cm^2\ V^{-1}\ s^{-1}$ in solution processed films comparable to those achieved from evaporated films. Other derivatives, including **53**, showed poorer mobilities, attributed to higher disorder in the amorphous films due to more conformational flexibility.[42]

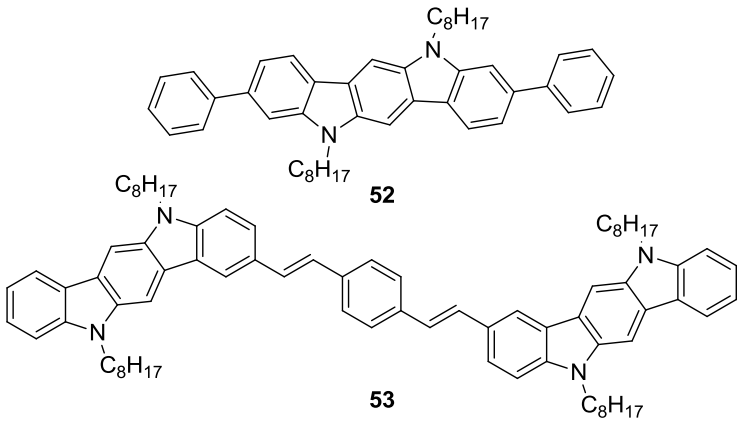

Figure 1.17 - Structure of carbazole hole transport materials

1.3.4 Fluorene in ambipolar systems

It is well established that fluorene is a thermally and kinetically stable unit with deep blue emission and a variety of polyfluorenes have found applications in OLEDs. The chemistry of fluorenes and polyfluorenes has been extensively studied and there are many well established strategies for their functionalisation. Substitution at the C(9) position is facile with both aryl and alkyl substituents, due to the acidity of the bridgehead hydrogens, scheme 1.7. The most common substituents in this position are alkyl chains, which act primarily to increase solubility and ease of processing. The introduction of aryl and perfluoroalkyl chains into transistor materials is also known to influence the intermolecular packing of a material and may have a positive effect on charge mobility and stability in certain cases. Substitution in the 2- and 7-positions is also easily achieved, commonly by introduction of halogen atoms as handles for further reaction, scheme 1.8. The synthesis of fluorene derivatives substituted in the 3- and 6-positions (scheme 1.9) has enabled comparisons of the electronic and photophysical properties with the more common 2,7-derivatives.[43,44] Reactivity and conjugation is more limited through the 3- and 6- positions, as demonstrated by lower molecular weight polymers and blue shifted emission of the 3,6-oligomers compared to their 2,7-counterparts.

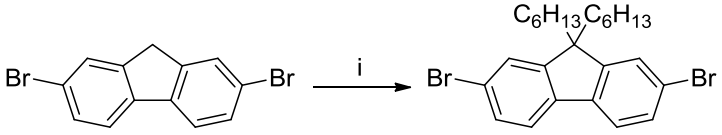

54 **55**

Reagents and conditions: i) NaOH, *n*-bromohexane, DMSO, *n*-Bu_4NBr

Scheme 1.7 - Substitution of the fluorene C9 position

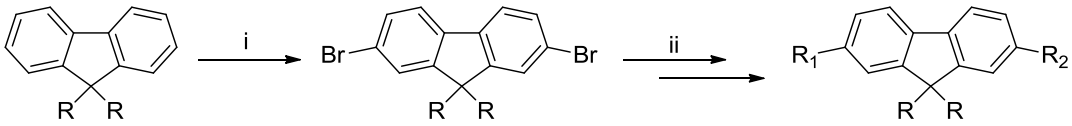

56 **57** **58**

Reagents and conditions: i) Br_2, $KBrO_3$, AcOH, H_2SO_4; ii) e.g. Suzuki-Miyaura cross-coupling reaction

Scheme 1.8 - Substitution of fluorene at the 2 and 7-positions

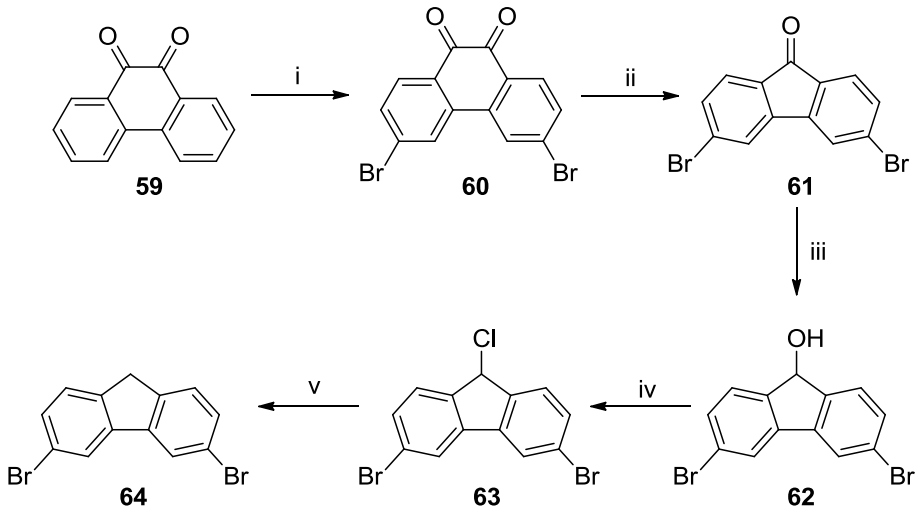

Reagents and conditions: i) Br_2, hv; ii) OH^-, $KMnO_4$; iii) $NaBH_4$; iv) HCl; v) Zn, CH_3COOH

Scheme 1.9 - Synthesis of 3,6-substituted fluorene

It is also possible to create a spiro centre at C(9), allowing control of the three dimensional structure of the material, scheme 1.10.

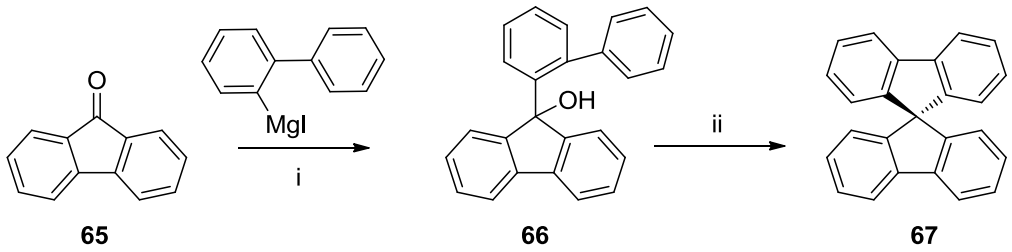

Reagents and conditions: i) THF; ii) HCl, AcOH

Scheme 1.10 - Synthesis of spirofluorene

It has been demonstrated that polyfluorenes can support electron transport when incorporated into a suitable device structure. It is vital to prevent the build-up of defects at device interfaces which can significantly hinder charge mobilities.[45] The Friend group reported electron mobilities of poly-9,9-dioctylfluorene (PFO) as high as 5 x 10^{-3} cm^2 V^{-1} s^{-1}, higher than the hole mobility observed of 3 x 10^{-4} cm^2 V^{-1} s^{-1}, figure 1.18. This implies that fluorene can support both electron and hole transport within a material and is therefore a suitable candidate for incorporation into D-A systems. Other work by Kajii *et al.* demonstrated that OFETs using PFO as an active layer exhibited ambipolar transport properties with both hole and electron mobilities of around 10^{-3} cm^2 V^{-1} s^{-1}.[46]

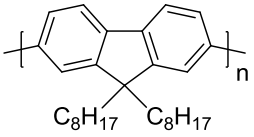

PFO
68

Figure 1.18 - Structure of PFO

The ability to create molecules with three-dimensional structures by taking advantage of spiro-fluorene centres may impart desirable properties on the material. For example, increased glass transition temperatures and morphological stability can be obtained. Chu *et al.* developed branched materials based on spiro(fluorene-9,9'-xanthene) derivatives as sky blue emitters for OLEDs (figure 1.19) that showed excellent thermal stability with high T_g up to 140 ^{o}C.[47] However, it should be noted that such complex molecules require lengthy and inefficient synthetic protocols.

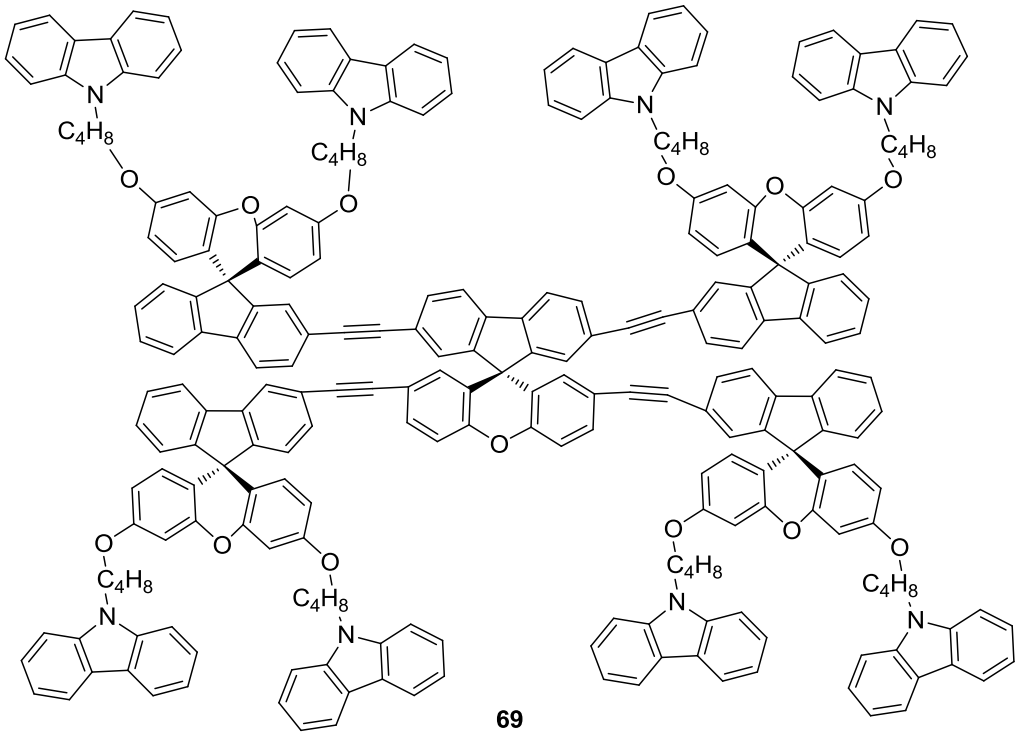

69

Figure 1.19 - Structure of a branched spiro(fluorene-9,9'-xanthene) derivative

1.4 Ambipolar systems containing carbazole, fluorene, oxadiazole or arylamine

There are many examples of compounds designed to incorporate two or more of the **Cbz**, **DPA**, **OXD** or **F** moieties into a single molecule in order to achieve desirable properties for application to optoelectronic applications; selected examples are discussed here.

A study of star shaped molecules with a D-π-A structure was carried out by Zou *et al.* using a triazine core as the electron-accepting moiety. The materials were shown to have fully or quasi reversible redox characteristics accompanied by high two-photon absorption cross-sections, attributed to the strong ICT character of the compounds, figure 1.20.[48] A strong two-photon absorption cross-section indicates that a material may be suitable for two-photon fluorescence excitation microscopy or 3D optical data storage among other applications.

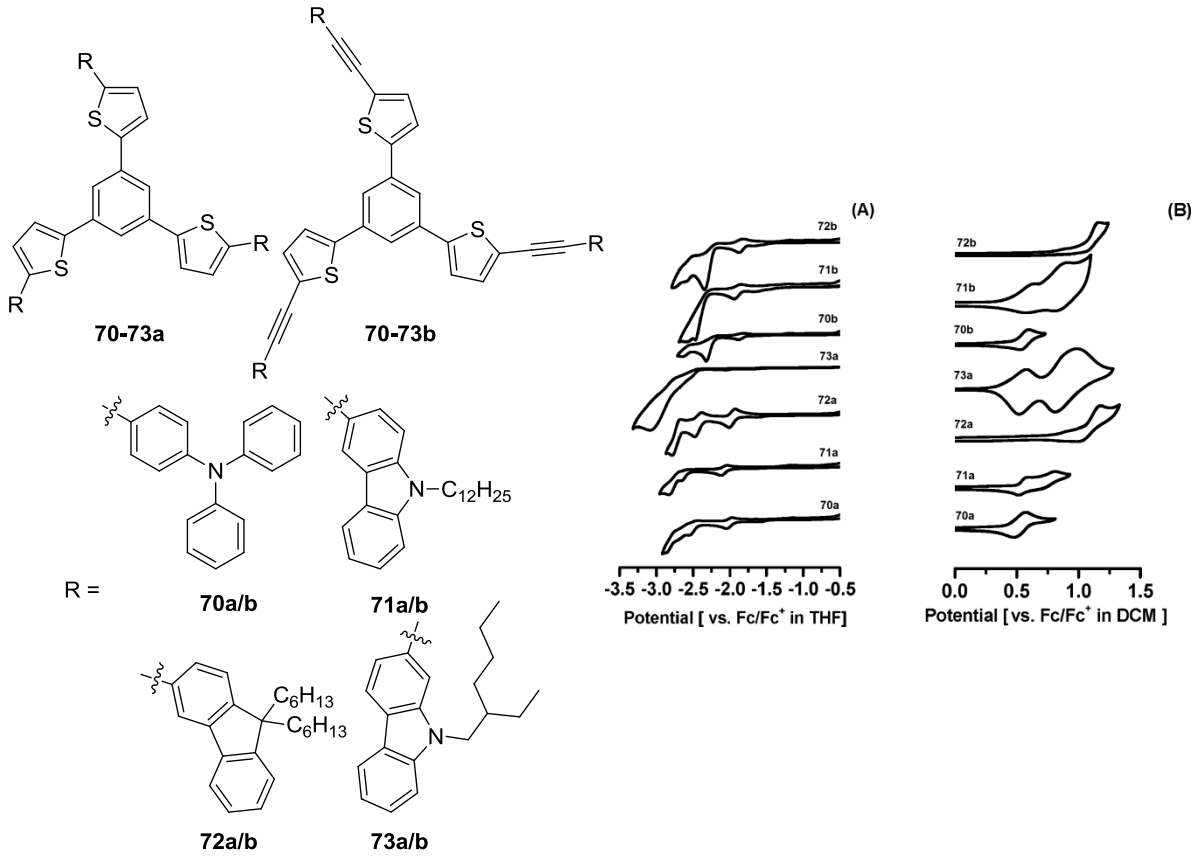

Figure 1.20 - Structure of TPA dyes and their cyclic voltammograms[48]

Work by Tao *et al.* to develop a new host for phosphorescent emission from iridium complexes led to a 1,3,4-oxadizole substituted with two carbazole units **74** which compared favourably with the commonly used carbazole host material CBP **74**, figure 1.21.[49] It was found that **74** has better thermal stability, a higher triplet energy, and HOMO and LUMO levels well matched to the electron and hole transport layers. The device characteristics (EQE: 18.5%) using the doped red emitter [$(piq)_2Ir(acac)$] were much improved compared to the device using CBP.[49]

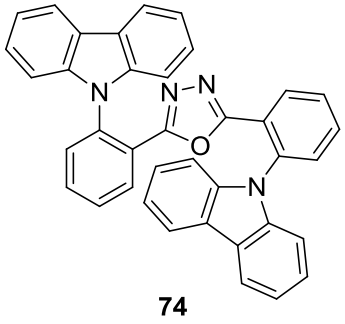

74

Figure 1.21 - Structure of bipolar host 74

Lai *et al.* synthesised ambipolar emitters **75** and **76** based on a diphenylamine-fluorene-benzimidazole structure. The diphenylamine and benzimidazole units were intended to aid hole and electron-transport, respectively.[50] The fluorene unit acted as an emissive spacer to prevent strong charge transfer interactions between the D and A components. The compounds demonstrated blue electroluminescence (EL) in single layer devices and acted as hosts to a yellow iridium complex [$(fbi)_2Ir(acac)$], figure 1.22. Time-of-flight (TOF) measurements showed that **75** and **76** supported both hole and electron transport as expected.[50]

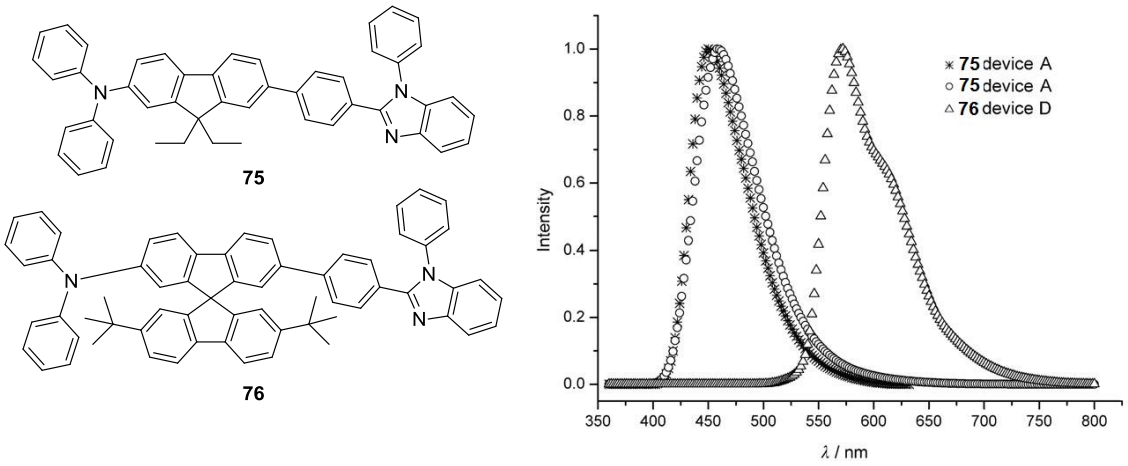

Figure 1.22 - Structure of ambipolar compounds and EL of single layer devices of 75 (A) and devices (D) using 75 and 76 as a host for a phosphorescent iridium emitter.[50]

Work by Müllen and collaborators on compounds **77** and **78** demonstrates the importance of the location of the donor and acceptor moieties with respect to one another, Figure 1.8. [51] OLED and TFT devices made from compounds **77** and **78** were starkly different in their device characteristics. **77** demonstrated p-type conduction in the TFT with calculated mobilities of 1 $x10^{-5}$ cm^2/ V s and an OLED emitting blue-green light with an EQE of up to 0.1%. This is in contrast to the devices of material **78** which exhibit insulating behaviour and non-functioning OLEDs.[51] This difference was attributed to exciplex formation in **78** devices due to

intermolecular charge separation, whereas **77** showed intramolecular donor-acceptor interactions: further evidence for this was provided by the strong PL quenching observed for **78** due to intermolecular aggregations.

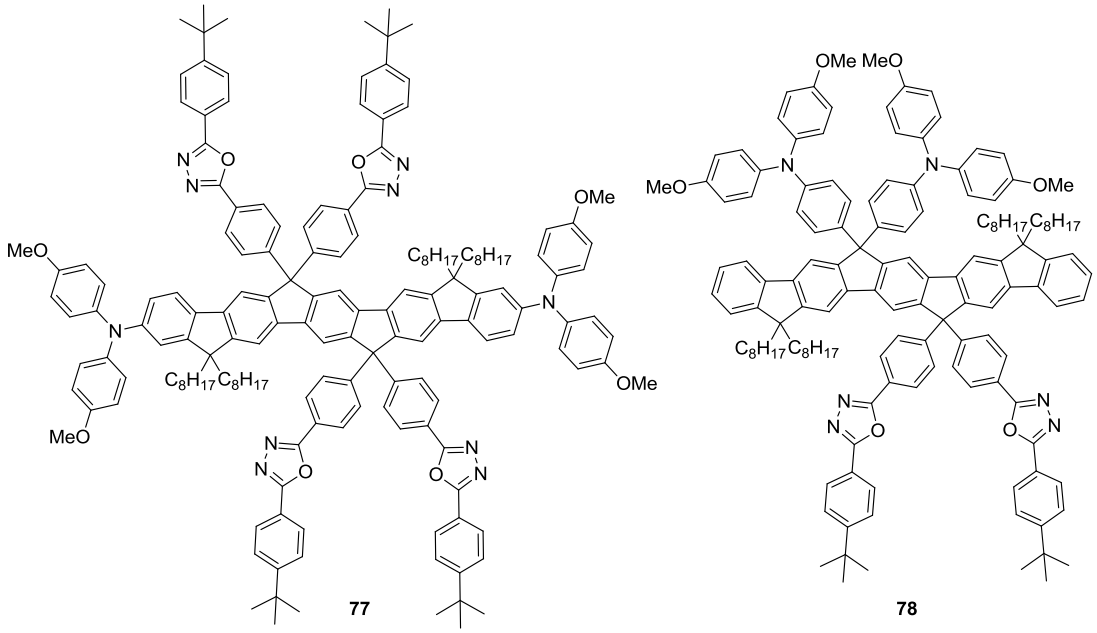

Figure 1.23 - Molecular structures of 77 and 78

Recent work by Zheng *et al.* describes the development of ambipolar host materials based on a D-A carbazole-diazafluorene motif, figure 1.24.[52] The compounds **79** and **80** exhibit ambipolar charge transport characteristics and the non-conjugated linking of the donor and acceptor moieties maintains high triplet levels of 2.82 and 2.83 eV, respectively. The PHOLED device based on MCAF using the blue emitter FIrpic, bis[2(4',6'-difluorophenyl)pyridinato-N,C(2')]-picolinate achieved current efficiencies of 32.2 cd A^{-1} with excellent EQE of 17.9% and power efficiency of 31.3 lm W^{-1}.[52] The excellent device characteristics reflect the charge carrier abilities and the efficient energy transfer from host to guest.

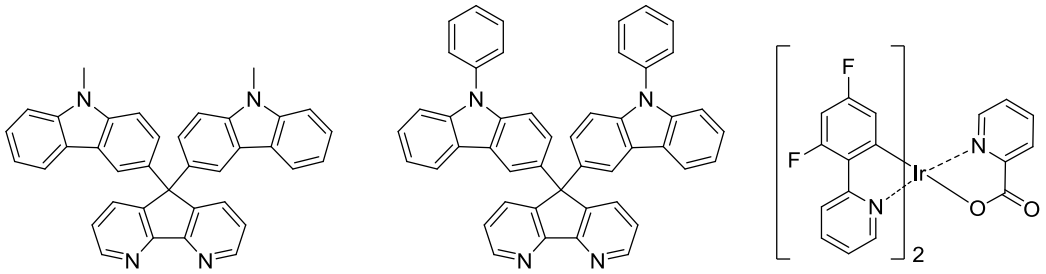

Figure 1.24 - Structure of ambipolar host materials based on carbazole-diazafluorenes and Iridium complex FIrpic

Lee *et al.* have developed D-A systems exhibiting electrical switching behaviour and investigated the effect of changing the donor moiety between **Cbz** and **DPA** when coupled with a phthalimide acceptor, figure 1.25.[53] **81** with a D-A-D molecular structure demonstrated reversible non-volatile negative-differential-resistance (NDR) characteristics, a phenomenon where increased voltages result in a reduced current. In contrast, **82** with the A-D-A structure exhibited insulating behaviour, attributed to limited hole mobility. It was also observed that the **DPA** substituted materials exhibited a higher on-off ratio than those with carbazole as donor groups.[53]

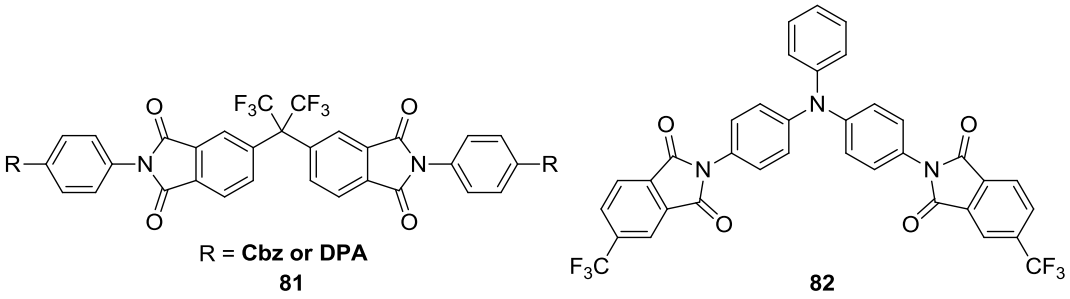

Figure 1.25 - Structures of D-A-D and A-D-A systems used for memory devices by Lee *et al.*

Recent work in our laboratory by Zheng *et al.* concerned the role of ICT in bipolar carbazole-oxadiazole systems, figure 1.26.[54] It is known that extensive ICT can reduce the HOMO-LUMO gap in a given system. This may result in reduced singlet and triplet energies that can be detrimental to the operation of devices using such a compound as a host, due to back energy transfer. Zheng demonstrated that by increasing the bulk of the substituent on the diphenyloxadizole fragment increases the triplet level, accompanied by a blue shift of both absorption and emission. It was also shown that substitutions on the 2- and 7-positions of the carbazole can lower the singlet level of the molecules and fine tuning of the energy levels is possible by careful molecular design.[54]

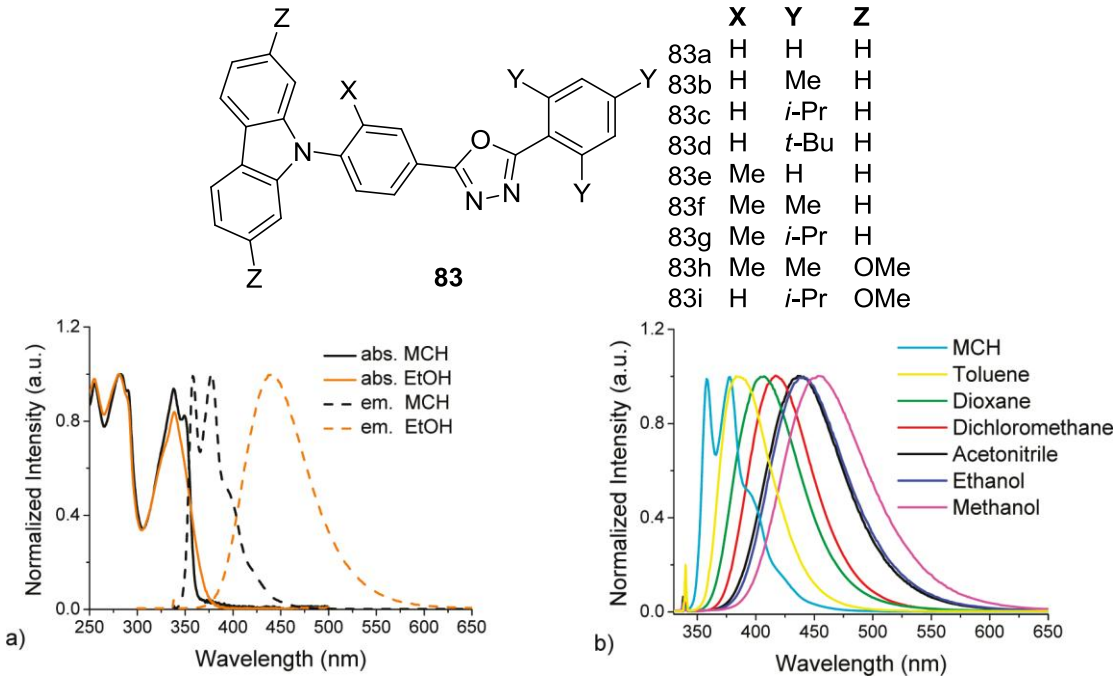

Figure 1.26 - Structures of bipolar carbazole-oxadiazole molecules and plots of absorption and emission of 83a in various solvents[54]

As an alternative to the all-conjugated bridges commonly used in D-A systems for host materials a tetraarylsilane bridge was investigated, figure 1.27.[55] The aim here was to raise the triplet level of the compound and interrupt conjugation between the donor and acceptor species, so that good electron and hole mobilities are maintained. High EQEs are achieved when the **DPA**-tetraarylsilane-benzimidazole compound **84** is used as a host material for blue (16.1%), green (22.7%), orange (20.5%) and white (19.1%) phosphorescent OLEDs.[55]

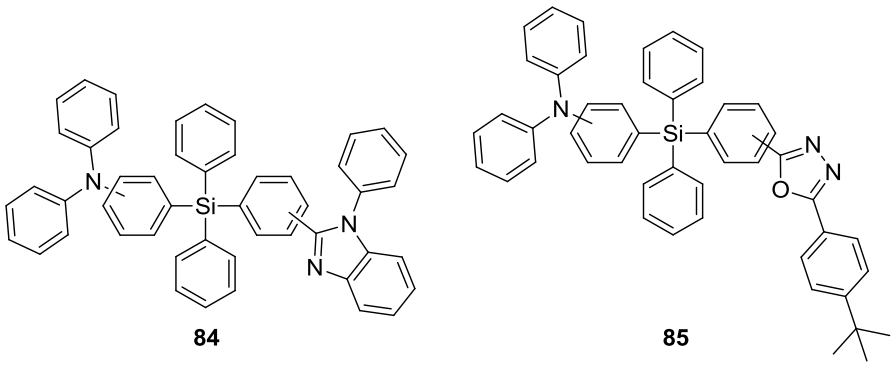

Figure 1.27 - Structures of D-A compounds containing a tetraaryl silane bridge

Design of a bipolar system **86** based on a fluorescent spirobifluorene backbone allowed an effective nitric oxide (NO) probe to be created.[56] An *ortho*-phenyldiamine unit in the molecule acts as both the electron donor and also as the receptor for NO, the 1,3,4-oxadiazole moiety

acts as the electron acceptor. In the absence of NO, there is strong photoinduced electron transfer (PET) from the diamine to the oxadiazole moiety. In the presence of NO EDADO-T is formed, altering the molecular structure and turning the PET off, resulting in strong fluorescence, figure 1.28.[56]

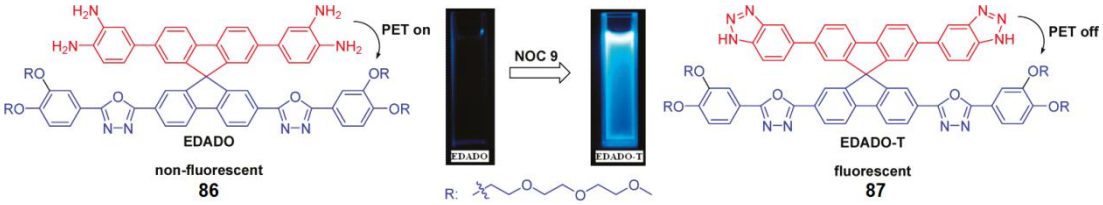

Figure 1.28 - Bipolar probe EDADO exhibits fluorescence in the presence of NO as EDADO-T[56]

Zhu *et al.* investigated some symmetrical molecules based on a fluorene-anthracene core with various charge transport moieties at the termini figure 1.29.[57] The molecules exhibit blue emission in the OLED shown, with emitter **88** giving CIE coordinates of (0.15, 0.13), close to the NTSC blue standard with maximum current efficiency of 2.0 cd A^{-1}. The materials also demonstrate high glass transition temperatures with low tendency to crystallise, giving good device stability.[57]

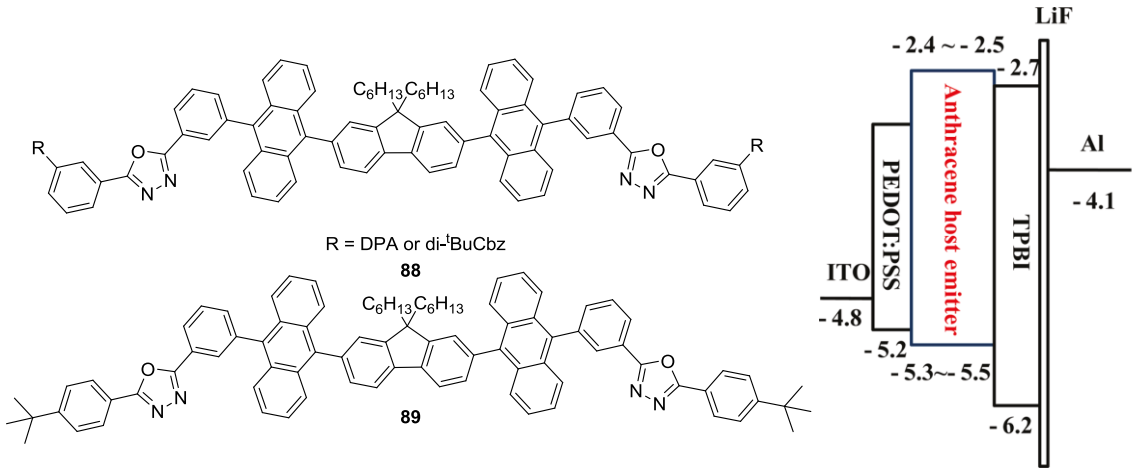

Figure 1.29 - Structures of fluorene-anthracene host emitters and device structure of OLEDs incorporating them[57]

Work in the Bryce group investigated triad molecules based on donor-bridge-acceptor structures using **DPA** or **Cbz** as donors, **F** as a bridging moiety and **OXDs** or pyridyl units as acceptors, figure 1.30.[58] They demonstrated that molecular design allows the emission colour and band gap of the compounds to be tuned from the blue to the green. The solution processible, thermally and chemically stable molecules are easily incorporated into simple, single layer OLED devices as a spin-coated active layer.[58]

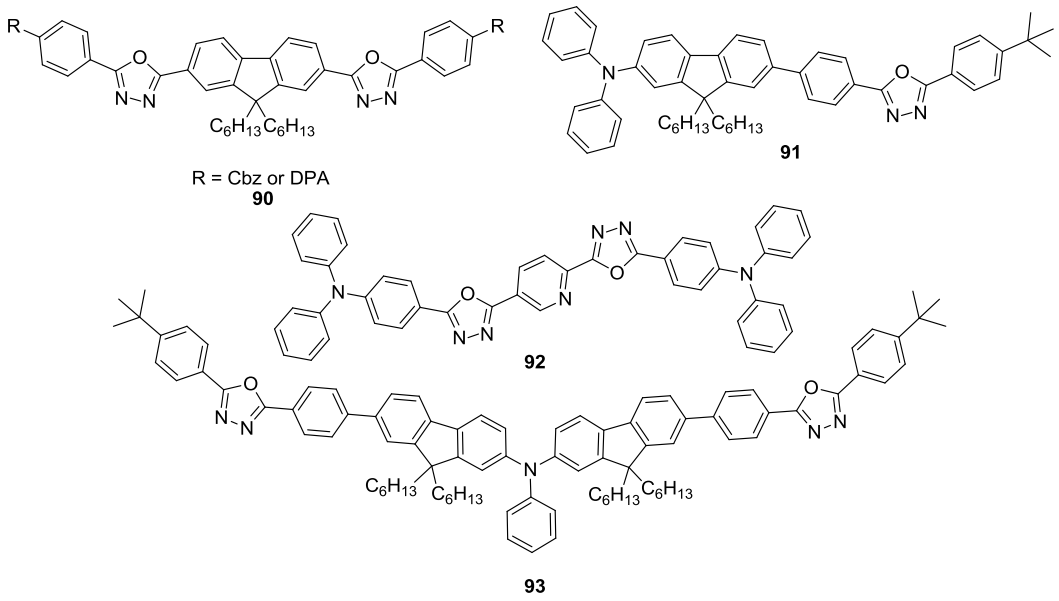

Figure 1.30 - Structures of triad molecules 90 – 93

In another study using the material **91** and **92**, switching characteristics were investigated. It was observed that the triad molecule **91** and D-A-D molecule **92** exhibited switching behaviour in a device structure Al/active layer/Al.[59] It is proposed that the donor and acceptor moieties provide charge transport and that the fluorene moiety is able to trap charge *via* formation of fluorenone defects giving rise to switching behaviour.[59]

1.5 Alternative Donors and Acceptors

Although arylamines and carbazoles are some of the most commonly used donor materials, particularly in the field of OLEDs, there are many other candidates that have been exploited for their electronic characteristics in organic materials chemistry. Zinc porphyrins, extended tetrathiafulvalenes (exTTFs) and ferrocenes have been used in various donor-acceptor arrays with C_{60}.[60-62] These fundamental electron transfer studies have probed the factors affecting the electron transfer processes – charge separation, recombination processes and attenuation factors (β) – a measure of the charge transfer capability of a bridge. These investigations assist our understanding of photosynthetic processes which may be applied to light-harvesting protocols to develop new energy technologies.[60] Aside from 1,3,4-oxadiazoles there are a multitude of electron-acceptors which have been used extensively. Discussed beloware some of the most common and well used donors and acceptors in organic materials chemistry.

An analogue of C_{60}, PCBM figure 1.31, is the most commonly used electron acceptor in bulk heterojunction solar cells. C_{60} is a strong electron acceptor, exhibiting three well resolved reduction waves in its cyclic voltammogram.[63] PCBM was synthesised by Wudl and coworkers and gives C_{60} much greater solubility resulting in its widespread use in solar cells.[64]

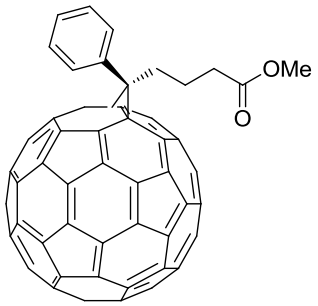

94

Figure 1.31 - Structure of PCBM

Strongly accepting C_{70} derivatives have also been used as acceptors in solar cells. A recent study by Heeger and coworkers demonstrated the new donor unit, **95** figure 1.32, with the acceptor $PC_{70}BM$.[65] The use of a small molecule donor compared with a polymeric donor allows more consistency to be achieved from batch to batch as the purity and uniformity of the material can be guaranteed and may also control the morphology of the device. Power conversion efficiencies (PCE) of 6.7% were reported for the optimised devices.[65]

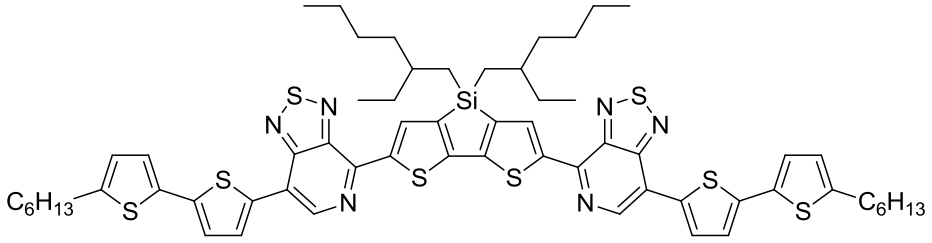

95

Figure 1.32 - Structure of new donor unit for use in solar cells

Zhu *et al.* presented a study of donor-acceptor systems using phenoxazine as a donor unit, figure 1.33. Phenoxazine possesses an ionisation potential 0.7 eV lower than carbazole and so is a stronger donor with a potentially more stable radical cation.[66] The materials exhibit reversible electrochemical oxidation and reduction, as well as evidence of ICT in the solution photophysics, indicating ambipolar characteristics. Good fluorescence quantum yields in solution for some derivatives demonstrate the potential for this donor to be incorporated into OLED devices. [66]

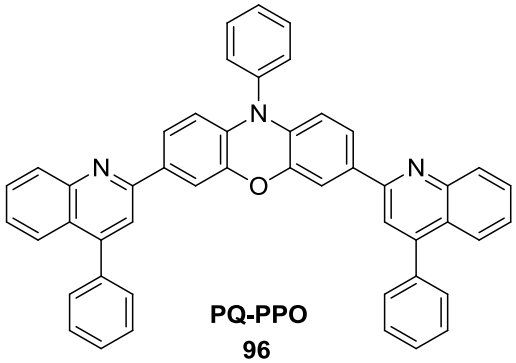

Figure 1.33 - A representative structure of a phenoxazine – acceptor system 96

Diphenylphosphine oxide has been used as an alternative acceptor by Hsu *et al.* in development of an ambipolar phosphorescent host material, **97**.[31] They take advantage of the film forming abilities of **97** and maintain limited conjugation in the structure by linking the carbazole and fluorene moieties *via* the non-conjugated C_9 position of fluorene, figure 1.34. The ambipolar nature of the host allows low operating voltages in the device and a good EQE of 14.8% was achieved with FIrpic, **81**, as the emitter.[31]

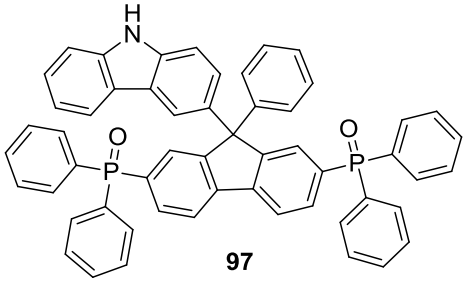

Figure 1.34 - Structure of host material 97

A recent study to compare the donor abilities of fluorene, carbazole and diphenylamine was carried out in our laboratory by Moss *et al.* using D-A-D systems where dibenzothiophene-*S,S*-dioxide was the acceptor moiety, figure 1.34 for a representative structure.[67] The framework was varied by altering the substitution positions on the donor and acceptor units. It was demonstrated that the donor strength increased in the order fluorene < carbazole < arylamine which was reflected in the increased red shifted ICT emission observed for the arylamine trimers particularly in polar solvents, figure 1.34. The emission could be effectively tuned by altering the structures of the materials.[67]

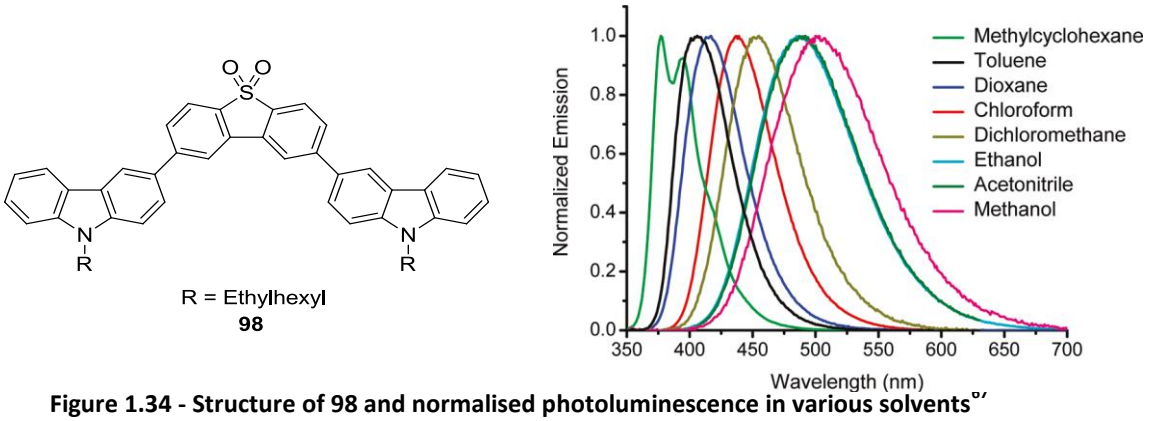

Figure 1.34 - Structure of 98 and normalised photoluminescence in various solvents[97]

1.6 Conclusions

This chapter has highlighted the importance of ambipolar D-A type systems for applications in organic materials. There is a large body of research that advocates the use of these types of systems to significantly improve device characteristics in many optoelectronic applications. It has been shown how the synthetic chemist can control the characteristics of a compound by careful manipulation of its structure and that the possibilities for structural modification are virtually without limit.

Within this area there is significant data to support the use of carbazoles, arylamines, fluorene and 1,3,4-oxadiazole units as key constituents of ambipolar systems. The advantages of these systems are their versatile electronic and structural characteristics combined with the ease of their synthetic manipulation. Although there is a wealth of data concerning these materials, there is still much room for new structural modifications aimed at the improvement of device characteristics. Studies in this area will be described in the following chapters.

Chapter 2: Single – Layer Deep Blue Molecular OLEDs Based on Carbazole – Fluorene – Oxadiazole Triad Molecules

---

2.1 Introduction

The devices discussed in this chapter will be based on all-organic fluorescent small molecules. Fluorescence occurs when a singlet excited state radiatively decays to the ground singlet state. Spin statistics dictates that the recombination of a hole and an electron results in the formation of one of four different states, one a singlet state and the other three triplets.[68] The ratio, therefore, of triplet to singlet states is 3:1. The emission of light from the triplet state (i.e. phosphorescence, the transition from a triplet excited state to a singlet ground state) is formally forbidden. In systems containing heavy metal atoms, for example iridium, the large spin-orbit coupling of the metal may allow intersystem crossing (ISC) to occur and hence phosphorescent emission.[68] Organometallic complexes, therefore, have the potential advantage of achieving a higher efficiency in an OLED by accessing the triplet state. However, the ease of colour tuning by synthesis, the advantage of simpler device structures and the lower cost of all-organic devices provides motivation for their continued development. Additionally, it has been demonstrated in recent years that the yield of formation of singlet excitons, η_s, may exceed the theoretically predicted value of 25%.[69] This means that the efficiency limits previously declared for fluorescent devices may be exceeded.

Segal *et al.* demonstrated that a higher proportion of singlet states may be produced in an OLED by control of the device structure.[70] Their work describes efforts to improve device efficiency by encouraging the mixing of charge-transfer (CT) states which are the precursors to singlet and triplet excitons, figure 2. By increasing the number of excited ^{1}CT states by the inclusion of a mixing layer consisting of DCM2:CBP, **108**, at the electron injection interface the OLED efficiency is increased three-fold compared to the device with no mixing layer, figure 2.1. This is attributed to the creation of nearly three times more singlet states than in the control OLED.[70] Time resolved spectroscopic studies confirm the nature of the emission to be fluorescent and not phosphorescent.

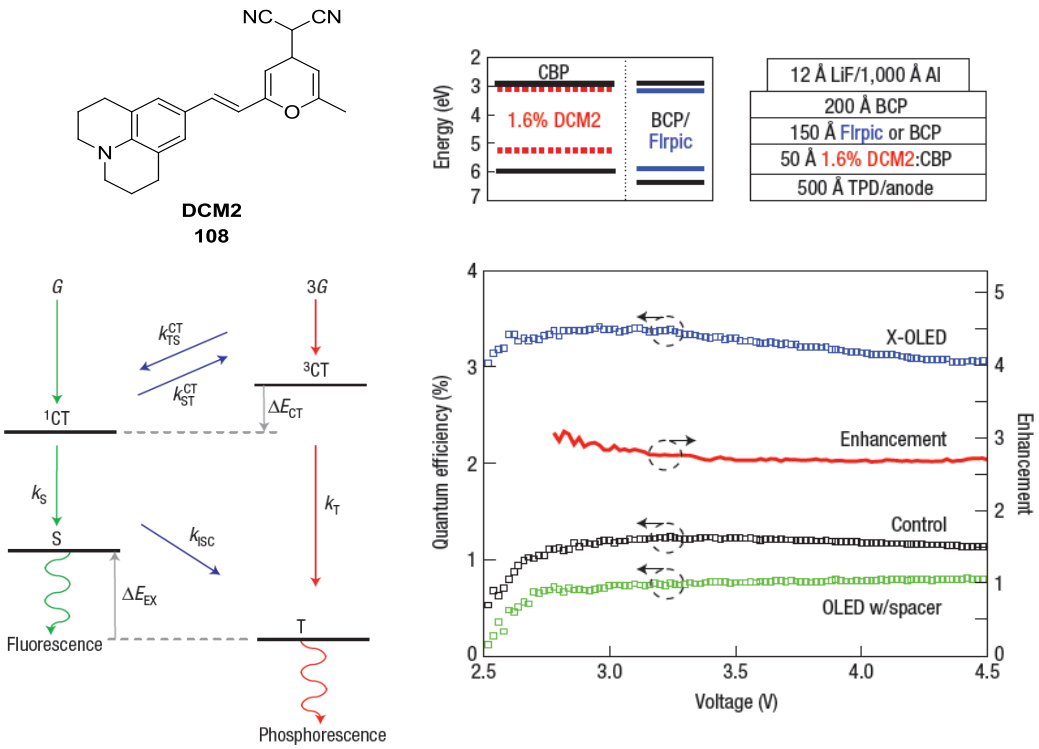

Figure 2.1- Proposed energy pathways for emission in displayed device structure and voltage vs. efficiency plot for the various OLEDs in the study[70]

2.1.1 Blue Emission

While there are currently very good red and green OLEDs available as elements in displays, deep blue devices remain challenging. The requirements for deep blue emitters are stringent; high efficiency, good thermal stability and saturated blue emission with Commision Internationale de l'Eclairage (CIE) coordinates of (0.14, 0.08) to satisfy the National Television System Committee (NTSC). It has been noted that very few deep blue devices achieve an external quantum efficiency (EQE; the ratio of number of emitted photons to number of injected electrons) greater than 1%.[71] Higher energy blue emission requires a larger HOMO – LUMO gap than red or green counterparts. This leads to challenges both in device stability and molecular design.

Common candidates for deep blue emission include derivatives of carbazole[72], arylamine[73], anthracene[18,74] or fluorene.[75] For example, Kim *et al.* described the incorporation of anthracene derivatives into devices with the structure shown in figure 2.2.[18] One of the derivatives achieved deep blue emission with CIE coordinates (0.156, 0.088), power efficiency of 1.87 lm W^{-1}, a luminance efficiency of 3.64 cd A^{-1} and an EQE of 7.18%.[18] When reported

these were the most impressive device results yet achieved for a fluorescent deep blue emitter; however it is important to note that the devices are complex multilayer structures. This requires expensive and complex fabrication procedures which are not readily applicable to large-area displays. The extra layers aid injection and transport of holes and electrons; if this could be achieved within one material by engineering the correct HOMO and LUMO levels and charge carrier characteristics, then a much simpler device may be fabricated.

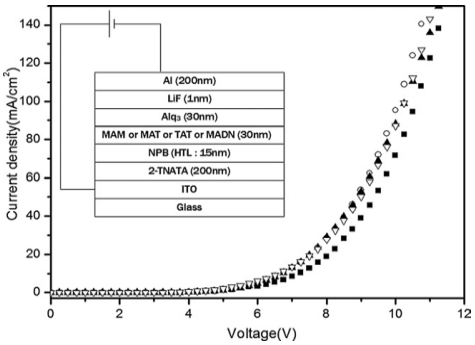

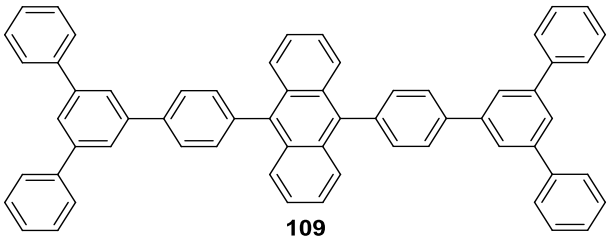

Figure 2.2- Structure of 109 and plots of voltage vs. current density for devices with multilayer structure indicated[18]

2.1.2 Donor-Acceptor Systems for Blue Emission

The importance of balanced hole and electron transport for OLED performace has been demonstrated.[5-7] Ambipolar materials that can support both electron and hole transport have been shown to be good candidates for efficient and deep blue emission in OLEDs.[71,76,77] Some of the main advantages are the proposed improvements in charge injection and simplification of device fabrication by reduction in the number of required layers.

Recent work by Reynolds *et al.* describes the incorporation of purine derivative **110** into an OLED.[71] The emissive layer consisted of **110** in a host matrix of *N,N'*-dicarbazolyl-3,5-benzene (mCP, **111**). An EQE of 3.1% was achieved with peak emission in the deep blue region at 430 nm with CIE coordinates of (0.15, 0.06).

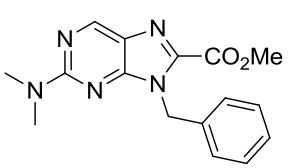

110

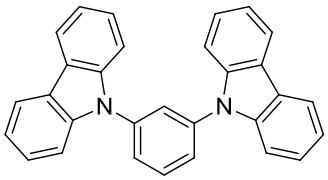

111

Figure 2.3- Structures of purine 110 and host material mCP

Lin *et al.* described the combination of a carbozlyl donor and a dimesitylboron acceptor systems for deep blue emission, **112** – **115**.[77] In the device structure ITO/NPB (40 nm)/CzPhB (20 nm)/TPBI (40 nm)/LiF (0.5 nm)/Al (100 nm) CzPhB exhibited deep blue emission with CIE coordinates (0.15, 0,09) with maximum EQE of 4.3%. The high performance is attributed to efficient injection of both holes and electrons into the bipolar emissive layer.[77]

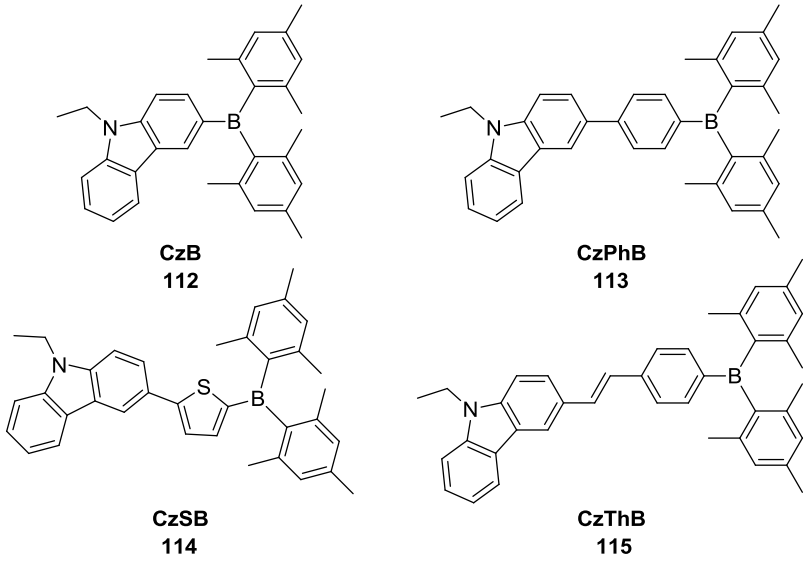

Figure 2.4- Stuctures of carbazole-dimesity boron D-A systems

Donor-acceptor arylamine-quinoline systems were synthesised by Hancock *et al.*[78] The donor-acceptor characteristics were demonstrated by solvatochromism studies showing a positive bathochromic shift in polar solvents indicating a stabilised ICT state. **117** was incorporated into devices with the architecture ITO/PEDOT/PVK/**117** /TPBI/LiF/Al; the emission was blue-green in colour with good brightness up to 15400 cd/m^2, 3.0% EQE and luminance efficiency of 7.9 cd/A.[78]

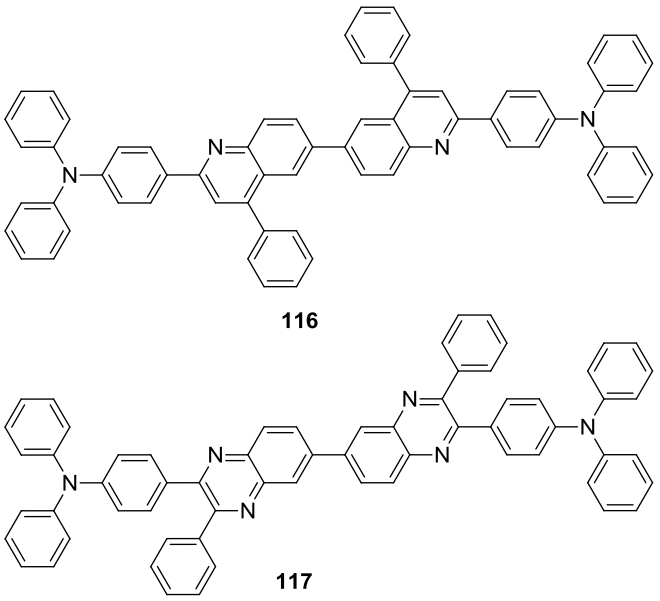

Figure 2.5- Structure of bipolar materials 116 and 117

A series of molecules based on triarylamine, anthracene and benzimidazole units was incorporated into simple device structures which demonstrated good performance whilst maintaining deep blue emission.[79] The material **118**, figure 2.6, achieved an EQE of 3.94% with CIE coordinates of (0.15, 0.14) in the device structure ITO/**118** (40 nm)/TPBI (40 nm)/LiF (1 nm)/Al (100 nm). This example demonstrates the potential to achieve impressive device characteristics whilst still using a simple device structure. The importance of incorporation of both a hole transporting and an electron transporting moiety within the same molecule is emphasised here and its success is demonstrated by the single layer device ITO/**118**(80 nm)/LiF (1 nm)/Al (100 nm) achieving an EQE of 2.66% and a maximum brightness of 8472 Cd m^2 at 8.7 V where both hole and electron injection are supported by the emissive material.[79]

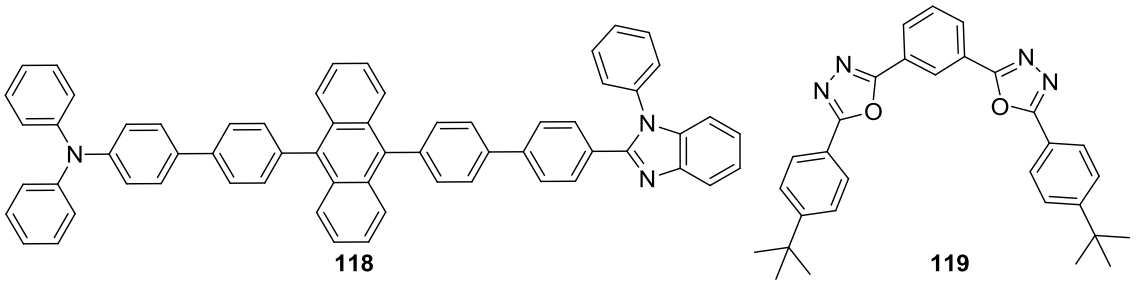

Figure 2.6- Structure of 118 and 119

2.1.3- Carbazole, Fluorene and Oxadiazole in Blue Emission

A recent study by Lei *et al.* utilised fluorene, carbazole and oxadiazole as units in blue emitters.[80] The emitters **120** – **124** were based on a truxene core substituted with conjugated fluorene based side arms. The fluorene units were substituted in the 2 and 9-positions with electron transporting (oxadiazole or triazole) units or hole transporting (carbazole) units. They were joined *via* non-conjugated linkers so as to limit the effect on the emission wavelength. The introduction of electron deficient units, triazole and oxadiazole, to analogues **120b** and **121**, improved the OLED performance by lowering the level of the LUMO and improving electron injection.[80] For the dihexylfluorene analogues **122** – **124** side chain interactions interfered with the film morphology and disrupted the quality of the OLED film – the materials with a spiro-fluorene **120** – **121** produced higher quality amorphous films.[80]

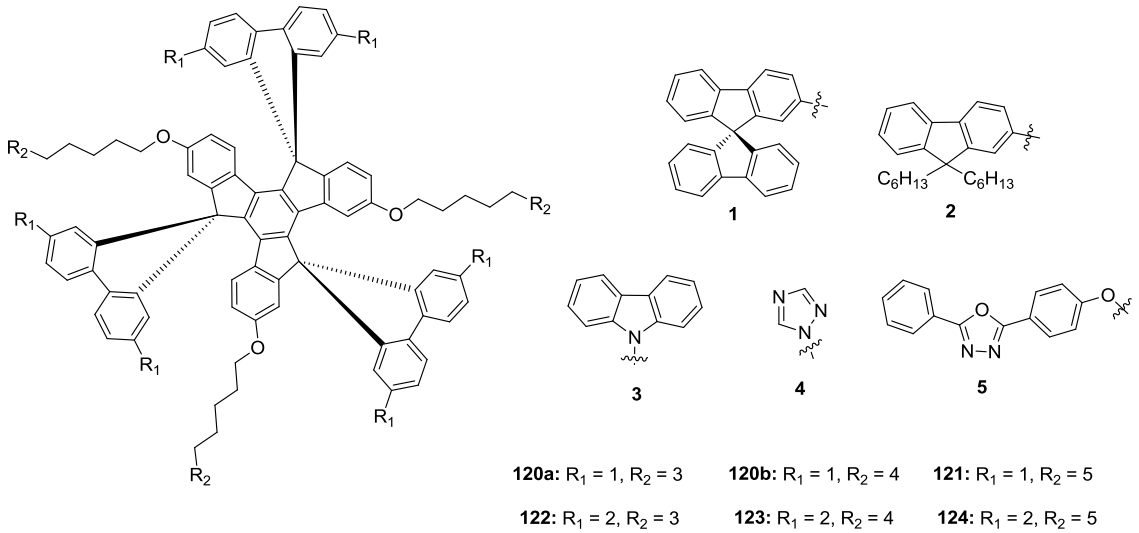

Figure 2.7- Structure of OLED candidates based on a truxene core

Previous work in the Bryce group has explored the effect of combining fluorene, oxadiazole and arylamine or carbazole into single molecules for light emitting applications. Fluorene is incorporated in the materials not only as a blue-emitting moiety but also to provide solubility through alkyl substituents to allow solution processing. Bipolar materials were synthesised and incorporated into OLEDs.[58] The incorporation of the hole-transporting arylamines resulted in a measurable increase in the HOMO of the compound as shown by DFT calculations and cyclic voltammetric studies in comparison with **OXD**-7, **119** a related electron transport unit. The bipolar materials demonstrated a bathochromic shift of emission in more polar solvents as discussed in chapter 1.

2.2 Results

This chapter describes the synthesis of a new series of ambipolar materials as candidates for deep blue molecular emitters. Our strategy combines the electron transport (acceptor unit), the hole transport (donor unit), and an emissive unit into one molecule. The objectives of the work were (i) to investigate how changes to molecular structure would tune the colour of fluorescence and (ii) to achieve efficient, stable and deep blue fluorescence in simple single-layer OLEDs. The synthesis, photophysical and device characteristics for deep blue OLEDs will be presented with a summary of DFT results (section 2.2).

2.2.1 Synthesis

The strategy adopted was to take a systematic approach, altering specific features of our materials to probe the effect of electronic, structural and morphological changes. The materials proposed for study are based upon the arylamine-fluorene-oxadiazole triad molecule, **91**, previously synthesised in our group by Kamtekar *et al. via* the route shown in scheme 2.1.[58] The synthesis of compound **125** from commercially available fluorene is described in the experimental chapter 6.

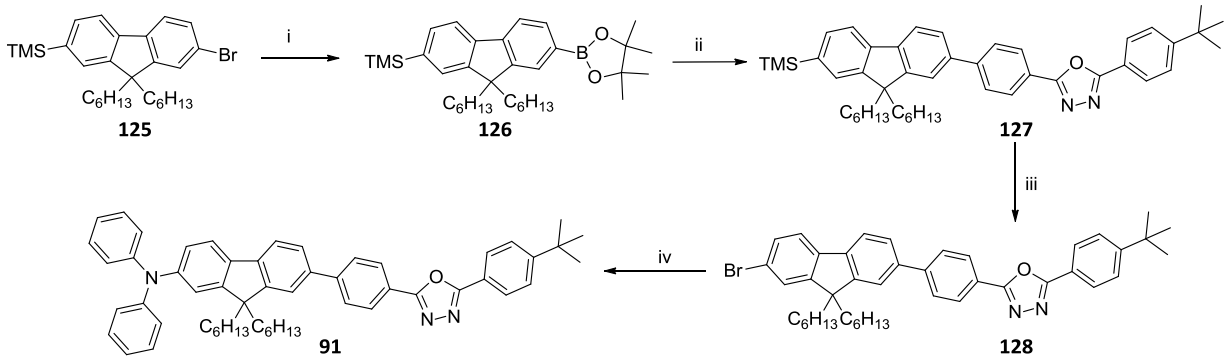

Reagents and Conditions: (i) *n*-BuLi, -78 °C, then 2-isopropyl-4,4,5,5-tetramethyl-1,3,2-dioxaborolane; (ii) **150**, $[Pd(PPh_3)_4]$, K_2CO_3, 80 °C; (iii) Br_2, NaOAc, THF, 0 °C; (iv) diphenylamine, $[Pd_2(dba)_3]$, $^tBu_3P$, NaO^tBu, PhMe, 80 °C.

Scheme 2.1 – Synthesis of arylamine-fluorene-oxadiazole triad molecule 91[58]

In order to facilitate asymmetric functionalisation of fluorene in the 2,7-positions one of two different strategies is required. One approach previously adopted by the Bryce group is to reversibly protect one of these positions to allow further functionalisation in one position as demonstrated in scheme 2.1.[81-83] Alternatively, forego a protection strategy and to substitute the 2 and 7-positions to give different levels of reactivity.[84]

Previous cyclic voltammetry (CV) studies on **91** and other analogues, have shown an irreversible feature in the oxidative scan of both arylamine and carbazole derivatives which are unsubstituted at the positions *para* to the nitrogen.[58,85] This feature is attributed to an electrochemical polymerisation process through these positions. To avoid this reaction, it was proposed to synthesise an analogue of **91** with these positions blocked by methyl groups to determine if device stability may be improved. Synthesis of the arylamine **131** was achieved by a Buchwald-Hartwig C-N coupling with the relevant amine and aryl chloride affording **131** in a 93% yield, shown in scheme 2.2.[19] The rest of the skeleton of **134** was built up by C-N cross-coupling reactions and Suzuki-Miyaura cross-coupling, scheme 2.2.

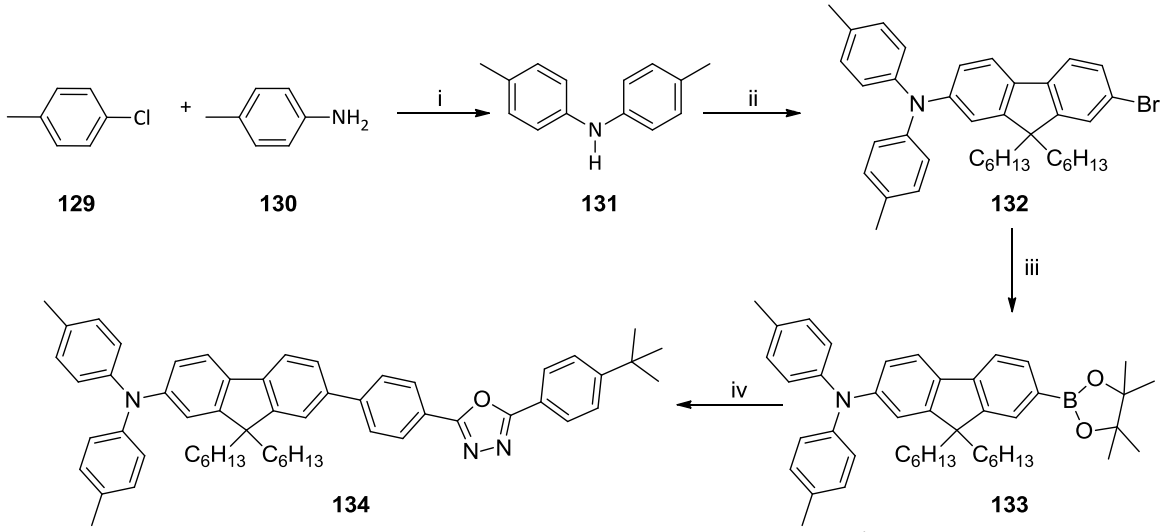

Reagents and Conditions: i) $[Pd_2(dba)_3]$ (0.5 mol%), JohnPhos (2 mol%), NaO^tBu, 80 ^oC, 15 h, 93%, ii) $[Pd_2(dba)_3]$ (1 mol%), dppf (3 mol%), NaO^tBu, toluene, 100 ^oC, 12 h, 50%, iii) nBuLi, THF, -78 ^oC then 2-isopropoxy-4,4,5,5-tetramethyl-1,3,2-dioxaboralane, -78 ^oC – RT, 15 h, 72%; iv) **150**, $[PdCl_2(PPh_3)_2]$, NaOH (aq), THF, 15 h, 62%

Scheme 2.2 – Synthesis of *para*-substituted arylamine analogue

When this route was applied to the synthesis of the carbazole analogue **140** it was discovered that the final C-N coupling *via* the Buchwald-Hartwig amination procedure adopted in scheme 2.2 resulted in poor yields of the desired product **140** and contamination with an unidentified luminescent impurity. The impurity was inseparable from **140** by column chromatography. This led to an alternative strategy being adopted. Iodination of commercially available 2-bromofluorene afforded 2-iodo-7-bromofluorene, which, after alkylation at the 9 position to improve solubility, was coupled *via* a ligand-mediated Ullmann reaction with carbazole selectively at the iodo-position in good yield. The product **138** was then borylated by a lithiation-quench procedure to furnish the Bpin-fluorene-carbazole unit **139**. Reaction of **139**

under standard Suzuki-Miyaura cross-coupling conditions afforded **140** in good yield, scheme 2.3, with excellent purity, by HPLC (representative trace for the series shown in experimental chapter), after column chromatography.

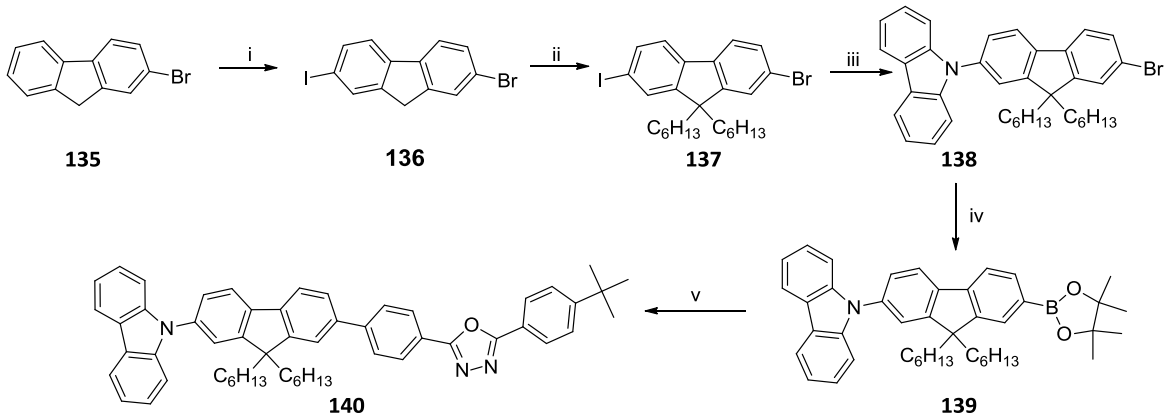

Reagents and Conditions: i) AcOH, H_2SO_4, KIO_3, I_2, 80^oC, 18 h; ii) tetra-*n*-butylammonium chloride, NaOH, *n*-bromohexane, RT, 20 h; iii) carbazole, CuI, 1,10-phenanthroline, K_2CO_3, DMF, 120 ^oC, 40 h; iv) nBuLi, 2-isopropoxy-4,4,5,5-tetramethyl-1,3,2-dioxaborolane, THF, -78 ^oC – RT, 15 h; v) **150**, $[PdCl_2(PPh_3)_2]$, NaOH (aq), THF, reflux, 15 h.

Scheme 2.3 – Synthesis of carbazole-fluorene-oxadiazole triad molecule

To alter both the electronic and morphological characteristics of the carbazole group a more strongly electron-donating dimethoxy-substituted carbazole and a bulky di-*tert*-butyl-substituted carbazole were proposed. The syntheses of the two carbazole species **142** and **143** are described in scheme 2.4. The Friedel-Crafts alkylation of carbazole proceded with polysubstitution occurring in the 1,3,6 and 8-positions of carbazole. The desired compound **143** was separated from the mixture by column chromatography.

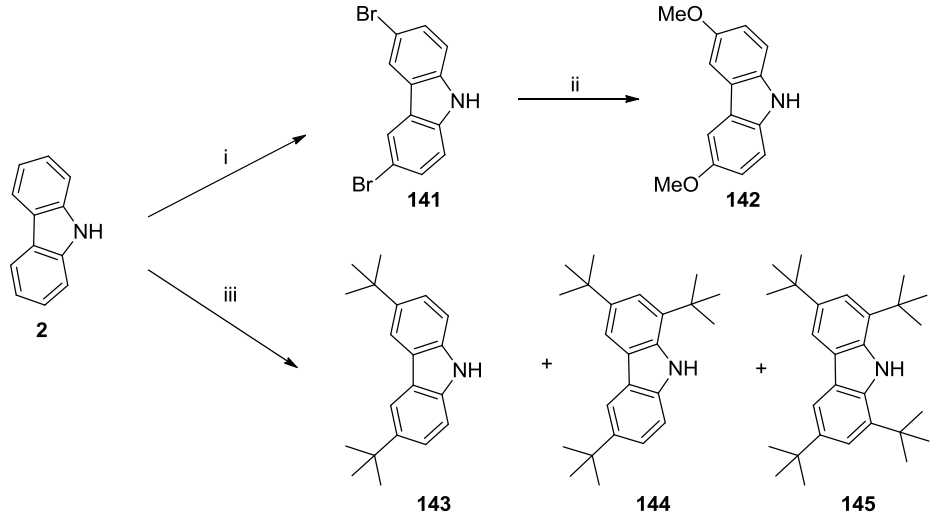

Reagents and Conditions: i) NBS, toluene/DMF, 0 ^oC, 0.5 h, 80%; ii) Na/MeOH, CuI, DMF, reflux, 3 h, 54%; iii) $ZnCl_2$, tert-butyl chloride, RT, 3h, 80% for **143**, 8% for **144**, 7% for **145**

Scheme 2.4 – Synthesis of di-methoxy and di-*tert*-butyl substituted carbazoles

To investigate the effects of systematically altering the electron transporting oxadiazole unit three different structures were proposed. The standard unit previously employed, **150**, introduction of an electron-withdrawing pyridyl unit to increase electron transport within the molecule, **151**, and the incorporation of an electron-donating thiophene unit, **155**. These oxadiazoles were synthesised *via* the tetrazole formed by reaction of a suitable benzonitrile derivative with sodium azide and ammonium chloride. The tetrazole is then reacted with an acid chloride in pyridine to afford the oxadiazole, scheme 2.5.

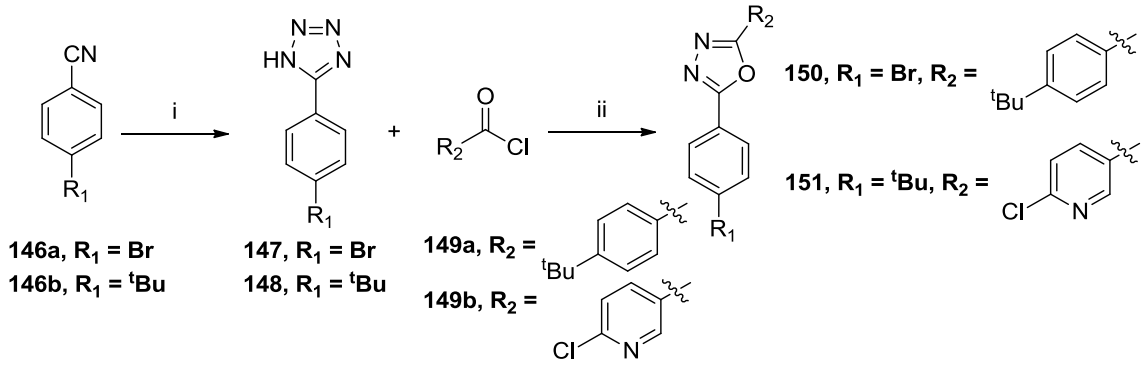

Reagents and Conditions: i) NaN_3, NH_4Cl, reflux, 4-15 h, 77% for **147**, 53% for **148**; ii) pyridine, reflux, 3h, 92% for **150**, 69% for **151**

Scheme 2.5 – Synthesis of oxadiazoles 150 and 151

155 was formed *via* a similar route, but required the initial bromination of 2-cyanothiophene, scheme 2.6.

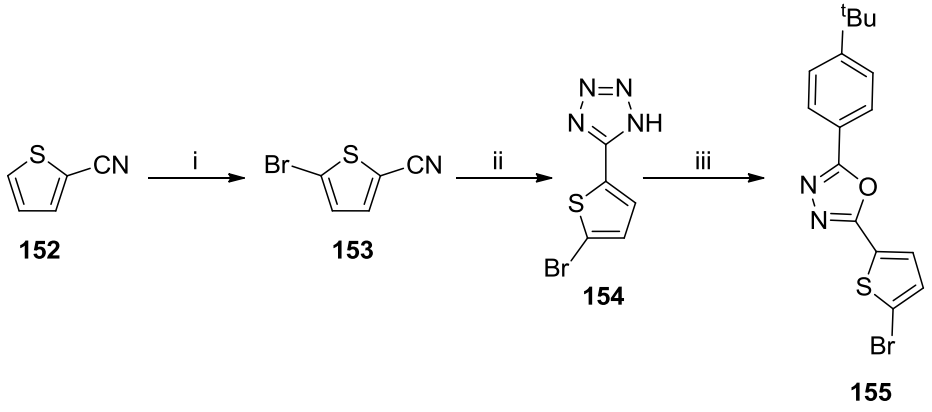

Reagents and Conditions: i) Ac_2O/AcOH, NBS, Br_2, RT, 3 h; ii) NaN_3, NH_4Cl, DMF, reflux; iii) 4-tert-butylbenzoyl chloride, pyridine, reflux, 15 h; overall yield 56%

Scheme 2.6 – Synthesis of oxadiazole 155

The three different oxadiazoles **150**, **151** and **155** were incorporated into triad molecules by the C-C cross-coupling procedure previously applied for the synthesis of **140**, scheme 2.7.

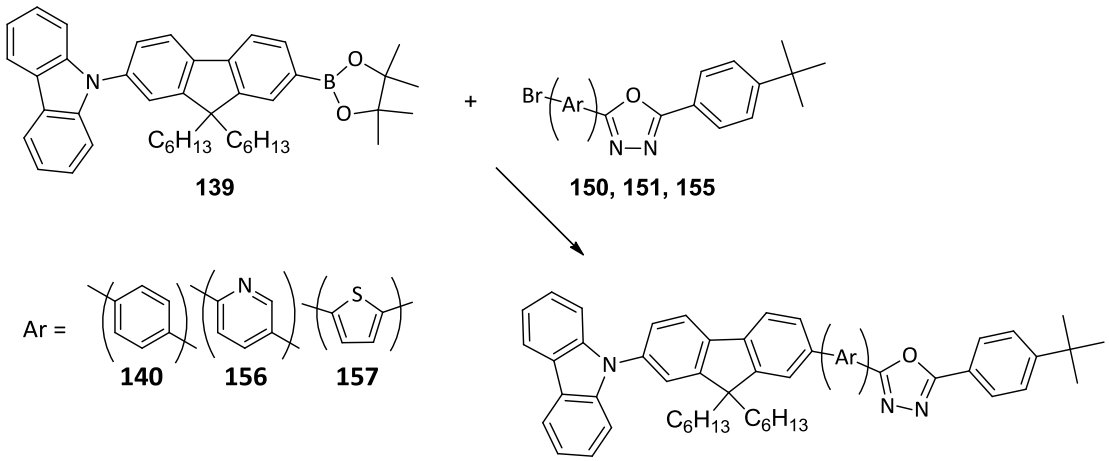

Reagents and Conditions: $[PdCl_2(PPh_3)_2]$, NaOH (aq), THF, reflux, 15 h; 78% for **140**, 72% for **156**, 84% for **157**

Scheme 2.7 - Synthesis of triad molecules 140, 156 and 157

Miyaura-borylation of oxadiazole **150** formed key intermediate **158**, which was then utilised to form the triad molecules with carbazole substituents, scheme 2.8.

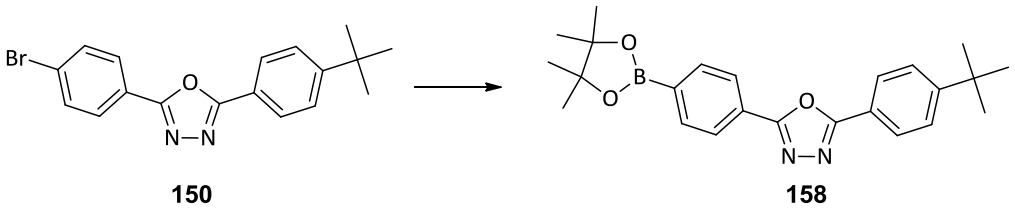

Reagents and Conditions: B_2pin_2, $[PdCl_2(dppf)]$, KOAc, DMF, 80 ^oC, 15 h, 83%

Scheme 2.8 – Synthesis of oxadiazole boronic ester 158

The modified trimers were then synthesised *via* the route described in scheme 2.9.

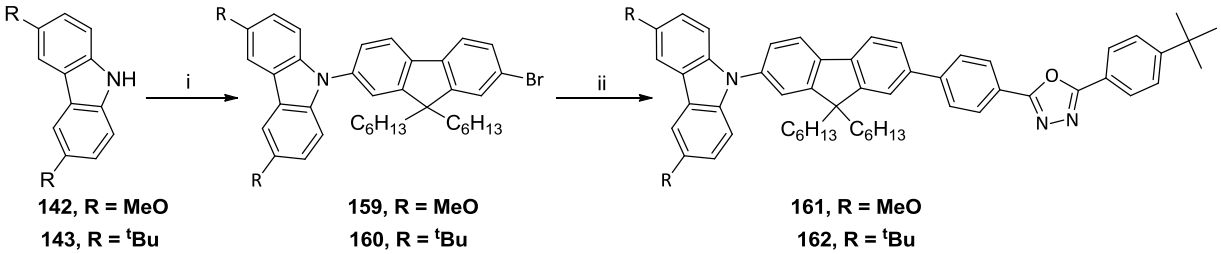

Reagents and Conditions: i) **142** or **143**, **137,** CuI, 1,10-phenanthroline, DMF, 120 ^oC, 15 h, 93% for **159**, 73% for **160; ii)** $[PdCl_2(PPh_3)_2]$, NaOH (aq), THF, reflux, 15 h; 73% for **161**, 77% for **162**

Scheme 2.9 – Synthesis of substituted-carbazole trimers 161 and 162

The final modification to the series was to alter the conjugation length between the donor and acceptor species. This was facilitated by the synthesis of a carbazole-oxadiazole dimer **163** with no fluorene and a molecule **165** containing a second fluorene unit. These syntheses were achieved by further C-N and C-C cross-coupling procedures (Schemes 2.10 and 2.11).

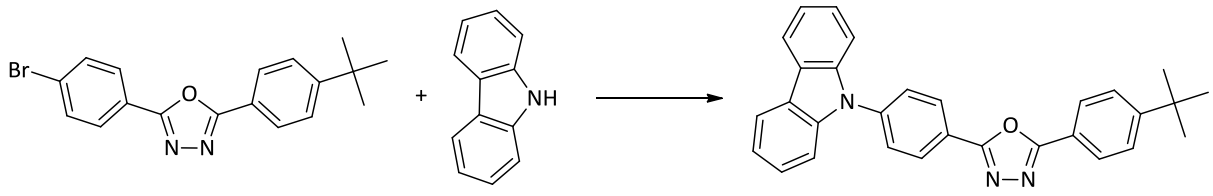

150 **33** **163**

Reagents and Conditions: $[Pd(OAc)_2]$, $P^tBu_3.HBF_4$, K_2CO_3, toluene, reflux, 24 h, 54%

Scheme 2.10 – Synthesis of carbazole-oxadiazole dimer 163

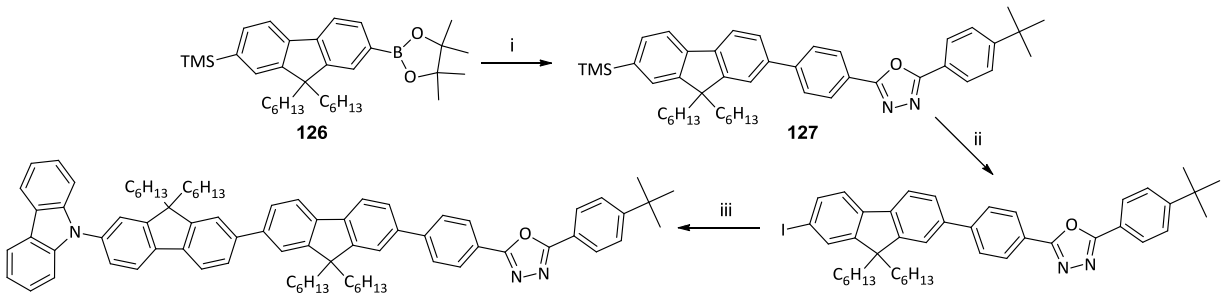

126 **127** **164** **165**

Reagents and Conditions: i) **150**, $[PdCl_2(PPh_3)_2]$, NaOH (aq), THF, reflux, 15 h, 88%; ii) Iodine monochloride, DCM, RT, 87%; iii) **139**, $[PdCl_2(PPh_3)_2]$, NaOH (aq), THF, reflux, 15 h, 91%

Scheme 2.11 – Synthesis of bifluorene material 165

Excellent purity for all the final products **134, 140, 156, 157, 161 – 163 and 165** was achieved and confirmed by HPLC analysis and NMR spectroscopy in all cases (representative HPLC trace and proton NMR spectrum shown in experimental chapter).

2.2.2 Cyclic Voltammetry Studies

The electrochemical properties of the compounds were investigated with assistance from Dr M. A Fox: selected scans are shown in figure 2.8. The measurements were carried out in DCM for oxidative scans and THF for reductive scans, both with tetrabutylammonium hexafluorophosphate (Bu_4NPF_6) as supporting electrolyte. The results are summarised in table 2.1 (for full scans, see appendix I).

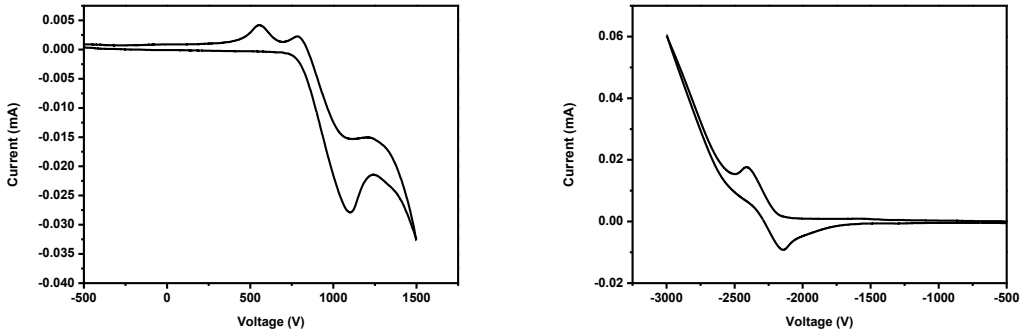

Figure 2.8 – Cyclic voltammograms showing oxidation (left: in DCM) and reduction (right: in THF) waves for 157 vs ferrocenium/ferrocene couple (FcH^+/FcH = 0.0 V).

Compound	$E_{1/2}$(Ox1)[a] (V)	E_c[a,b] (V)	$E_{1/2}$(Ox2)[a] (V)	$E_{1/2}$(Red1)[c] (V)
91	0.42			
134	0.32			
140	0.86[d]	0.54		
156	0.89[d]	0.57		-2.19
157	0.85[d]	0.56		-2.28
161	0.48		1.19[e]	
162	0.75			
163	1.00[d]	0.50[f]		
165	0.80[d]	0.54	1.03[d]	

[a]Scan between 1.5 V and -0.5 V vs ferrocenium/ferrocene couple (FcH^+/FcH = 0.0 V) in DCM.
[b]From cathodic wave of the 'dimer' formed after oxidation.
[c]Scan between -0.5 V and -2.5 V vs FcH^+/FcH (0.0 V) in THF.
[d]Estimated from 'reversible wave' at low sample concentration.
[e]Irreversible wave, anodic wave value given.
[f]Third cathodic wave observed at -0.40 V after oxidation.

Table 2.1- Cyclic voltammetry data for OLED candidates

All of the compounds show an oxidation wave due to either the electron-donating carbazole group or the diphenylamino group. As previously observed, compounds without substituents in the 3- and 6-positions display an irreversible oxidation wave at high sample concentrations. This is due to a dimerisation process which is more favoured with increased sample concentration and duration of oxidation. Materials **161** and **162** which are substituted in this position do not exhibit the irreversible oxidation observed in the other materials due to the reactive position being blocked. Compound **161** has a lower oxidation potential than **162** consistent with the stronger donor characteristics of the methoxy substituents compared with the *tert*-butyl substituents. Compound **165** displays a second oxidation occurring on one of the fluorene units, figure 2.9. Reduction waves are only observable in the solvent window for

compounds **156** and **157** at -2.19 V and -2.28 V, respectively, which can be assigned to a reduction of the pyridyl and thienyl units.

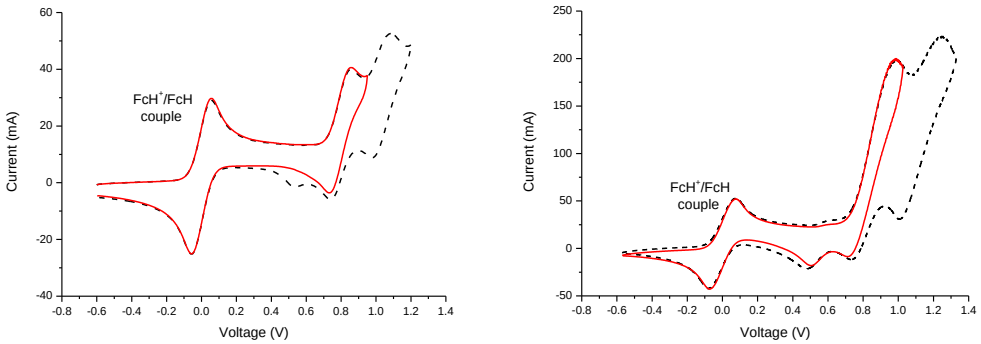

Figure 2.9- Cyclovoltammograms showing two oxidation waves for 165 in low (left) and high sample concentrations.

The oxidation potential decreases for the diphenylamino-substituted compounds compared with the carbazole analogues. This is consistent with the expectation that a stronger donor will cause the oxidation potential to decrease due to easier formation of the cation radical.[67]

2.2.3 Photophysics

The results of solution photophysical studies on all the materials are summarised in Tables 2.2 and 2.4 showing absorption, emission and PLQY data. The absorption and emission were measured in a variety of solvents to investigate the solvatochromic properties of the systems.

A comparison of the parent compound **91** and the carbazole analogue **140** shows some stark differences. The absorption and emission spectra of **140** shows a dramatic blue-shift in comparison to its diphenylamino analogue **91** of 40 and 47 nm respectively, figure 2.10. This blue-shift is a positive indicator for the potential success of incorporating **140** into a deep blue OLED.

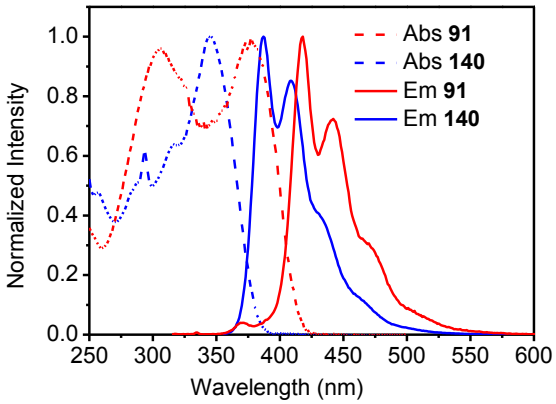

Figure 2.10- Absorption and emission spectra of **91** and **140** in cyclohexane solution.

Absorption data, summarised in table 2.2, (for other spectra, see appendix I) shows that all the compounds have a strong absorption band between 345-370 nm and that those derivatives containing a diphenylamino unit are red-shifted in comparison to the unsubstituted-carbazole-fluorene-oxadiazole compounds. It appears that the extinction coefficients are related to the number of fluorene units incorporated into the molecule; ε = 47000-63000 for **140**, **156**, **157**, **161** and **162**, ε = 100000 for **165** and ε = 27000 for **163**. There are significant solvatochromic shifts on going from cyclohexane to acetonitrile solutions for **156**, **161**, **162** and **163** and, interestingly, negative solvatochromism is observed for these compounds.

Compound	λ_{abs} (nm) Cyclohexane	ε ($cm^{-1}mol^{-1}dm^3$)	λ_{abs} (nm) MeCN	Solvatochromic Shift (cm^{-1})
91	305	31600		
	377	32400		
134	296	45300		
	386	35600		
140	345	61500	344	-80
156	363	63200	353	-780
157	370	56700	370	0
161	363	46700	351	-940
	312	60500	311	
162	353	57800	350	-240
	321	43400	321	
163	349	26500	339	-850
	339	30800	331	
	285	34600	291	
	284	51600	284	
165	357	99500	358	80

Table 2.2 - Solution absorption properties of the OLED candidates

The solution emission characteristics are summarised in table 2.4. (For all spectra, see appendix I). Every compound exhibited blue emission with vibronic bands observable in cyclohexane solution due to locally excited (LE) emission. All compounds exhibit very high fluorescence quantum yields of over 80%. All carbazole-containing compounds exhibit a deep blue emission maximum between 383 and 412 nm, with the exception of **163** which is deeper blue at 358 nm. The blue-shift of **163** compared with **140** demonstrates that the absence of fluorene increases the energy gap between the excited and ground states in **163** compared with **140**. All other modifications to **140** result in a red-shift of emission in cyclohexane. The diphenylamino containing compounds are more red-shifted in their emission than their carbazole analogues.

All of the materials show positive solvatochromism in their PL spectra. This is due to stabilised intramolecular charge transfer (ICT) emission in more polar solvents. The weakest solvatochromism effect is observed for **165**, the compound with two fluorene units. This suggests that the ICT character in this compound is smaller than the others, which can be explained by the increased distance between the donor and acceptor moieties. The spectra showing the extent of solvatochromism in different solvents for **165** and **161** are shown below, (for other compounds see appendix I) demonstrating the lack of solvatochromism in **165**.

The trend in the positive solvatochromic shifts in the emissions listed in Table 2.4 follow the trend in the negative solvatochromic effects observed in the absorption data. The charge transfer character in the excited states of **156**, **162**, **163** and especially **161** must be relatively strong, whereas the CT character in **157** and **165** is weaker. The Stokes shifts in cyclohexane solutions for all the compounds except **163** are consistent in the range of 2040-3010 cm^{-1}, whereas for **163** it is small at 720 cm^{-1}. This implies that the excited state geometry in **163** is quite similar to its ground state geometry and thus there is a substantial blue shift in its emission compared to **140**. Small geometry rearrangements are likely in the excited states for **140**, **156**, **157**, **161**, **162** and **165** and presumably involve the fluorene units present in these molecules.

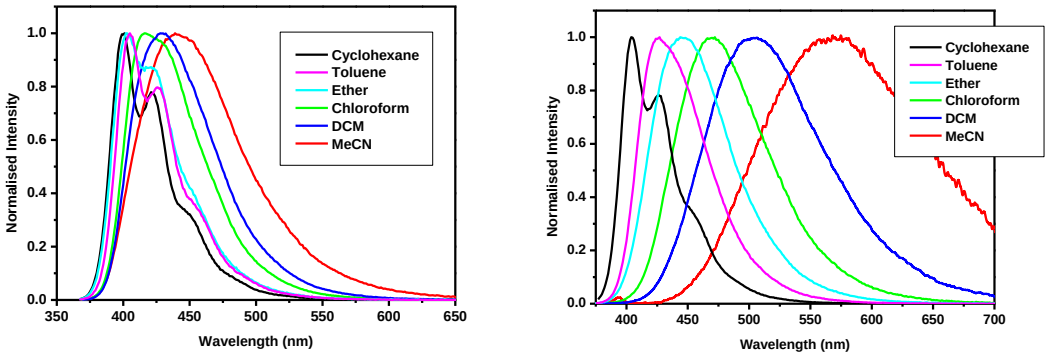

Figure 2.11 - Plot of emission of a) 165 and b) 161 in various solvents

The extent of charge transfer may be quantitatively assessed by applying the Lippert-Mataga equation (eq. 1).

$$\nu_A - \nu_F = \frac{2\Delta f}{hca^3}\left(\mu_E - \mu_G\right)^2 + const$$

Where :

$\nu_A - \nu_F$ = *energy difference between ground and excited states*

h = *planck const*

c = *speed of light*

a = *radius of cavity of fluorophore*

Δf = *orientation polarisability*

μ_E = *excited state dipole moment*

μ_G = *ground state dipole momen*

$$\left(\Delta\mu\right)^2 = \frac{hca^3\Delta\bar{\nu}\times const}{2\Delta f}A$$

Equation 2.1 – The Lippert-Mataga equation

A plot of Δν/Δf for the various solvents, where the non-polar solvent cyclohexane is compared with the more polar solvents, will allow a value for the change in dipole moment of the system to be calculated. The plot should be linear, and deviations from this indicate specific solvent effects such as hydrogen bonding, better solvation, acid-base chemistry or charge-transfer interactions. This equation contains many assumptions, e.g. that the fluorophore is spherical and there are no specific solvent interactions. Additionally, the polarisability of the fluorophore and the direction in which the ground and excited states dipole moments point is considered to be the same. The electrons are assumed to redistribute around the excited state

of the dipole in the time span of the transition but the nuclei do not. Therefore, this equation must be considered only an approximation.[86]

Compound	a (Å)	Δμ (D)
140	7	21
134	7	28
156	7	11
157	7	16
162	7	23
161	7	27
163	4.7	12
165	**9**	21

Table 2.3 - calculated dipole moment values using the Lippert-Mataga formalism

The value of Δμ gives an indication of the change in dipole moment of the fluorophore in the excited state and the separation of charge in the excited state. As materials **140, 156, 157, 162, 161** and **134** are of similar size, the magnitude of Δμ can be related to the amount of charge transfer between donor and acceptor units in the excited state. The largest value of Δμ was obtained for **134**, this is expected due to the increased strength of the arylamine donor compared to carbazole. The value of Δμ for **161** is larger than **140**, demonstrating that the addition of methoxy groups increased the donor strength of the carbazole. This causes an increase in the change in dipole moment between the ground and excited states resulting in a value for Δμ very similar to that of **134.**

Thin film emission data were measured with assistance from Dr L.-O. Palsson from thermally evaporated thin films for all the OLED candidates and are summarised in table 2.4. In all cases, the film emission is red-shifted with respect to the solution emission from cyclohexane by 2050-3550 cm^{-1}. The PLQY values are between 0.17-0.38 for the thin films and are much lower than those obtained in cyclohexane solution.

2.2.4 Theoretical Calculations

Density Functional Theory (DFT) calculations were carried out on the OLED candidates by Dr M. A. Fox at Durham University at the B3LYP/6-31G* level. For all of the compounds the hexyl groups were replaced with ethyl groups to reduce the computational effort required. The data are summarised in Figure 2.12.

The HOMO-LUMO energy diagram obtained from the calculations demonstrates that the introduction of the carbazole group lowers the HOMO level compared to those containing a diphenylamino substituent and so increases the band gap. This agrees with the observed blue-shift in fluorescence emission in both solution state and films. The largest band-gap of 3.75 eV is calculated for **163**, which is mirrored by its deep blue emission and may be explained by the lack of conjugation between a carbazole and fluorene unit in the HOMO molecular orbital. The addition of the thiophene and pyridyl unit to the oxadiazole moiety results in an increase in the electron affinity of the materials and hence a smaller band gap, again comparing favourably with the observed red shift in emission properties for these compounds.

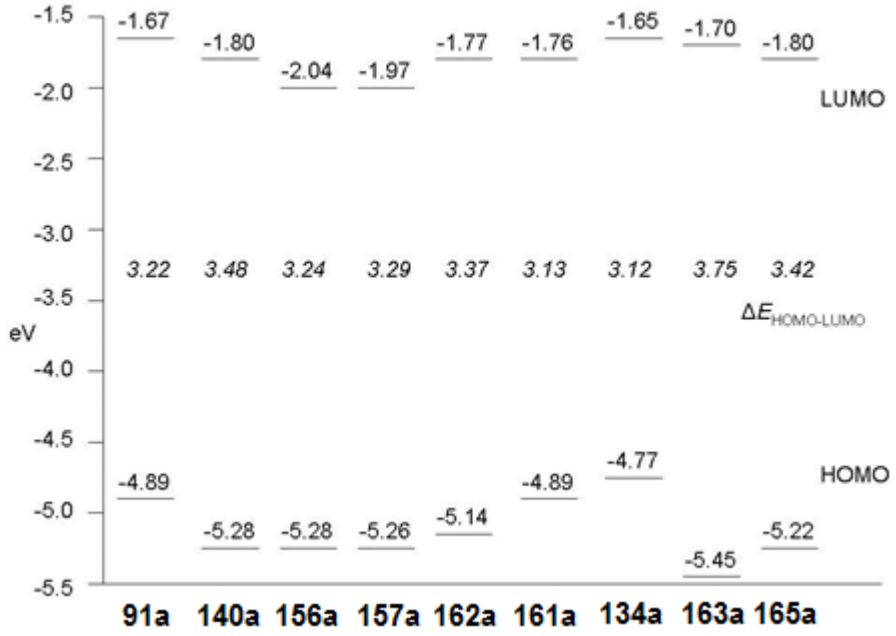

Figure 2.12 – MO energy diagram for HOMO and LUMO levels of OLED candidates

(Computations performed by Dr M. A. Fox)

Compound	λ_{max} Cy* (nm)[a]	λ_{max} Toluene (nm)[a]	λ_{max} Et_2O (nm)[a]	λ_{max} $CHCl_3$ (nm)[a]	λ_{max} DCM (nm)[a]	λ_{max} MeCN (nm)[a]	Solvatochromic Shift (cm^{-1})	solution ϕ_f[c]	λ_{max} thin film[e] (nm)	Thin film ϕ_f[f]
91	430, 455[g]	-	-	483[g]	-	562[g]	5460	0.88[d, g]	467	0.30
134	426, 451, (482)[b]	446	464	498	528	575	6080	0.84	495	0.21
140	383, 405, (432)[b]	398, 418	409	425	439	464	4560	0.88	430	0.38
156	392, 415, (444)[b]	416, 429	428	452	468	505	5710	0.99	450	0.36
157	412, 435, (466)[b]	422, 446	422, 442	454	460	472	3090	0.86	467	0.17
161	402, 424, (453)[b]	426	446	469	503	583	7720	0.96	465	0.17
162	395, 417, (442)[b]	408, (426)[b]	419	444	462	498	5240	0.80	450	0.20
163	358, 377, (395)[b]	378	383	402	414	439	5150	0.95	410	0.29
165	400, 420, (449)[b]	405, 426, (454)[b]	403, 422	416	430	439	2220	0.99	450	0.21

*Cyclohexane

[a]Excitation at lowest energy λ_{abs} of compound in appropriate solvent

[b]Shoulder

[c]Quantum yields measured in cyclohexane solution in an integrating sphere with excitation at lowest energy λ_{abs} of compound in cyclohexane. Estimated error of +/-0.05

[d] Quantum yield measured in in DCM solution, measured against quinine sulfate and fluorescein standards. Estimated error of +/-0.05

[e] Excitation wavelengths (λ_{ex}) for **140** at 350 nm, for **156**, **157** and **161** at 370 nm and for **162**, **163** and **165** at 340 nm

[f] PLQY data obtained using an integrating sphere as described in the literature[87]; estimated errors ±5%.

[g]Data taken from previous publication, measurements carried out by Dr K. T. Kamtekar[58]

Table 2.4 – Solution and thin film (obtained by thermal evaporation) emission properties of OLED candidate

All the compounds show a large arylamine or carbazole character in the HOMO, but a small contribution of arylamine or carbazole character in the LUMO. This is consistent with large charge separation in the excited state and therefore the observed solvatochromism in fluorescence in different solvents. Figure 2.13 shows the frontier molecular orbitals for **140** which are representative of the series with the HOMO localised predominantly on the carbazole and the LUMO extending over the oxadiazole and fluorene units.

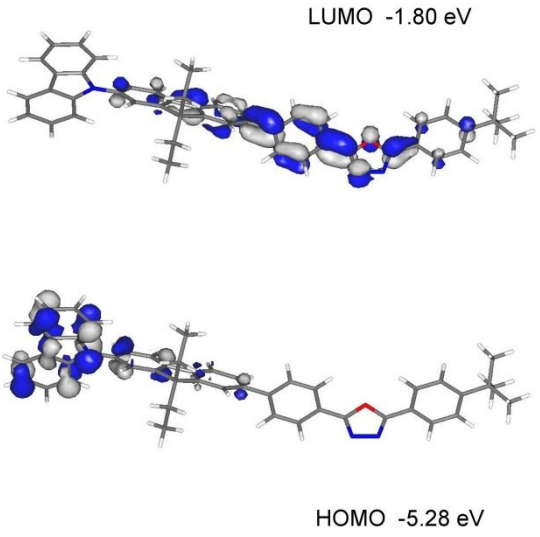

Figure 2.13 – Frontier molecular orbital plots for 140

(Computations performed by Dr M. A. Fox)

2.2.5 DSC and TGA measurements

Differential scanning calorimetry (DSC) and thermal gravimetric analysis (TGA) measurements were carried out on the OLED candidates to determine the glass transition temperatures (T_g) and the 5% mass loss temperatures of the different materials. These data can help to evaluate the potential stability of a material under device operation. A low T_g may result in instability under device operation and low thermal stability can also indicate potential degradation of devices. All the compounds exhibit a high temperature for their 5% mass loss indicating good thermal stability. In addition, the T_g values are high enough to allow device operation without morphology changes in the films.[28]

Compound	T_g (°C)	5% mass loss by TGA (°C)
140	82.5	423
156	92.0	424
157	84.5	418
162	112.5	423
161	91.0	421
165	85.0	430
134	77.0	395
177	90.0	421

Table 2.5- Glass transition temperatures and 5% mass loss temperatures for OLED candidates

2.3 Device Results

Devices reported in Sections 2.2.7 and 2.2.8 were fabricated by Ms. Alison Fisher and Dr Christopher Pearson in Professor Petty's laboratory in the School of Engineering, Durham University. The present author was closely involved in the interpretation of the data. All devices were constructed with the simple single-active-layer architecture ITO/PEDOT-PSS/emitter/Ca(or CsF)/Al, shown in figure 2.14.

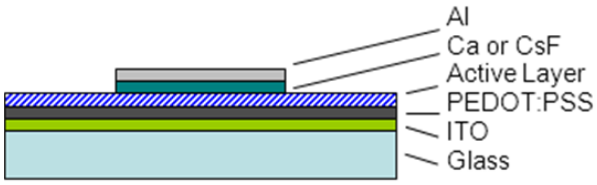

Figure 2.14 - Schematic diagram of device structure used for OLEDs in this work

2.3.1 Diphenylamino compared with carbazole as a donor in deep blue OLEDS

The first investigation compared the new compound **140** with the previously investigated **91** as an OLED emitter.[58] As previously discussed, the HOMO-LUMO gap of **140** is larger than **91** and both the solution absorption and emission spectra of **140** are blue shifted with respect to **91**.

Figure 4a compares the electroluminescence (EL) spectra for **91** and **140**, revealing a blue shift of around 56 nm in the emission of **140**: the peak emission is 487 nm for **91** and at 431 nm for **140**, figure 2.15. These data are consistent with the calculated increase in HOMO-LUMO gap for **140** compared with **91**. The deep blue colour obtained, figure 2.15, for devices with **140** lies very close to the NTSC standard for blue light (0.14, 0.08). In addition, the method of active layer deposition, i.e thermal evaporation or spin-coating, has very little effect on the emission

colour for **140**. In comparison **91** exhibits a small blue shift in its EL upon thermal evaporation compared with spin-coating, figure 2.15.

Devices with an active layer deposited by spin-coating show a five-fold increase in external quantum efficiency (EQE) for devices of **140** (1.25%) compared with **91** (0.26%), table 2.6. The conductivity of **91** is larger than **140**, demonstrated by figure 2.17 (photocurrent/current vs electric field plots), this is rationalised by the lowered HOMO level in **140** which increases the barrier for hole injection into the emissive layer from the ITO/PEDOT-PSS anode. The improved EQE for the devices may be due to improved balance in the hole and electron carrier ability of **140** compared with **91**.

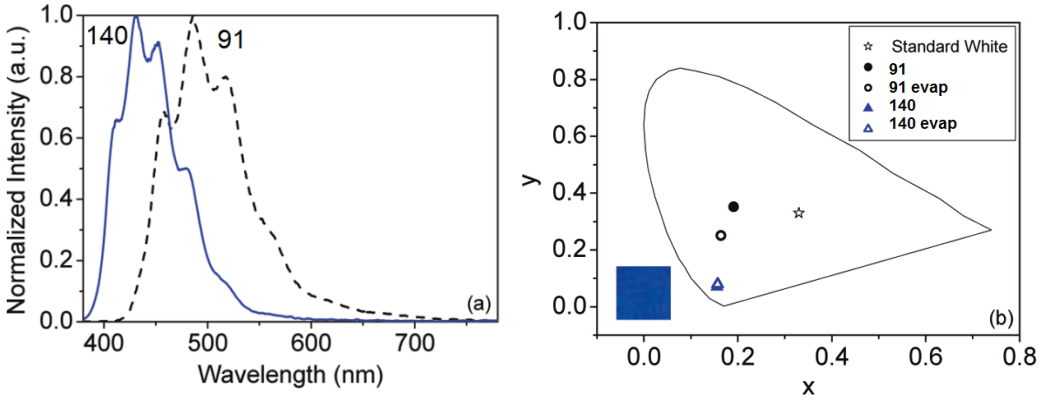

Figure 2.15 - (a) EL spectra of devices based on spin-coated layers of 91 and on 140; (b) comparison of CIE coordinates of devices comprising 91 and 140, measured at J~150 Am^{-2} for 91 and J~50 Am^{-2} for 140. Active layers in OLEDs produced by spin-coating and thermal evaporation. Inset is a photograph of the deep-blue OLED of 140.

After a direct comparison of **140** with the previous investigation of **91** the method of emissive layer deposition was investigated. The relevant data are contrasted in table 2.6 for the different devices. It can be seen that evaporation of the emissive layer improves the EQE for both materials in OLED devices, figure 2.16. In addition, the power efficiency, current efficiency and brightness are improved for devices of **140** with an evaporated layer rather than spin-coated. The efficiencies achieved for these simple device architectures with a deep blue fluorescent emitter are among the highest reported in the literature, up to 4.71% for **140** in devices with an evaporated layer.

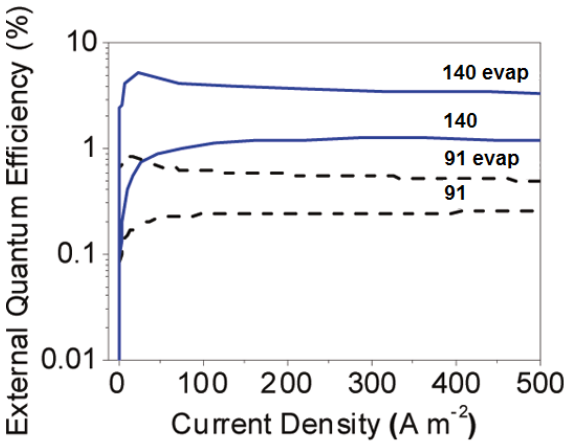

Figure 2.16 - External quantum efficiencies of 91 and 140. Data are shown for OLEDs in which the active layer has been deposited by both spin-coating and thermal evaporation (data denoted as 91 evap and 140 evap).

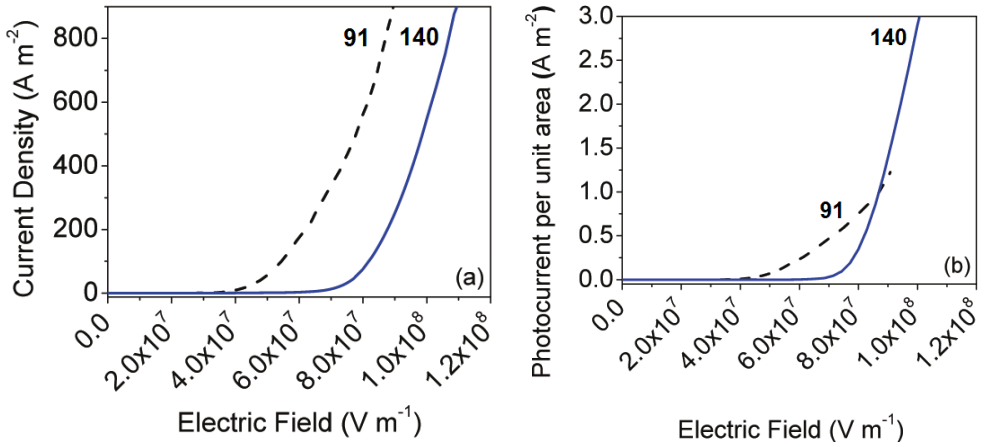

Figure 2.17 - (a) Current density as a function of electric field; (b) photocurrent per unit area as a function of electric field. Active layers in OLEDs produced by spin-coating.

The surface morphologies of the films were investigated using atomic force microscopy (AFM) and photoluminescence (PL) measurements. The spin-coated films were relatively smooth and amorphous in appearance, whereas the films produced from thermal evaporation show distinct grain formation, figure 2.18. Fluorescence quantum yield measurements carried out on the thin films did not demonstrate a significant difference in spun films compared with thermally evaporated ones, table 2.6. Based on these observations it is probable that the improved EQE values are due to improved charge carrier mobilities in the more crystalline evaporated films. In addition, the emission zone may be moved further away from the device interfaces, reducing quenching effects that reduce device efficiency

	91 (Spin-coated[f])	91 (Evaporated)	140 (Spin-coated[f])	140 (Evaporated)
Emissive Layer Thickness (nm)	110	70	70	105
Peak Emission (nm)	487	484	431	431
FWHM (nm)	87	105	67	81
CIE[a] x	0.191	0.164	0.156	0.157
CIE[a] y	0.352	0.251	0.069	0.079
Turn-on Electric Field (V m^{-1}) (Turn-on Voltage, V)	2.96 x 10^7 (3.53)	6.24 x 10^7 (4.30)	4.50 x 10^7 (3.15)	3.99 x 10^7 (4.18)
EQE[b] (%)	0.26	0.63	1.25	4.71
Current Efficiency[c] (cd A^{-1})	-	0.93	0.47	1.49
Power Efficiency[c] (lm W^{-1})	-	0.30	0.18	0.53
Brightness[c] (cd m^{-2})	-	943.2	483.1	1520.0
λ_{max} (nm)	468[e]/447[f]	467	427[e]/439[f]	430
PLQY[d]	0.27[e]/0.22[f]	0.30	0.50[e]/0.33[f]	0.38

[a] CIE coordinates of spin-coated **91** measured at an applied current of 0.5 mA (J ~ 150 A m^{-2}). All other OLEDs measured at an applied current of 1 mA (J ~ 50 A m^{-2}).

[b] EQE measured at 100 ±30 cd m^{-2}.

[c] Measured under an applied current of 20 mA (J ~10^3 A m^{-2})

[d] Data obtained using an integrating sphere as described in the literature;[87] errors ±5%; excitation wavelength λex 380 nm (compound **91**), 350 nm (compound **140**).

[e] film spun from a DCM solution.

[f] film spun from a toluene solution.

Table 2.6 - Comparison of characteristics of spin-coated and evaporated devices and their emission properties

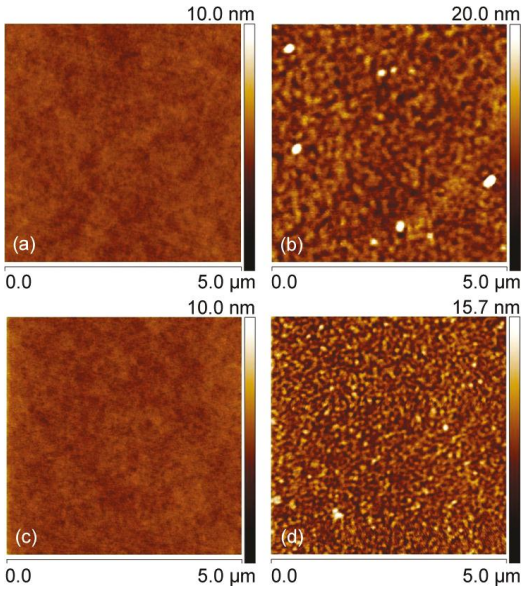

Figure 2.18 - AFM images of films of (a) spin-coated 91 (film thickness =53 nm); (b) evaporated 91 (64 nm); (c) spin-coated 140 (61 nm); and (d) evaporated 140 (59 nm).

In conclusion, it has been demonstrated that the replacement of the diphenylamino moiety in **91** with a carbazole improves OLED characteristics, most notably, colour, brightness and

efficiency. Furthermore, when the emissive layer is deposited by thermal evaporation instead of spin-coating, device characteristics are further enhanced.

2.3.2 Carbazole-based OLED materials

Based on the results garnered from the comparison of **91** and **140**, it was concluded that the structure-property relationships of the other compounds would be best investigated in devices based on evaporated emissive layers. The device architectures for these devices are as depicted in figure 2.14 and the EL, current-voltage, EQE and colour characteristics are shown in figures 2.19 – 2.22, respectively. Other device characteristics are summarised in table 2.7.

AFM images of the films of the materials revealed a granular morphology for all the different materials in thermally evaporated films, in keeping with those observed for **91** and **140**, figure 2.18. The grain size of the granular regions varied from 125-278 nm (±10%). The largest grain size was observed for **157**, at 278 nm, the inclusion of the 5-membered thiophene ring (compound **157**) rather than the 6-membered phenyl or pyridyl unit in the other compounds introduces a change in the backbone of the material and may have an effect on the packing in thin films. The smallest grains were observed for **163** at 125 nm. Again, this compound which lacks a fluorene unit is structurally different from the other analogues and one might expect this to be reflected in morphological differences of the thin films.

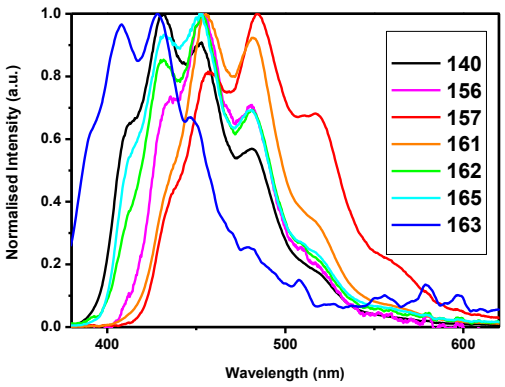

Figure 2.19 - EL spectra for devices with OLED candidates 140, 156, 157, 161, 162, 165 and 163 as the emissive layer

	140	156	157	161	162	165	163
Turn on V[a] (V)	4.18	3.87	3.04	2.80	3.03	3.68	3.22
EQE[b] (%)	4.71	0.20	0.38	1.48	1.89	0.36	0.54
Wavelength of maximum emission[c] (nm)	431	453	484	455	453	428	452
FWHM (nm)	81	66	87	63	73	70	81
CIE[d] *x* at 1 mA	0.157	0.158	0.181	0.150	0.151	0.161	0.164
CIE[d] *y* at 1 mA	0.079	0.120	0.273	0.177	0.096	0.049	0.114
Brightness[e] (cd m^{-2})	72.25	1.739	35.81	7.511	99.60	6.312	7.767
Current efficiency[e] (cd A^{-1})	1.419	0.034	0.703	0.147	1.956	0.124	0.153
Power efficiency[e] (lm W^{-1})	0.665	0.014	0.409	0.125	0.960	0.075	0.084

[a]Turn on voltage given at 1 nA of photocurrent. [b]EQE measured at 100 cd m^{-2}. [c]Peak emission of **162** and **163** measured under an applied current of 10 mA and 2 mA respectively. All other OLEDs measured at 20 mA (J ~10^3 A m^{-2}). [d]CIE coordinates measured at an applied current of 1 mA. [e]Brightness, current efficiency and power efficiency measured under an applied current of 1 mA.

Table 2.7 - Electroluminescence data for OLEDs based on compounds 140, 156, 157, 161, 162, 165 and 163

Compounds **156** and **157** were designed to alter the acceptor characteristics of the emitter. The I-V characteristics are within experimental error very similar, but show a higher current than observed for **140**. The DFT calculations predict a very similar HOMO level for **156** and **157** with an increased electron affinity; this suggests that the increased current is due to increased electron current in devices of **140**. The devices of **156** and **157** exhibit a decreased voltage compared with devices based on **140**, table 2.7. However, they do not show improved efficiencies and the decrease in the HOMO-LUMO gap for **156** and **157** has a detrimental effect on the deep blue emission of their devices.

Increasing the donor strength of the carbazole moiety by introducing methoxy substituents in **161** increases the HOMO level which shifts the emission colour to the green. Raising the HOMO level does have the effect of decreasing the turn-on voltage of the device to 2.80 V, the lowest for any of the materials studied. The other modification to the carbazole moiety was carried out in **162**. Introduction of the *t*-butyl groups does not cause a large change in the band gap and this is reflected in the retention of the deep blue emission in the desired region of the CIE diagram. In addition, the **162** device has improved brightness and current and power efficiencies compared with devices of **140**, with a good EQE of 1.9%, the second highest in the series.

163 and **165** were synthesised to investigate the role of the fluorene unit on the optoelectronic properties. The second fluorene unit in **165** does not affect the EL colour, which

is consistent with the similar calculated band gaps, table 2.7. Removing fluorene from the backbone (**163**) blue shifts the EL compared with devices based on **140**. However, the improved blue characteristics are accompanied by a significant decrease in device efficiency and brightness, table 2.7. The HOMO-LUMO data for **165** are markedly different to **163**, but this is not reflected in the I-V data, figure 2.20. The two compounds exhibit very similar I-V curves: it may be reasoned that poorer charge injection in **163** – due to decreased electron and hole affinity compared with **140** – is offset by improved charge carrier mobility in the thin films of **163**. This may be ascribed to the more pronounced structural alteration in **163** (removal of the fluorene unit) resulting in larger film morphology changes compared **140** and the other members of the series.

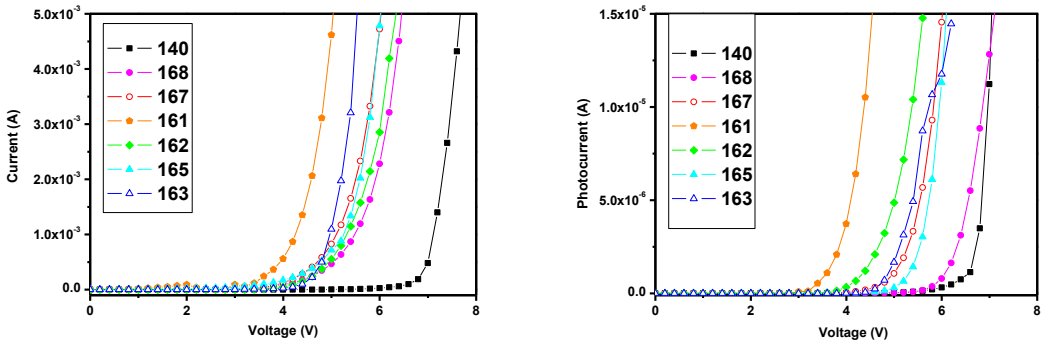

Fig. 2.20 - (a) Current-voltage and (b) Photocurrent-voltage characteristics of the devices incorporating the new materials. Device architecture: ITO/PEDOT:PSS/X/Ca/Al (X = 140, 156, 157, 161, 162, 163 and 165)

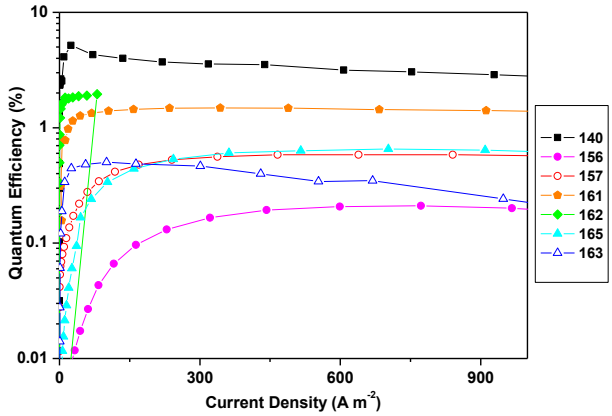

Fig. 2.21 - External Quantum Efficiency of devices incorporating materials 140, 156, 157, 161, 162, 163 and 165

The compounds with the largest calculated band gaps, **163, 140, 165 and 162** have the deepest blue EL emission. A plot of $1/CIE_y$ vs. the calculated band gap (eV) reveals an approximately linear correlation, showing that an increased band gap will shift the CIE coordinates closer to the blue. Compounds **156** and **165** lie off the linear plot.

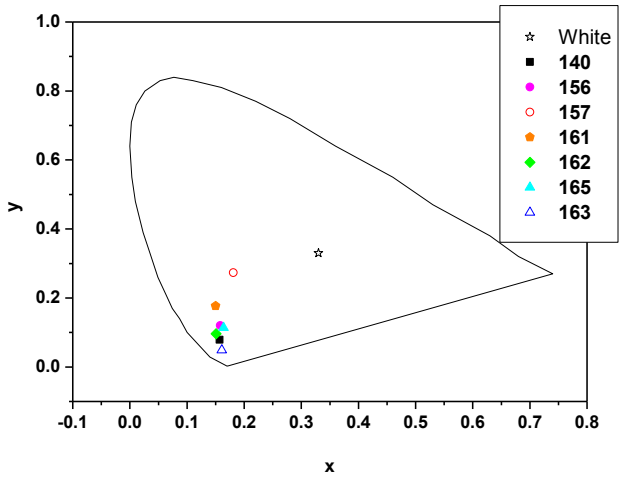

Figure 2.22 - CIE diagram indicating the colour emission of each device compared to standard white light.

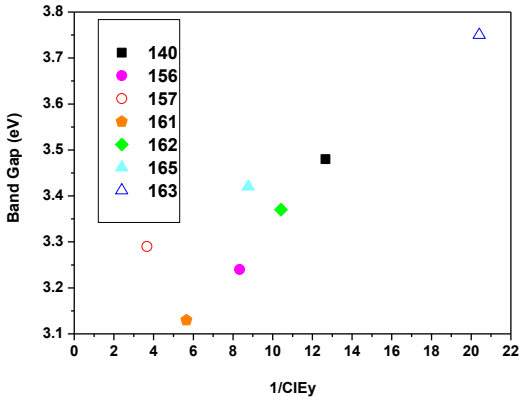

Figure 2.23 - Dependence of band gap, E_g (from Figure 2.12), on 1/CIEy for OLEDs based on the different molecules.

2.4 Conclusions

From the results obtained some design rules have emerged for the application of these types of materials for OLED applications. The inclusion of the carbazole group is essential to achieve a deep blue emission, as compounds using an arylamine motif shift the emission out of the deep blue region of the CIE diagram. It has been shown that substitution of the carbazole

group with substituents can have a positive effect on device efficiency and improve the compound's electrochemical stability. However, when the donor ability is enhanced by methoxy substituents then the colour of the OLED is shifted to the green. Inclusion of the fluorene group is instrumental in achieving high efficiency in these devices. It can be concluded that the DFT calculations provide an accurate assessment of the EL colour for most of the compounds in this series. However, prediction of other device characteristics including efficiency and brightness are not as easily assessed. It seems that the balance of the hole and electron mobilities within the materials is important in determining some device parameters.

Notably, the OLEDs fabricated in this work from compounds **140** and **162** are competitive with the most efficient deep-blue OLEDs based on all-organic small-molecule fluorophores. There are very few literature reports of OLEDs of this type with emission close to the National Television System Committee (NTSC) standard blue co-ordinates of (0.14, 0.08) that achieve EQE values >1% or current efficiencies >1 cd A^{-1}.[52,57,71] OLEDs based on **140**, incorporating a 2,5-diphenyl-1,3,4-oxadiazole acceptor group and a carbazole donor unit, exhibited the highest external conversion efficiency, of approximately 4.2%. This device emitted deep-blue electroluminescence, with CIE (*x*, *y*) co-ordinates of (0.16, 0.07), close to the NTSC standard blue co-ordinates of (0.14, 0.08).These materials are very attractive for further development due to the combination of good processability of the molecules, their bipolar structure, colour tunability and efficient performance of OLEDs using a simple non-doped device architecture.

Chapter 3: Bipolar Materials for White Light Emission and Improved Charge Transport in OLEDs

---

3.1 Introduction

The previous chapter demonstrated how the series of molecules based on **140** and its analogues have been successfully incorporated into simple, efficient and deep blue OLEDs. This chapter describes the attempts to combine these blue emitters with suitable yellow dyes in devices for white light emission.

3.1.1 White Light Emission from Blended OLED devices containing two active compounds

There is much active research currently to produce efficient white organic light emitting devices (WOLEDs) both for displays and as solid-state lighting sources. It is well known that the current dominant technology, incandescent lightbulbs, lose the majority of their energy (~95%) as heat rather than light. It has been estimated by the US Energy Information Administration that in 2009 about 13.6% of total US energy consumption was for lighting. Therefore, there is clearly great motivation to develop alternative, efficient lighting solutions.

White light is defined by the Commission Internationale d'Eclairage (CIE) as having coordinates of (0.33, 0.33). There have been extensive reviews of this area of research in recent years.[30,38,89,90] There are various ways that one might achieve white light emission from a device, but the approach adopted here takes advantage of the efficient deep blue of **140** already in hand, blended with commercially available fluorescent and phosphorescent yellow dyes.

Blending blue and yellow emitters to form a WOLED device is a strategy that has been adopted before.[91,92] An example of a successful blended device to produce white light was demonstrated by Alam *et al.*[93] A blend of blue PFO, **68**, and red-orange MEH-PPV, **166**, resulted in white emission with CIE coordinates of (0.32, 0.33) very close to the CIE defined white point, figure 3.1. Formation of nanocrystalline regions of PFO was attributed to the success of the white devices by hindering energy transfer from the high energy blue to the lower energy red

emitter. When a larger weight percentage of MEH-PPV (>30 wt. %) was included an amorphous film with no nanocrystalline regions is formed and energy transfer is increased resulting in red-shifted emission.[93] This study demonstrates the importance of film morphology and aggregation effects in such blended devices.

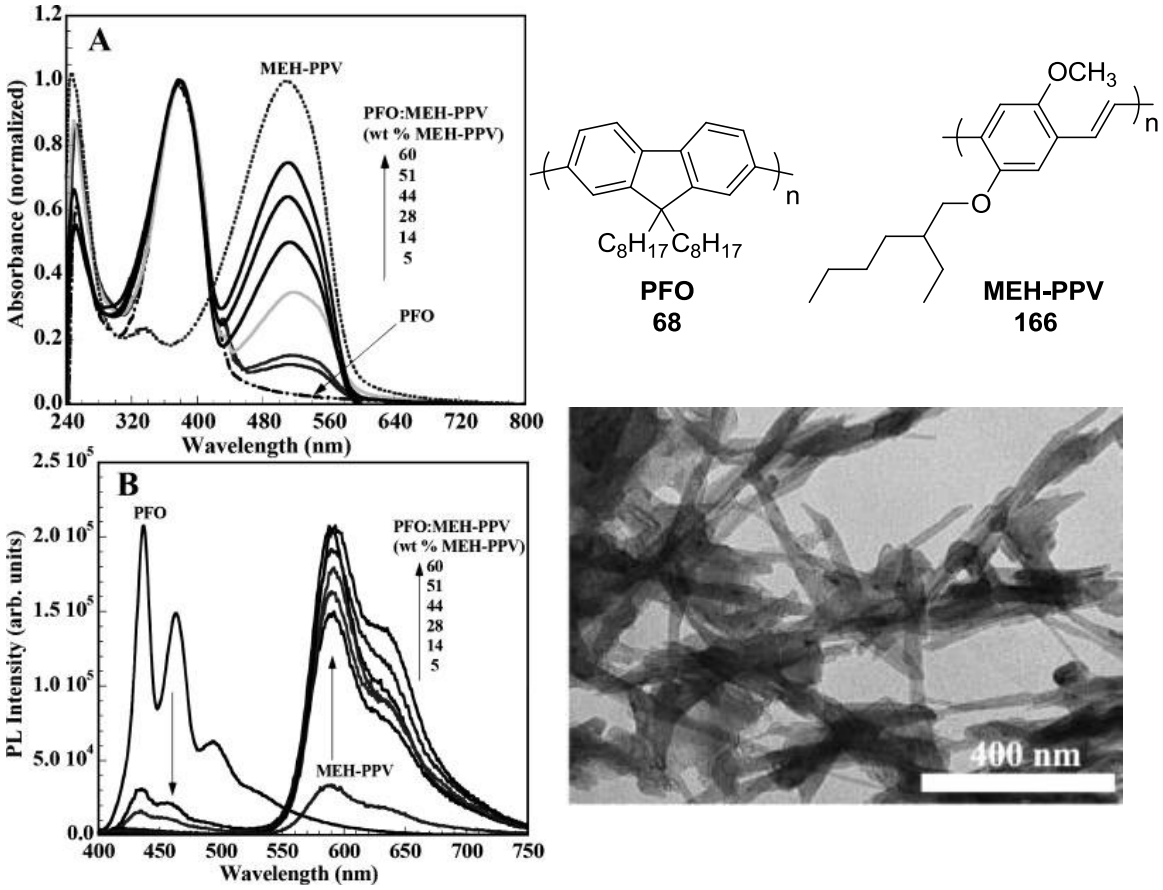

Figure 3.1 - (A) Optical absorption (normalised) and (B) PL spectra of thin films of PFO, MEH-PPV and their blends spin-coated from chloroform solutions; Structures of PFO and MEH-PPV, TEM image of PFO:MEH-PPV blend with 5 wt.-% MEH-PPV showing nanocrystalline structures [93]

A system utilising a high energy polymer host doped with two iridium dyes was fabricated by Cao and coworkers, figure 3.2.[94] Doping concentrations of the two dyes were at 0.14% blended with PFO in the device with structure ITO/PEDOT:PSS/PVK/blend/Ba which achieved white emission with CIE coordinates (0.33, 0.33) and maximum efficiency of 5.5 lm W^{-1} and 9 cd A^{-1}.[94] In this case the host is responsible for both charge transport and blue emission. The red ($(Piq)_2Ir(acaF)$) (**168**) and green ($Ir(Bu\text{-}ppy)_3$) (**167**) phosphorescent emitters provide the other colour elements via energy transfer from the host or through direct charge recombination.

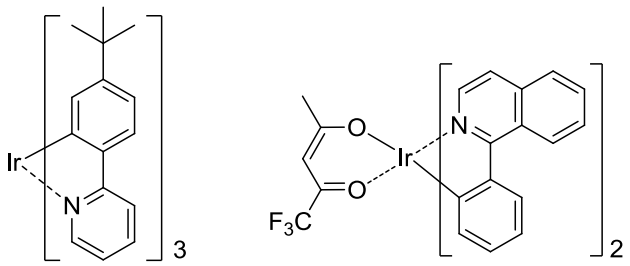

Ir(Bu-ppy)$_3$ **(Piq)$_2$Ir(acaF)**

167 **168**

Figure 3.2 - Structures of iridium dopants

In an example by Brovelli *et al.* unwanted energy transfer is prevented by a non-covalent encapsulation of one of the emitters, figure 3.3.[95] The blue emitting polymer PFBP.MeCβ-CD.THS, **171**, is encapsulated with a cyclodextrin strongly hindering energy transfer to the green-emitting polymer F8BT. The white emission achieved had CIE coordinates of (0.28, 0.34) with a power efficiency of 0.39 cd A^{-1}.[95]

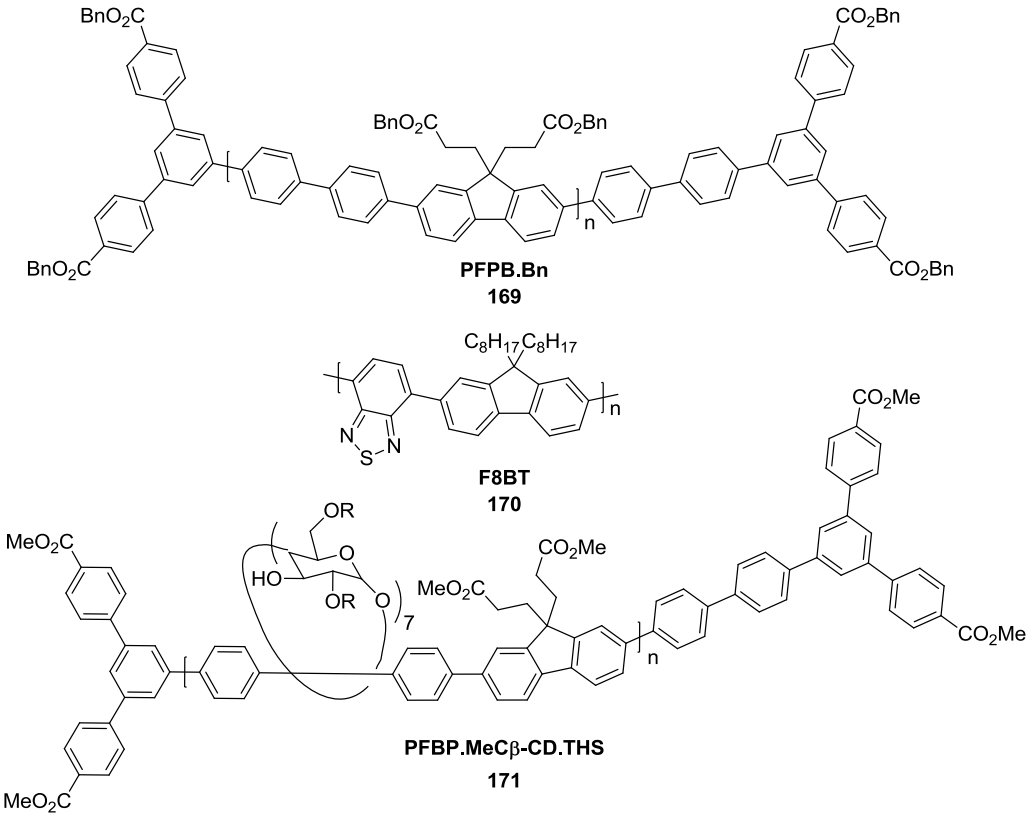

Figure 3.3 - Structures of polymers used to produce a WOLED by Brovelli *et al.*[95]

3.2 Results and Discussion

Our strategy was to blend the deep blue emitter **140** with commercially available yellow dyes, a fluorescent phenyl-substituted poly(*p*-phenylenevinylene) polymer, **PDY-132** (**173**) and a phosphorescent complex, iridium(III)bis(4-phenylthieno[3,2-*c*]pyridinato-N,C2')acetylacetonate, **PO-01** (**172**), figure 3.4. One of the main aims in this study was to produce very simple device structures that are reproducible and are relatively cheap to fabricate. The blue material **140** acts as the wide band gap host, charge transporter and provides the deep blue emission. Doping with increasing quantities of the complementary yellow material should result in a change in colour across the CIE diagram passing through or near the white point.

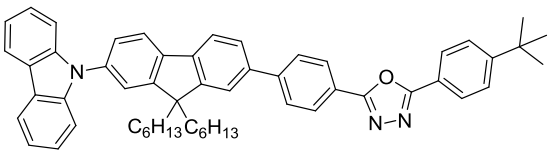

140

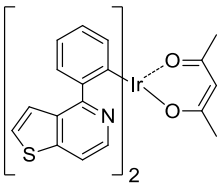

PO-01
172

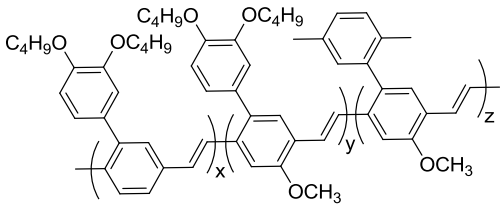

PDY-132
173

Figure 3.4 - Structures of materials used

3.2.1 Device results

The device structure utilised is the same as previously discussed and is shown in figure 2.14. Devices were fabricated by Ms. Cristina Roldán-Carmona in the Department of Engineering, Durham University. The present author was closely involved in interpreting the data.

In devices based on a blend of **140** and **PDY-132**, as the amount of **140** increased in the blend the emission colour changes from yellow to green and then along a straight line across the CIE diagram to deep blue, figure 3.5. Because of this shift to the green part of the spectrum a white emission is not achieved with this blended device. The shift in the colour of the emission is attributed to reorganisation of the polymer chains as more **140** is introduced into the blend resulting in different aggregates forming, affecting the colour purity. The OLED characteristics are presented in table 3.1.

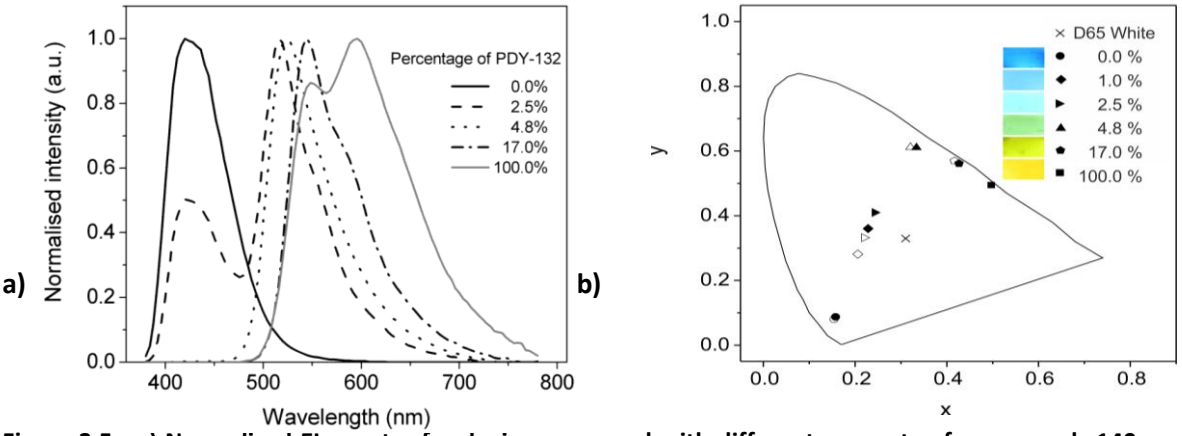

Figure 3.5 - a) Normalised EL spectra for devices prepared with different amounts of compounds 140 and PDY-132 as weight ratios. All samples are spin coated from toluene solution and spectra were recorded at a current of 1 mA. b) CIE (x,y) coordinates for devices, prepared with different amounts of compounds 140 and PDY-132 at 1 mA (black symbols) and 10 mA (white symbols). Photographs of the light output are shown

Weight concentration of PDY-132 (%)	EQE_{max} (%)	Brightness[a] (cd m^{-2})	Power efficiency[a] (lm W^{-1})	Brightness[b] (cd m^{-2})	Power efficiency[b] (lm W^{-1})	$CIE_{x,y}$[a]
0.0	0.90	21	0.26	290	0.29	0.16, 0.09
1.0	1.00	120	1.05	990	0.70	0.23, 0.36
2.5	1.10	161	1.44	1370	1.05	0.24, 0.40
4.8	1.35	234	1.98	2560	1.72	0.33, 0.61
17.0	2.73	540	3.44	4000	1.87	0.43, 0.56
100.0	1.73	159	0.58	570	0.17	0.50, 0.49

[a] At a current intensity of 1 mA ± 1 cd m^{-2}.

[b] At a current intensity of 10 mA ± 10 cd m^{-2}.

Table 3.1 - Optoelectronic properties of ITO/PEDOT-PSS/140–PDY-132/Ca/Al devices with different concentrations of PDY-132. All samples spin coated from toluene solutions.

The devices incorporating **PO-01** with **140** show that efficient energy transfer from the blue host to the yellow iridium dye is occurring. All blue emission is lost with blends containing >0.4 wt. % of the iridium complex. By varying the amount of **172** in the device it is possible to achieve emission very close to the desired white point, figure 3.6, with an optimum emission achieved with 0.14% (by weight) of **PO-01** giving CIE coordinates of (0.32, 0.31) at a current of 1 mA; device characteristics are displayed in table 3.2. At increased drive currents an

irreversible red-shift in the emission was observed. This may be due to a morphological change resulting in less efficient energy transfer to the yellow iridium complex, figure 3.6.

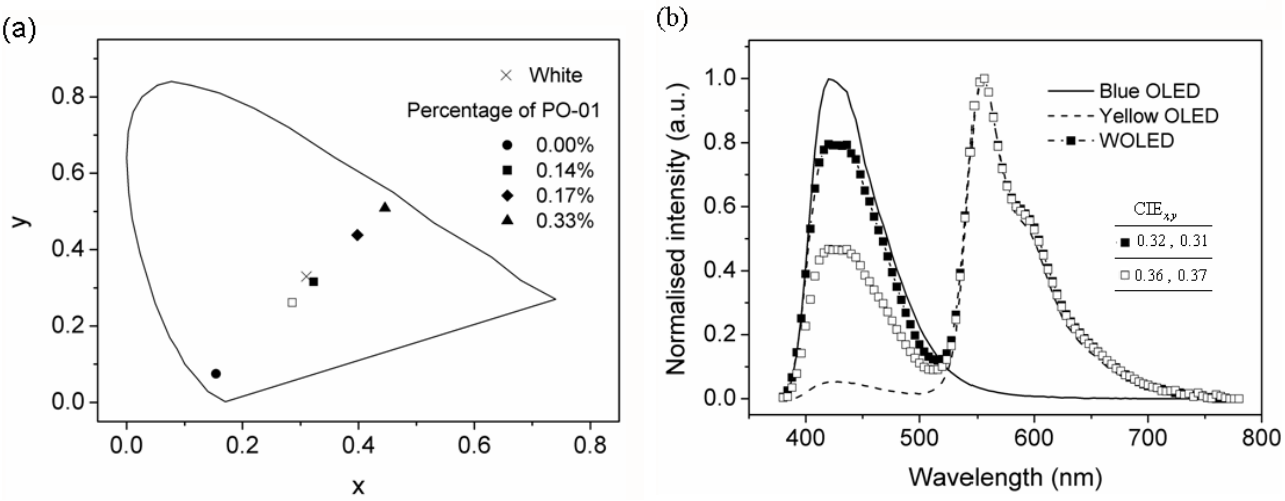

Figure 3.6 - (a) CIE (*x,y*) coordinates for devices, prepared with different amounts of compounds 140 and PO-01 at 1 mA. The white square is for a WOLED containing 0.14% of OXD-7, measured at 10 mA. The D65 white reference point is indicated by the cross. (b) Normalised EL spectra for the white OLED at 1 mA before (filled squares) and after (white squares) the application of a 10 mA current. The EL spectra of the blue and yellow OLEDs (0.0% and 0.33% compound PO-01, respectively) are also shown.

Devices	Solvent[a]	119[b]	PO-01[b]	EQE(%)[c]	L^d (cd m^{-2})	η_l (lm W^{-1})	L^e (cd m^{-2})	η_l (lm W^{-1})	$CIE_{x,y}$[f]
					1 mA		10 mA		
Blue OLED	Toluene	-	-	0.90	21	0.26	290	0.29	0.16, 0.09
	T:C	30	-	3.00	49	0.44	390	0.26	0.16, 0.09
WOLED 1	Toluene	-	0.140	0.72	58	0.53	720	0.56	0.32, 0.31
2	T:C	30	0.021	2.50	221	1.83	1580	0.98	0.30, 0.31
3	T:C	30	0.021	2.25	219	2.16	1620	1.18	0.30, 0.31
Yellow OLED	Toluene	-	0.330	0.70	171	1.43	2430	1.64	0.45, 0.51
	T:C	30	0.140	3.37	910	6.45	7820	4.50	0.45, 0.51

[a] Solvent used in the spinning solution. (T:C) represents toluene:chlorobenzene 1:1 (v/v).
[b] Weight concentration (%).
[c] Maximum value for the external quantum efficiency.
[d] uncertainty ± 1 cd m^{-2}.
[e] uncertainty ± 10 cd m^{-2}
[f] At a current intensity of 1 mA.

Table 3.2 - Optoelectronic properties of ITO/PEDOT-PSS/140–PO-01–119/Ca/Al OLEDs for different concentrations of PO-01 and 119 molecules, including the external quantum efficiency EQE, the luminance *L*, the luminous efficacy η_l, and the $CIE_{x,y}$ coordinates. WOLED 3 is prepared under the same conditions as WOLED 2 but using a cathode of CsF.

3.3 Improving Electron Transport Properties in White and Blue OLEDs

Organic compounds commonly used as the emissive material in OLEDs are known to be predominantly hole transporting e.g. poly(phenylene vinylene) (PPV) or polyfluorene (PF) (although there is some debate about the charge transport properties of PF). This means that they have low electron affinities and in a device hole injection is often dominant over electron injection. The incorporation of extra electron-transporting layers in a device, either by blending in an electron-transport material with the emitter, or increasing the electron-affinity of the emissive material by chemical design, has been shown to improve the efficiency of OLEDs.[5,6]

An example of the device improvements that may be achieved by such a strategy is work by Grice *et al*. incorporating a triazole polymer, **TRIDSB** (**174**) figure 3.7, into a device with structure ITO/PPV/TRIDSB/Al which improved quantum efficiency four-fold to 0.08% compared with 0.02% in the device without **TRIDSB**.[96]

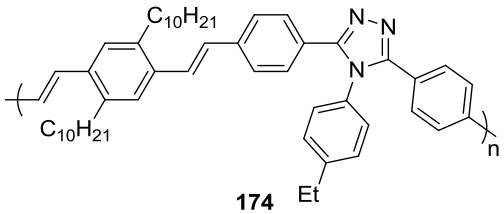

174

Figure 3.7 - Structure of triazole polymer TRIDSB

1,3,4-Oxadiazoles are effective electron transport materials with high thermal stability and high photoluminescent quantum yield (PLQY). This was demonstrated effectively by Brown *et al.* when they introduced a 2-(4-biphenylyl)-5-(4-*tert*-butylphenyl)-1,3,4-oxadiazole (butyl-PBD) (**175**) as a dispersion in poly(methylmethacrylate) as a electron-transport hole-blocking (ETHB) layer in a PPV-based OLED, figure 3.8.[97] The devices demonstrate a ten-fold improvement in efficiency compared to the parent PPV device.

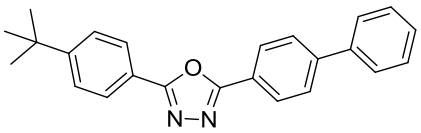

175

Figure 3.8 - Structure of butyl-PBD

Work by Ahn *et al.* in Durham showed that the oxadiazole-containing electron-transport material DFD (**176**) significantly improves OLEDs based on poly[2-(2-ethylhexyloxy)-5-methoxy-1,4-phenylenevinylene] (**MEH-PPV**), figure 3.9.[98] The device containing 95% of the ET material in the blend was two orders of magnitude more efficient than the non-blended (pure MEH-PPV) device.

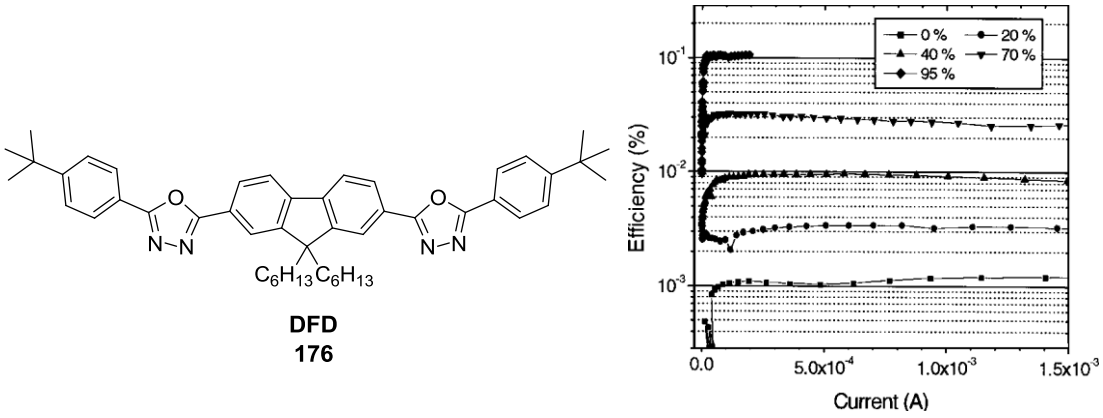

Figure 3.9 - Structure of DFD and graph displaying EQE vs. current for OLEDs fabricated with MEH-PPV/DFD blended layers[98]

Other work in Durham has demonstrated a similar improvement in device efficiency when blending **OXD**-based materials into the emissive layer of OLED devices.[99,100]

3.3.1 Synthesis

Based on observations of improved device efficiency upon incorporation of oxadiazole units compounds **177** and **178** were designed with the aim to improve the electron transporting properties of **140** by introducing additional oxadiazole units, at different sites in the backbone, figure 3.10.

The synthesis of **177** was achieved through a series of functional group transformations of 5-bromoisophthalic acid **179** to yield the bis-oxadiazole **184**, scheme 3.1. The steps to **182** have been reported in the literature.[101] The final step of the sequence was a standard Suzuki-Miyaura cross-coupling with **139** which proceeded in an excellent 87% yield.

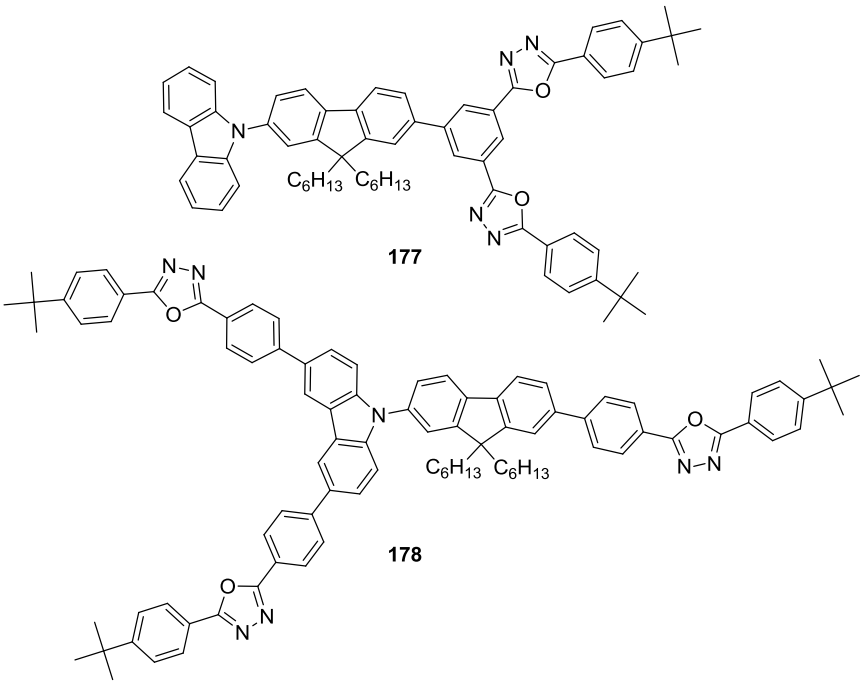

Figure 3.10 - Molecular structures of 177 and 178

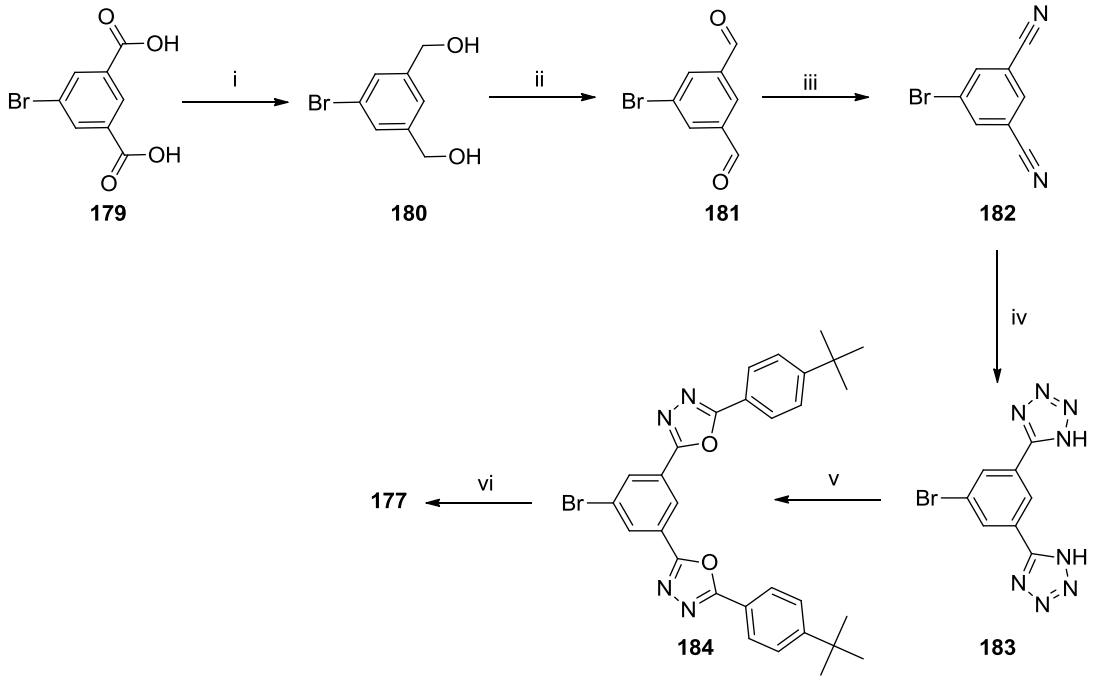

Reagents and Conditions: i) BH_3.THF, THF, 25 ^{o}C, 16 h, 99%; ii) PCC, DCM, 25 ^{o}C, 1 h, 81%; iii) I_2, NH_3 (aq), THF, RT, 49%; iv) NH_4Cl, NaN_3, DMF, reflux, 100%; v) *tert*-butylbenzoyl chloride, pyridine, reflux, 76% vi) **139**, $[PdCl_2(PPh_3)_2]$, NaOH (aq), THF, 60 ^{o}C, 15 h, 87%

Scheme 3.1 – synthesis of bis-oxadiazole 177

The synthesis of **178** was achieved through a series of cross-coupling procedures using previously synthesised intermediates, scheme 3.2.

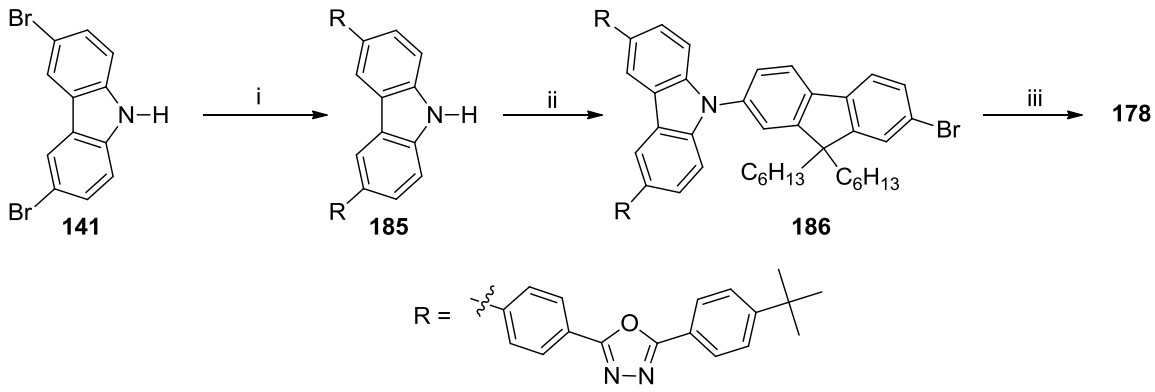

Reagents and Conditions: i) **158**, $[PdCl_2(PPh_3)_2]$, NaOH (aq), THF, 60 °C, 47%, ii) **137**, CuI, 1,10-phenanthroline, DMF, 120 °C, 15 h, 51%, **158**, $[PdCl_2(PPh_3)_2]$, NaOH (aq), THF, 60 °C, 80%

Scheme 3.2 – Synthesis of 178

Compound **178** was unsuitable for vapour deposition due to its low volatility. Investigations into spin-coating the material for devices are underway.

3.3.2 Results and Discussion

The first investigations into improving device efficiency through improved electron transport were made by incorporating electron-transporting **OXD-7** (**119**), figure 3.12, into the WOLEDs containing **140** blended with **PO-01**. Addition of OXD-7 to leads to a significant decrease in sample current and a marked increase in EQE, up to 3.3% when using 30% blend of **119**, figure 3.12. The blended layer was spin-coated from a 1 : 1 toluene : chlorobenzene solution which results in the colour of these devices red-shifting compared to those containing films spun from toluene. This meant that a white device could be produced using a smaller weight percentage of the iridium complex **172**. A device structure of ITO/PEDOT-PSS/**140**–**PO-01**(0.021%)–**119**(30%)/Ca/Al for WOLED 2, gave CIE coordinates (0.30, 0.31) very close to the D65 reference point. The EQE of this device was 2.5%, significantly greater than the figure of 0.72% achieved for WOLED 1, table 3.2. Figure 3.11 shows a photo of devices for the pure blue OLED (**140**, yellow (**PO-01** 0.33%) and WOLED 2 devices.

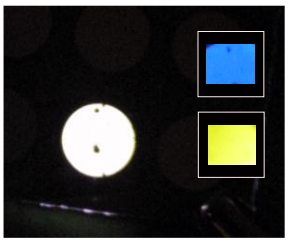

Figure 3.11 - Photographs of reference blue and yellow devices and WOLED 2 recorded at a constant current of 1 mA

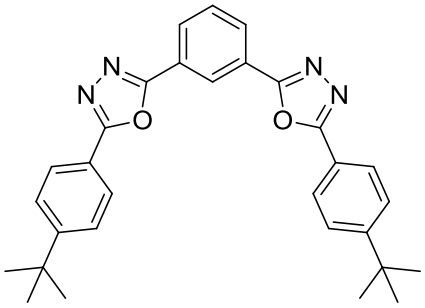

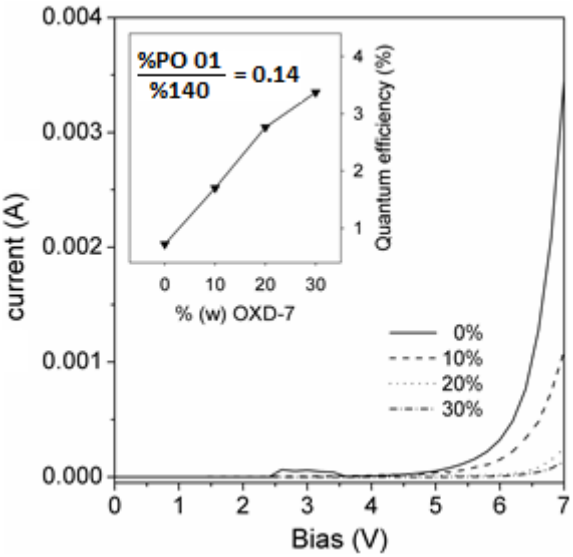

Figure 3.12 - Molecular Structure of 119 and current versus bias data for OLEDs of a blend of 140 and PO-01 with different percentages of 119 in the film. All samples spin coated from 1:1 (by volume) toluene: chlorobenzene solutions. In all cases, the yellow : blue dye ratio is 0.14 (by weight). The inset shows the external quantum efficiency variation with the weight concentration of OXD-7.

Because of the improved device characteristics observed when **119** was blended into various OLED and WOLED devices compound **177** incorporating an additional **OXD** unit was designed. Results are summarised in tables 3.3 and 3.4. Devices based on pure **177** exhibit a similar emission colour as **140** but with a reduced EQE, 0.27% compared to 0.90%. Devices containing blends of PDY-123 and **PO-01** with **177** were made. Those devices containing PDY-123 do not pass close to the desired white point, again displaying a shift to the green followed by transition to the blue point. The devices doped with the iridium complex **PO-01** do show emission very close to the white point at levels of 0.1 weight% of **PO-01**. The CIE coordinates for this emission are (0.33, 0.31), but the EQE is 0.42%, compared to 2.5% achieved in WOLED 2 where the ET material was incorporated separately. Device characteristics for these OLEDs are described in tables 3.3 (**177** with PDY-123) and 3.4 (**177** with **PO-01**).

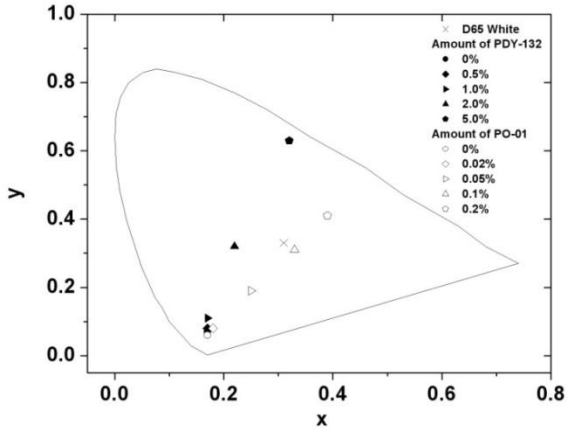

Figure 3.13 - CIE (*x,y*) coordinates for devices, prepared with different amounts of compound 177 and PDY-132 (filled symbols) and 177 and PO-01 (open symbols) at 1 mA. All samples spin coated from chlorobenzene solutions. The CIE coordinates of D65 white are also included for reference.

Weight concentration of PDY-132 (%)	EQE_{max} (%)	Brightness[a] (cd m^{-2})	Power efficiency[a] (lm W^{-1})	Brightness[b] (cd m^{-2})	Power efficiency[b] (lm W^{-1})	$CIE_{x,y}$[a]
0.0	0.27	3	1.9E-3	70	5.7E-2	0.17, 0.07
0.5	0.34	7	6.0E-2	90	7.0E-2	0.17, 0.08
1.0	0.48	12	0.11	130	9.7E-2	0.17, 0.11
2.0	0.58	62	0.55	540	0.36	0.22, 0.32
5.0	1.47	394	2.4	3510	1.6	0.32, 0.63

[a] At a current intensity of 1 mA ± 1 cd m^{-2}.
[b] At a current intensity of 10 mA ± 10 cd m^{-2}.

Table 3.3 - Optoelectronic properties of ITO/PEDOT/177 –PDY-132/Ca/Al devices with different concentrations of PDY-132. All samples spin coated from chlorobenzene solutions.

The reduced performance of the OLEDs containing **177** compared to those containing a blend of **140** and **OXD**-7 may be attributed to a variety of effects. The different orientation of the oxadiazole moieties within the molecule is changed in **177**. The oxadiazoles are conjugated in a *meta* orientation compared to *para* in **140**. This will result in a reduced conjugation of the oxadiazole with the rest of the molecule and may affect the charge transfer properties.

In addition, the orientation of the **OXD**-7 molecules in relation to the **140** molecules is likely to be important within the film. In **177**, this orientation is fixed in the Y-shaped structure. A blend of **OXD**-7 and **140** can adopt many different intermolecular orientations and interactions within the film which may aid electron transport and therefore increase the efficiency of

charge recombination. A final parameter to consider is the solvent used to spin-cast the films. In the **OXD**-7 blends, a mixed solvent was required compared to pure toluene in the **177** blends. It has been demonstrated previously that solvent effects can be very important in affecting device performance.[102,103]

Weight concentration of PO-01 (%)	EQE_{max} (%)	Brightness[a] (cd m^{-2})	Power efficiency[a] (lm W^{-1})	Brightness[b] (cd m^{-2})	Power efficiency[b] (lm W^{-1})	$CIE_{x,y}$ [a]
0.0	0.27	3	1.9E-3	70	5.7E-2	0.17, 0.07
0.02	0.25	3	1.7E-2	62	3.6E-2	0.18, 0.08
0.05	0.33	2	1.1E-2	150	8.5E-2	0.25, 0.19
0.1	0.42	14	8.8E-2	350	0.19	0.33, 0.31
0.2	0.46	27	0.17	690	0.33	0.39, 0.41

[a] At a current intensity of 1 mA ± 1 cd m^{-2}.

[b] At a current intensity of 10 mA ± 10 cd m^{-2}.

Table 3.4 - Optoelectronic properties of ITO/PEDOT/177 – PO-01/Ca/Al devices with different concentrations of PO-01. All samples spin coated from chlorobenzene solutions.

3.3.3 Conclusions

Blended single-active-layer organic light emitting devices in which a deep blue carbazole-based dye, **140**, is mixed with yellow emitting materials have been fabricated and their electro-optical behaviour studied as a function of blend composition. Two different yellow dyes were used: a fluorescent phenyl-substituted poly(*p*-phenylenevinylene) polymer, **PDY-132**, and an iridium-based phosphorescent dye, **PO-01**. Although OLEDs based on the pure yellow compounds possessed similar CIE co-ordinates, the blended layer devices behaved very differently. As compound **140** was added to **PDY-132**, the OLED colour shifts from yellow to green, and finally to blue; the locus of the data points misses the D65 white point. The effect is attributed to structural reorganisation of the polymer chains in the yellow material. In contrast, blends of **140** with **PO-01** pass very close to the white point, and achieve CIE co-ordinates $x = 0.30$; $y = 0.31$.

Devices using **140** as the emitter show improved performance when blended with an electron-transporting material **OXD**-7, with EQEs increasing up to three-fold in spin-coated devices. However, incorporation of additional electron-transporting units within the same molecule, as

in **177**, does not have the same effect on the device results. This suggests that morphological factors and the orientation of molecules within the films are important considerations. However, the new bis- and tris-oxadiazole derivatives **177** and **178** may be suitable electron-transport materials in combination with other emitters.

Chapter 4: Synthesis and Intramolecular Charge Transfer in Arylamine-Oxadiazole Donor-Acceptor Molecular Wires

---

4.1. Introduction

In depth understanding of electron-transfer processes and charge distribution in organic systems is of current interest in many areas of science. Much recent activity has focussed on the design and study of novel organic molecular wires.[102,103] Practical applications in molecular electronics as well as fundamental knowledge of electron transfer processes relevant to both biological and chemical systems make this area attractive for study. Design of simplified molecular systems may allow the complex photochemical charge separation that occurs in photosynthesis to be more easily modelled; this is of great interest for solar energy applications among others.

Charge transfer may occur by a hopping or tunnelling mechanism.[104] Rates of electron transfer in a given system will depend on many factors including the nature of the donor and acceptor moiety, the bridge, the distance between donor and acceptor, the orientation of the bridge and also electronic coupling between the donor, acceptor and bridge.

Charge transfer in many organic systems occurs by a coherent tunnelling process in which the energy barrier is determined by the electronic structure of the bridge molecule, a superexchange mechanism. This tunnelling process occurs when donor and acceptor states mix with the bridge states, which are higher in energy than the donor and acceptor. During the charge transfer process charge is not located on the bridge. The rate of electron transfer in these systems is dependent on the β coefficient and decays exponentially with distance, equation 4.1(a).

For a molecular wire to transport charge over long distances with good efficiency, the distance dependence of the electron transfer should be weak. This can occur when the energies of the bridge states are comparable to that of the donor in the wire, and the bridge may be oxidised or reduced directly and electron transfer occurs through a hopping mechanism, figure 4.1. The

distance dependence of this type of charge transport is weaker than for the superexchange mechanism, equation 4.1(b).

$$a) \quad k_{ET} = k_0 e^{-\beta(r-r_0)}$$

$$b) \quad k_{ET} = k_0(1/r)$$

Equation 4.1 - a) electron transfer rate equation for a superexchange mechanism; b) electron transfer rate equation for a hopping mechanism

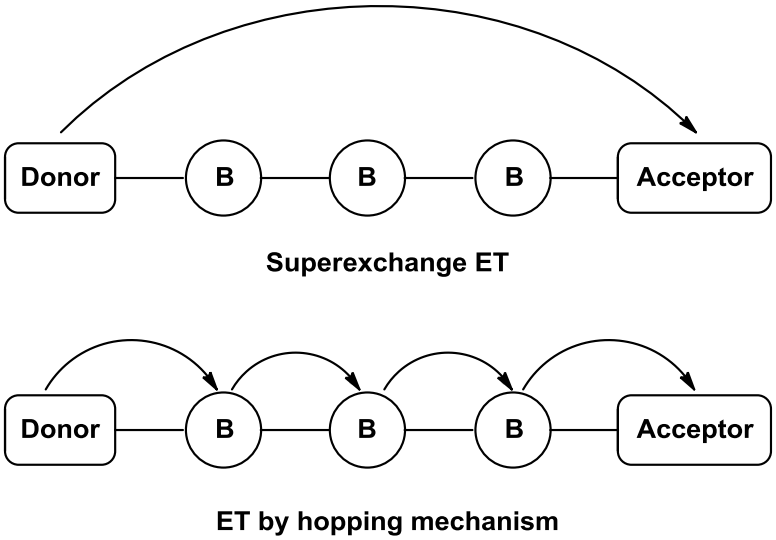

Figure 4.1 - Mechanisms of intramolecular charge transfer; i) superexchange with an exponential distance dependence on rate; ii) charge transfer by a hopping mechanism where the distance dependence is proportional to 1/r

Oligo-*p*-phenylenevinylene (OPV) bridges in D-π-A wires are excellent candidates, demonstrating electron-transfer with small length dependence, figure 4.2.[102] Fluorescence of tetracene in the D-π-A systems is observed to be strongly quenched by the pyromellitimide acceptor; this electron transfer process was investigated using femtosecond optical pump-probe spectroscopy. The rate of electron transfer showed very little distance dependence with a β value of 0.04 $Å^{-1}$ calculated where exponential distance decay is assumed.[102] The electron transport in this example occurs *via* a hopping mechanism.

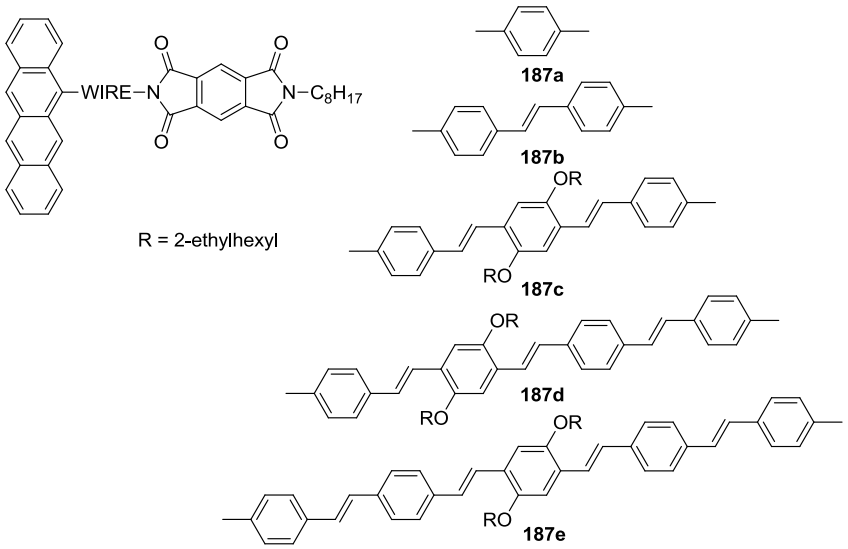

Figure 4.2 - Structures of molecular wire candidates using an OPV bridge

Hanss *et al.* investigated electron transfer through D-π-A systems using a oligo-*p*-xylene bridge, which demonstrates contrasting ET characteristics to the OPV bridges, figure 4.3.[105] *p*-Xylene units do not exhibit any significant increase in their oxidation potentials as the length of the bridge is increased. Furthermore, because of the significant dihedral angle between two linked *p*-xylene units there should not be a large increase in π conjugation as the wire length is increased. The electronic structure in the bridge is relatively length-independent compared with the analogous more conjugated *p*-phenyl or 2,7-fluorenyl systems. Absorption spectra demonstrate an incremental red-shift in the absorption of the *p*-phenyl wires whereas the *p*-xylene wires do not exhibit such a change; this supports the argument that the length scale does not affect the electronic structure for the *p*-xylene series.[105] Time resolved fluorescence decay for the *p*-xylene systems was recorded for MLCT emission and a strong length dependence was observed, giving a β value of 0.52 $Å^{-1}$ for the electron transfer by tunnelling.[105] The comparison of this value with other systems using the same wire but different donors and acceptors demonstrates that the β value is a parameter of the entire system rather than being bridge specific.[103]

Studying fundamental hole-transfer processes in arylamine systems is of great interest due to their wide use in organic material applications. Müllen and collaborators investigated the charge transport properties of D-π-D type materials **191** using ladder-fluorene bridging elements, figure 4.4.[104] The *n* = 1 system with a length scale of 2.2 nm demonstrated communication between the two amine centres *via* a hopping mechanism, observed in an inter-valent charge transfer (IVCT) band upon chemical oxidation by $SbCl_5$. Similar DPA-π-DPA

systems with OPE bridges on similar length scales did not exhibit a well-resolved IVCT band indicating limited communication between the two amine centres.[106,107] The increased communication in **191** is attributed to stronger conjugation through the planarised ladder-fluorene system.[104]

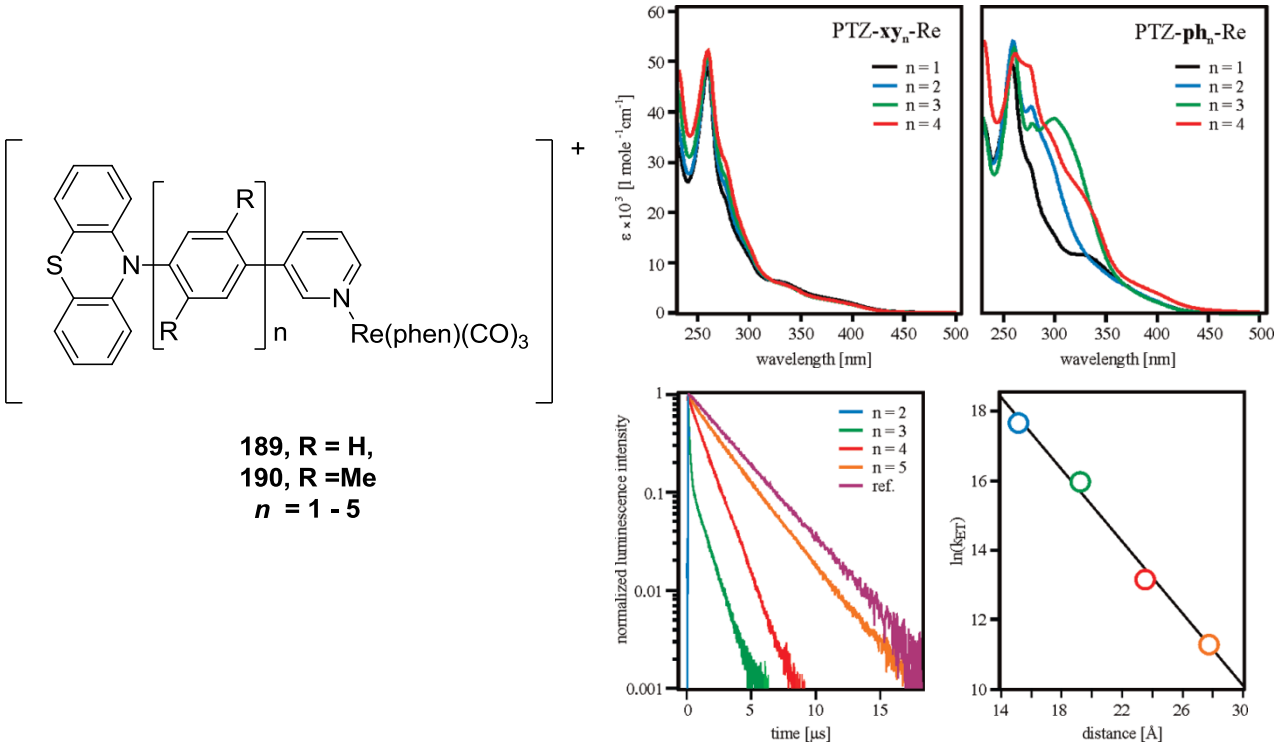

189, R = H,
190, R =Me
***n* = 1 - 5**

Figure 4.3 - (a) Structures of wire candidates 189 and 190 (PTZ = phenothiazine) (b) absorption spectra of wire candidates in dichloromethane solution (c) plot of fluorescence decay and distance dependence on rate of ET for *p*-xylene molecular wires with plot for reference complex $[Re(phen)(CO)_3(pyridine)]^+$

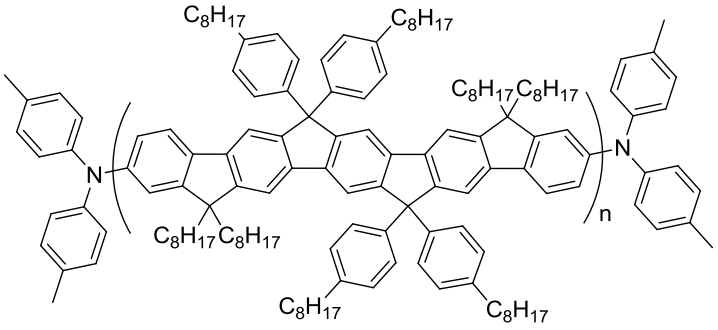

191
n = 1, 2 or 3

Figure 4.4 - Structure of D-π-D system 191

Dias *et al.* investigated co-oligomers of fluorene and dibenzothiophene-*S,S*-dioxide and the nature of fluorescence in these types of systems, figure 4.5.[108] Strong positive

solvatochromism and dual fluorescence was observed, due to locally excited (LE) or intramolecular charge transfer (ICT) states, in polar ethanol at low temperatures. The ICT state is stabilised by higher solvent polarity and is accompanied by structural rearrangement to a twisted intramolecular charge transfer (TICT) state.

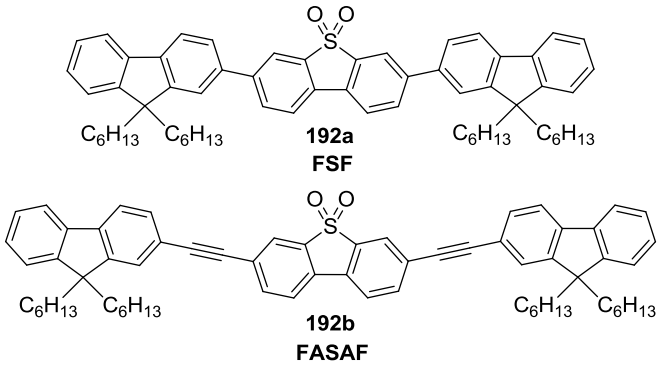

Figure 4.5 - Structures of 192a and 192b

The Bryce group have investigated a series of triphenylamine-(CΞC)$_n$-2,5-diphenyl-1,3,4-oxadiazole dyad molecules **193a-d**, figure 4.6.[109,110] Strong solvatochromism was observed in their PL spectra ascribed to strong ICT interactions. Further studies using two-photon excitation supported the evidence for efficient ICT showing sensitivity to the dielectric medium and the extent of conjugation.

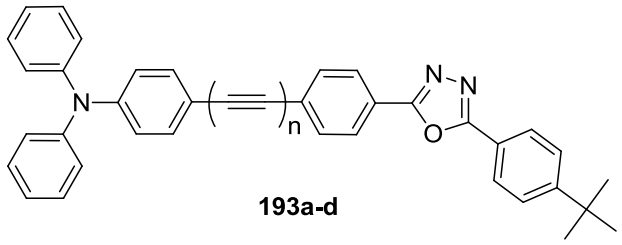

Figure 4.6 - Strucure of DPA-OXD D-A systems (*n* = 1-4)

It has been shown that the magnitude of charge transfer through conjugated bridges is sensitive not only to the nature of the bridge but also the structure of the donor and acceptor groups. Therefore, a comprehensive study of selected donor and acceptor couples with various conjugated bridges will allow a systematic study of the fundamental processes occurring. An advantage of utilising the triarylamine and oxadiazole as donor and acceptor groups, respectively, is that the resulting dyad molecules display a strong fluorescence which allows many analytical techniques to be utilised.

4.2 Results and discussion

4.2.1 Oligo-*p*-phenyleneethynylene molecular wires

There have been some investigations into OPE molecular wires carried out in a collaboration by the groups of Martin and Guldi. Symmetrical C_{60}-OPE-C_{60} molecular wires were synthesised and their electronics in the ground and excited states were probed. In the ground state there were no significant interactions between the C_{60} groups but fluorescence and transient absorption spectroscopy revealed efficient deactivation of the excited state by energy transfer, rather than electron transfer, from the OPE oligomer to the low lying C_{60} singlet states.[111]

Lu *et al.* investigated the transition from a tunnelling to hopping mechanism on different length scales in OPE wires. By assembling amine functionalised OPE wires **194a – 194g** on a gold surface and measuring resistance with a scanning tunnelling microscope – break junction (STMBJ) technique the transition from a tunnelling to a hopping charge transport mechanism is seen as the length of wire is increased. A clear transition can be observed in the plot of log of resistance vs. molecular length at **194c** where a hopping charge transport mechanism becomes prominent, figure 4.7.

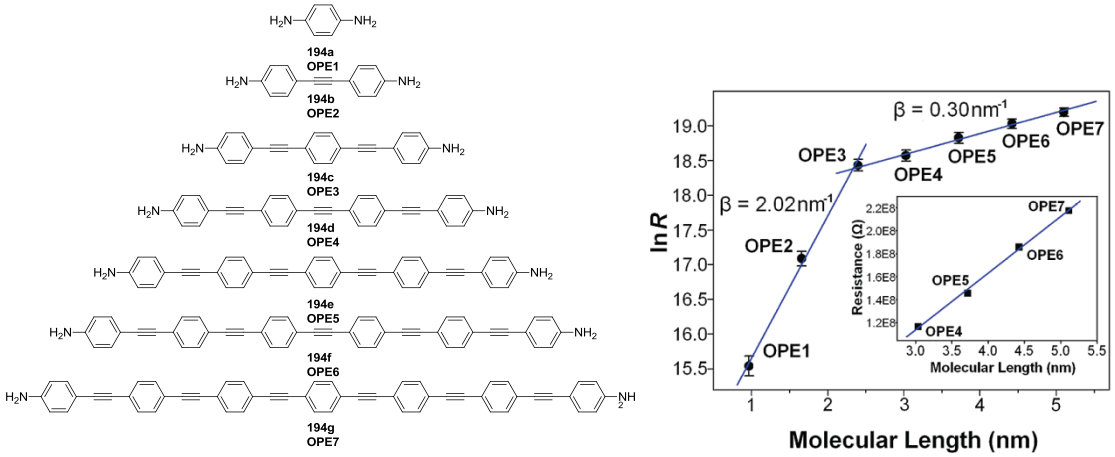

Figure 4.7 - Structure of OPEs 194a – g and plot of resistance versus molecular length data from STMBJ measurements

Atomic force microscopy (AFM) was used by Liu *et al.* to investigate the electron transfer processes occurring in various OPE molecular wires, figure 4.8. They used a monolayer of the wires on a metal substrate in conjunction with AFM to make their measurements. They observed that for the systems investigated the resistance scaled exponentially with the

molecular length as would be expected with a tunnelling mechanism of electron transfer. They calculated an attenuation factor of 0.21 ± 0.01 $Å^{-1}$ for the OPEs.[112]

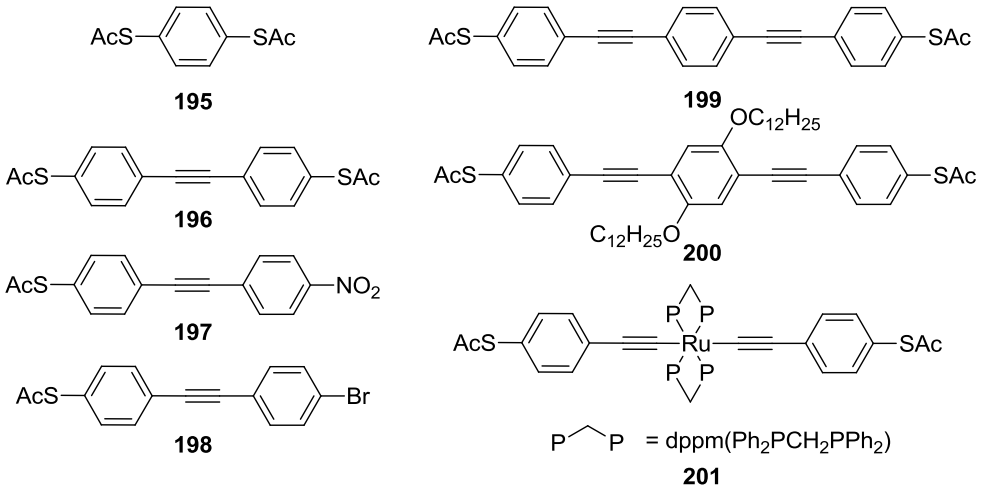

Figure 4.8 - Structure of OPE wires used by Liu *et al.*

4.2.2 Design and Synthesis of new D-OPE-A Wires

Our targets **202-206** (Figure 4.9) were a series of OPE derivatives of various lengths with D and A substituents at the termini. The same oxadiazole acceptor as used in **140** was chosen, along with the di-*p*-tolyl substituted arylamine donor, which is known to possess greater electrochemical stability than the unsubstituted triarylamine.[58,85] Our aim was to construct a comprehensive picture of the effectiveness of the OPE bridge combined with the chosen donor and acceptor units. In addition to the synthesis of the D-π-A systems, the D-π-D and A-π-A systems were pursued as comparative model systems.

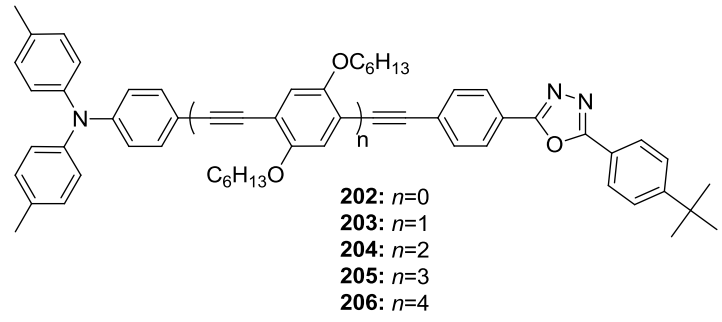

Figure 4.9 - Structures of the target series of oligo-*p*-phenyleneethynylene molecular wires

The general synthetic protocol for OPE systems involves palladium-catalysed cross-coupling reactions of terminal alkynes and aryl iodides or bromides. For improved solubility of the molecules the phenyl rings of the bridge were substituted with hexyloxy chains. To achieve the asymmetric addition of groups to the growing molecular wire was to use an orthogonal

protection of the di-alkynylphenylene building blocks. This strategy has been used previously to great effect.[113]

Alkylation of hydroquinone, **207**, with 1-bromohexane following the standard literature procedure yielded **208** in 90% yield.[114] Further reaction of **208** with potassium iodate and iodine in an acidic solution yielded key intermediate **209** in 32% yield shown in scheme 4.1.[113]

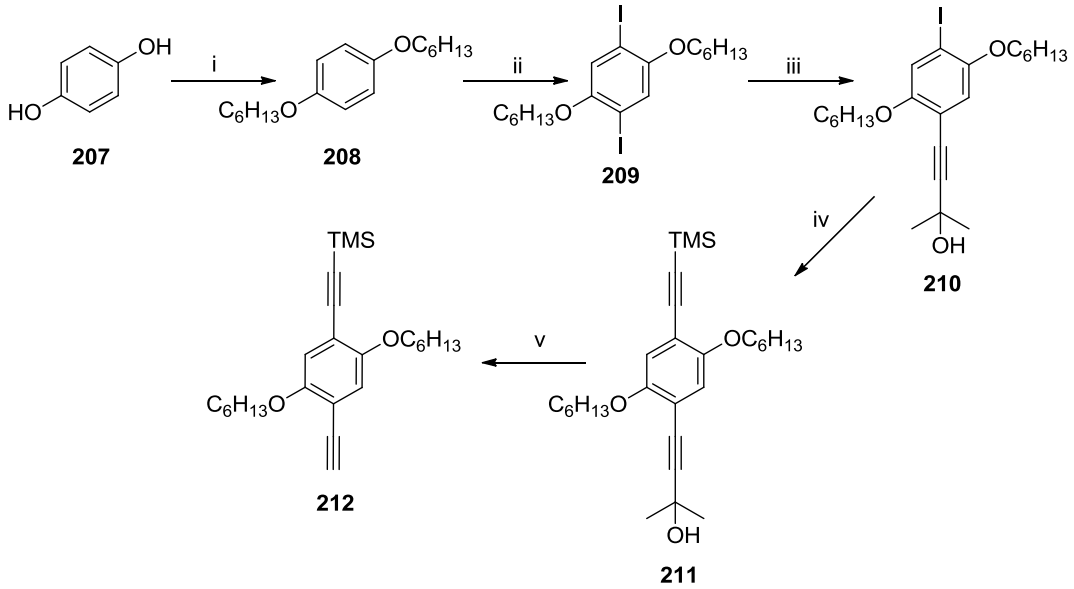

Reagents and Conditions: i) KOH, EtOH, 1-bromohexane, 65 ^{o}C, 4 h, 90%; ii) KIO_3, I_2, $AcOH/H_2SO_4/H_2O$, reflux, 6 h, 32%; iii) 2-methylbut-3-yn-2-ol, Et_3N, $[PdCl_2(PPh_3)_2]$,CuI, 50 ^{o}C, 15 h, 51%; iv) TMSA, Et_3N, $[PdCl_2(PPh_3)_2]$,CuI, 50 ^{o}C, 1 h, 93%; v) NaOH, toluene, 100 ^{o}C, 3 h, 51%

Scheme 4.1 - Synthesis of 212

Reaction of compound **209** with 2-methylbut-3-yn-2-ol *via* standard Sonogashira reaction yielded the monoprotected alkyne **210**. Protection first with the polar alcohol acetylene allows easy separation of the product from any remaining starting material or bis-substituted side products. Further reaction of **210** with trimethylsilyl acetylene yielded the doubly protected compound **211**. Exclusive deprotection of the alcohol protecting group was achieved under anhydrous conditions with NaOH in toluene. This reaction proceeded in a moderate 51% yield but with the advantage that unreacted starting material was easily recovered from the reaction. Compound **212** is an important building block allowing easy addition of singular units to the growing OPE backbone, scheme 4.1.[113]

The synthesis of the triarylamine end group was achieved by standard cross-coupling procedures followed by the deprotection of amine **214** to yield the free acetylene **215** quantitatively, scheme 4.2.[113]

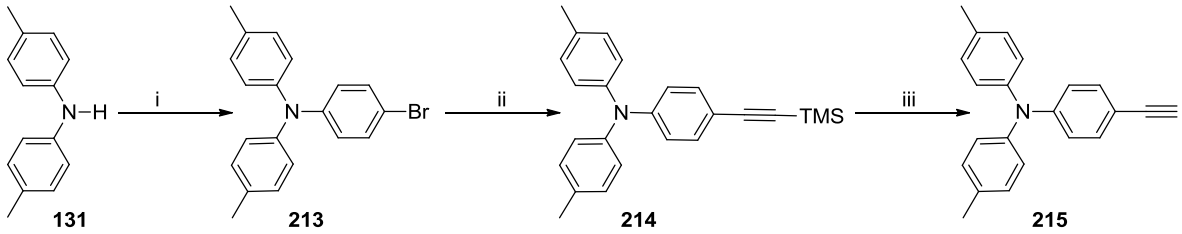

Reagents and Conditions:i) 1-iodo-4-bromobenzene, $[Pd_2(dba)_3]$, dppf, NaO^tBu, toluene, 100°C, 15 h, 54%; ii) TMSA, $Pd(PPh_3)_4$, CuI, reflux, 15 h, 56%; iii) K_2CO_3, MeOH, RT, 2 h, 100%

Scheme 4.2 – Synthesis of 215

The n=0 member of the family **202** was formed in 92% yield *via* Sonogashira reaction of **215** with **216** (formed *via* standard oxadiazole procedure – see experimental chapter), scheme 4.3.

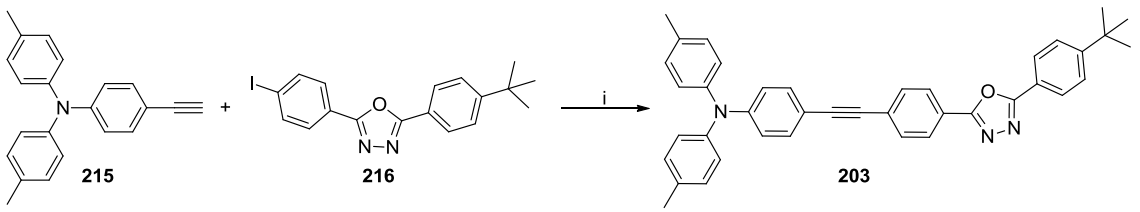

Reagents and Conditions: i) $[Pd(PPh_3)_4]$, CuI, Et_3N/THF, reflux 15 h, 92%

Scheme 4.3 - Synthesis of 203

The alkyne-functionalised oxadizole **218** was synthesised *via* a Sonogashira reaction of **150** with 2-methylbut-3-yn-2-ol in 98% yield. Deprotection of the alkyne with sodium hydroxide in toluene afforded the reagent **218**, scheme 4.4.[113]

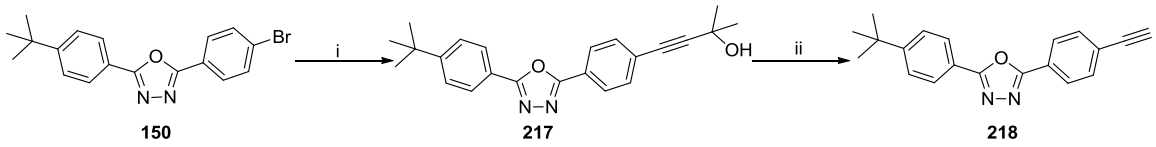

Reagents and Conditions: i) 2-methylbut-3-yn-2-ol, $[PdCl_2(PPh_3)_2]$, CuI, Et_3N, 50 °C, 2 h, 98%; ii) NaOH, toluene, reflux, 0.5 h, 66%

Scheme 4.4 – Synthesis of 218

The previously synthesised oxadiazole end group **150** was initially employed in the attempted Sonogashira reaction with **212**. However, the reaction was unsuccessful both at room temperature and at reflux. The oxidatively homocoupled butadiyne derivative **219** was isolated and **150** was recovered, scheme 4.5. This unwanted reaction presumably occurred due to the

diminished reactivity of the bromo substituent of **150** compared with the standard iodo-reagent. Additionally the use of the dichloro-palladium (II) catalyst has been known to increase the occurrence of alkyne homocoupling due to the need to generate the active palladium (0) catalyst *in situ*.[115-117] Therefore the analogous iodo-oxadiazole **216** was synthesised with the intention of employing the tetrakistriphenylphosphine palladium catalyst to suppress the homocoupling reaction.

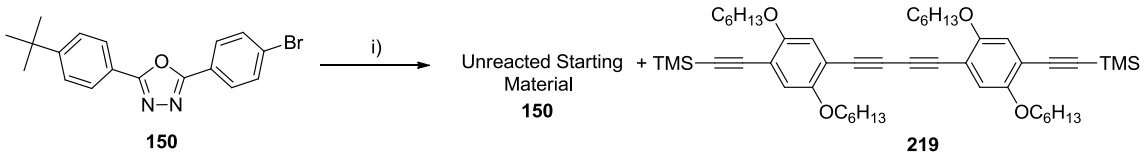

150 **219**

Reagents and Conditions: i) 212, $[PdCl_2(PPh_3)_2]$, CuI, Et_3N, reflux, 15 h, **150** 95% recovered, **219** 71%

Scheme 4.5 – Attempted Sonogashira coupling of 150 and 212

When the reaction of **216** and **212** was carried out using **a** palladium (0) catalyst a stark difference in reactivity and conversion was observed. An 85% yield of the desired product **220** was obtained along with a small amount of in *situ* deprotection of the TMS alkyne which upon further reaction gave the bis-oxadiazole derivative **221** in 8% yield, scheme 4.6.

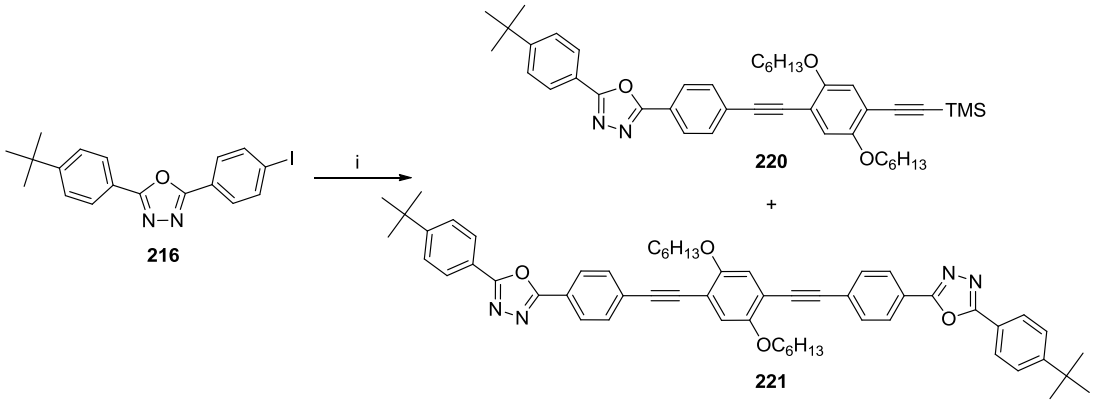

216 **220** **221**

Reagents and Conditions: i) **212**, $[Pd(PPh_3)_4]$, CuI, Et_3N, reflux, 15 h, **220** 85%, **221** 8%

Scheme 4.6 – Synthesis of 220 and 221

These optimised reaction conditions were applied to future Sonogashira reactions and allowed the synthesis of the desired series of OPE molecular wires. Deprotection of **220** with potassium carbonate in methanol at room temperature afforded **222** quantitatively, scheme 4.7.

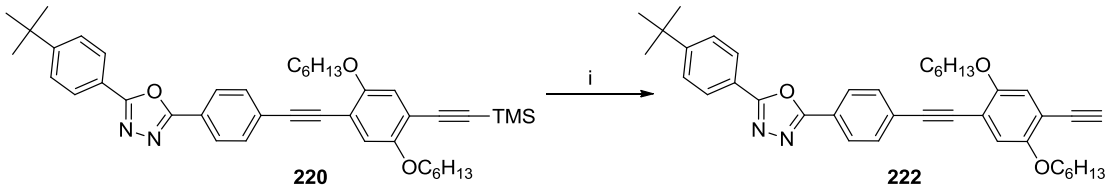

Reagents and Conditions: i) K_2CO_3, MeOH, THF, RT, 2 h, 100%

Scheme 4.7 – Deprotection of 220

With the various key intermediates in hand, the synthesis of the *n* = 1 – 4 compounds could be achieved through the correct combination of these compounds and Sonogashira protocols. The *n* = 1 derivative **203** was synthesised as described in scheme 4.8. The synthesis of the amine intermediate **223** by Sonogashira cross-coupling of **215** with **209** also furnished the bis-substituted D-D *n* = 1 system **224**.

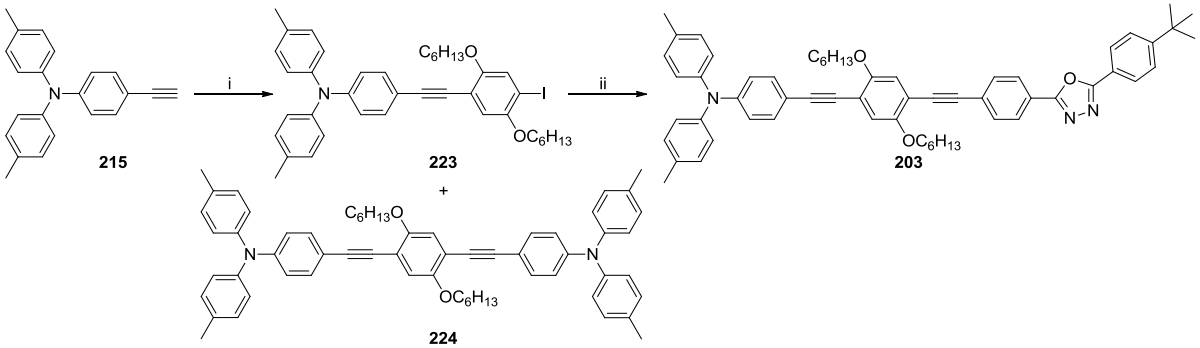

Reagents and Conditions:i) **209**, $[Pd(PPh_3)_4]$, CuI, Et_3N, reflux, 15 h, **223** 53%, **224** 14%; ii) **216**, $[PdCl_2(PPh_3)_2]$, CuI, Et_3N, 50 ^oC, 13 h, 86%

Scheme 4.8 – Synthesis of 203

Synthesis of the *n* = 2 analogue **204** was achieved using a similar strategy, scheme 4.9.

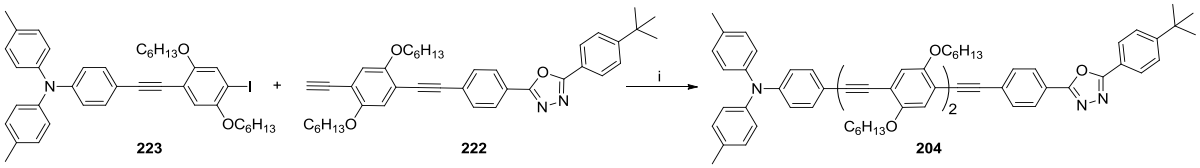

Reagents and Conditions: i) $[Pd(PPh_3)_4]$, CuI, Et_3N/THF, 70 ^oC, 15 h, 49%

Scheme 4.9 – Synthesis of 204

Extension of the amine intermediate **222** by a single phenylethynyl unit allowed the *n* = 3 derivative **205** to be formed through reaction with the extended oxadiazole **226**, scheme 4.10.

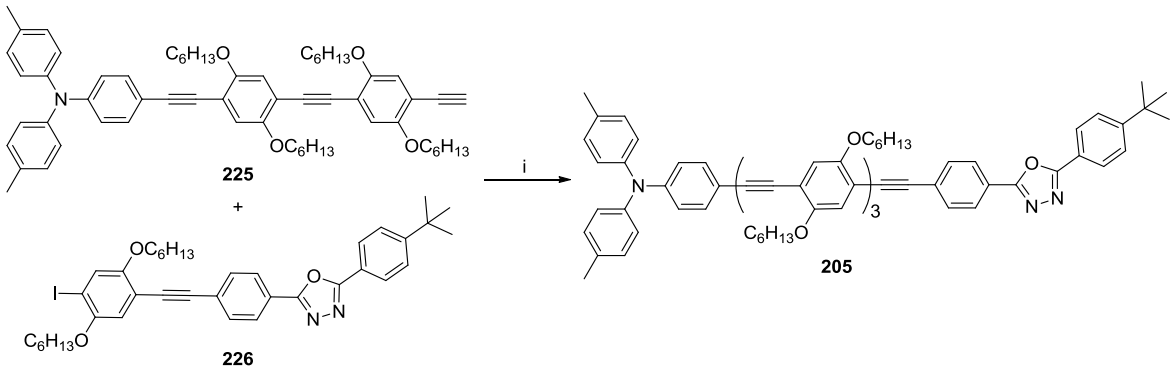

Reagents and Conditions:i) $[Pd(PPh_3)_4]$, CuI, Et_3N, THF, reflux, 15 h, 22%

Scheme 4.10 – Synthesis of 205

The synthesis of the final analogue required in this series – the *n* = 4 molecule **206** – is shown in scheme 4.11. This reaction resulted in some bis-substitution of the diiodo compound **209**, resulting in formation of the side product **227** in 24% yield.

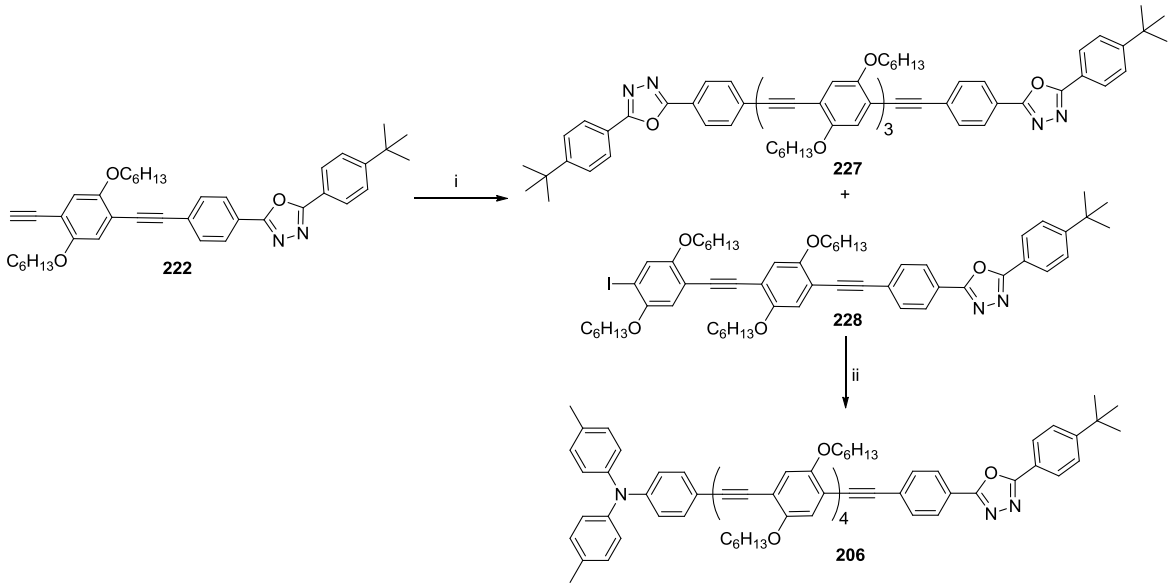

Reagents and Conditions:i) **209**, $[Pd(PPh_3)_4]$, CuI, Et_3N, THF, reflux, **228** 54%, **227** 24%; ii) **225**, $[Pd(PPh_3)_4]$, CuI, Et_3N, THF, reflux, 13 h, 85%

Scheme 4.11 – Synthesis of 206

The symmetrical molecule **229** was also synthesised as described in scheme 4.12.

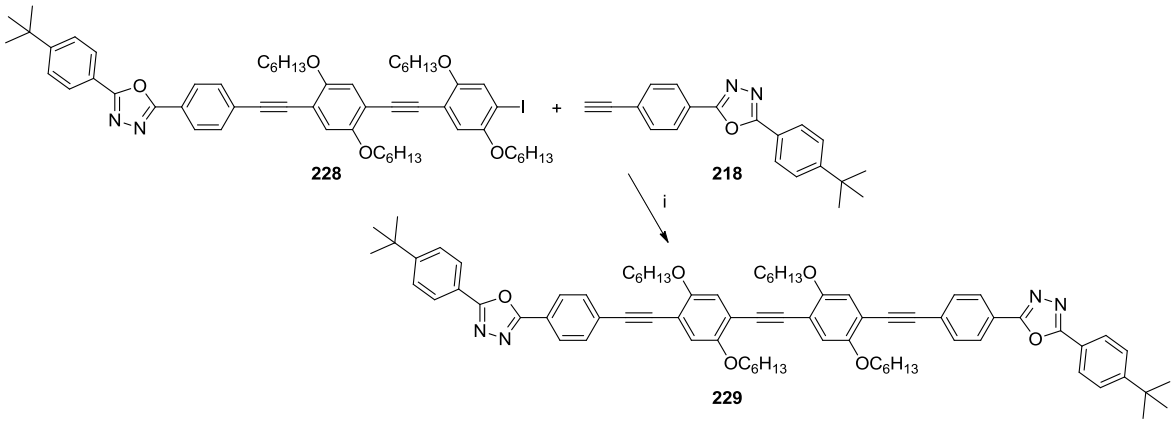

Reagents and Conditions:i) [$Pd(PPh_3)_4$], CuI, Et_3N, THF, reflux, 15 h, 72%

Scheme 4.12 – Synthesis of A-A system 229

4.2.3 Photophysics

Photophysical studies were carried out on the D-π-A systems **202** – **206** as well as the D-π-D system **224** and A-π-A system **229**. Steady state solution fluorescence studies probed the extent of LE or ICT states in different solvents. The data are summarised in table 4.1.

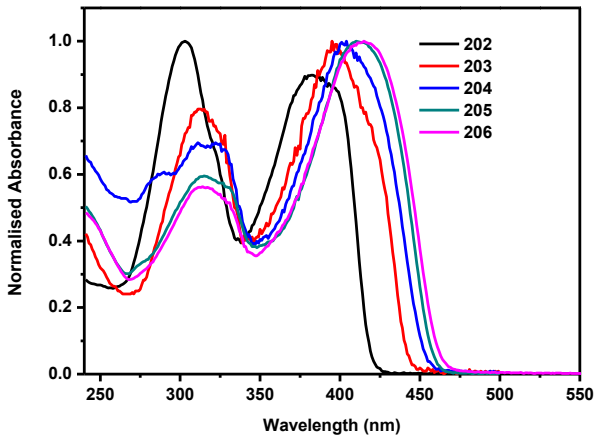

Figure 4.10 - Normalised absorption spectra for OPE molecular wires 202 – 206 in cyclohexane solution

The absorption data for the *n* = 1 – 5 series **202** – **206** demonstrate a progressive red shift with increasing distance between donor and acceptor as the number of phenyleneethynylene units increases, figure 4.10 (absorption spectra for **224** and **229** in appendix II). The red shift in absorption and emission can be rationalised by an increase in the conjugation length as the number of bridging units is increased. In addition to the shift in the wavelength of the absorption, the relative intensity of the two major absorption bands changes systematically. As

the length of the material increases the higher energy absorption (~300-320 nm) decreases in intensity while the lower energy absorption (~380-415 nm) increases in intensity.

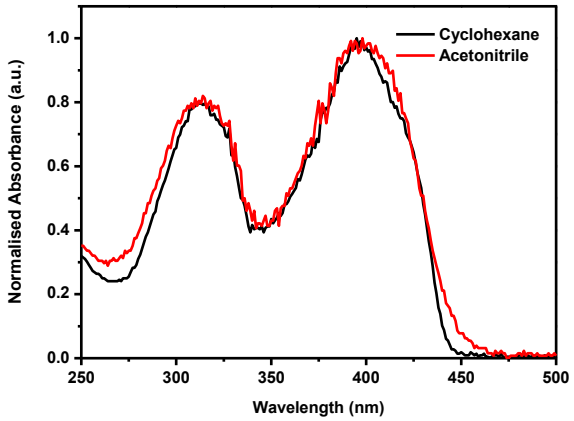

Figure 4.11 - Absorption spectra of 203 in cyclohexane and acetonitrile solutions

A comparison of the absorption spectrum of **203** in non-polar cyclohexane and polar acetonitrile, figure 4.11, shows a small red shift in acetonitrile on the red edge of the main absorption band. This is suggestive of a low energy ICT band in the absorption spectrum; this feature is observed with the other D-A systems studied.

Fluorescence spectra of the molecules in solution show two main features. In non-polar solvents emission from a LE state, due to a π-π* transition, and an ICT state can be observed. As the polarity of the solvent is increased the LE emission disappears and only the ICT emission is retained. Strong solvatochromism is observed which decreases in intensity as the molecular length increases. Figure 4.12 shows the spectra for the shortest and longest derivatives, **202** and **206**, respectively (other plots are shown in appendix II).

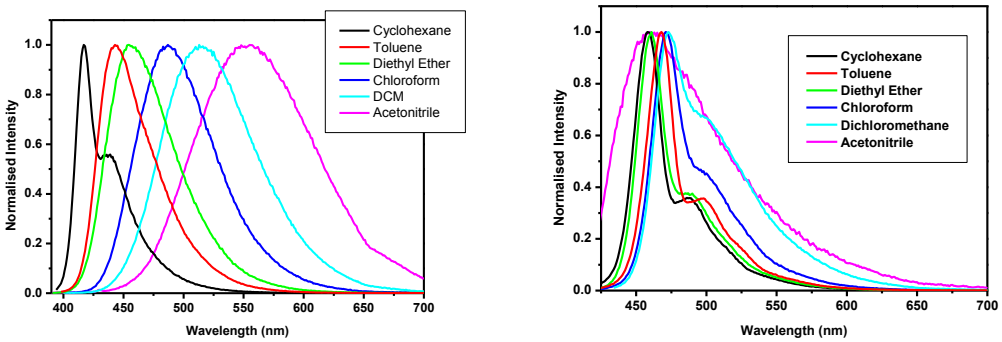

Figure 4.12 - Emission spectra in a variety of solvents of different polarity for 202 (left) and 206 (right)

The quantum yields of all of the materials in cyclohexane solution were consistently high in the range of 0.71 – 0.94, table 4.1. In polar acetonitrile solution, however, the D-A systems exhibit lower PLQY values between 0.15 and 0.34. This indicates the presence of radiationless decay pathways. However, the model symmetrical systems **224** and **229** have higher PLQYs in polar solvent of 0.82 and 0.96, respectively. This suggests the presence of more radiationless decay pathways in the asymmetric systems, probably due to intermolecular interactions with the polar solvent.

4.2.4 Time resolved fluorescence spectroscopy

Time correlated single photon counting (TCSPC) spectroscopy was used to analyse the fluorescence decay of the molecules in solvents of varying polarity (experimental details in chapter 6). These measurements were carried out at the Department of Physics, Durham University with the assistance of Dr Lars Pålsson. The decay lifetimes as calculated from the TCSPC spectra are displayed in table 4.2. Two main decay features can be observed: a fast decay on the picosecond timescale (15 – 40 ps) and a longer lived decay on the nanosecond timescale (0.7 – >10 ns). For all the molecules as the detection wavelength of the emission decay was moved to higher wavelengths the decay lifetime increases and the fast decay process is eliminated. The fast decay component may be ascribed to a planarisation process of the bridge in the molecule and the longer lived decay due to an intramolecular CT state.

The decays for **202** were longer lived than the timescale of the experiment, meaning that accurate lifetimes could not be calculated from the decays obtained. As the lifetime of the species is longer than the time between laser pulses, **202** may not have relaxed to its ground state before another excitation occurs. This can lead to unwanted photobleaching effects. A plot of the recorded decays is displayed in figure 4.13. In order to obtain accurate lifetimes for these species a system with a laser with longer intervals between pulses should be used.

Figures 4.13 and 4.14 show a comparison of the decays for the different molecules in non-polar cyclohexane solution and polar DCM solution when detected near their emission onset where the LE state decay is observable (all plots in appendix II). A trend can be observed that as the length of the wire is increased the amplitude of the fast decay component, due to the LE state, also increases, particularly in non-polar cyclohexane solutions. This can be rationalised by the fact that the planarisation process required to produce the CT state requires more

energy as the length of the wire increases. In the shorter **202** in polar DCM solution the fast LE decay is not observable, figure 4.13, indicating that less energy is required to stabilise the ICT state when the D-A distance is shorter; the fast decay is also not observed in **202**. The symmetrical analogues **224** and **229**, demonstrated by **224**, figure 4.12, also show a similar trend in their decay lifetimes.

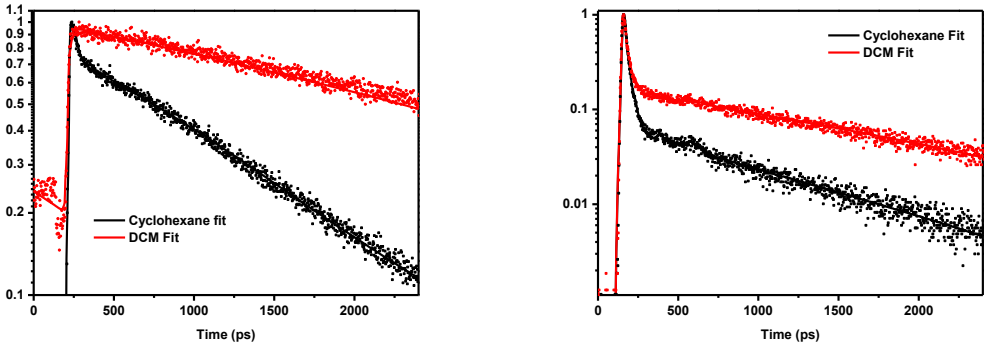

Figure 4.13 – Luminescence decays recorded at the emission onset of compounds 203 (left) and 205 (right) in cyclohexane and DCM (excitation wavelength: 385 nm)

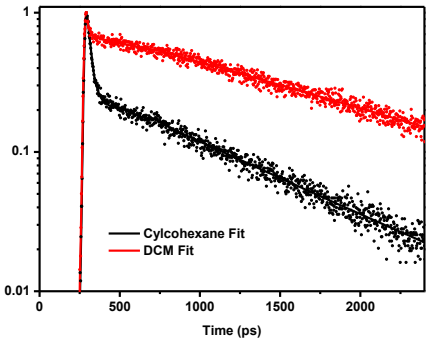

Figure 4.14 – Luminescence decays recorded at the emission onset of compound 224 in cyclohexane and DCM (excitation wavelength: 385 nm)

Compound	λ_{abs} (nm) Cy	λ_{abs} (nm) MeCN	ε (cm^{-1} mol^{-1} dm^3)[a]	λ_{max} Cy (nm)[b]	λ_{max} Toluene (nm)[b]	λ_{max} Et_2O (nm)[b]	λ_{max} $CHCl_3$ (nm)[b]	λ_{max} DCM (nm)[b]	λ_{max} MeCN (nm)[b]	Solvatochromic Shift (cm^{-1})	ϕ[d]	ϕ[e]
202	207, 303, 384	300, 381	67800, 46600, 41900	417, 437	443	455	487	514	555	5960	0.92	0.19
203	205, 313, 396	314, 398	20400, 12400, 15300	438, 465	453, 480	465	494	533	608	6380	0.90	0.21
204	206, 322, 402	324, 408	54500, 20800, 29100	450, 478	460, 489	459	480	521	573	4770	0.90	0.15
205	205, 318, 412	320, 417	223000, 98100, 165000	456, 485	465, 495	458, 488	471, (505)[c]	500	485	1310	0.94	0.16
206	208, 314, 415	322, 411	160000, 76700, 138000	458, 488	468, 498	461, 488	472, (498)[c]	473, (500)[c]	462	190	0.71	0.37
229	204, 329, 399	328, 405	42800, 33900, 44200	445, 472, (494)[c]	452, 479	446, 473	455, 482	456, (482)[c]	454, (478)[c]	450	0.89	0.82
224	211, 300, 396	297, 401	84700, 35600, 65600	428, 451, (473)[c]	436, 462	431, (453)[c]	447	457	485	2750	0.94	0.96

[a]Extinction coefficient calculated for compound in cyclohexane solution

[b]Excitation at lowest energy λ_{abs} of compound in specified solvent

[c]Shoulder

[d]Quantum yields measured in cyclohexane solution with excitation at lowest energy λ_{abs} of compound in cyclohexane. Estimated error of +/-0.05

[e]Quantum yields measured in acetonitrile solution with excitation at lowest energy λ_{abs} of compound in acetonitrile. Estimated error of +/-0.05

Table 4.1 – Solution photophysical characteristics of compounds 202-206, 224 and 229

		Cyclohexane			Diethyl Ether			DCM		
203	Detection Wavelength (nm)	430	460	500	430	470	575	500	550	650
	Lifetime τ (ps)*	20.2 972.9	- 984	- 970	9.5 1214	- 1205	- 1297	- 35000	- 34300	- 35200
204	Detection Wavelength (nm)	420	450	480	440	480	520	460	480	520
	Lifetime τ (ps)*	150.6 954	- 776	- 770	- 927	- 1052	- 1035	- 1529	- 1601	- 1577
205	Detection Wavelength (nm)	420	440	480	440	470	510	450	470	500
	Lifetime τ (ps)*	33.4 952	55.4 751	- 779	33.0 899	- 868	- 780	33.9 1712	- 1690	- 1420
206	Detection Wavelength (nm)	410	450	510	430	450	520	440	470	560
	Lifetime τ (ps)*	60.6 770	58.1 772	- 729	48.1 827	48.6 788	- 757	258.2 1891	- 1386	- 2379
229	Detection Wavelength (nm)	420	440	450	420	440	450	430	450	500
	Lifetime τ (ps)*	24.7 892	- 836	- 871	12.9 1052	- 980	- 980	15.7 1080	- 1026	- 1025
224	Detection Wavelength (nm)	410	430	440	410	420	440	430	430	460
	Lifetime τ (ps)*	16.3 817	- 843	- 841	4.7 918	- 932	- 941	6.9 1323	- 1302	- 1292

***Uncertainties in lifetime measurements: for lifetimes less than 50 ps ± 5 ps; for lifetimes up to 1 ns ± 0.1 ns; for lifetimes over 1 ns ± 30%**

Table 4.2 – Lifetimes as calculated from TCSPC measurements for wire compounds (excluding 202) at various detection wavelength.

4.2.5 Cyclic Voltammetry

It was observed in chapter 2 that the electrochemical oxidation of unsubstituted carbazole and diphenylamine substituted derivatives resulted in polymerisation at high concentration. This present series of OPEs has di-*p*-tolylamine substituents as the donor moiety in order to improve their electrochemical stability by blocking the reactive 4-position on the phenyls of the arylamine. The cyclic voltammetry data are presented in table 4.3.

Compound	$E_{1/2}$(Ox1)[a]	$E_{1/2}$(Ox2)[a]	$E_{1/2}$(Ox3)[a]	$E_{1/2}$(Red1)[b]
202	0.45	-	-	-
203	0.48	0.96	-	-
204	0.39	0.85[c]	1.22[c]	-
205	-	-	-	-
206	0.33	-	-	-
224	0.48	0.96[c]	-	-1.87[c]
229	0.74	1.01[c]	-	-

[a] Scan between 1.5 V and -0.5 V vs ferrocenium/ferrocene couple (FcH^+/FcH = 0.0 V) in DCM.
[b] Scan between -0.5 V and -2.5 V vs FcH^+/FcH (0.0 V) in THF.
[c] Irreversible wave, anodic wave value given.

Table 4.3 – Cyclic voltammetry data for compounds 202 – 206, 224 and 229

The previous CV study of **194a-d** by Palsson *et al.*[110] was performed in acetonitrile solution, but the OPEs in this study were insoluble in this solvent, so DCM was used as solvent for oxidations and THF for reductions, by analogy with the compounds in chapter 2. A well resolved oxidation wave was not observed for **205** and with the exception of **224** reduction waves were not observed for any of the OPE wires within this solvent window. Representative CV scans of **224** are shown in figure 4.13 (other scans are shown in appendix II). A significant trend is that the first oxidation potential, due to oxidation of the triarylamine to the radical cation, occurs at lower potentials as the wire length is increased.

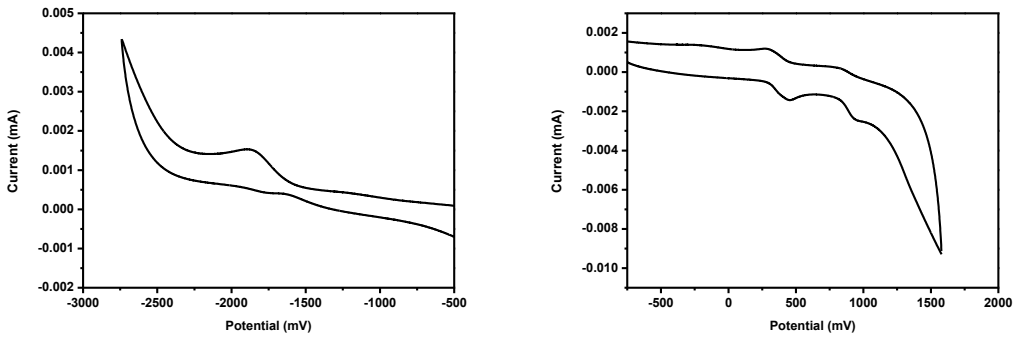

Figure 4.15 – CV trace for 224 reduction (in THF) left and oxidation (in DCM) right

4.3 Planarised and Twisted Donor-acceptor systems

In addition to probing charge transfer between arylamine and **OXD** units by varying the length of an OPE bridge, we have also investigated the extent of charge transfer between these D and A units when the extent of conjugation in similar length-scale molecules is altered. For this study our targets were **134** and **230 - 232** with a triphenylene linker with the phenyl rings being forced into a coplanar configuration or intentionally twisted out of planarity, figure 4.16.

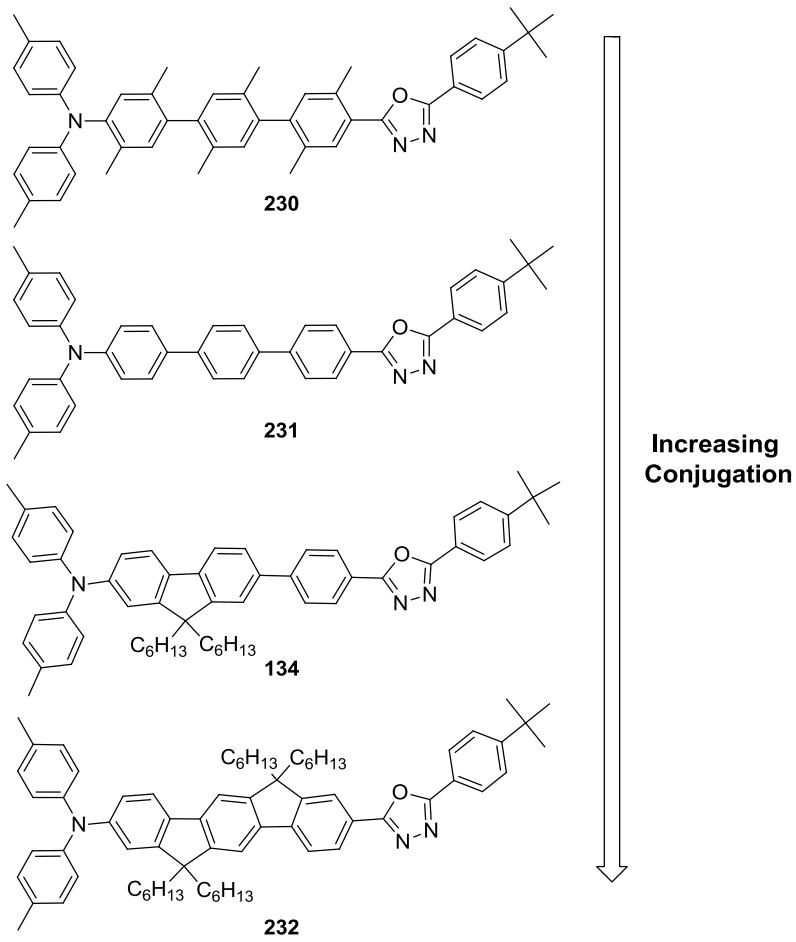

Figure 4.16 – Proposed structures of donor-acceptor wires with different levels of conjugation

4.3.1 Synthesis

Compound **134** had previously been synthesised for OLED studies (scheme 2.2).

The synthetic route to **231** was achieved by Suzuki-Miyaura cross-coupling procedures utilising key intermediate **235** and previously synthesised amine **213** and oxadiazole **158**, schemes 4.13 and 4.14.

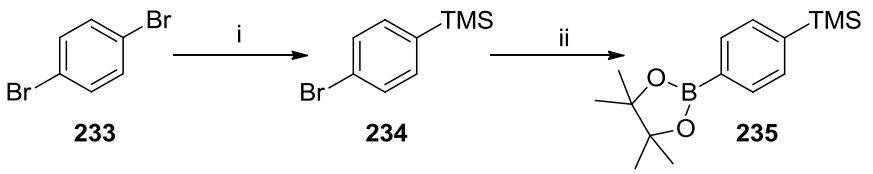

Reagents and Conditions: i) nBuLi, TMSCl, Et_2O, -78 ^oC, 4 h, 88%; ii) B_2pin_2, [$PdCl_2$(dppf)], KOAc, DMF, 80 ^oC, 15 h, 96%

Scheme 4.13 – Synthesis of key intermediate 235

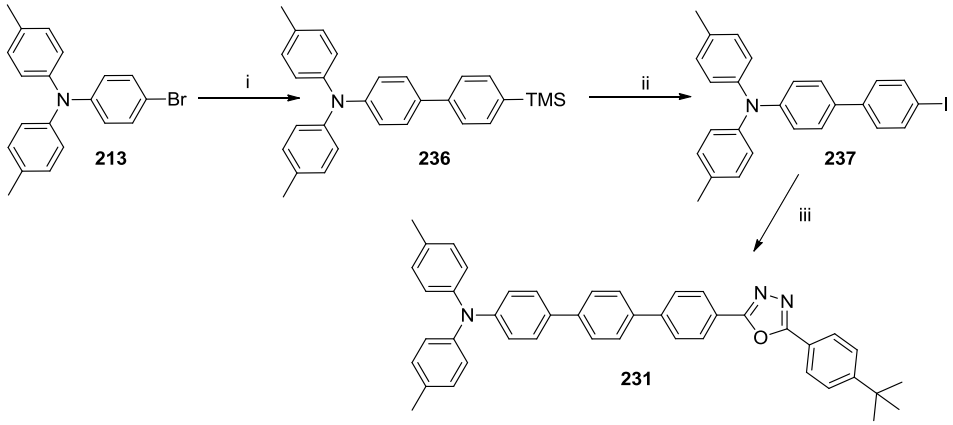

Reagents and Conditions:i) **235**, [$PdCl_2(PPh_3)_2$], NaOH (aq), THF, reflux, 15 h, 78%; ii) ICl, DCM, RT, 2 h, 100%; iii) **158**, [$PdCl_2(PPh_3)_2$], NaOH (aq), THF, reflux, 15 h, 57%

Scheme 4.14 – Synthesis of phenylene D-A wire 231

The synthesis of the out-of-conjugation materials was made more difficult by the hindered nature of the halogen due to the presence of the *ortho*-methyl groups. Initially this resulted in lower yields in cross-coupling reactions under previously used conditions and difficulty in lithiation reactions at the halogen site. By exploring a variety of different reaction conditions and altering the catalysts and ligands the reaction conditions have been optimised and the desired molecule **230** was obtained in good yield.

The synthetic routes to the twisted oxadiazole **244** and key phenyl boronic ester intermediate **246** are described in schemes 4.15 and 4.16.

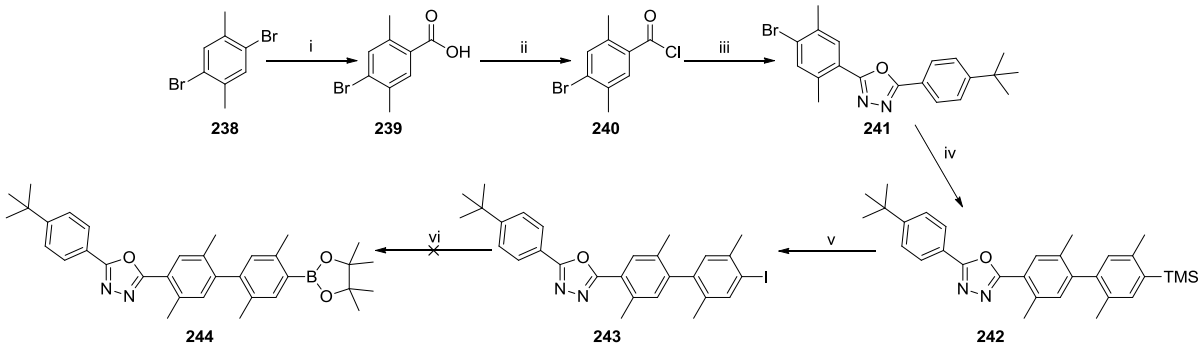

Reagents and Conditions: i) nBuLi, CO_2, Et_2O, -78 ^oC – RT then HCl (aq), 16 h, 82%; ii) $SOCl_2$, DCM, reflux, 2 h, 100%; iii) **150**, pyridine, reflux, 4 h, 56%; iv) **246**, $[PdCl_2(PPh_3)_2]$, NaOH (aq), THF, 60 ^oC, 15 h, 60%, v) ICl, DCM, 2 h, 99%; vi) B_2pin_2, $[PdCl_2(dppf)]$, KOAc, DMF, 80 ^oC, 15 h

Scheme 4.15 – Synthesis of the oxadiazole 243 and attempted borylation

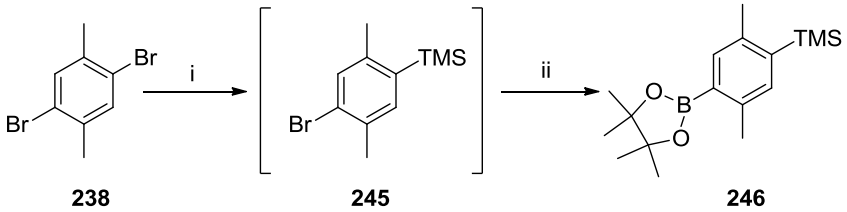

Reagents and Conditions: i) nBuLi, TMSCl, -78 ^oC – RT, 15 h; ii) B_2pin_2, $[PdCl_2(dppf)]$, KOAc, DMF, 80 ^oC, 15 h, 46% yield over both steps

Scheme 4.16 – Synthesis of key phenyl boronic acid intermediate 246

Further synthesis of the oxadiazole portion of the molecule was achieved *via* a Suzuki-Miyaura cross-coupling procedure with the intermediate **246**, scheme 4.15. Conversion of the TMS group to the iodo-analogue was almost quantitative. The Miyaura-borylation on **243** was attempted and while some of the desired product **244** was observed by ^1H NMR analysis of the crude product mixture, it could not be separated by chromatographic techniques. An alternative disconnection to obtain the boronic ester **254** of the amine portion as the coupling partner for the iodo-oxadiazole **243** was explored.

The synthesis of the twisted amine portion of the molecule proved to be less trivial. The initial plan was to couple di-*p*-tolylamine with 1,4-dibromo-2,5-dimethylbenzene as described in scheme 4.18. However, standard Buchwald-Hartwig C-N coupling conditions that had previously been employed gave only a very low yield of **247**, likely due to the steric bulk of the methyl groups *ortho* to the halogens. Yields of **247** of 11% and 15% were obtained for $Pd_2(dba)_3$/dppf catalyst systems using NaO^tBu as base without and with *tert*-butanol additive,

respectively. Using the iodo-substituted coupling partner **250** with both a ligand-mediated Ullman procedure (CuI, 1,10-phenanthroline and K_2CO_3) and under palladium catalysed conditions were also low yielding, table 4.4. Ultimately a method was found utilising a relatively cheap palladium source (10% Pd/C) that provided excellent yields for mono-reaction of C-N coupling with bromides.[118] This reaction allowed the synthesis of secondary amine **252** then tertiary amine **253**. Bromination of **253** with NBS quantitatively gave amine **247**, followed by the boronic ester **254** through a lithiation-quench procedure, scheme 4.17.

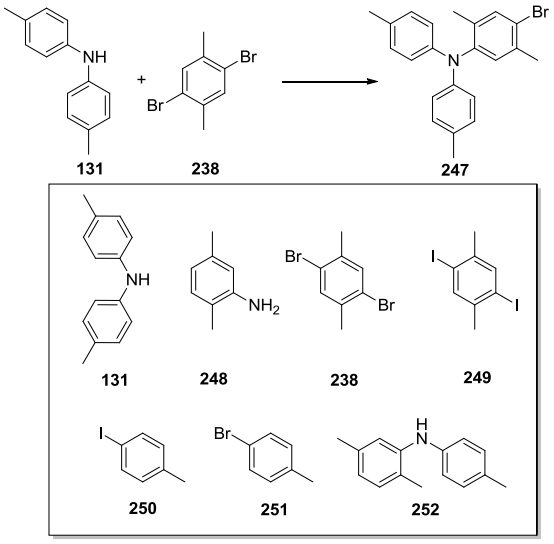

Amine	Halide	Solvent	Base	Temp (°C)	Catalyst System	2°Amine Yield (%)	3°Amine Yield (%)
131	**238**	Toluene	NaO^tBu	100	$Pd_2(dba)_3$/dppf	-	11
131	**238**	Toluene/ ^tBuOH	NaO^tBu	100	$Pd_2(dba)_3$/dppf	-	15
131	**249**	DMF	K_2CO_3	120	CuI/1,10-phenanthroline	-	5
248	**250**	Toluene	NaO^tBu		$Pd_2(dba)_3/P^tBu.HBF_4$	34	-
248	**250**	Mesitylene	NaO^tBu	160	10% Pd/C / dppf	96	-
252	**251**	Mesitylene	NaO^tBu	180	10% Pd/C / dppf	-	88

Table 4.4 – Reaction conditions and yields for C-N coupling reactions

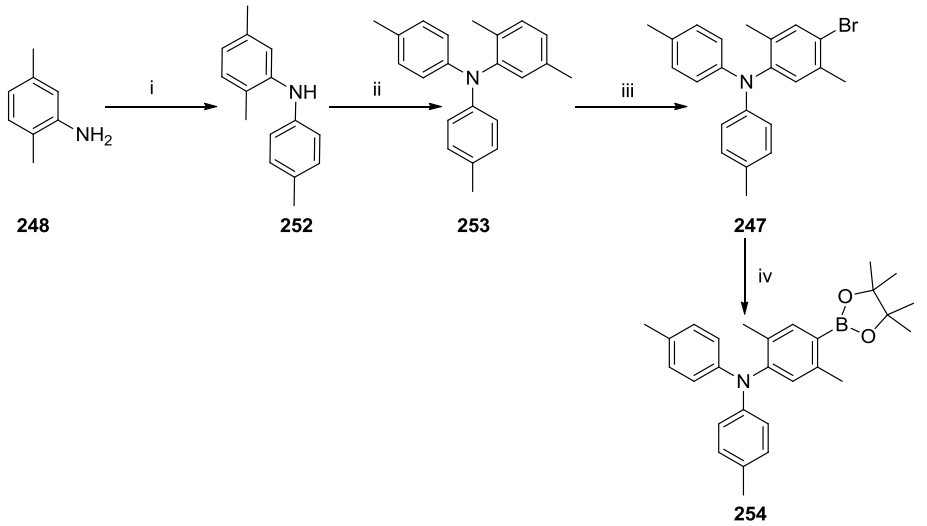

Reagents and Conditions: i) 4-iodotoluene, 10% Pd/C, dppf, NaO^{t}Bu, mesitylene, 160 ^{o}C, 24 h, 96%; ii) 4-bromotoluene, 10% Pd/C, dppf, NaO^{t}Bu, mesitylene, 180 ^{o}C, 24 h, 88%; iii) NBS, DCM, 0 ^{o}C, 1.5 h, 100%; iv) nBuLi, 2-isopropoxy-4,4,5,5-tetramethyl-1,3,2-dioxaborolane, Et_2O, -78 ^{o}C – RT, 45%

Scheme 4.17 – Synthesis of intermediate 254

The final target **230** was acquired through a Suzuki-Miyaura cross-coupling reaction of **254** and **243** in 82% yield, scheme 4.18.

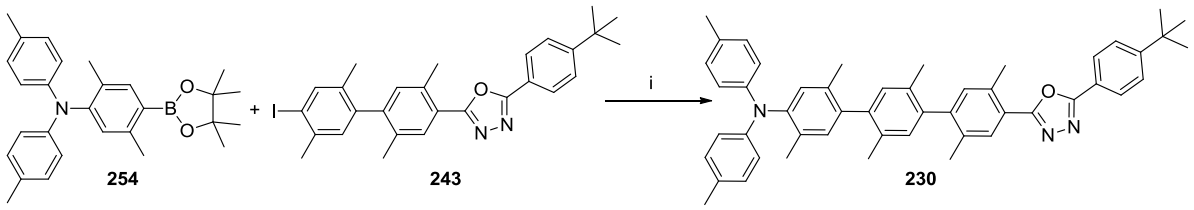

Reagents and Conditions:i) $[PdCl_2(PPh_3)_2]$, NaOH (aq), THF, 60 ^{o}C, 15 h, 82%

Scheme 4.18 – Synthesis of twisted wire 230

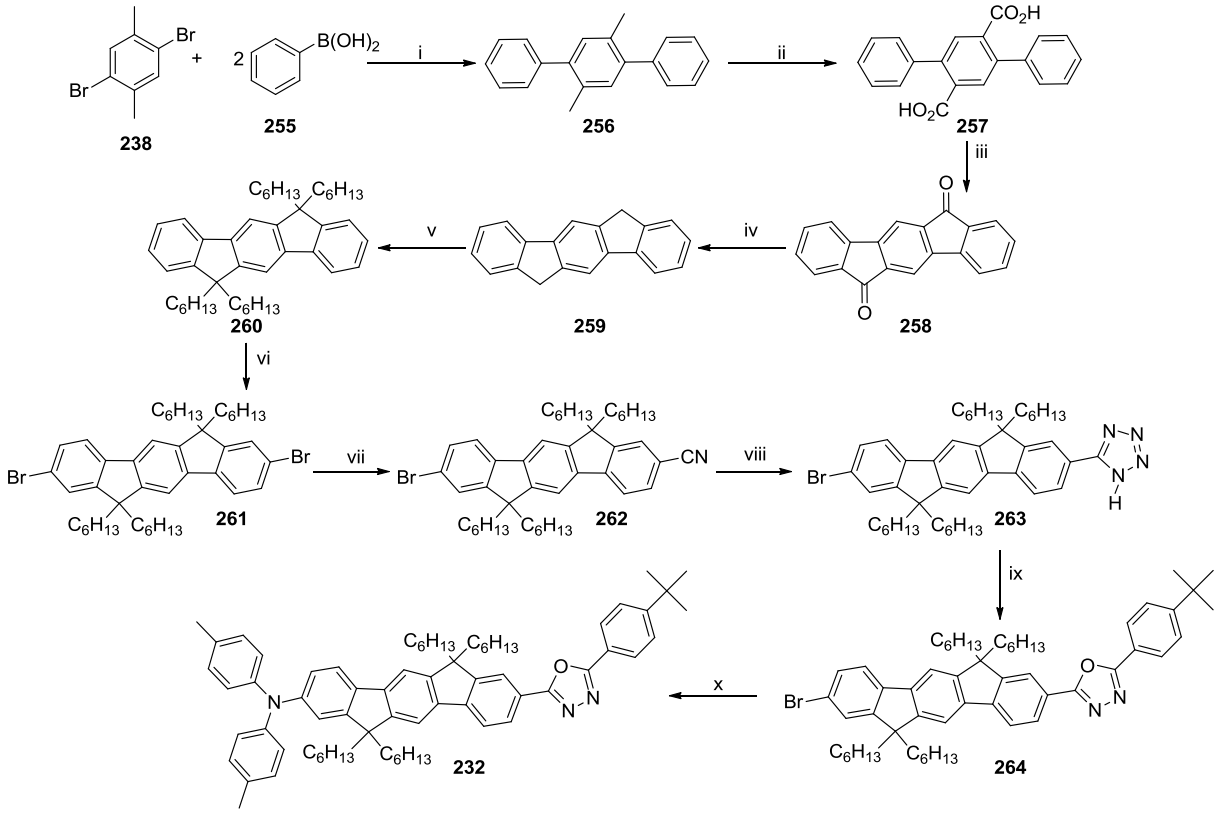

Reagents and Conditions:i) $[Pd(OAc)_2]$, K_2CO_3, nBu_4NBr, H_2O, 70 ^oC, 2 h, 68%; ii) $KMnO_4$, pyridine/H_2O, reflux, 24 h, 95%; iii) H_2SO_4, H_2O, RT, 2 h, 89%; iv) KOH, $N_2H_4.H_2O$, diethylene glycol, 180 ^oC, 20 h, 75%; v) nBuLi, 1-bromohexane, THF, -78 ^oC – RT, 20 h, 31%; vi) $FeCl_3$, Br_2, $CHCl_3$, RT, 91%; vii) CuCN, DMF, reflux, 20 h then acidified $FeCl_3$ solution, 90 ^oC, 0.3 h, 50%; viii) NaN_3, NH_4Cl, DMF, reflux, 15 h, 36%; ix) 4-*tert*-butylbenzoyl chloride, pyridine, reflux, 20 h, 96%; x) **131**, $[Pd_2(dba)_3]$, dppf, NaO^tBu, toluene, 100 ^oC, 15 h, 57% (impure product)

Scheme 4.19 – Synthesis of planarised wire 232

The proposed synthetic route for the planarised analogue **232** is outlined in Scheme 4.19, employing a literature synthesis of the ladder fluorene **260** [119] followed by a cyanation reaction to allow the formation of the oxadiazole ring directly linked to the fluorene system, scheme 4.21.

However, complete purification of the final three intermediates **262, 263** and **264** was not achieved through column chromatography. A small proportion of an unidentified fluorescent material could not be removed from **232** (NMR evidence given in experimental chapter).The R_f values of the final product **232** and the impurity **265** were very similar in various solvent systems (Rf and solvent details are given in experimental chapter) and purification was not possible. An alternative route, scheme 4.20, was undertaken to try and produce a pure sample of **232**. However, the same impurity was observed in the product mixture at the cyanation

stage and was again inseperable from the desired product **262** and the difference in R_f of **262** compared with the unsubstituted material was too small for separation by column chromatography. The synthesis of a pure sample of **232** was, therefore, not achieved.

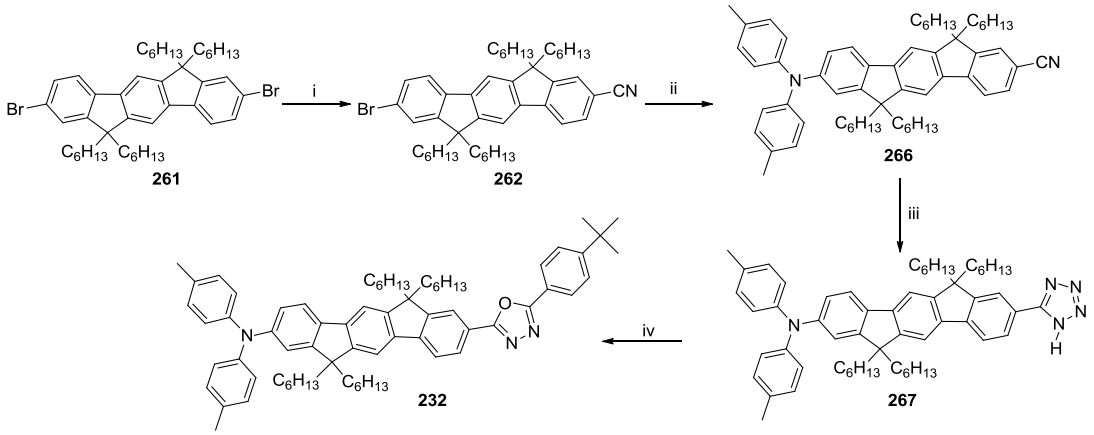

Reagents and conditions: CuCN, DMF, reflux, 20 h then acidified $FeCl_3$ solution, 90 ^{o}C, 0.3 h, 50% ii) di-*p*-tolylamine, $[Pd_2(dba)_3]$, dppf, NaO^tBu, toluene, 100 ^{o}C; iii) NH_4Cl, NaN_3, DMF reflux; iv) 4-*tert*-butylbenzoyl chloride, pyridine, reflux (impure product)

Scheme 4.20 – Proposed alternate synthesis of 232

4.3.2 Conclusions

Molecular wires based on a DPA-OPE-**OXD** structure have been synthesised by a Sonogashira protocol using orthogonally protected phenylene units. Photophysical studies of these materials demonstrate there is less efficient intramolecular energy transfer through the molecules as the wire length is increased. This is shown by evidence of a more predominant LE state in the longer molecular wires compared with the shorter molecular wires, where ICT emission is dominant even in non-polar solvents. There is evidence that as solvent polarity is increased the ICT state is dominant in the fluorescence, but low PLQYs for the molecules in polar acetonitrile also suggest the presence of significant non-radiative decay pathways. In order to gain more insight into the kind of transport occurring in these systems and the nature of the fluorescence some further measurements should be carried out including transient absorption measurements and time resolved emission spectroscopy across the entire emission spectrum with a streak camera. These measurements are underway.

Members of the series of planarised and twisted wires **134**, **230** and **231** have been synthesised *via* Suzuki-Miyaura cross-coupling procedures. The synthesis of the fully planarised wire **232** has not been achieved due to difficulties in purification. An alternate route should be

undertaken in future work in order to obtain the material at the required purity. It appears that the impurity is appearing at the cyanation stage, so an alternative route with cyanation at a later stage after the C-N bond forming reaction may be successful. With the full series in hand photophysical studies of the molecules can be pursued.

Chapter 5: Donor-Acceptor Compounds for Dye Sensitised Solar Cells

5.1 Introduction

Currently, one of the most promising and intensely researched areas in molecular electronics is that of light-harvesting materials to be used in organic photovoltaics (OPVs). Solid-state silicon solar cell technology is currently dominant in the marketplace, but the promise of low-cost fabrication of cells based on molecular, nanocrystalline or polymeric materials presents real competition. Their potential to produce coloured, transparent or flexible cells allows for more choice and integration than in current technology. A promising class of OPV is the dye sensitised solar cell (DSSC) which is currently the subject of vigorous research.[120-122]

The first efficient DSSC was reported by O'Reagan *et al.* in 1991, based on a nanocrystalline TiO_2 semiconductor sensitised by ruthenium complex **268** (figure 5.1) with an iodide – triiodide electrolyte.[123] The devices achieved power conversion efficiencies (PCE) - the incident photon to current conversion efficiency - of over 7%. The basis of a DSSC, shown in figure 5.1, is the photoexcitation of a dye material adsorbed on a semiconductor (usually TiO_2), which injects an electron into the conduction band of the semiconductor material. Charge transfer occurs through the semiconductor and the excited dye material is reduced to its original state by the electrolyte solution. The reason this process works is the limitation of back electron transfer processes which can be explained by the different lifetimes of the various electron transfer processes. This has been investigated in some detail by various groups.[111,112,124-127]

The work in this chapter focusses on the design of the molecular dye material used within the solar cell. There are many factors which may affect the efficacy of a dye in a DSSC. The dye should bind strongly to the TiO_2 nanoparticles *via* an anchoring group, typically a carboxylate or similar group, and it must strongly absorb solar radiation. The dye must also be able to inject charge into the TiO_2 through its LUMO and have a HOMO of an appropriate energy to be easily reduced by the hole-transport material once the dye is oxidised.

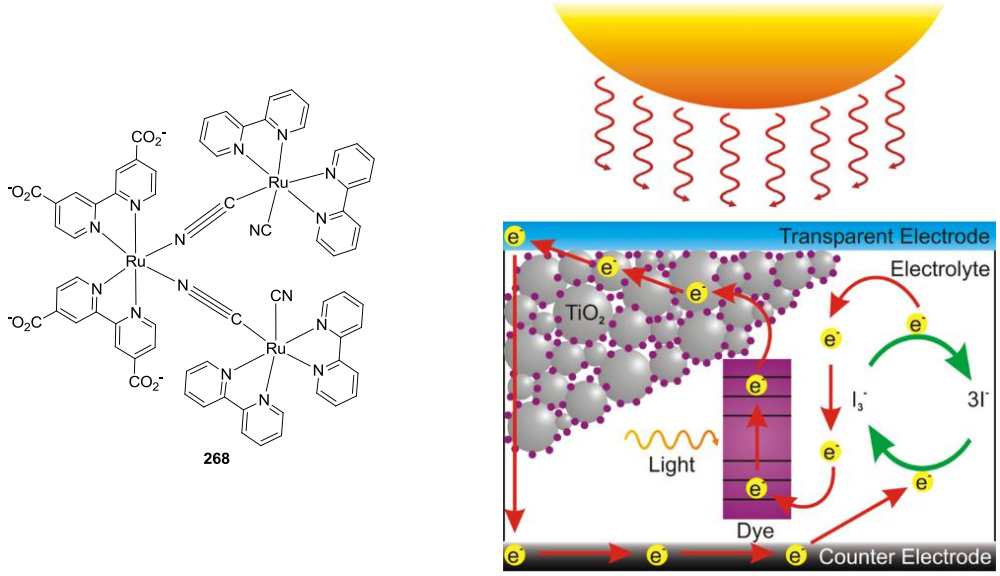

Figure 5.1 - Structure of 268 and working principles of a DSSC[128]

One advantage of all-organic dye materials is that they may easily achieve very high molar extinction coefficients compared with metal complexes. An indoline based organic dye **269**, figure 5.2, achieves an extinction coefficient of 68,700 mol^{-1} cm^{-1} at 526 nm, compared with 13,900 mol^{-1} cm^{-1} at 541 nm for the conventional ruthenium dye N-719, **270**.[120,121,129] Another advantage of the all-organic sensitisers is that their relative cost is potentially lower than complexes containing rare metals. It is also possible to control molecular design so as to manipulate spectral coverage in the materials' absorbance.

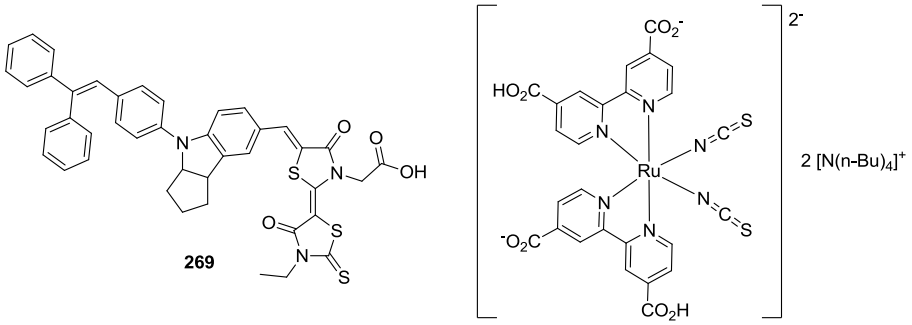

N-719
270

Figure 5.2 - Structures of dyes 269 and 270

Baheti *et al.* discuss the importance of the linker in D-A organic dye molecules to provide separation of the HOMO on the donor, and the LUMO, on the acceptor.[125] This separation improves the intramolecular charge separation, hindering unwanted charge recombination during device operation. They investigated different linkers in a DPA-linker-cyanoacrylic acid

motif, figure 5.3. Improved device characteristics were observed in the fluorene-based dyes compared with the biphenyl analogues. This was attributed to both a larger absorption extinction coefficient in the **F**-based dyes **272a** and **272b** and also to more efficient intramolecular charge transfer resulting in more efficient charge separation in the **F** materials.[125]

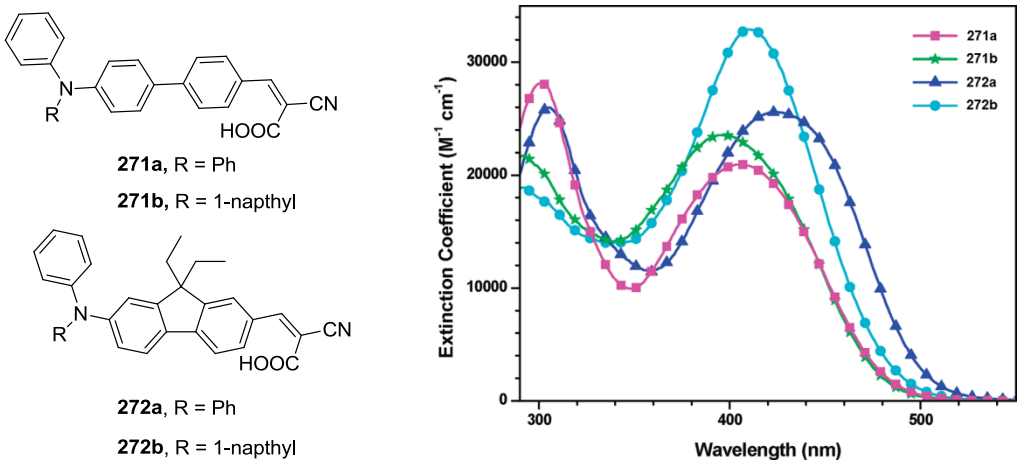

Figure 5.3 - Structure of dyes based on a fluorene or biphenyl linker and their absorption spectra in dichloromethane solution and molar extinction coefficients[125]

To investigate further the effect of changing the spacer furan was incorporated adjacent to the linker, compound **273**, figure 5.4.[130] Thiophene linkers have been shown to improve device efficiency compared with phenyl analogues as thiophene lowers the energy barrier to the charge transfer transition due to its smaller resonance energy barrier; the furan moiety is expected to show this effect. The dye **273** exhibited good power conversion efficiencies of 7.36%, comparable to those of a device containing N-719.[130]

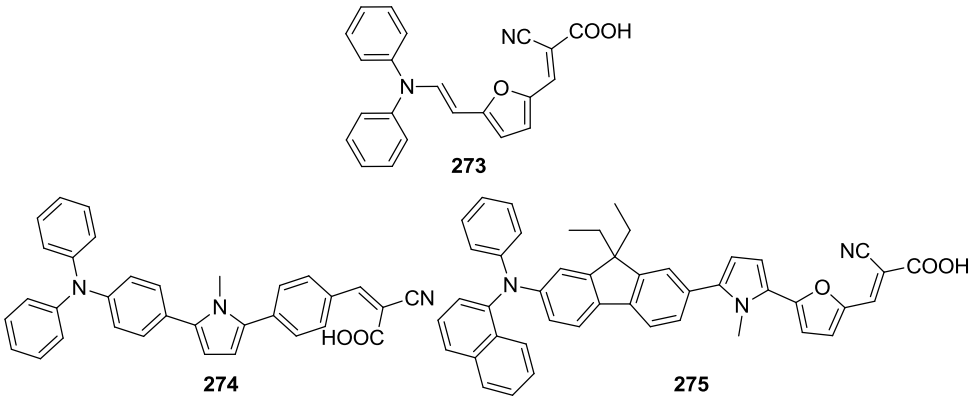

Figure 5.4 - Structure of dye materials 273, 274 and 275

Yen *et al*. introduced an electron rich spacer, pyrrole, into their dye materials **274** and **275**, figure 5.4.[127] The advantage of such a spacer is the potential to red-shift the absorbance of the

material and also to improve charge separation in the excited state due to limited interaction with neighbouring aromatic units due to larger dihedral angles between the pyrrole and neighbouring groups. The compound **274** achieved a power conversion efficiency of 6.18% in cells with TiO_2 semiconductor, I^-/I_3^- electrolyte and platinum electrodes.[127]

Incorporation of long aliphatic chains to dye molecules has been shown to be effective in preventing unwanted charge recombination. This has been demonstrated by Hagberg *et al.* and Tsai *et al.* who incorporated methoxy substituents or long alkyl chains in close proximity to the donor portion of the dye resulting in improved device characteristics.[106,107] It is proposed that such substitution may help to prevent unwanted recombination of electrolyte with electrons injected into the TiO_2.

Recently Grätzel and co-workers incorporated a donor-π-acceptor based dye **276b**, figure 5.5 into a cell using a Co(II)/Co(III) electrolyte. This electrolyte has a higher reduction potential than iodide based electrolytes, this means that less voltage is lost upon regeneration of the sensitiser. In addition there were many design features of the dye that act to improve its characteristics for DSSCs. The long alkyl chains may help to prevent unwanted charge recombination processes. The zinc porphyrin unit helps to give the dye a very high extinction coefficient and to absorb strongly over the whole visible spectrum with high internal power conversion efficiencies (IPCE) at most wavelengths, figure 5.5. These improvements resulted in a record power conversion efficiency of over 12%.[131]

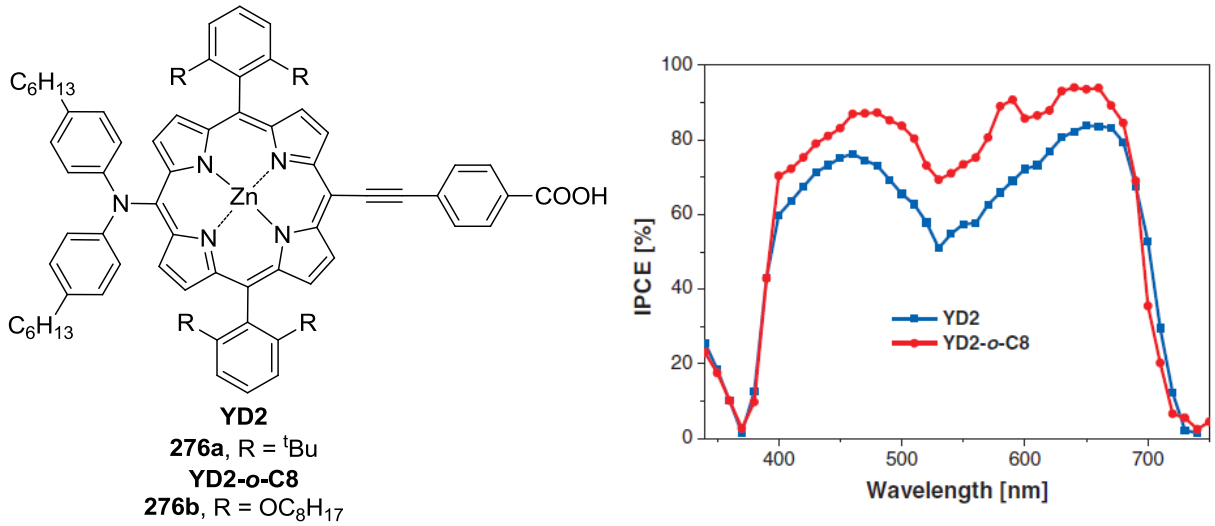

YD2
276a, R = ^{t}Bu
YD2-*o*-C8
276b, R = OC_8H_{17}

Figure 5.5 - Structure of dye 276a and b and plot of IPCE over the visible spectrum

5.2 Results and Discussion

5.2.1 Synthesis

The proposed materials for this study were based upon a donor-linker-acceptor-anchoring group structure, figure 5.7. The materials are based on those we had used in OLEDs previously (Chapter 2) and were designed to probe the effect of altering the anchoring group of the dye on the DSSC performance. In addition, we observe that the vast majority of solar cell candidates are geared towards the absorption of the entire solar spectrum which results in the dyes being very strongly coloured materials. We recognised that molecules that absorb more in the blue region of the spectrum offer the potential to fabricate transparent devices that may be used for a number of desirable applications.

1,3,4-Oxadiazoles have to our knowledge only been used in one other study as constituents of dye materials for DSSCs.[132] Devices using the materials (figure 5.6) achieved PCEs of between 2.79% and 3.21% indicating that materials using an **OXD** acceptor in conjunction with an arylamine donor and suitable anchoring group may be suitable for DSSC applications. Our molecules also include a fluorene moiety, which should improve the molar extinction coefficients of the materials compared with those in this study, as demonstrated in chapter 2.

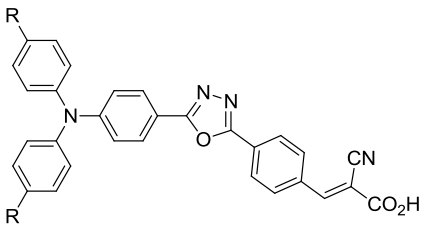

R = H, Me, C_2H_5, $C(CH_3)_3$, OMe

277

Figure 5.6 – Structure of 277

The choice of anchoring groups to investigate was made upon the basis of precedent for the cyanoacrylic acid,[125,132] carboxylic acid,[129,131] and catechol[133] anchoring groups to successfully bind to TiO_2 in DSSCs. In addition to investigating the effect of using these groups we wanted to explore the potential of a benzyl alcohol and cyano anchoring groups in DSSCs.

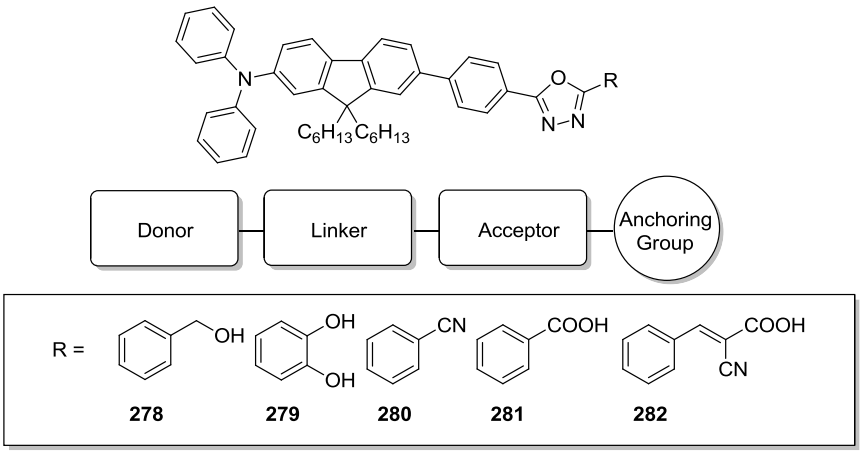

Figure 5.7 – Structure of target molecules for DSSC applications

Our initial route for the synthesis of the various DSSC candidates is shown in scheme 5.1. Monosubstitution of dibromohexylfluorene **55** *via* a Buchwald-Hartwig amination procedure followed by a Suzuki-Miyaura cross-coupling reaction with 4-benzonitrile boronic ester (**284** – see experimental chapter for details) coupling partner gave intermediate **285**. Reaction of this intermediate with sodium azide and ammonium chloride produced the key tetrazole intermediate **286**. Our aim was to react **286** with a variety of acid chlorides to produce the desired DSSC candidates. However, synthesis of the catechol acid chloride **288a** proved difficult. At room temperature the reaction of thionyl chloride with the catechol acid gave a complex mixture of products. An alternative reaction with the methoxy substituted acid gave no reaction with thionyl chloride at room temperature or at reflux, scheme 5.2. In parallel an alternative synthetic route was being carried out which proved to be more satisfactory, so this route was abandoned.

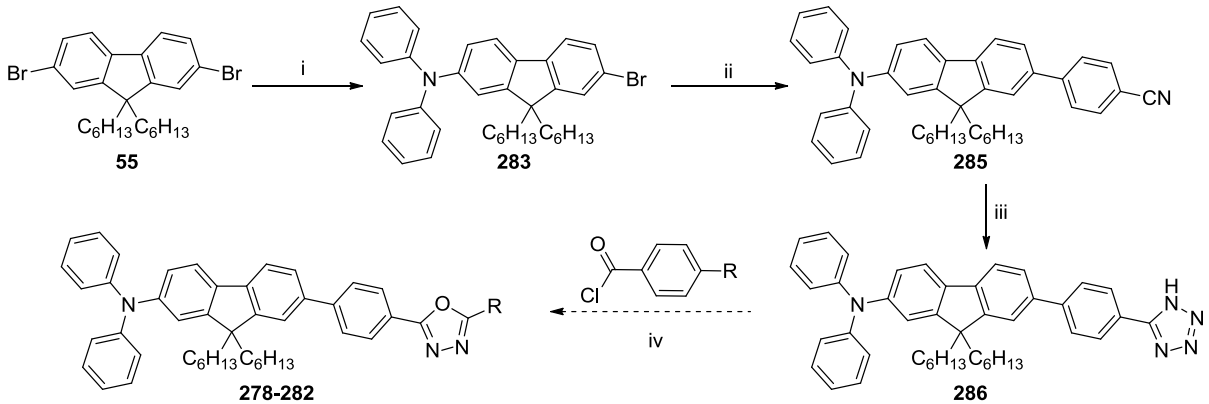

Reagents and Conditions: i) diphenylamine, NaO^{t}Bu, 10% Pd/C, dppf, mesitylene, 160 ^{o}C, 15 h, 29%; ii) **284**, $[PdCl_2(PPh_3)_2]$, NaOH (aq), THF, 65 ^{o}C, 15 h, 72%; iii) NH_4Cl, NaN_3, DMF, reflux, 24 h, 57%; iv) pyridine, reflux, 5 h

Scheme 5.1. – Proposed synthetic route to DSSC candidates

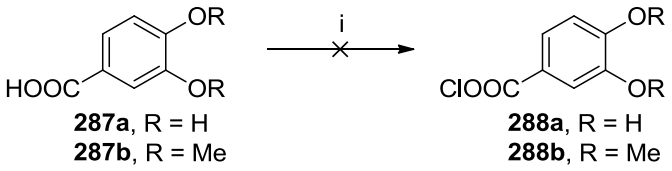

287a, R = H
287b, R = Me

288a, R = H
288b, R = Me

Reagents and Conditions: i) $SOCl_2$, DCM/THF, RT – reflux

Scheme 5.2 – Attempted synthesis of acid chlorides 287a and 288b

The alternative route adopted was to synthesise **283** as in scheme 5.1 and couple this with an appropriate oxadiazole boronic ester. Oxadiazole boronic esters have previously been synthesised *via* a Miyaura-borylation procedure in excellent yields (chapter 2, **158**).

Scheme 5.3 shows the synthesis of compound **278** with a terminal benzyl alcohol group. The original intention was to brominate the oxadiazole **291** to produce **292** which could then be functionalised further in that position. However, the Miyaura-borylation of **292** gave the unexpected product **293** in 66% yield, due to substitution of the benzyl bromide with an acetate group, derived from the potassium acetate base. This reactivity was used advantageously in the last step, where a hydroxide base was used to substitute again at the benzyl position to achieve the desired benzyl alcohol product **278** in 76% yield.

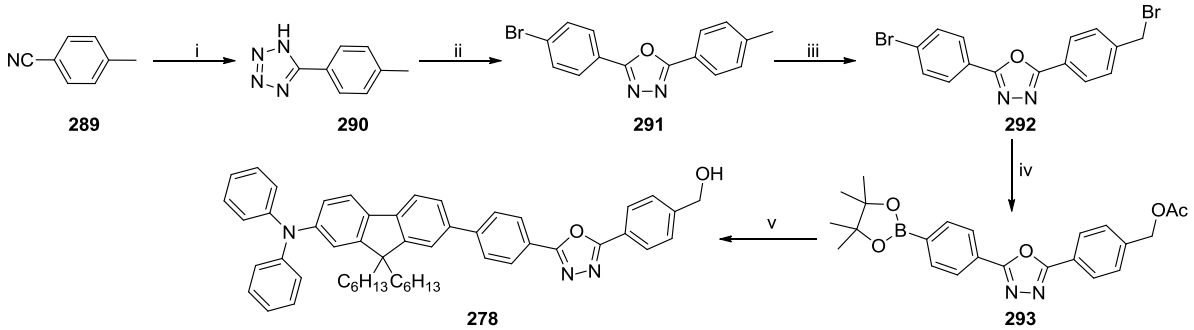

289 **290** **291** **292** **293** **278**

Reagents and Conditions: i) NH_4Cl, NaN_3, DMF, reflux, 15 h, 91%; ii) 4-bromobenzoyl chloride, pyridine, reflux, 72 h, 57%; iii) NBS, benzoyl peroxide, 1,2-dichloroethane, 70 ^oC, 15 h, 48%; iv) B_2pin_2, [$PdCl_2$(dppf)], KOAc, DMF, 80 ^oC, 15 h, 66%; v) **283**, [$PdCl_2(PPh_2)$], NaOH (aq), THF, 65 ^oC, 76%

Scheme 5.3 – Synthesis of 278

Our proposed route to compound **279** with a terminal catechol group was *via* protection of the alcohol groups by benzyl groups. These were removed in the last step by catalytic hydrogenation with palladium on carbon and hydrogen gas to give **279**, scheme 5.4. However, the final catechol product was found to be insoluble and therefore not purified successfully by column chromatography and was unsuitable for further study.

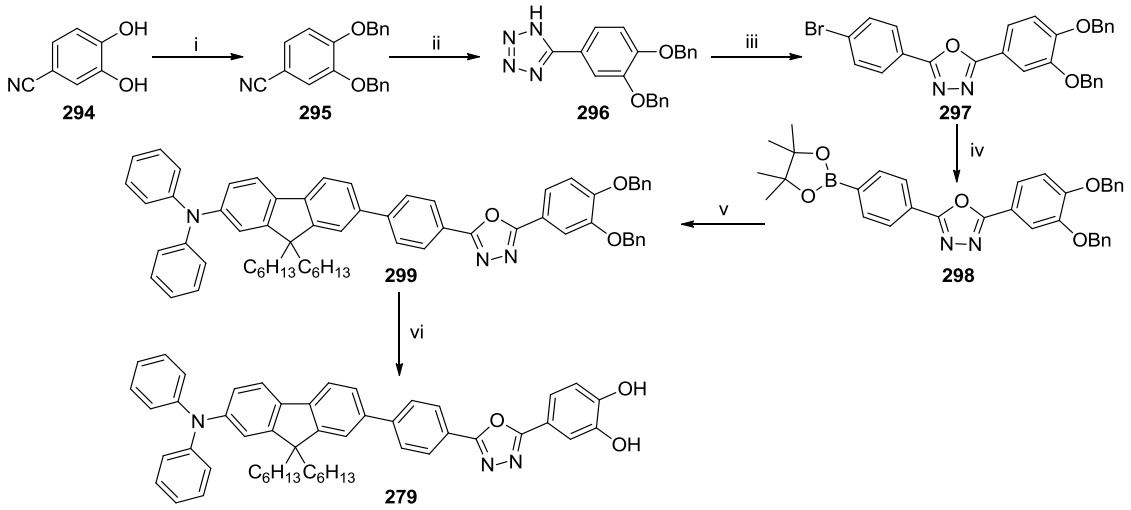

Reagents and Conditions: i) benzyl bromide, potassium carbonate, DMF, 120 ^{o}C, 20 h, 100%; ii) NH_4Cl, NaN_3, DMF, reflux, 20 h, 32%; iii) 4-bromobenzoyl chloride, pyridine dried over KOH, reflux, 15 h, 24%; iv) B_2pin_2, $[PdCl_2(dppf)]$, KOAc, DMF, 80 ^{o}C, 15 h, 59%; v) **283**, $[PdCl_2(PPh_3)_2]$, NaOH (aq), THF, 65 ^{o}C, 15 h, 98%: vi) 10% Pd/C, H_2 (g), THF, RT, 15 h

Scheme 5.4 – Synthesis of 279

The formation of other oxadiazoles bearing the nitrile, carboxylic acid or cyanoacrylic acid anchoring groups was not possible directly through the procedures previously adopted in chapters 2 and 3. It was found that the oxadiazole forming stage of the reaction was unsuccessful in the presence of a strongly electron withdrawing group on the tetrazole reagent, scheme 5.5. This can be explained by the resonance canonical form of **300b** shown in scheme 5.5, illustrating the reduced nucleophilicity of the tetrazole species by delocalisation of the anion.

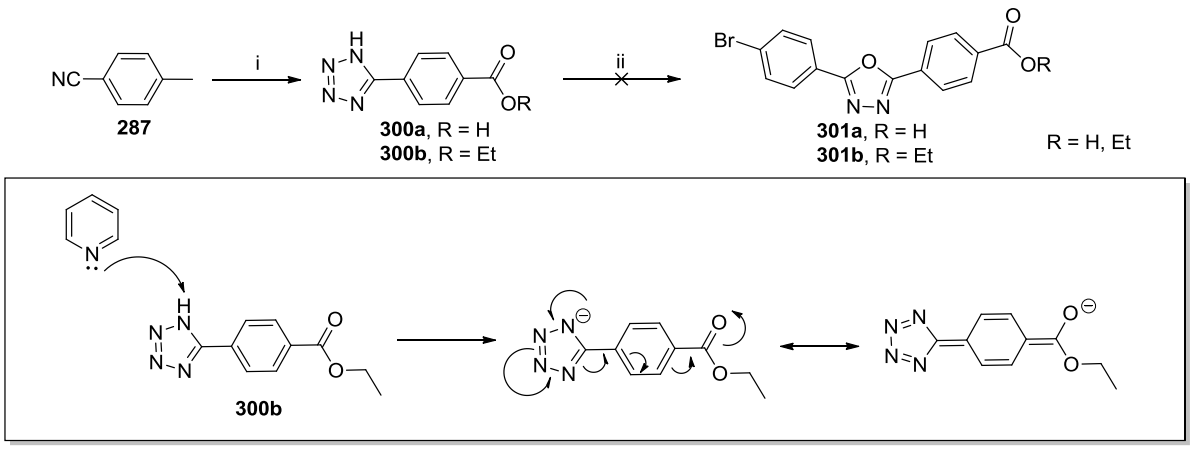

Scheme 5.5 – Attempted synthesis of 301 and resonance canonical forms of tetrazole reducing nucleophilicity of the anion

This lack of reactivity of **300** meant that an alternative route to the required oxadiazoles was devised *via* coupling of a hydrazide with an acid chloride using a peptide coupling agent TBTU. Scheme 5.6 shows a successful test reaction to obtain **305**.

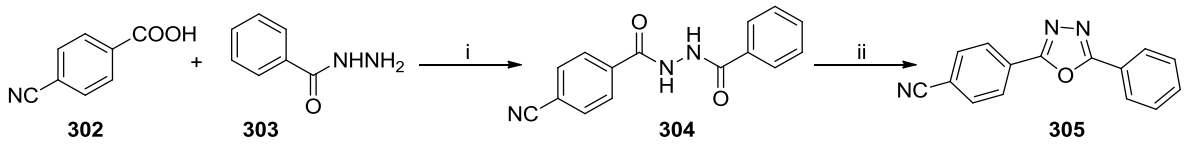

Reagents and Conditions: i) TBTU, THF, DIPEA, RT, 0.75 h, 56%; ii) $POCl_3$, reflux, 15 h, 79%

Scheme 5.6 – Test synthesis of a cyanophenyl oxadiazole

The success of this test reaction led to the synthesis of the cyano-functionalised material, **280** shown in scheme 5.7. Subsequently the terminal cyano group of **280** was converted to the carboxylic acid analogue **281** by reaction with aqueous potassium hydroxide.

The final dye candidate was **282** substituted with a cyanoacrylic acid anchoring group (Scheme 5.8). The alcohol of **278** was oxidised to the aldehyde **309** with PCC. Compound **309** was then converted to **282** by the Knoevenagel condensation using cyanoacetic acid.

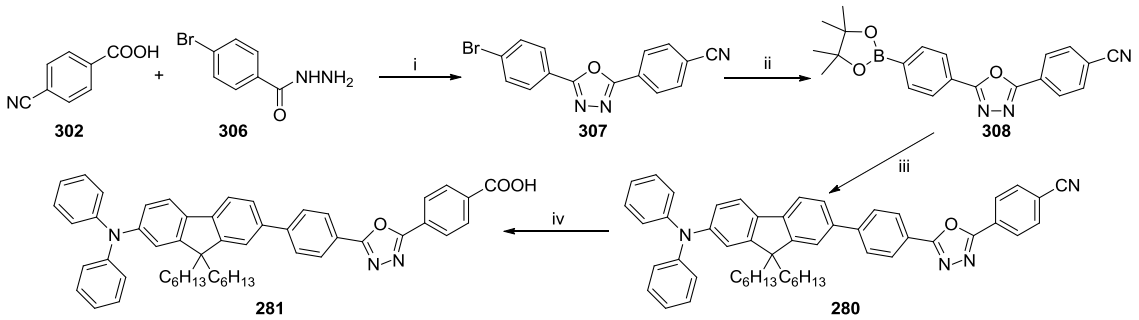

Reagents and Conditions: i) TBTU, THF, DIPEA, RT, 24 h, then $POCl_3$, reflux 12 h, 16%; ii) B_2pin_2, $[PdCl_2(dppf)]$, KOAc, DMF, 80 ^oC, 15 h, 51%; iii) **283**, $[PdCl_2(PPh_3)_2]$, NaOH (aq), THF, 65 ^oC, 33%; iv) KOH (aq), $EtOH/H_2O$, reflux, 15 h, then HCl (aq), 57%

Scheme 5.7 – The synthesis of the nitrile and carboxylic acid derivatives 280 and 281

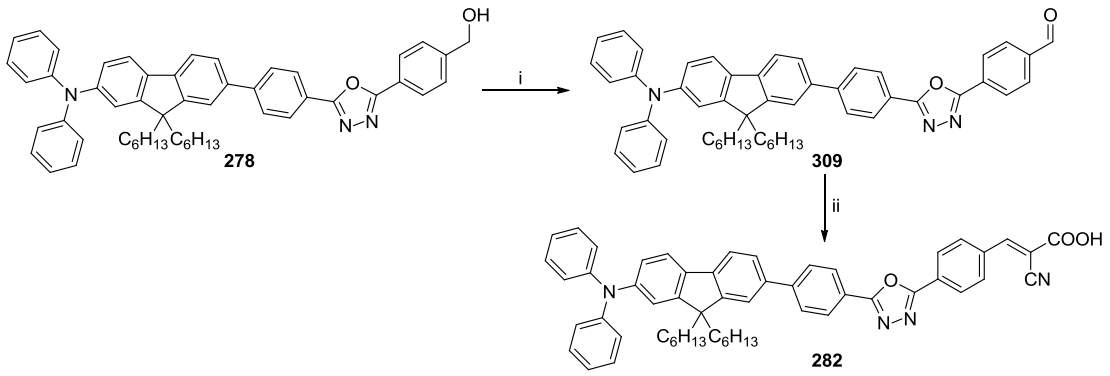

Reagents and Conditions: i) PCC, DCM, RT, 1 h, 60%; ii) cyanoacetic acid, NH_4OAc, AcOH, reflux, 15 h, 50%

Scheme 5.8 – Synthesis of 282

Characterisation by ^1H NMR spectroscopy of the dyes which contained a very polar anchoring group was hindered by aggregation of these materials in some solvents. The hydrophilic head group and hydrophobic body of the dye, particularly the long hexyl chains, result in a structure with surfactant-like features. This was particularly evident with the cyanoacrylic acid derivative **282**. The ^1H NMR spectrum of **282** in deuterated chloroform, Fig. 5.8a, acetone, dichloromethane or toluene resulted in very broad peaks. When **282** was dissolved with a very polar solvent, CD_3OD, with CS_2 as a co-solvent (to improve solubility) the spectrum was resolved, figure 5.8b. This can be attributed to increased intermolecular interactions of the anchoring group with the polar CD_3OD disrupting micelle formation of **282**. The same effect was observed with the acid and catechol substituted dyes **279** and **281**. The broadening of the carbon NMR spectra of the same compounds was less problematic in $CDCl_3$ due to the larger difference between shift values in the sample.

5.2.2 Thin Films

Thin-film studies were carried out with assistance from Dr Mateusz Wielopolski at the École Polytechnique Fédérale de Lausanne (EPFL) in Professor Jacques Moser's laboratory. Absorption spectroscopy of thin films is a standard technique used to determine whether a dye successfully binds to the nanocrystalline TiO_2. The four materials, **278**, **279**, **281** and **282** were used to form films. However, only the dyes **281** and **282** with the carboxylic acid and cyanoacrylic acid anchoring groups, respectively, were found to bind to the TiO_2, observed by a shift of the absorption spectrum compared to pristine TiO_2, figure 5.10. This meant that of the series **278** – **282** only **281** and **282** would be suitable for the fabrication of DSSCs.

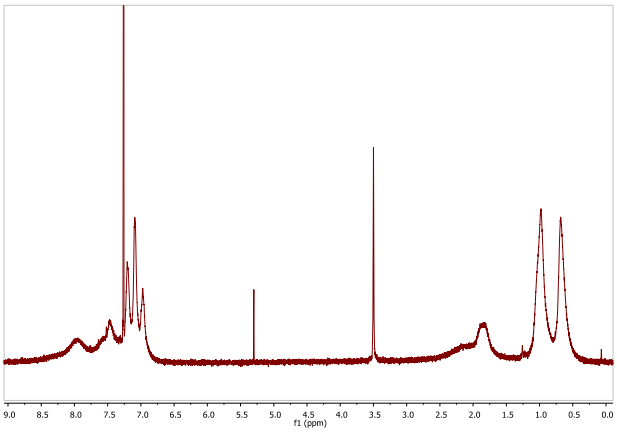

a) ^{1}H NMR spectrum of **282** in $CDCl_3$

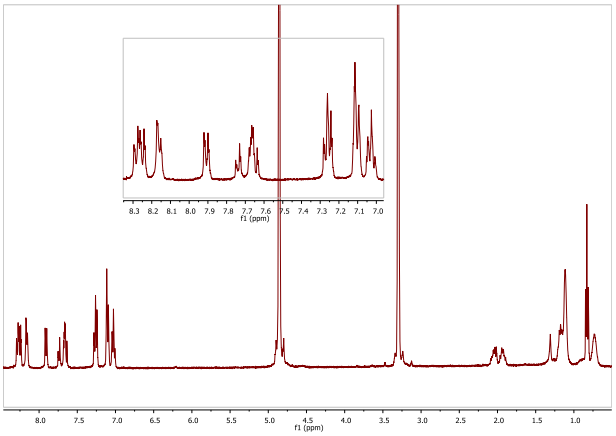

b) ^{1}H NMR spectrum of **282** in CD_3OD/CS_2, inset, expansion of aromatic region

Figure 5.8 – NMR spectra of 282 in different solvents

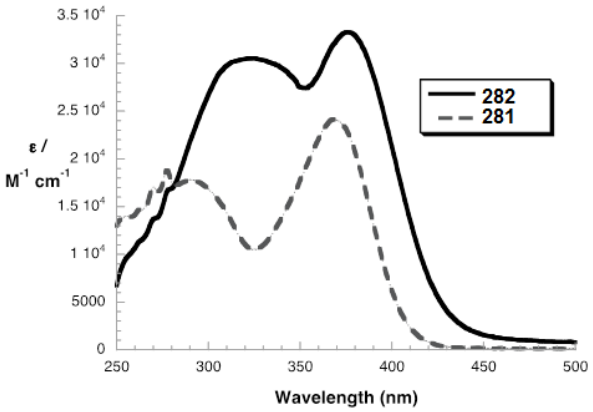

Figure 5.9 – Absorption spectra of 281 and 282 in a ^{t}BuOH/MeCN solution.

Figure 5.9 shows the absorption spectra of the two investigated dyes **281** and **282** in 1:1 MeCN : ^{t}BuOH solution. The absorption of **282** is significantly red-shifted to 470 nm (red edge of the absorption) compared with **281** which absorbs up to 435 nm, which implies a slightly more extended π-conjugation in **282**. In both dyes the two broad maxima (**282**: λ_{max} 325 nm and 385 nm; **281** λmax 295 nm and 370 nm) correspond to π-π* charge transfer (CT) absorptions of the triphenylamine (TA) / fluorene (F) moieties with relative shifts that correlate with the length of the π-conjugation as mentioned above. The extinction coefficients are 3.3 x 10^4 M^{-1} cm^{-1} and 2.3 x 10^4 M^{-1} cm^{-1} for **282** and **281**, respectively at their absorption maxima.

In order to study their applicability for photovoltaic devices, both dyes **281** and **282** were adsorbed on 5 µm thick transparent TiO_2 films. Figure 5.10 shows the corresponding absorption spectra after 16 h dye loading on TiO_2. The spectral changes as compared with bare TiO_2 corroborate the adsorption of the two dyes onto the semiconductor surface. **281** exhibits a significant red-shift of its absorption edge by almost 30 nm due to the interaction with TiO_2. This suggests a shift of charge density from the dye to TiO_2 upon adsorption and a simultaneous extension of the π-conjugation. In **282** the absorption is blue-shifted upon adsorption and a broad shoulder develops between 315 and 360 nm which makes the film nearly transparent.

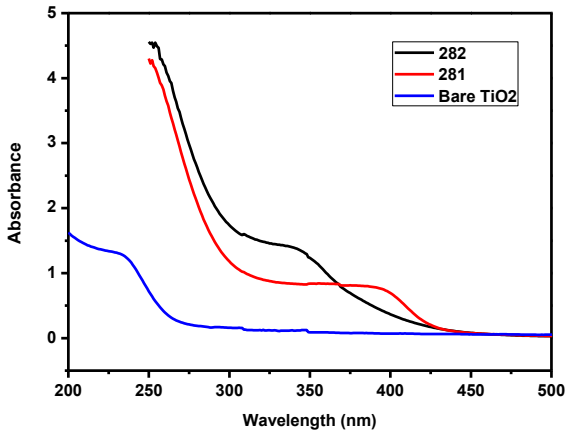

Figure 5.10 – Absorption spectra of bare TiO_2 film and 281 and 282 on 5 µm thick TiO_2 films.

5.2.3 Time resolved spectroscopy

Photophysical analysis of solution and thin films of **281** and **282** was carried out at the EPFL in Professor Jacques Moser's laboratory with assistance from Dr Mateusz Wielopolski. Photophysical analysis served to ascertain the suitability of these materials as candidates for dyes in DSSCs. In order to probe the charge transfer properties of the dyes and their kinetics in solution and as adsorbed on TiO_2 we employed various time-resolved spectroscopic techniques.

For a comparative study and to gain a complete image of all processes involved in the charge transfer from the dye to the semiconductor we also investigated the reference systems **278** and **280** as well as **281** and **282**. The cyano anchor in **280** has only very weak electron accepting properties, whereas the hydroxyl anchor in **278** lacks them compared with the other dyes **281** and **282**. Hence, important conclusions about the spectroscopic fingerprints of the excited state species can be drawn from the femtosecond transient absorption spectra of the solutions of **278** and **280**.

Photoexcitation of **278** leads only to the population of the singlet excited state, whereas the electron accepting features in **280** cause photoexcitation to result in a charge separated state. In line with this hypothesis, the transient absorption spectrum of a solution of **278** clearly resembles the features of the photoinduced singlet excited state of the fluorene moiety. The singlet excited state forms immediately after laser excitation and is identified by a small shoulder at 480 nm and a broad maximum between 550 and 700 nm, Figure 5.10. The deactivation of the singlet excited state occurs following first order kinetics with a rate of k_S = 4.6×10^9 s^{-1}. However, **280** exhibits a transformation of the singlet features on a 1 ps timescale (k_2 = 1.5×10^{12} s^{-1}) into those of a radical cation of the arylamine, which corresponds to the broad maximum between 470 and 580 nm, and a sharper peak at 670 nm, figure 5.11. The cation radical decays with very fast kinetics (k_{CR} = 4.3×10^{10} s^{-1}) on a timescale of less than 30 ps in solution. The broad spectral shape of the radical cation stems from the conjugation of the donor into the bridge allowing delocalisation of the positive charge upon oxidation of the arylamine.

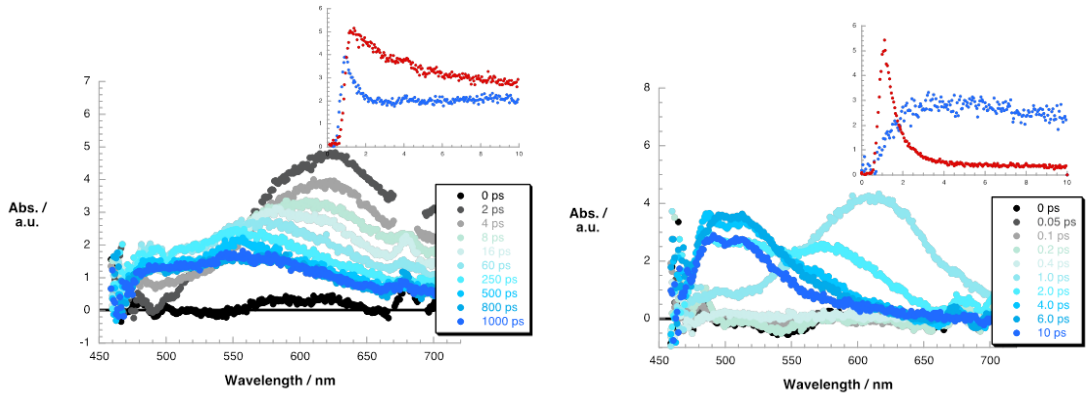

Figure 5.11 – Differential absorption spectra obtained upon femtosecond flash photolysis (λ_{exc} = 400 nm) of tBuOH/MeCN (1:1 v/v) solutions of (left) 278 and (right) 280 with several time delays at room temperature. Insets: corresponding time profiles illustrating the kinetics of the signals at different wavelengths (left – blue: 550 nm, red: 630 nm; right – blue: 480 nm, red: 610 nm).

The femtosecond transient absorption spectra of the solutions of **281** and **282**, figure 5.12, exhibit the same fingerprints as mentioned above. In **282** with the strong cyanoacrylate acceptor the singlet features transform into the corresponding radical ion pair features on a time scale of less than 2 ps (k_S = 1.2 x 10^{12} s^{-1}). The latter decay with dynamics following first order kinetics with a rate similar to **280** (k_{CR} = 5.0 x 10^{10} s^{-1}). In **281**, on the other hand, the singlet features vanish more slowly (k_S = 5.8 x 10^9 s^{-1}) and the corresponding radical cation signature does not evolve.

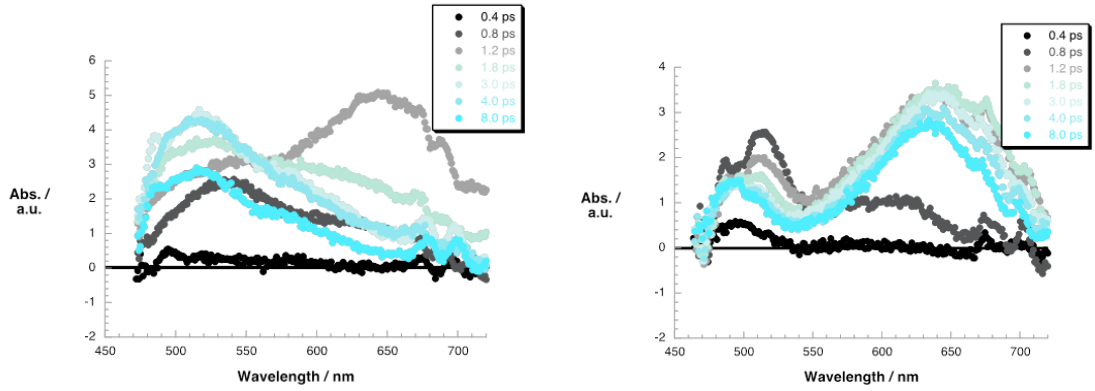

Figure 5.12 – Differential absorption spectra obtained upon femtosecond flash photolysis (λ_{exc} = 400 nm) of tBuOH/MeCN (1:1) solutions of 282 (left) and 281 (right) with several time delays at room temperature.

It has been observed that **282** binds to the electron acceptor TiO_2 and the process of charge injection into the conduction band of the semiconductor occurs extremely quickly. After 0.6 ps the signature of the oxidised state is observable in the spectrum figure 5.12a. After 300 ps this charge injection is followed by a decay ($\tau_{1/2}$ = 168 ps) to 60% of the initial intensity, which then

remains constant on the timescale of the experiment (1100 ps). The electron injection into **281** occurs on a slightly slower timescale due to a lower electron affinity of the carboxylic acid anchor compared with the cyanoacrylate of **282**. In contrast to **282**, the formation of the singlet excited state is the initial observable state for **281**, figure 5.13b. The singlet state then transforms to the oxidised arylamine cation on an 8 ps timescale, which then behaves similarly to **282**.

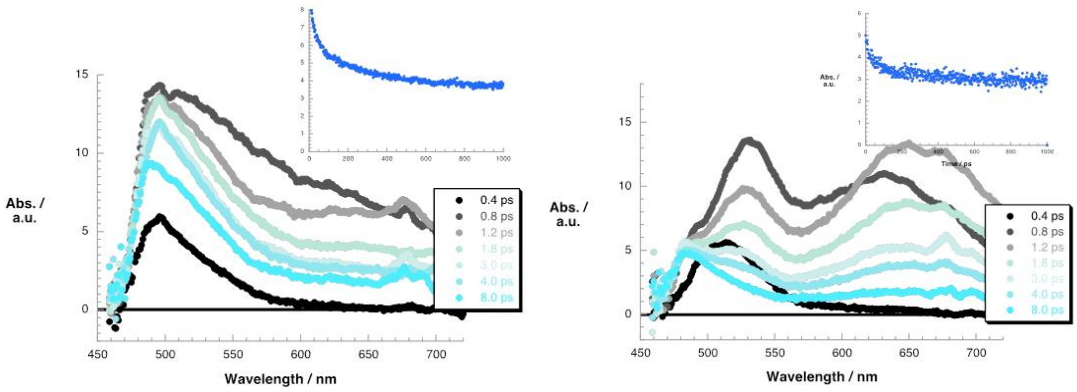

Figure 5.13 Differential absorption spectra obtained upon femtosecond flash photolysis (λ_{exc} = 400 nm) of 282 (left) and 281 (right) on 5 µm thick TiO_2 with several time delays at room temperature. Insets: corresponding time profiles illustrating the kinetics of the signals at 490 nm.

To probe the kinetics of dye regeneration and charge recombination complementary nanosecond flash photolysis studies were employed with dyes **281** and **282**. As expected, the characteristic features of the oxidised state, namely the broad absorption between 440 and 580 nm and the sharper peak around 670 nm, Figure 5.14, were observed on the nanosecond time scale. The signals decay with remarkably slow kinetics, i.e. 1.3 x 10^3 s^{-1} for **282** and 8.3 x 10^2 s^{-1} for **281**. A possible explanation is that (as shown by molecular modelling of such systems – see chapter 2) there is a large dihedral angle of more than 30^o between the **F** unit and the adjacent phenyl rings. This restricts the π-conjugation in the backbone and blocks the back electron transfer from TiO_2 to the oxidised dye, which in turn leads to these long recombination times of more than 1.2 ms. This proposal is further corroborated by the fact that the addition of a I^-/I_3^- redox electrolyte induces a ten-fold decrease of the lifetime of the triarylamine cation radical signal. Hence, in the presence of a redox electrolyte solution the regeneration of the oxidised dye occurs through the electrons from the electrolyte, which is much faster than the back electron transfer from TiO_2.

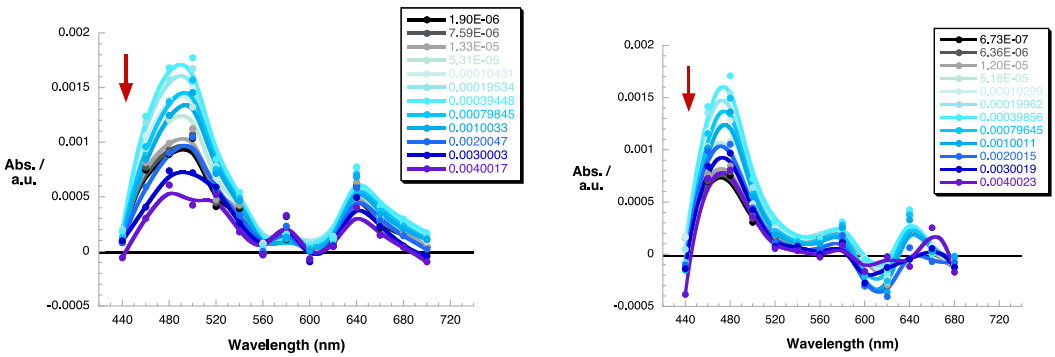

Figure 5.14 – Differential absorption spectrum obtained upon nanosecond flash photolysis (λ_{exc} = 420 nm) of 282 (left) and 281 (right) on 5 µm thick TiO_2 with several time delays at room temperature.

5.2.4 Device studies

Preliminary fabrication and analysis of solar cell devices were carried out at the EPFL by Magdalena Marszalek, as described in chapter 6. Figure 5.15 shows the current-voltage characteristics of DSSCs using **281** and **282** as the sensitiser dye. Table 5.1 lists the device characteristics of the dyes under different levels of exposure to solar radiation.

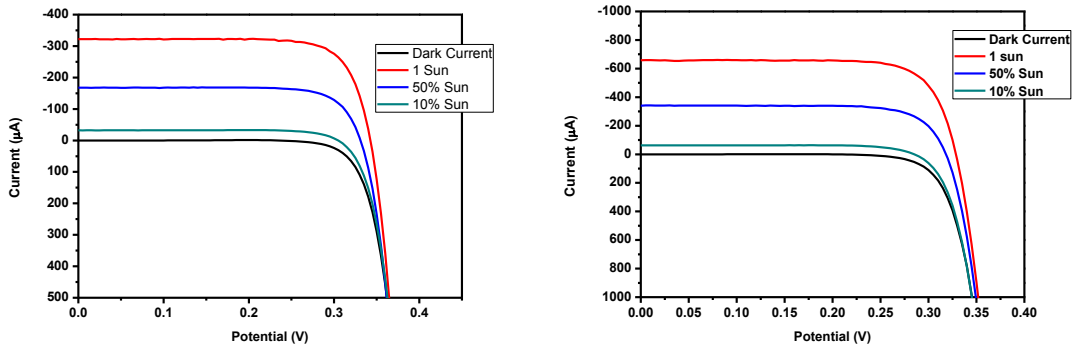

Figure 5.15 – Current-voltage plots for (a) 281 and (b) 282

It can be concluded that **282** performs better overall than **281** in the DSSC, with higher current and power conversion efficiency (PCE) achieved. The PCE for the two materials in devices reach 1.06 and 2.02% for **281** and **282**, respectively, indicating the considerable potential for these types of materials as low-voltage transparent sensitisers for DSSCs. It is their transparency which sets these systems apart from the vast majority of dye molecules which have been exploited in DSSCs. Further studies on these systems will be carried out, exploring the internal power conversion efficiencies (IPCE) for the materials over the UV and visible spectrum.

Dye	P_{in} (mW/cm^2)	J_{sc} (mA/cm^2)	V_{oc} (mV)	FF	PCE (%)
281	9.6	0.2	579	0.78	0.98
	51.2	1.1	644	0.76	1.03
	100.5	2.1	672	0.76	1.06
282	9.6	0.4	556	0.76	1.71
	51.7	2.1	624	0.75	1.92
	100.1	4.2	648	0.74	2.02

Table 5.1 - Detailed photovoltaic parameters of the devices made with the dyes 281 and 282 and iodide-based electrolyte at different light intensities. P_{in} is the incident intensity of AM1.5 solar light, J_{SC} is the photocurrent density measured at short circuit, V_{OC} is the open-circuit photovoltage and FF is the fill factor (FF = $P_{max}/(J_{sc}V_{oc})$)

5.3 Conclusions

A series of all-organic dyes **279** – **282** with different terminal substituents has been synthesised and their assembly on TiO_2 has been investigated. Initial studies have demonstrated that **281** and **282** may be excellent candidates for transparent low-voltage DSSC applications, particularly **282** which has a cyanoacrylic acid anchoring group. Physical studies demonstrate that upon photoexcitation charge injection occurs into the electron acceptor TiO_2 with the formation of long-lived charge separated states for both **281** and **282**. Synthetic modifications to these materials may be implemented to improve their characteristics in DSSCs. Substitution on the arylamine[106,107] has been shown to reduce unwanted charge recombination and an extension of the backbone of the material to the bifluorene analogue may serve to increase the molar extinction coefficient of the molecule without altering the absorption wavelength significantly. Further studies are underway to investigate the internal power conversion efficiency (IPCE) of the dyes with respect to the whole visible spectrum and in the UV region alone. In addition the synthesis of a bifluorene analogue of **282** is underway, **283** figure 5.16, with the aim of improving the molar extinction coefficient of the dye to maximise absorption of light without shifting the absorption wavelengths.

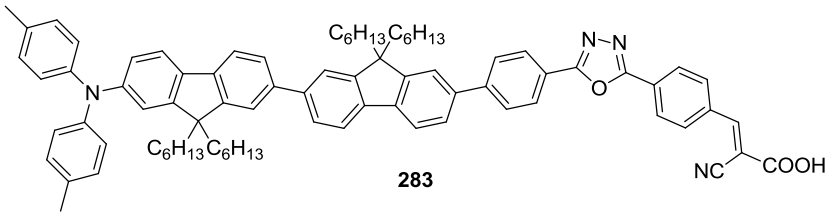

283

Figure 5.16 – Structure of proposed bifluorene DSSC candidate **283**

Chapter 6: Experimental Procedures

6.1 General Experimental Procedures

All air-sensitive reactions were conducted under a blanket of argon which was dried by passage through a column of phosphorus pentoxide. All commercial chemicals were used without further purification unless otherwise stated. Anhydrous toluene, tetrahydrofuran (THF) and diethyl ether (Et_2O) were dried through an HPLC column on an Innovative Technology Inc. solvent purification system. Anhydrous pyridine was dried over KOH pellets. Column chromatography was carried out using 40-60 μm mesh silica. Analytical thin layer chromatography was performed on 20 mm pre-coated plates of silica gel (Merck, silica gel $60F_{254}$), visualisation was made using ultraviolet light (254 nm). NMR spectra were recorded on: Bruker Avance-400 (^{1}H NMR: 400 MHz, ^{13}C NMR: 101 MHz), Varian Mercury-200 (^{1}H NMR: 200 MHz), Varian Mercury-400 (^{1}H NMR: 400 MHz, ^{13}C NMR: 126 MHz), Varian Inova-500 (^{1}H NMR: 500 MHz, ^{13}C NMR 126 MHz) and Varian VNMRS-700 (^{1}H NMR: 700 MHz, ^{13}C NMR 176 MHz) spectrometers. Melting points were determined in open-ended capillaries using a Stuart Scientific SMP3 melting point apparatus at a ramping rate of 5 °C/min. Mass spectra were measured on a Waters Xevo OTofMS with an ASAP probe. Electron ionisation (EI) mass spectra were recorded on a Thermoquest Trace or a Thermo-Finnigan DSQ. Elemental analyses were obtained on an Exeter Analytical Inc. E-440 elemental analyser. Ion analyses were performed on a Dionex 120 Ion Chromatography detector. HPLC analysis was carried out using a PerkinElmer Series 200 HPLC instrument equipped with a diode array detector, usually monitoring at 254 nm. The column was a Phenamenex HyperClone 5 μm ODS (C10) 120 Å, 250 x 4.6 mm; flow rate 1 mL min^{-1}.

UV-visible absorption spectroscopy

Absorption spectra of solutions in quartz cuvettes of path length l = 1 cm with an absorbance, A, < 0.3 at 400 nm were measured on a Unicam UV2-100 spectrometer operated with the Unicam Vision software. Baseline correction was achieved by reference to pure solvent. Extinction coefficients (ε, dm^3 mol^{-1} cm^{-1}) were calculated using the Beer-Lambert law, $A = \varepsilon cl$, (c is the concentration, mol dm^{-3}) by recording the absorption spectrum for a sample weighed on an analytical balance.

One-photon photoluminescence spectroscopy

Excitation and emission photoluminescence spectra were recorded on an Horiba Jobin Yvon SPEX Fluorolog-3 spectrofluorometer. Samples were held in quartz fluorescence cuvettes, *l* = 1 cm x 1 cm. Solutions had *A* = 0.10-0.15 at 400 nm to minimise inner filter effects.

Cyclic Voltammetry

Cyclic voltammetry experiments were carried out using a BASCV50W electrochemical workstation in a three-electrode cell equipped with a platinum disk (Ø 1.6 mm) working electrode, platinum wire counter electrode and a non-aqueous Ag/Ag^+ reference electrode (0.01 M $AgNO_3$ in dry MeCN), with iR compensation. CV data for compounds were obtained in dry DCM (oxidations) and dry THF (reductions) with 0.1 M tetrabutylammonium hexafluorophosphate (Bu_4NPF_6) as a supporting electrolyte, under an argon atmosphere. The potential of the reference electrode in benzonitrile (0.1 M Bu_4NPF_6) was checked against the ferrocene/ferrocenium couple (Fc/Fc^+), which showed the average potential against the reference electrode of +0.187 V. Where no reduction wave is shown, no reduction waves could be resolved on scanning to -2.0 V.

6.2 General Synthetic Procedures

General Miyaura Borylation Procedure

In a flame dried flask under an atmosphere of argon 1 equivalent of the aryl halide was dissolved in DMF (2 cm^3 per mmol of halide) and degassed with argon for 20 min. To this stirred solution B_2pin_2 (1.4 equivalents) and potassium acetate (1.6 equivalents) were added and the mixture degassed for a further 10 min, after which time [$PdCl_2$(dppf)] (2 mol%) was added and the reaction mixture heated to 80 ^oC for 15 h. The mixture was then cooled, water added and extracted with diethyl ether. The organic extracts are combined and the solvent removed under reduced pressure. The crude product was purified by column chromatography on silica gel.

General Suzuki Miyaura Cross-Coupling Procedure

In a flame dried flask under an atmosphere of argon the relevant aryl halide and boronic ester or acid were dissolved in anhydrous THF (2 cm^3 per mmol of halide) and degassed for 20 min. To this stirred solution aqueous NaOH (2-2.5 equivalents) was added and the mixture degassed

for a further 10 min. After this time [$PdCl_2(PPh_3)_2$] (2 mol%) was added and the reaction mixture heated to 65 ^oC for 15 h under argon. The reaction mixture was then allowed to cool, filtered through a plug of Celite, washed with water and extracted with diethyl ether. The solvent was removed from the combined organic extracts under reduced pressure and the crude product purified by column chromatography on silica gel.

General Ligand Mediated Ullmann C-N Coupling Procedure

In a flame dried flask under an atmosphere of argon the iodide, amine, copper iodide (10 mol%), 1,10-phenanthroline (20 mol%) and potassium carbonate (2 equivalents) were added. The flask was evacuated and backfilled with argon followed by the addition of degassed, anhydrous DMF *via* the septum. The reaction mixture was stirred and heated to 120 ^oC for 15 h. After which time, the reaction was cooled and the solvent removed by evaporation under reduced pressure. The crude product was purified by column chromatography on silica gel.

General Buchwald-Hartwig Amination Procedure A

In a flame dried flask under an atmosphere of argon the amine (1 equivalent) and the aryl halide (1.2 equivalents), [$Pd_2(dba)_3$] (0.5 mol%), JohnPhos (1 mol%) and NaO^tBu (2.5 equivalents) were added. The flask was evacuated and backfilled with argon. Anhydrous toluene was added through the septum (along with either the halide or amine if a liquid) and the reaction was heated to 100 ^oC for 15 h. After this time the reaction mixture was cooled and filtered through a Celite plug, the solvent removed and the crude product purified by column chromatography on silica gel.

General Buchwald-Hartwig Amination procedure B

In a flame dried flask under an atmosphere of argon the amine (1 equivalent) and the aryl halide (1.2 equivalents for mono substitution and 2.5 equivalents for bis-substitution), NaO^tBu (1.5 equivalents for mono substitution and 2.5 equivalents for bis-substitution), 10% Pd/C (2 mol%) and dppf (3 mol%) were added. To these solids thoroughly degassed mesitylene (1 cm^3 per 1 mmol of amine) was added and the mixture degassed for a further 10 min. The reaction mixture was heated to 160 ^oC for 15 h under an atmosphere of argon. The reaction mixture was then cooled, put through a Celite plug, poured onto water and extracted with diethyl ether. The organic extracts were combined and the solvent removed under reduced pressure. The crude product was purified by column chromatography on silica gel.

General Sonogashira Cross-Coupling Procedure

In a flame dried flask under an atmosphere of argon the aryl halide and terminal alkyne were dissolved in a mixture of anhydrous THF and triethylamine. The stirred solution was degassed with argon for 15 min followed by the addition of the palladium catalyst ($[Pd(PPh_3)_4]$ or $[PdCl_2(PPh_3)_2]$). The reaction mixture was then heated to 60 ^oC for 15 h, after which time the reaction was cooled and the solvent removed under reduced pressure. The crude productwas purified by column chromatography on silica gel.

6.3 Experimental Procedures for Chapter 2

54; 2,7-Dibromo-9*H*-fluorene

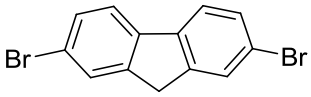

Commercially available fluorene (**4**) (50.00 g, 0.301 mol) was dissolved in glacial acetic acid (450 cm^3) at 70 °C with stirring. To this solution 98% H_2SO_4 (4.3 cm^3) was added dropwise. The reaction was cooled to 50 °C and a solution of bromine (24.6 cm^3, 0.48 mol) in glacial acetic acid (40 cm^3) was added dropwise keeping the temperature between 40 and 55 °C to avoid crystallisation of fluorene. When about half the bromine was added crystallisation of the product occurs and $KBrO_3$ (17.00 g, 0.10 mol) was added simultaneously with the rest of the bromine in small portions with vigorous stirring. The reaction mixture was then stirred for a further 4 h at room temperature and then cooled to 10 °C. The solid was filtered and washed with 70% acetic acid (100 cm^3) and then washed with water until the washings were pH 7. The product **54** was obtained as a yellow powder (76.1 g, 78%), no further purification was necessary. NMR data were consistent with literature.[134] ^1H NMR (400 MHz, $CDCl_3$): δ 7.69 (2 H, d, *J* = 0.9 Hz), 7.62 (2 H, m), 7.55 – 7.48 (2 H, m), 3.89 (2 H, s).

55; 2,7-Dibromo-9,9-dihexyl-9*H*-fluorene

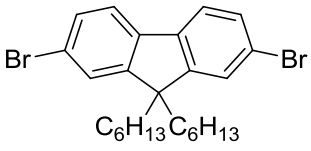

Under an atmosphere of argon 2,7-dibromo-9*H*-fluorene (**54**) (50.00 g, 0.15 mol) and 1-bromohexane (70.2 cm^3, 0.62 mol) were dissolved in anhydrous THF (500 cm^3). The solution was cooled to 0 °C followed by the addition of ^{t}BuOK (38.88 g, 0.35 mol) in anhydrous THF (50 cm^3), maintaining a temperature of 0 – 5 °C, over 1 h. The reaction mixture was then stirred for 4 h at room temperature and then filtered from the potassium bromide precipitate and washed

with DCM. Solvent was removed from the filtrate under reduced pressure, dissolved in DCM, washed with water and then dried. The crude product was then purified by column chromatography on silica gel using petroleum ether (b.p. 40 – 60 °C) as eluent. Recrystallisation from hexane gave **55** as a white crystalline solid (61.0 g, 81 %). NMR data were consistent with the literature.[134] ^{1}H NMR (400 MHz, $CDCl_3$): δ 7.52 (2H, d, *J* = 8.0 Hz), 7.45 (2H, dd, *J* = 2 Hz and 8.0 Hz), 7.44 (2H, d, *J* = 2 Hz), 1.95 – 1.87 (4H, m), 1.16 – 1.08 (4H, m), 1.08 – 0.98 (8H, m), 0.78 (6H, t, J = 7.1), 0.62 – 0.53 (4H, m).

125; (7-Bromo-9,9-dihexyl-9*H*-fluoren-2-yl)trimethylsilane

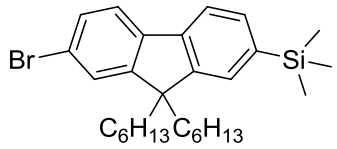

In a flame dried flask 2,7-dibromo-9,9-dihexyl-9*H*-fluorene (**55**) (7.93 g, 16.1 mmol) was dissolved in anhydrous THF (100 cm^3) under an atmosphere of argon and then cooled to -78 °C. To this stirred solution *n*-butyl lithium (6.43 cm^3, 16.1 mmol) was added dropwise, the solution was then stirred for 1 h. Trimethylsilyl chloride (2.04 cm^3, 16.1 mmol) was added to the stirred solution, which was then warmed to room temperature and stirred for a further 30 min. The reaction mixture was quenched with water, extracted into petroleum ether (b.p. 40 – 60 °C), washed with water, dried ($MgSO_4$) and concentrated by evaporation under reduced pressure. The crude product was purified by column chromatography on silica gel using petroleum ether (b.p. 40 – 60 °C) as eluent. The product **125** was obtained as a colourless oil (7.12 g, 92 %). NMR data were consistent with the literature.[82] ^{1}H NMR (400 MHz, $CDCl_3$): δ 7.65 (1H, m), 7.58 (1H, m), 7.44 (4H, m), 1.92 (4H, m), 1.05 (12H, m), 0.78 (6H, m), 0.61 (4H, m), 0.30 (9H, s).

126; (9,9-Dihexyl-7-(4,4,5,5-tetramethyl-1,3,2-dioxaborolan-2-yl)-9*H*-fluoren-2-yl)trimethylsilane

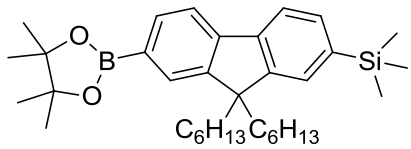

In a flame dried flask (7-bromo-9,9-dihexyl-9H-fluoren-2-yl)trimethylsilane (**125**) (7.11 g, 14.7 mmol) was dissolved in anhydrous THF (100 cm^3) under an atmosphere of argon and cooled to -78 °C. To this stirred solution *n*-butyl lithium (6.43 cm^3, 16.1 mmol) was added dropwise and stirred for 30 min, followed by addition of 2-isopropoxy-4,4,5,5-tetramethyl-1,3,2-dioxaborolane (3.01 g, 16.2 mmol). The reaction mixture was then warmed to room temperature and stirred for 12 h. Brine solution was added to the reaction mixture, the mixture was then extracted with diethyl ether and washed with water, dried ($MgSO_4$) and concentrated by evaporation under reduced pressure. The crude product was purified by column chromatography on silica gel using petroleum ether (b.p. 40 – 60 °C) with 0 – 5 % ethyl

acetate as eluent. The product **126** was obtained as a white solid (4.43 g, 57%). The NMR data were consistent with the literature.[58] ^{1}H NMR (200 MHz, $CDCl_3$): δ 7.80 (1 H, m), 7.75 (1 H, s), 7.73 – 7.66 (2 H, m), 7.53 – 7.44 (1 H, m), 7.46 (1 H, s), 1.97 (4 H, m), 1.39 (12 H, s), 1.15 – 0.94 (12 H, m), 0.75 (6 H, m), 0.70 – 0.44 (4 H, m, *J* = 8.0, 4.7 Hz), 0.30 (9 H, s).

127; 2-(4-*Tert*-butylphenyl)-5-(4-(9,9-dihexyl-7-(trimethylsilyl)-9*H*-fluoren-2-yl)phenyl)-1,3,4-oxadiazole

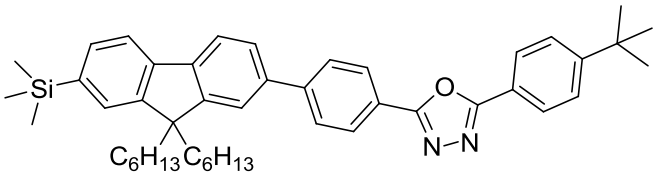

The standard Suzuki-Miyaura cross-coupling procedure was followed using the following quantities: (9,9-dihexyl-7- (4,4,5,5-tetramethyl-1,3,2-dioxaborolan-2-yl) - 9H -fluorene-2-yl) trimethylsilane (**126**) (4.13 g, 7.76 mmol), 2-(4-bromophenyl) - 5 - (4-*tert*-butylphenyl) - 1,3,4-oxadiazole (**150**) (3.25 g, 8.54 mmol), aqueous sodium hydroxide (2.4 g in 40 cm^3 H_2O), $[PdCl_2(PPh_3)_2]$ (0.27 g, 0.39 mmol). The crude product was purified by column chromatography on silica gel using petroleum ether 40-60 °C with 5 % ethyl acetate as eluent to yield the product **127** as a white solid (3.84 g, 88%). The NMR data were consistent with the literature.[58] ^{1}H NMR (499 MHz, $CDCl_3$): δ 8.24 (2H, d, J = 8.5 Hz), 8.10 (2H, d, J = 8.5 Hz), 7.84 (2H, d, J = 8.5 Hz), 7.80 (1H, d, J = 8.0 Hz), 7.72 (1H, d, J = 8.0 Hz), 7.63 (2H, m), 7.57 (2H, d, J= 8.5 Hz), 7.52 (2H, m), 2.03 (4H, m), 1.40 (9H, s), 1.09 (12H, m), 0.78 (6H, t, J = 6.9 Hz), 0.75 (4H, m), 0.33 (9H, s); ^{13}C (125 MHz, $CDCl_3$): δ 165.53, 165.23, 156.20, 152.70, 151.07, 145.74, 142.19, 141.90, 140.35, 139.50, 132.76, 128.55, 128.47, 128.20, 127.66, 126.94, 123.37, 122.33, 122.00, 121.09, 120.04, 56.03, 40.99, 36.04, 32.32, 32.01, 30.42, 24.55, 23.36, 14.87, 0.00.

131; Di-*p*-tolylamine

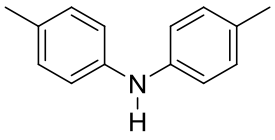

The standard Buchwald-Hartwig cross-coupling procedure was followed using the following quantities: $[Pd_2(dba)_3]$ (0.12 g, 0.13 mmol), JohnPhos (0.08 g, 0.25 mmol), NaO^tBu (3.40 g, 35.4 mmol) and *p*-toluidine (**130**) (3.25 g, 30.0 mmol), 1-chloro-4-methylbenzene (**129**) (3.00 cm^3, 25.3 mmol) and toluene (20 cm^3). The crude product was purified by column chromatography on silica with 9 : 1 (v/v) hexane : ethyl acetate as eluent. The product **131** was obtained as a white solid (4.65 g, 93%). The NMR data were consistent with the literature.[19] ^{1}H NMR (400 MHz, $CDCl_3$): δ 7.07 (4H, d, J = 8.5 Hz), 6.96 (4H, d, J = 8.5 Hz), 5.55 (1H, s), 2.31 (6H, s).

132; 7-Bromo-9,9-dihexyl-*N*,*N*-di-*p*-tolyl-9*H*-fluoren-2-amine

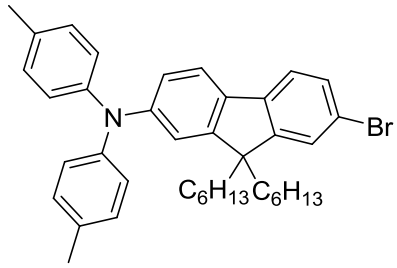

The general Buchwald-Hartwig amination procedure A was followed using the following quantities: 2,7-dibromo-9,9-dihexyl-9*H*-fluorene (**55**) (1.00 g, 2.03 mmol), di-*p*-tolylamine (**131**) (0.40 g, 2.03 mmol), dppf (0.03 g, 0.04 mmol), [$Pd_2(dba)_3$] (0.01 g, 0.01 mmol), sodium *tert*-butoxide (0.23 g, 2.43 mmol) and toluene (30 cm^3). The crude product was purified by column chromatography on silica gel with hexane and 5% DCM as eluent to yield the product **132** as a white solid (0.62 g, 50%). ^{1}H NMR (500 MHz, $CDCl_3$): δ 7.50 – 7.35 (4H m), 7.03 (9H, m), 6.95 (d, *J* = 7.9 Hz, 1H), 2.32 (6H, s), 1.88 – 1.73 (4H, m), 1.22 – 0.94 (12H, m), 0.81 (6H, t, *J* = 7.2 Hz), 0.64 (4H, m); ^{13}C NMR (126 MHz, $CDCl_3$): δ 153.05, 151.83, 148.20, 145.75, 140.36, 134.43, 132.39, 130.05, 126.14, 124.37, 122.52, 120.47, 120.06, 118.20, 55.52, 40.39, 31.76, 29.83, 23.94, 22.83, 21.07, 14.32; HRMS (ASAP$^+$) calcd for $C_{39}H_{46}{}^{79}BrN$ 607.2814. Found: 607.2802; Mp. 106.3 – 107.1 °C.

133; 9,9-Dihexyl-7-(4,4,5,5-tetramethyl-1,3,2-dioxaborolan-2-yl)-*N*,*N*-di*p*-tolyl-9*H*-fluoren-2-amine

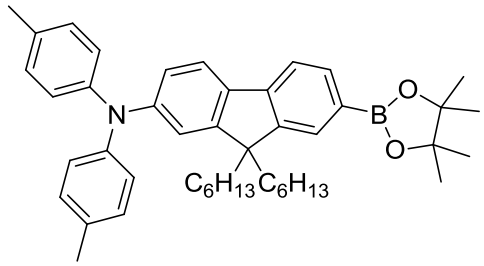

In a flame dried flask under an atmosphere of argon 7-bromo-9,9-dihexyl-*N*,*N*-di*p*-tolyl-9*H*-fluoren-2-amine (**132**) (0.30 g, 0.49 mmmol) was dissolved in anhydrous THF (70 cm^3) and cooled to – 78 °C. To this stirred solution *n*-butyllithium (0.79 cm^3, 1.97 mmol) was added dropwise and stirred for 30 min. To this solution 2-isopropoxy-4,4,5,5-tetramethyl-1,3,2-dioxaboralane (0.41 cm^3, 2.00 mmol) was added dropwise. The reaction mixture was left to stir for 7 h at which point it was quenched by the addition of brine (30 cm^3). The reaction mixture was extracted with diethyl ether, the organic phases washed with water, dried ($MgSO_4$) and concentrated. The crude product was purified by column chromatography on silica gel with 40 – 60 petroleum ether and 2% ethyl acetate as eluent. The product was recrystallised from isopropanol to give **133** as white crystals (0.23 g, 72%). ^{1}H NMR (500 MHz, $CDCl_3$): δ 7.77 (1H, d, *J* = 7.5 Hz), 7.70 (1H, s), 7.61 (1H, d, *J* = 7.5 Hz), 7.54 (1H, d, *J* = 8.0 Hz), 7.06 (9H, m), 6.99 – 6.92 (2H, dd, J = 8.0 and 2.0 Hz), 2.33 (6H, s), 2.04 – 1.74 (4H, m), 1.39 (12H, s), 1.21 – 0.95 (12H, m), 0.80 (6H, t, *J* = 7.2 Hz), 0.73 – 0.51 (4H, m); ^{13}C NMR (126 MHz, $CDCl_3$): δ 152.92, 149.95, 148.20, 145.83, 144.38, 135.45, 134.03, 132.31, 130.02, 128.85, 124.33, 122.52, 120.87, 118.50, 118.39, 83.87, 55.27, 40.35, 31.78, 29.88, 25.21, 23.93,

22.85, 21.08, 14.35; HRMS (ASAP$^+$) calcd for $C_{45}H_{59}{}^{10}BNO_2$: 655.4675. Found: 655.4680; Mp. 159.5 – 160.0 ^oC.

134; 7-(4-(5-(4-*Tert*-butylphenyl)-1,3,4-oxadiazol-2-yl)phenyl)-9,9-dihexyl-*N*,*N*-di*p*-tolyl-9*H*-fluoren-2-amine

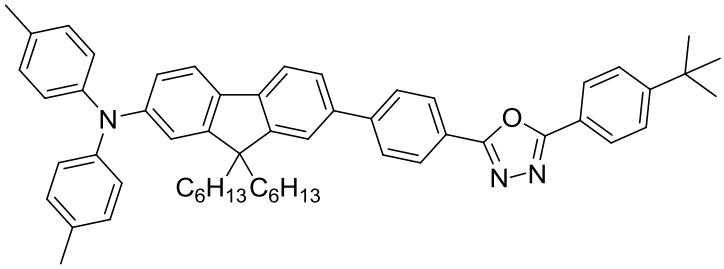

The standard Suzuki-Miyaura cross-coupling procedure was followed using the following quantities: 9,9-dihexyl-7-(4,4,5,5-tetramethyl-1,3,2-dioxaborolan-2-yl) -*N*,*N*-di-*p*-tolyl-9*H*-fluoren-2-amine (**132**) (0.11 g, 0.18 mmol), 2-(4- bromophenyl)-5-(4-*tert*-butylphenyl)-1,3,4-oxadiazole (**150**) (0.08 g, 0.22 mmol), [$PdCl_2(PPh_3)_2$] (6 mg, 0.01 mmol), NaOH (0.5 g in 5 cm^3) and THF (30 cm^3). The crude product was purified by column chromatography on silica gel with DCM as eluent to yield the product **134** as a yellow solid (0.09 g, 62%). ^{1}H NMR (500 MHz, $CDCl_3$): δ 8.23 (d, J = 8.5 Hz, 2H), 8.10 (d, J = 8.5 Hz, 2H), 7.83 (d, J = 8.5 Hz, 2H), 7.68 (d, J = 8.0, 1H), 7.64 – 7.53 (m, 6H), 7.07 (m, 9H), 6.99 (dd, J = 8.0, 2.0 Hz, 1H), 2.34 (s, 6H), 2.03 – 1.81 (m, 4H), 1.38 (s, 9H), 1.23 – 0.99 (m, 12H), 0.81 (t, J 7.2 Hz, 6H), 0.69 (m, 4H); ^{13}C NMR (126 MHz, $CDCl_3$): δ 164.89, 164.65, 155.56, 152.58, 151.68, 148.14, 145.80, 145.18, 141.64, 137.71, 134.89, 132.41, 130.06, 127.80, 127.57, 127.04, 126.32, 124.39, 122.58, 121.41, 120.69, 119.60, 118.32, 55.41, 40.51, 35.37, 31.78, 31.41, 29.90, 24.04, 22.84, 21.09, 14.34; HRMS (ASAP$^+$) calcd for $C_{57}H_{63}N_3O$ 805.4971. Found: 805.4966; Mp. 89.5 – 91.0 °C. Purity was judged to be >99% by HPLC analysis.

136; 2-Bromo-7-iodo-9*H*-fluorene

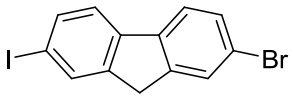

To a solution of 2-bromo-9*H*-fluorene (**135**) (16.00 g, 65.3 mmol) in glacial acetic acid (500 cm^3) and 20% sulfuric acid (50 cm^3) potassium iodate (2.80 g, 13.1 mmol) followed by iodine (9.12 g, 35.9 mmol) were added. The reaction mixture was stirred at 80 °C for 18 h. The reaction mixture was then cooled, diluted with water (400 cm^3) and extracted with DCM (3 x 150 cm^3). The organic phase was washed with water (500 cm^3), aqueous $NaHCO_3$ (100 cm^3), brine solution (150 cm^3), dried over sodium thiosulfate, filtered and reduced. The solid was dissolved in DCM to which methanol was added to precipitate the product. The product **136** was isolated as a white solid (15.80 g, 65%).

NMR data were consistent with the literature.[84] ^{1}H NMR (200 MHz, $CDCl_3$): δ 7.93 – 7.85 (m, 1H), 7.76 – 7.57 (m, 3H), 7.57 – 7.43 (m, 2H), 3.87 (s, 2H).

137; 2-Bromo-9,9-dihexyl-7-iodo-9*H*-fluorene

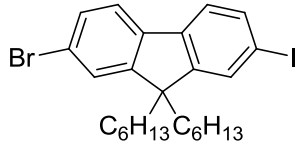

To a solution of 2-bromo-7-iodo-9*H*-fluorene (**136**) (15.80 g, 42.6 mmol) in DMSO (150 cm^3), tetra *n*-butylammonium chloride (2 g) was added followed by sodium hydroxide solution (4.26 g in 20 cm^3 H_2O). To this orange solution *n*-bromohexane was added. The reaction mixture was then stirred at room temperature for 20 h. Water was added and the mixture was extracted with ethyl acetate. The organic layers were washed with aqueous HCl, dried, filtered and concentrated. The crude product was purified by column chromatography on silica gel with petroleum ether (b.p. 40 – 60 ^{o}C) as eluent followed by recrystallisation from ethanol. The product **137** was isolated as pale yellow crystals (15.6 g, 68%). The NMR data were consistent with the literature.[84] ^{1}H NMR (400 MHz, $CDCl_3$): δ 7.70 – 7.57 (m, 2H), 7.56 – 7.47 (m, 1H), 7.47 – 7.34 (m, 3H), 1.97 – 1.81 (m, 4H), 1.09 (m, 12H), 0.78 (t, *J* = 7.1 Hz, 6H), 0.58 (s, 4H).

138; 9-(7-Bromo-9,9-dihexyl-9*H*-fluoren-2-yl)-9*H*-carbazole

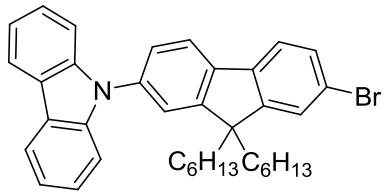

The standard ligand mediated Ullmann cross-coupling procedure was followed using the following quantities: 2-bromo-9,9-dihexyl-7-iodo-9*H*-fluorene (**137**) (1.00 g, 1.85 mmol), carbazole (**2**) (0.37 g, 2.22 mmol), copper iodide (0.03 g, 0.19 mmol), 1,10-phenanthroline (0.07 g, 0.37 mmol), potassium carbonate (0.71 g, 3.7 mmol) and DMF (8 cm^3). The crude product was purified by column chromatography on silica with 98 : 2 (v/v) petroleum ether (b.p. 40 – 60 ^{o}C) : DCM as eluent. The product **138** was isolated as a white foamy solid (0.86 g, 80%). The NMR data were consistent with the literature.[84] ^{1}H NMR (700 MHz, $CDCl_3$): δ 8.18 (d, *J* = 8.0 Hz, 2H), 7.88 (d, *J* = 8.0 Hz, 1H), 7.66 – 7.61 (m, 1H), 7.55 (m, 1H), 7.54 – 7.51 (m, 1H), 7.45 – 7.41 (m, 2H), 7.35 – 7.29 (m, 1H), 2.04 – 1.93 (m, 4H), 1.23 – 1.04 (m, 12H), 0.84 – 0.69 (m, 10H); ^{13}C NMR (176 MHz, $CDCl_3$): δ 153.21, 152.21, 140.95, 139.31, 139.29, 136.81, 136.77, 130.21, 126.27, 125.91, 123.38, 121.77, 121.43, 121.21, 120.92, 120.37, 119.91, 109.70, 55.69, 40.18, 31.48, 29.55, 23.82, 22.53, 13.90.

139; 9-(9,9-Dihexyl-7-(4,4,5,5-tetramethyl-1,3,2-dioxaborolan-2-yl)-9*H*-fluoren-2-yl)-9*H*-carbazole

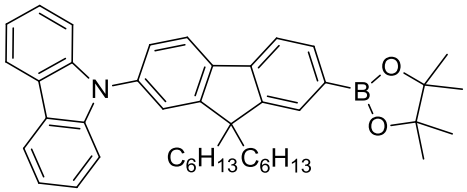

In a flame dried flask under an atmosphere of argon 9-(7-bromo-9,9-dihexyl-9*H*-fluoren-2-yl)-9*H*-carbazole (**138**) (1.60 g, 2.77 mmol) was dissolved in anhydrous THF (150 cm^3). This solution was cooled to -78 °C followed by the dropwise addition of *n*-BuLi (4.40 cm^3, 11.1 mmol). This solution was then stirred for 1 h at which time 2-isopropoxy-4,4,5,5-tetramethyl-1,3,2-dioxaborolane (2.30 cm^3, 11.2 mmol) was added. The reaction mixture was then stirred whilst gradually warming to room temperature over the next 15 h. Brine solution was then added to the mixture, which was then extracted into diethyl ether. The organic phases were washed with water, dried ($MgSO_4$) and concentrated. The crude product was purified by column chromatography on silica gel with 4 : 1 (v/v) petroleum ether (b.p. 40 – 60 ^oC) and DCM as eluent to yield the product **139** as a foamy white solid (0.879 g, 51%). ^1H NMR (700 MHz, $CDCl_3$): δ 8.17 (d, *J* = 8.0Hz, 2H), 7.97 – 7.90 (m, 1H), 7.87 (dd, *J* = 7.5, 1.0 Hz, 1H), 7.80 (s, 1H), 7.78 (dd, *J* = 7.5, 1.0 Hz, 1H), 7.56 – 7.50 (m, 2H), 7.47 – 7.39 (m, 4H), 7.31 (ddd, *J* = 8.0, 7.0, 1.5 Hz, 2H), 2.10 – 1.94 (m, 4H), 1.41 (s, 12H), 1.20 – 0.99 (m, 12H), 0.87 – 0.63 (m, 5H); ^{13}C NMR (176 MHz, $CDCl_3$): δ 153.16, 150.16, 143.20, 141.00, 140.20, 136.71, 133.93, 128.90, 125.86, 125.65, 123.33, 121.81, 121.21, 120.31, 119.82, 119.14, 109.78, 83.90, 55.43, 40.12, 31.47, 30.89, 29.57, 24.94, 23.80, 22.51, 13.98; HRMS ($ASAP^+$) calcd for $C_{38}H_{53}{}^{10}BN_3O_4$: 625.4165. Found: 625.4183; Mp. 138.0 – 140.0 °C.

140; 2-(4-(7-(9*H*-Carbazol-9-yl)-9,9-dihexyl-9*H*-fluoren-2-yl)phenyl)-5-(4-*tert*-butylphenyl)-1,3,4-oxadiazole

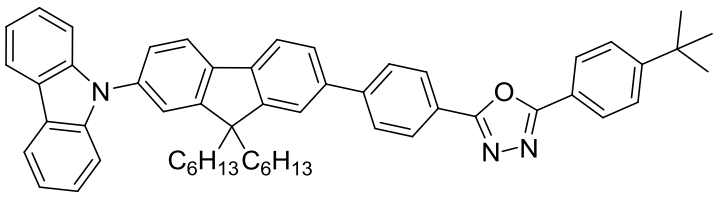

The standard Suzuki-Miyaura cross-coupling procedure was followed using the following quantities: 9 - (9,9-dihexyl - 7 - (4,4,5,5-tetramethyl - 1,3,2 -dioxaborolan-2-yl) - 9*H* -fluoren-2-yl) -9*H*- carbazole (**139**) (0.21 g, 0.33 mmol), 2-(4-bromophenyl)-5-(4-*tert*-butylphenyl)-1,3,4-oxadiazole (**150**) (0.15 g, 0.40 mmol), [$PdCl_2(PPh_3)_2$] (0.14 g, 0.02 mmol), NaOH (0.5 g in 5 cm^3 H_2O) and THF (30 cm^3). The crude product was purified by column chromatography on silica gel first with 7 : 3 (v/v) petroleum ether : diethyl ether as eluent and then a second time with DCM as eluent to yield the product **140** as a white solid (0.20 g, 78%). ^1H NMR (700 MHz, $CDCl_3$): δ 8.25 (d, *J* 8.0 Hz,

2H), 8.17 (d, *J* = 8.0 Hz, 2H), 8.10 (d, *J* 8.0 Hz, 2H), 7.95 (d, *J* = 8.0 Hz, 1H), 7.89 – 7.83 (m, 3H), 7.70 (d, *J* = 8.0 Hz, 1H), 7.66 (s, 1H), 7.60 – 7.52 (m, 4H), 7.48 – 7.38 (m, 4H), 7.31 (t, *J* =7.0 Hz, 2H), 2.12 – 1.99 (m, 4H), 1.38 (s, 9H), 1.22 – 1.04 (m, 12H), 0.79 (m, 10H); ^{13}C NMR (126 MHz, $CDCl_3$): δ 164.96, 164.57, 155.63, 153.16, 152.20, 144.90, 141.23, 140.75, 139.99, 139.23, 136.89, 128.03, 127.64, 127.06, 126.63, 126.34, 126.16, 126.11, 123.62, 122.94, 122.07, 121.74, 121.37, 121.32, 120.64, 120.61, 120.15, 110.02, 55.92, 40.56, 35.38, 31.75, 31.40, 29.87, 24.17, 22.87, 14.28; HRMS (ASAP$^+$) calcd for $C_{55}H_{57}N_3O$: 775.4502. Found: 775.4529; Mp: 99 °C. Purity was judged to be >99% by HPLC analysis.

141; 3,6-Dibromo-9*H*-carbazole

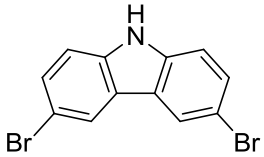

9*H*-carbazole (**2**) (8.00 g, 47.8 mmol) was dissolved in toluene (50 cm^3) and DMF (20 cm^3) in a two neck round bottomed flask under an atmosphere of argon and cooled in an ice bath to 0 °C. *N*-bromosuccinimide (18.69 g, 0.11 mol) was added to the solution whilst maintaining the temperature at 0 °C. The reaction mixture was then stirred for 0.5 h. After this time, the mixture was poured onto water and left standing for 12 h. The precipitate was filtered and recrystallised from 5 : 1 methanol and hexane. The product **141** was isolated as off-white crystals (12.4 g, 80%). The NMR data were consistent with the literature.[135] ^{1}H NMR (200 MHz, $CDCl_3$): δ 8.13 (d, *J* = 2.0 Hz, 2H), 8.09 (s br, 1H), 7.52 (dd, *J* = 8.5, 2.0 Hz, 2H), 7.31 (d, *J* = 8.5 Hz, 2H); MS EI$^+$: m/z 324.9 ([M], 100 %), 243.9 (40 %), 164.0 (38 %).

142; 3,6-Dimethoxy-9*H*-carbazole

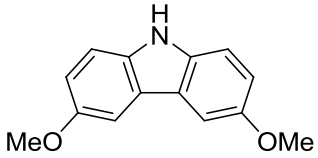

Sodium methoxide (20.00 g, 0.37 mol) was dissolved in anhydrous DMF (80 cm^3) under an atmosphere of argon. To this stirred mixture, copper iodide (14.09 g, 74.0 mmol) and 3,6-dibromo-9*H*-carbazole (**141**) (6.00 g, 0.0185 mol) were added. The reaction mixture was heated to reflux for 3 h. The mixture was filtered while hot, ethyl acetate (150 cm^3) was added and the solution was washed with brine (2 x 100 cm^3). The crude product was purified by column chromatography on silica gel with 1 : 1 (v/v) DCM : petroleum ether (b.p. 40 -60 ^{o}C) as eluent and the product was then recrystallised from a mixture of hexane and ethanol. The product **142** was isolated as white crystals (1.4 g, 54%) The NMR data were consistent with the literature.[136] ^{1}H NMR (200 MHz, $CDCl_3$): δ 7.78 (1 H, s), 7.51 (d, *J* = 2.5 Hz, 2H), 7.32 (d, *J* = 9.0 Hz, 2H), 7.06 (dd, *J* = 9.0, 2.5 Hz, 2H), 3.94 (6 H, s).

143, 144 and 145

9*H*-carbazole (**2**) (8.00 g, 47.8 mmol) and zinc chloride (19.56 g, 0.14 mol) were dissolved in nitromethane (100 cm^3) under an atmosphere of argon. To this stirred solution *tert*-butyl chloride (15.70 cm^3, 0.14 mol) was added dropwise. The reaction mixture was stirred at 20 °C for 5 h and then hydrolysed with water (100 cm^3). The product was extracted into DCM, the organic layers washed with water, dried ($MgSO_4$) and the solvent evaporated. The crude product was purified by column chromatography on silica gel with 7 : 3 (v/v) petroleum ether (b.p. 40 – 60 ^oC) : DCM as eluent, the fractions obtained were recrystallised from methanol.

143; 3,6-Di-*tert*-butyl-9*H*-carbazole

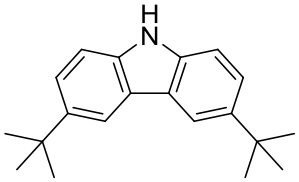

Fraction three was isolated as colourless crystals (10.7 g, 80%) The NMR data were consistent with the literature.[137] ^{1}H NMR (400 MHz, $CDCl_3$): δ 8.11 – 8.04 (m, 2H), 7.84 (s, 1H), 7.47 (dd, *J* = 8.5, 2.0 Hz, 2H), 7.33 (dd, *J* = 8.5, 2.0 Hz, 2H), 1.46 (s, 18H).

144; 1,3,6-Tri-*tert*-butyl-9*H*-carbazole

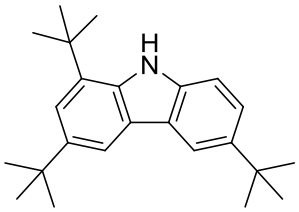

Fraction two was isolated as colourless crystals (1.3 g, 8%). The NMR data were consistent with the literature.[137] ^{1}HNMR (400 MHz, $CDCl_3$) 8.20 (d, *J* = 2.0 Hz, 1H), 8.14 – 8.02 (m, 2H), 7.62 – 7.51 (m, 2H), 7.47 (d, *J* = 8.5 Hz, 1H), 1.67 (s, 9H), 1.59 (s, 9H), 1.58 (s, 9H).

145; 1,3,6,8-Tetra-*tert*-butyl-9*H*-carbazole

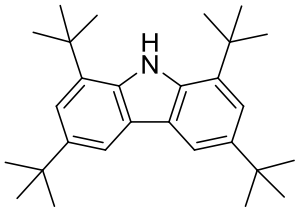

Fraction one was isolated as colourless crystals (1.3 g, 7%). The NMR data were consistent with the literature.[137] ^{1}HNMR (400 MHz, $CDCl_3$): δ 8.41 (s, 1H), 8.24 (d, *J* = 1.5 Hz, 2H), 7.68 (d, *J* = 1,5 Hz, 2H), 1.85 (s, 18H), 1.74 (s, 18H).

147; 5-(4-Bromophenyl)-1*H*-tetrazole

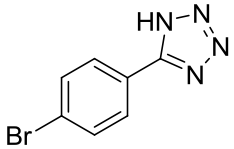

4-Bromobenzonitrile (**146a**) (5.00 g, 27.5 mmol), sodium azide (2.14 g, 33.0 mmol) and ammonium chloride (1.76 g, 33.0 mmol) were combined in a flame dried flask. Anhydrous DMF was added to the dry reagents and the mixture was heated at 105 °C for 12 h. The reaction mixture was allowed to cool to room temperature and was then poured onto cold water and acidified to pH 3 with dilute HCl precipitating a white solid. The solid was filtered and washed with water. The product was

obtained as a white solid (4.79 g, 77%). The NMR data were consistent with the literature.[138] ^{1}H NMR (400 MHz, $CDCl_3$): δ 7.84 (d, *J* = 8.5 Hz, 2H), 7.99 (d, *J* = 8.5 Hz, 2H).

148; 5-(4-*Tert*-butylphenyl)-1*H*-tetrazole

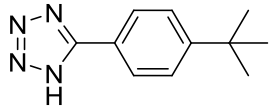

4-*Tert*-butylbenzonitrile (**146b**) (2.51 cm^3, 14.8 mmol), sodium azide (1.16 g, 17.7 mmol) and ammonium chloride (0.95 g, 17.7 mmol) were combined in a flame dried flask. Anhydrous DMF was added to the dry reagents and the mixture was heated at 105 °C for 12 h. The reaction mixture was allowed to cool to room temperature and was then poured onto cold water and acidified to pH 3 with dilute HCl precipitating a white solid. The solid was filtered and washed with water. The product **148** was obtained as a white solid (1.59 g, 53%). The NMR data were consistent with the literature.[139] ^{1}H NMR (400 MHz, DMSO-d_6): δ 7.95 (d, *J* = 8.0 Hz, 2H), 7.61 (d, *J* = 8.0 Hz, 1H), 1.30 (s, 9H).

150; 2-(4-Bromophenyl)-5-(4-*tert*-butylphenyl)-1,3,4-oxadiazole

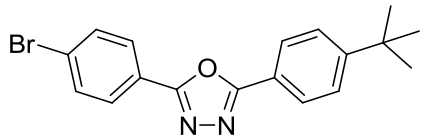

5-(4-Bromophenyl)-1H-tetrazole (**147**) (2.11 g, 9.20 mmol) was dissolved in pyridine (30 cm^3) and 4-tertbutylbenzoyl chloride (**149b)** (1.98 cm^3, 10.1 mmol). The mixture was stirred and heated to 100 °C for 3 h. The reaction mixture was then cooled and poured onto water precipitating a pale yellow solid. The solid was filtered and recrystallised from ethanol. The product **150** was obtained as white crystals (3.2 g, 92%). The NMR data were consistent with the literature.[58] ^{1}H NMR (400 MHz, DMSO-d_6): δ 8.04 (m, 4H), 7.83 (m, 2H), 7.63 (m, 2H), 1.32 (s, 9H).

151; 2-(4-*Tert*-butylphenyl)-5-(6-chloropyridin-3-yl)-1,3,4-oxadiazole

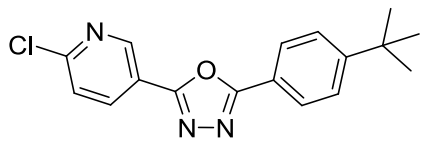

5-(4-*tert*-butylphenyl)-1*H*-tetrazole (**148**) (1.62 g, 8.00 mmol) and 6-chloronicotinoyl chloride (**149b**) (1.55 g, 8.80 mmol) were dissolved in pyridine (30 cm^3). The mixture was stirred and heated to 100 °C for 3 h. The reaction mixture was then cooled and poured onto water precipitating a pale yellow solid. The solid was filtered and recrystallised from ethanol. The product **151** was obtained as white crystals (1.73 g, 69%). ^{1}H NMR (700 MHz, DMSO-d_6): δ 9.12 (dd, *J* = 2.5, 1.0 Hz, 1H), 8.51 (dd, *J* = 8.0, 2.5 Hz, 1H), 8.06 (d, J = 8.5 Hz, 2H), 7.78 (dd, *J* = 8.5, 1.0 Hz, 1H), 7.67 – 7.60 (d, J = 8.5 Hz, 1H), 1.31 (s, 9H) ppm; ^{13}C NMR (176 MHz, DMSO-d_6): δ 165.01, 161.84, 155.78, 153.42, 148.26, 138.02, 127.19, 126.72, 125.58,

120.76, 120.02, 35.34, 31.26; HRMS (ASAP$^+$) calcd for $C_{17}H_{17}N_3OCl$: 314.1060. Found: 314.1063; Mp: 172.0 – 173.0 ^oC.

155; 2-(5-Bromothiophen-2-yl)-5-(4-*tert*-butylphenyl)-1,3,4-oxadiazole

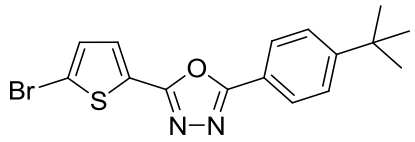

Thiophene-2-carbonitrile (**152**) (8.00 g, 73.3 mmol) was dissolved in a mixture of acetic anhydride (28 cm^3) and acetic acid (4.5 cm^3). To this stirred solution NBS (13.05 g, 73.3 mmol) and bromine (3.8 cm^3, 73.3 mmol) were added. The reaction mixture was stirred at room temperature for 3 h. The mixture was poured onto water and ice, to which sodium bisulfite solution was added. After extraction with DCM the organic layer was washed with a saturated sodium $NaHCO_3$ solution, dried over Na_2SO_4 and evaporated. The crude product **153** (8.00 g, 42.5 mmol) was dissolved in anhydrous DMF (80 cm^3) to which ammonium chloride (2.70 g, 51 mmol) and sodium azide (3.31 g, 51 mmol) were added. The mixture was heated at 120 °C for 15 h. The reaction mixture was cooled, poured onto water and acidified to pH 3 with aqueous HCl to precipitate a white solid. To a solution of this solid [assumed to be crude 5-(5-bromothiophen-2-yl)-1*H*-tetrazole (**154**)] (9.61 g) in pyridine (50 cm^3) 4-*tert*-butylbenzoyl chloride (9.75 cm^3, 49.9 mmol) was added and heated to 100 °C for 15 h. The reaction mixture was cooled and poured onto water to precipitate the crude product, which was filtered, washed with water and dried under high vacuum. The crude product was purified by chromatography on silica with DCM as eleunt, the solid obtained was recrystallised from ethanol. The product **155** was obtained as white crystals (11.4 g, 43%). ^1H NMR (700 MHz, $CDCl_3$): δ 8.02 – 7.99 (2 H, m), 7.56 (1 H, d, *J* = 3.9), 7.55 – 7.51 (2 H, m), 7.14 (1 H, d, *J* = 3.9) 1.36 (9 H, s); ^{13}C NMR (176 MHz, $CDCl_3$): δ 164.18, 159.52, 155.55, 131.05, 129.65, 126.78, 126.06, 120.63, 117.79, 53.40, 35.09, 31.08; HRMS (ASAP$^+$) calcd for $C_{16}H_{16}N_2OS^{79}Br$: 363.0167. Found: 363.0152; Mp. 179.8 – 181.3 °C.

156; 2-(6-(7-(9*H*-Carbazol-9-yl)-9,9-dihexyl-9*H*-fluoren-2-yl)pyridin-3-yl)-5-(4-*tert*-butylphenyl)-1,3,4-oxadiazole

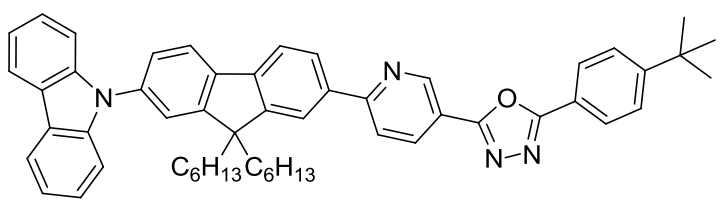

The standard Suzuki-Miyaura cross-coupling procedure was followed using the following quantities: 9-(9 , 9 - dihexyl - 7 - (4,4,5,5 – tetramethyl - 1,3,2 - dioxaborolan-2-yl) - 9H -fluoren-2-yl)-9H-carbazole (**139**) (0.20 g, 0.32 mmol), 2-(4-*tert*-

butylphenyl)-5-(6-chloropyridin-3-yl)-1,3,4-oxadiazole (**151**) (0.12 g, 0.38 mmol), [$PdCl_2(PPh_3)_2$] (0.14 g, 0.02 mmol), NaOH (0.5 g in 5 cm^3 H_2O) and THF (30 cm^3). The crude product was purified by column chromatography on silica gel first with 7 : 3 (v/v) petroleum ether (b.p. 40 – 60 ^oC) : diethyl ether as eluent and then a second time with DCM as eluent to yield the product **156** as a pale yellow solid (0.18 g, 72%). ^1H NMR (700 MHz, $CDCl_3$): δ 9.47 (1 H, d, *J* = 2.2), 8.52 (1 H, dd, *J* = 8.3, 2.2), 8.21 – 8.15 (4 H, m), 8.12 (2 H, d, *J* = 8.3), 8.03 (1 H, d, *J* = 8.3), 8.01 – 7.96 (1 H, m), 7.92 (1 H, d, *J* = 7.9), 7.64 – 7.56 (4 H, m), 7.50 – 7.41 (4 H, m), 7.33 (2 H, dd, *J* = 10.7, 3.9), 2.20 – 2.04 (4 H, m), 1.40 (9 H, s), 1.21 – 1.04 (12 H, m), 0.87 – 0.81 (4 H, m), 0.79 (6 H, t, *J* = 7.2); ^{13}C NMR (176 MHz, $CDCl_3$): δ 165.03, 162.54, 159.93, 155.68, 153.31, 151.87, 147.81, 142.30, 140.97, 139.60, 137.21, 136.96, 134.78, 126.90, 126.50, 126.15, 125.92, 125.87, 123.41, 121.86, 121.57, 121.36, 120.82, 120.38, 120.34, 120.28, 119.93, 118.49, 109.76, 55.70, 40.29, 35.14, 31.52, 31.12, 29.62, 23.95, 22.54, 13.99; HRMS ($ASAP^+$) calcd for $C_{54}H_{57}N_4O$: 777.4532. Found: 777.4551; Mp. 110.0 – 111.5 °C. Purity was judged to be >99% by HPLC analysis.

157; 2-(5-(7-(9*H*-Carbazol-9-yl)-9,9-dihexyl-9*H*-fluoren-2-yl)thiophen-2-yl)-5-(4-*tert*-butylphenyl)-1,3,4-oxadiazole

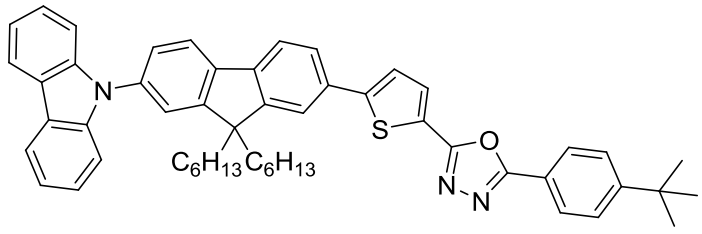

The standard Suzuki-Miyaura cross-coupling procedure was followed using the following quantities: 9-(9 , 9 - dihexyl - 7 - (4,4,5,5 – tetramethyl - 1,3,2 - dioxaborolan-2-yl) - 9H -fluoren-2-yl)-9H-carbazole (**139**) (0.4 g, 0.64 mmol), 2-(5-bromothiophen-2-yl)-5-(4-*tert*-butylphenyl)-1,3,4-oxadiazole (**151**) (0.28 g, 0.77 mmol), [$PdCl_2(PPh_3)_2$] (0.14 g, 0.02 mmol), NaOH (0.5 g in 5 cm^3 H_2O) and THF (30 cm^3) The crude product was purified by column chromatography on silica gel first with 7 : 3 (v/v) petroleum ether (b.p. 40 – 60 ^oC) : diethyl ether as eluent and then a second time with DCM as eluent to yield the product **157** as a pale yellow solid (0.42 g, 84%). ^1H NMR (700 MHz, $CDCl_3$): δ 8.20 (2 H, d, *J* 7.8), 8.09 (2 H, d, *J* 8.5), 7.97 – 7.91 (1 H, m), 7.85 (1 H, d, *J* 3.8), 7.83 (1 H, d, *J* 7.8), 7.74 (1 H, dd, *J* 7.8, 1.6), 7.70 (1 H, d, *J* 1.3), 7.62 – 7.55 (4 H, m), 7.51 – 7.43 (5 H, m), 7.36 – 7.31 (2 H, m), 2.14 – 2.02 (4 H, m), 1.40 (9 H, s), 1.25 – 1.07 (12 H, m), 0.89 – 0.76 (10 H, m); ^{13}C NMR (176 MHz, $CDCl_3$): δ 164.10, 160.58, 155.39, 152.90, 152.11, 149.70, 141.12, 140.98, 139.51, 136.86, 132.23, 130.53, 126.79, 126.06, 125.94, 125.39, 123.83, 123.71, 123.42, 121.82, 121.12, 120.92, 120.52, 120.42, 120.40, 119.96, 109.76, 55.63, 40.28, 35.11, 31.50, 31.13,

29.61, 23.93, 22.54, 14.01; HRMS (ASAP$^+$) calcd for $C_{53}H_{55}N_3OS$: 781.4066. Found: 781.4071; Mp. 102.0 – 105.0 °C. Purity was judged to be >99% by HPLC analysis.

158; 2-(4-*Tert*-butylphenyl)-5-(4-(4,4,5,5-tetramethyl-1,3,2-dioxaborolan-2-yl)phenyl)-1,3,4-oxadiazole

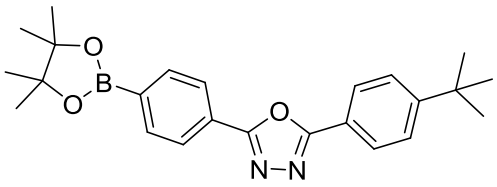

The standard Miyaura borylation procedure was followed using the following quantities: 2-(4-bromophenyl)-5-(4-*tert*-butylphenyl)-1,3,4-oxadiazole (**150**) (1.50 g, 4.2 mmol), 4,4,4',4',5,5,5',5'-octamethyl-2,2'-bi(1,3,2-dioxaborolane) (B_2pin_2) (1.17 g, 4.6 mmol) and potassium acetate (1.24 g, 12.6 mmol), [$PdCl_2$(dppf)] (10 mg, 0.1 mmol) and DMF (10 cm^3). The crude product was purified by column chromatography on silica gel with 9 : 1 (v/v) petroleum ether (b.p. 40 – 60 ^oC) : ethyl acetate as eluent to yield **158** as a white solid (1.41 g, 83%). ^1H NMR (700 MHz, $CDCl_3$): δ 8.12 (2 H, d, *J* = 8.3), 8.07 (2 H, d, *J* = 8.6), 7.95 (2 H, d, *J* = 8 .3), 7.54 (2 H, d, *J* = 8.6), 1.37 (18 H, s), 1.36 (9 H, s); ^{13}C NMR (176 MHz, $CDCl_3$): δ 164.78, 164.38, 155.36, 135.27, 126.81, 126.16, 126.02, 125.90, 121.05, 84.19, 35.08, 31.10, 24.87; HRMS (ASAP$^+$) calcd for $C_{24}H_{30}BN_2O_3$: 404.2386. Found: 404.2389.

159; 9-(7-Bromo-9,9-dihexyl-9*H*-fluoren-2-yl)-3,6-dimethoxy-9*H*-carbazole

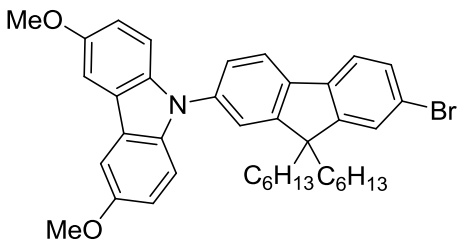

The standard ligand mediated Ullmann cross-coupling procedure was followed using the following quantities: 2-bromo-9,9-dihexyl-7-iodo-9*H*-fluorene (**137**) (1.00 g, 1.85 mmol), 3,6-di-methoxy-9*H*-carbazole (**142**) (0.42 g, 1.85 mmol), copper iodide (0.03 g, 0.19 mmol), 1,10-phenanthroline (0.07 g, 0.37 mmol), potassium carbonate (0.51 g, 3.7 mmol) and DMF (8 cm^3). The crude product was purified by column chromatography on silica with 98 : 2 (v/v) petroleum ether (b.p. 40 – 60 ^oC) : DCM as eluent to yield the product **159** as a white solid (1.10 g, 93%). ^1H NMR (500 MHz, $CDCl_3$): 7.86 (1 H, d, *J* = 7.8), 7.66 – 7.58 (3 H, m), 7.57 – 7.50 (4 H, m), 7.38 (2 H, d, *J* 8.9), 7.09 (2 H, dd, *J* 8.9, 2.5), 3.99 (6 H, s), 2.06 – 1.94 (4 H, m), 1.24 – 1.05 (12 H, m), 0.82 (6 H, t, *J* 7.1), 0.79 – 0.65 (4 H, m); ^{13}C NMR (126 MHz, $CDCl_3$) δ: 154.30, 153.43, 152.42, 139.65, 139.05, 137.55, 136.58, 130.47, 126.51, 125.72, 123.90, 121.58, 121.52, 121.43, 121.17, 115.47, 110.93, 103.20, 56.39, 55.93, 40.47, 31.79, 29.86, 24.11, 22.85, 14.33; HRMS (ASAP$^+$) calcd for $C_{39}H_{45}NO_2{}^{79}Br$: 638.2634. Found: 638.2622; Mp. 91.5 – 92.0 °C

160; 9-(7-Bromo-9,9-dihexyl-9*H*-fluoren-2-yl)-3,6-di-*tert*-butyl-9*H*-carbazole

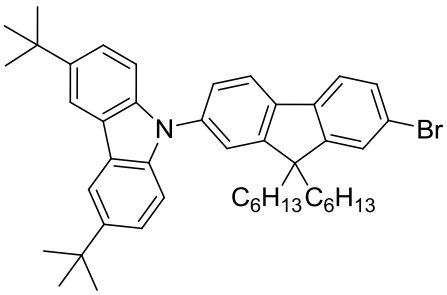

The standard ligand mediated Ullmann cross-coupling procedure was followed using the following quantities: 2-bromo-9,9-dihexyl-7-iodo-9*H*-fluorene (**137**) (1.00 g, 1.85 mmol), 3,6-di-*tert*-butyl-9*H*-carbazole (**143**) (0.52 g, 1.85 mmol), copper iodide (0.03 g, 0.19 mmol), 1,10-phenanthroline (0.07 g, 0.37 mmol), potassium carbonate (0.51 g, 3.7 mmol) and DMF (8 cm^3). The crude product was purified by column chromatography on silica with 98 : 2 (v/v) petroleum ether (b.p. 40 – 60 ^oC) : DCM as eluent to yield **160** as a white solid (1.00 g, 78%). ^1H NMR (400 MHz, $CDCl_3$): δ 8.17 (d, *J* = 1.0 Hz, 2H), 7.85 (d, *J* = 8.0 Hz, 1H), 7.62 (d, 1H), 7.56 – 7.48 (m, 5H), 7.47 (d, *J* = 2.0 Hz, 1H), 7.39 (d, *J* = 1.0 Hz, 1H), 7.37 (s, 1H), 2.03 – 1.92 (m, 4H), 1.48 (s, 18H), 1.22 – 0.99 (m, 12H), 0.86 – 0.61 (m, 10H); ^{13}C NMR (101 MHz, $CDCl_3$): δ 153.82, 152.20, 151.09, 141.88, 138.24, 137.78, 136.29, 129.18, 125.24, 124.46, 122.58, 122.39, 120.35, 120.26, 120.14, 119.85, 115.34, 108.16, 54.67, 39.24, 33.76, 31.03, 30.54, 28.62, 22.84, 21.60, 13.06; HRMS ($ASAP^+$) calcd for $C_{45}H_{56}N^{79}Br$: 689.3596. Found: 689.3611; Mp. 77.0 – 79.5 °C

161; 2-(4-*Tert*-butylphenyl)-5-(4-(7-(3,6-dimethoxy-9*H*-carbazol-9-yl)-9,9-dihexyl-9*H*-fluoren-2-yl)phenyl)-1,3,4-oxadiazole

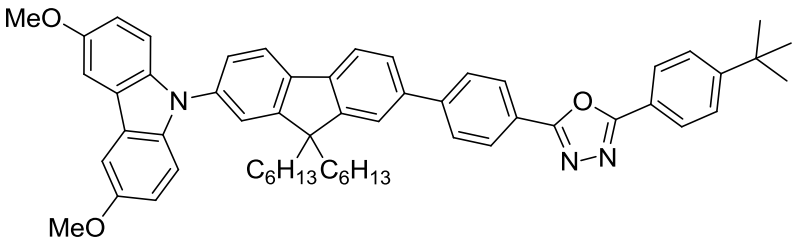

The standard Suzuki-Miyaura cross-coupling procedure was followed using the following quantities: 9-(7-bromo-9,9-dihexyl-9*H*-fluoren-2-yl)-3,6-di-methoxy-butyl-9*H*-carbazole (0.50 g, 0.78 mmol) (**159**), 2-(4-*tert*-butylphenyl)-5-(4-(4,4,5,5-tetramethyl-1,3,2-dioxaborolan-2-yl)phenyl)-1,3,4-oxadiazole (**158**) (0.32 g, 0.78 mmol), [$PdCl_2(PPh_3)_2$] (0.01 g, 0.02 mmol), NaOH (0.7 g in 5 cm^3 H_2O) and THF (30 cm^3). The crude product was purified by column chromatography on silica gel first with 7 : 3 (v/v) petroleum ether : diethyl ether as eluent and then a second time with DCM as eluent to yield **161** as a pale yellow solid (0.48 g, 73%). ^1H NMR (700 MHz, $CDCl_3$): δ 8.26 (d, *J* = 8.5 Hz, 2H), 8.11 (d, *J* = 8.5 Hz, 2H), 7.93 (d, *J* = 8.5 Hz, 1H), 7.90 – 7.82 (m, 3H), 7.70 (dd, *J* = 8.0, 1.5 Hz, 1H), 7.67 (d, *J* = 1.5 Hz, 1H), 7.60 (d, *J* = 2.0 Hz, 2H), 7.58 (d, *J* = 8.5 Hz, 2H), 7.56 – 7.53 (m, 2H), 7.39 (d, *J* = 8.5 Hz, 2H), 7.08 (dd, *J* = 8.5, 2.5 Hz, 2H), 3.98 (s, 6H), 2.15 – 2.00 (m, 4H), 1.40 (s, 9H), 1.22 – 1.05 (m, 12H), 0.89 – 0.72 (m, 10H); ^{13}C NMR (176 MHz, $CDCl_3$): δ 164.69,

164.31, 155.35, 154.03, 152.86, 151.89, 144.66, 140.56, 139.25, 138.85, 137.18, 136.40, 127.70, 127.36, 126.80, 126.34, 126.06, 125.42, 123.62, 122.69, 121.47, 121.35, 121.15, 120.99, 120.26, 115.18, 110.68, 103.00, 56.15, 55.55, 40.29, 35.10, 31.49, 31.13, 29.61, 23.92, 22.53, 14.00; HRMS (ASAP$^+$) calcd for $C_{57}H_{62}N_3O_3$: 836.4791. Found: 836.4827; Mp. 109.0 – 110.5 °C. Purity was judged to be >99% by HPLC analysis.

162; 2-(4-*Tert*-butylphenyl)-5-(4-(7-(3,6-di-*tert*-butyl-9*H*-carbazol-9-yl)-9,9-dihexyl-9*H*-fluoren-2-yl)phenyl)-1,3,4-oxadiazole

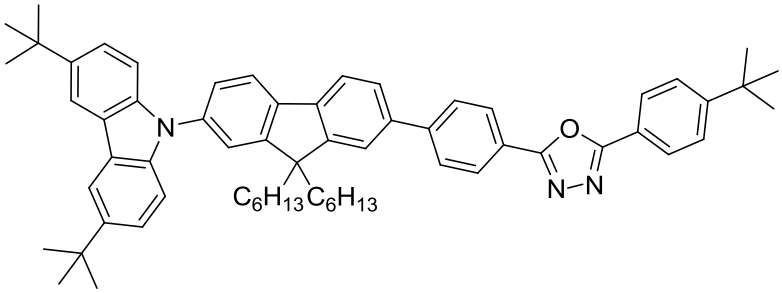

The standard Suzuki-Miyaura cross-coupling procedure was followed using the following quantities: 9-(7-bromo-9,9-dihexyl-9*H*-fluoren-2-yl)-3,6-di-*tert*-butyl-9*H*-carbazole (**160**) (0.30 g, 0.43 mmol), 2-(4-*tert*-butylphenyl)-5-(4-(4,4,5,5-tetramethyl-1,3,2-dioxaborolan-2-yl)phenyl)-1,3,4-oxadiazole (**158**) (0.18 g, 0.43 mmol), $[PdCl_2(PPh_3)_2]$ (0.01 g, 0.02 mmol), NaOH (0.5 g in 5 cm^3 in H_2O) and THF (30 cm^3). The crude product was purified by column chromatography on silica gel first with 7 : 3 (v/v) petroleum ether (b.p. 40 – 60 ^{o}C) : diethyl ether as eluent and then a second time with DCM as eluent to yield **162** as a white solid (0.30 g, 77%). ^{1}H NMR (700 MHz, $CDCl_3$): δ 8.26 (d, *J* = 8.0 Hz, 2H), 8.18 (d, *J* = 2.0 Hz, 2H), 8.11 (d, *J* = 8.5 Hz, 2H), 7.93 (d, *J* = 8.5 Hz), 7.90 – 7.84 (m, 3H), 7.70 (dd, *J* = 8.0, 1.5 Hz,, 1H), 7.67 (s, 1H), 7.61 – 7.54 (m, 4H), 7.50 (dd, *J* = 8.5, 2.0 Hz, 1H), 7.42 (d, *J* = 8.5 Hz, 3H), 2.12 – 2.01 (m, 4H), 1.49 (s, 18H), 1.39 (s, 9H), 1.21 – 1.08 (m, 12H), 0.85 – 0.76 (m, 10H); ^{13}C NMR (176 MHz, $CDCl_3$): δ 164.69, 164.32, 155.37, 152.78, 151.92, 144.70, 142.83, 140.64, 139.30, 139.23, 138.82, 137.19, 127.71, 127.37, 126.81, 126.33, 126.06, 125.42, 123.56, 123.38, 122.68, 121.46, 121.41, 121.16, 120.96, 120.25, 116.31, 109.20, 55.56, 40.33, 35.11, 34.74, 32.03, 31.53, 31.14, 29.65, 23.93, 22.57, 14.03; HRMS (ASAP$^+$) calcd for $C_{63}H_{74}N_3O$: 888.5832. Found: 888.5859; Mp. 137.0 – 139.0 °C. Purity was judged to be >99% by HPLC analysis.

163; 2-(4-(9*H*-Carbazol-9-yl)phenyl)-5-(4-*tert*-butylphenyl)-1,3,4-oxadiazole

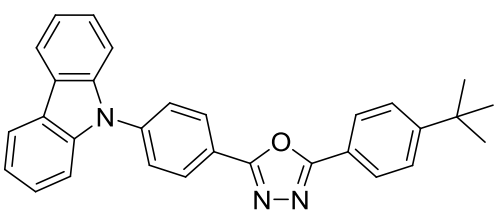

To a flame dried flask under an atmosphere of argon 2 - (4 - bromophenyl) - 5 - (4 – *tert* -

butylphenyl)-1,3,4-oxadiazole (**150**) (0.4 g, 1.12 mmol), 9*H*-carbazole (**2**) (0.22 g, 1.34 mmol) and potassium carbonate (0.46 g, 3.36 mmol) were added. Anhydrous toluene (10 cm^3) was added to the reagents and degassed for 1 hr. To this stirred solution palladium (II) acetate (7.5 mg, 0.03 mmol) and tri-*tert*-butylphosphonium tetrafluoroborate (29 mg, 0.10 mmol) were added and the reaction mixture heated to reflux for 22 h. The reaction mixture was cooled, washed with brine and extracted with diethyl ether. The combined organic phases were washed with water, dried ($MgSO_4$) and concentrated. The crude product was purified by column chromatography on silica gel first with 7 : 3 (v/v) petroleum ether (b.p. 40 – 60 ^oC) : diethyl ether as eluent and then a second time with DCM as eluent. The product obtained was recrystallised from acetonitrile to yield **163** as colourless crystals (0.27 g, 54%). ^1H NMR (700 MHz, $CDCl_3$): δ 8.39 (d, *J* = 8.5 Hz, 2H), 8.17 (d, *J* = 8.0 Hz, 2H), 8.11 (d, *J* = 8.5 Hz, 2H), 7.79 (d, *J* = 8.5 Hz, 2H), 7.59 (d, *J* = 8.5 Hz, 2H), 7.51 (d, *J* = 8.0 Hz, 2H), 7.49 – 7.42 (m, 2H), 7.37 – 7.31 (m, 2H), 1.39 (s, 9H); ^{13}C NMR (176 MHz, $CDCl_3$): δ 164.88, 163.78, 155.52, 140.80, 140.29, 128.52, 127.24, 126.82, 126.19, 126.11, 123.77, 122.63, 120.99, 120.54, 120.45, 109.69, 35.12, 31.11; HRMS ($ASAP^+$) calcd for $C_{30}H_{26}N_3O$: 444.2076. Found: 444.2074; Mp. 171.5 – 173.0.

164; 2-(4-*Tert*-butylphenyl)-5-(4-(9,9-dihexyl-7-iodo-9*H*-fluoren-2-yl)phenyl)-1,3,4-oxadiazole

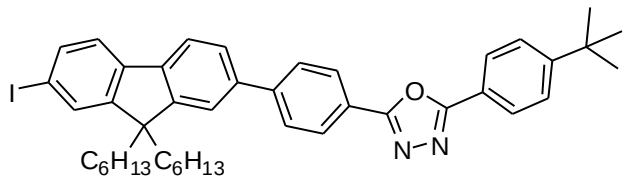

A solution of 2-(4-tertbutylphenyl) - 5 - (4-(9,9-dihexyl - 7 - trimethylsilyl) - 9H - fluorene-2-yl)phenyl) - 1,3,4 – oxadiazole (**127**) (0.63 g, 0.92 mmol) in DCM (20 cm^3) was cooled to 0 °C in an ice bath. To this stirred solution 1M iodine monochloride (1.5 cm^3, 1.5 mmol) was added. The reaction mixture was stirred for 1.5 h, quenched with aqueous sodium thiosulfate, extracted into DCM, washed with brine, concentrated under reduced pressure and recrystallised from ethanol. The product **164** was obtained as white crystals (0.64 g, 93%). ^1H NMR (700 MHz, $CDCl_3$): δ 8.24 (d, J = 8.5 Hz, 2H), 8.10 (d, J = 8.5 Hz, 2H), 7.82 (d, J = 8.5 Hz, 2H), 7.76 (d, J = 8.0 Hz, 1H), 7.70 (d, J = 1.0 Hz, 1H), 7.69 (dd, J = 8.0, 1.0 Hz, 1H), 7.64 (dd, J = 8.0, 1.5 Hz, 1H), 7.59 (d, J = 1.5 Hz, 1H), 7.57 (d, J = 8.5 Hz, 1H), 7.48 (d, 8.5 Hz, 1H), 2.00 (m, 4H), 1.39 (s, 9H), 1.09 (m, 12H), 0.78 (t, J = 7.5 Hz, 6H), 0.67 (m, 4H); ^{13}C NMR (176 MHz, $CDCl_3$): δ 164.68, 164.27, 155.43, 153.42, 151.05, 144.60, 140.28, 140.10, 139.24, 135.96, 132.12, 127.68, 127.35, 126.79, 126.25, 126.05, 122.70, 121.59, 121.35, 121.11, 120.26, 92.88, 55.50, 40.22, 35.09, 31.41, 31.12, 29.58, 23.75, 22.54, 13.97; MS (EI^+): 736 (M^+, 100%); Anal. Calcd. For $C_{43}H_{49}IN_2O$: C, 70.10; H, 6.70; N, 3.80. Found: C, 70.34; H: 6.77; N: 3.72; Mp: 139.5 – 140.9 ^oC

165; 2-(4-(7'-(9*H*-Carbazol-9-yl)-9,9,9',9'-tetrahexyl-2,2'-bi(9*H*-fluoren)-7-yl)phenyl)-5-(4-*tert*-butylphenyl)-1,3,4-oxadiazole

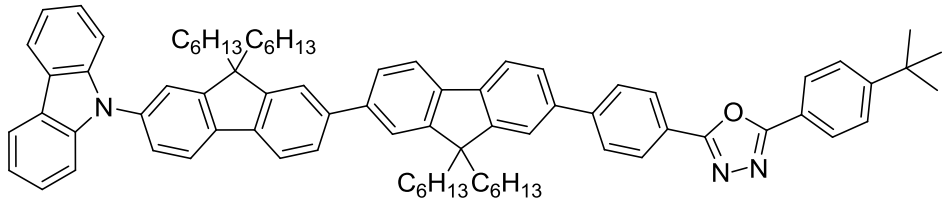

The standard Suzuki-Miyaura cross-coupling procedure was followed using the following quantities: 9-(9,9-dihexyl-7-(4,4,5,5-tetramethyl-1,3,2-dioxaborolan-2-yl)-9*H*-fluoren-2-yl)-9*H*-carbazole (**139**) (0.20 g, 0.32 mmol), 2-(4-*tert*-butylphenyl)-5-(4-(9,9-dihexyl-7-iodo-9*H*-fluoren-2-yl)phenyl)-1,3,4-oxadiazole (**164**) (0.26 g, 0.35 mmol), $Pd(PPh_3)_2Cl_2$, NaOH (0.5 g in 5 cm^3 H_2O) and THF (30 cm^3). The crude product was purified by column chromatography on silica gel first with 7 : 3 (v/v) petroleum ether (b.p. 40 – 60 ^oC) : diethyl ether as eluent and then a second time with DCM as eluent to yield **165** as a white solid (0.32 g, 91%). ^1H NMR (700 MHz, $CDCl_3$): δ 8.27 (d, *J* = 7.0 Hz, 2H), 8.20 (d, *J* = 8.0 Hz, 2H), 8.12 (dd, *J* = 8.0, 1.5 Hz, 2H), 7.96 (d, *J* = 7.5 Hz, 1H), 7.87 (m, 4H), 7.79 – 7.64 (m, 6H), 7.64 – 7.54 (m, 4H), 7.54 – 7.40 (m, 4H), 7.33 (t, *J* = 7.5 Hz, 2H), 2.21 – 2.01 (m, 8H), 1.40 (s, 9H), 1.23 – 1.05 (m, 24H), 0.97 – 0.72 (m, 20H); ^{13}C NMR (176 MHz, $CDCl_3$): δ 164.69, 164.35, 155.33, 152.86, 151.96, 151.91, 151.82, 144.83, 141.07, 141.02, 140.81, 140.70, 140.09, 139.81, 139.58, 138.64, 136.36, 127.69, 127.37, 126.81, 126.37, 126.29, 126.22, 126.07, 125.90, 125.83, 123.38, 122.62, 121.86, 121.51, 121.49, 121.19, 120.85, 120.37, 120.23, 120.16, 119.86, 109.81, 60.37, 55.55, 55.44, 40.38, 40.30, 35.11, 31.51, 31.46, 31.15, 29.67, 29.63, 23.95, 23.85, 22.56, 22.54, 14.02, 14.01; HRMS ($ASAP^+$) calcd for $C_{80}H_{90}ON_3$ 1108.70784. Found: 1108.70900; Mp. 113.5 – 115.0 °C. Purity was judged to be >99% by HPLC analysis.

Software Version	: 6.3.1.0504	Date	: 01/03/2010 18:05:43
Reprocess Number	: bioactivehplc1: 4068		
Sample Name	: KEL2-3 4xdil	Data Acquisition Time	: 01/03/2010 17:09:42
Instrument Name	: HPLC1	Channel	: A
Rack/Vial	: 0/3	Operator	: dch5lwl
Sample Amount	: 1.000000	Dilution Factor	: 1.000000
Cycle	: 3		

Result File : C:\HPLC1\Data\Aileen\KEL2-3 4xdil_2010__03_01_HPLC1_005.rst
Sequence File : C:\HPLC1\KEL MAR1.seq

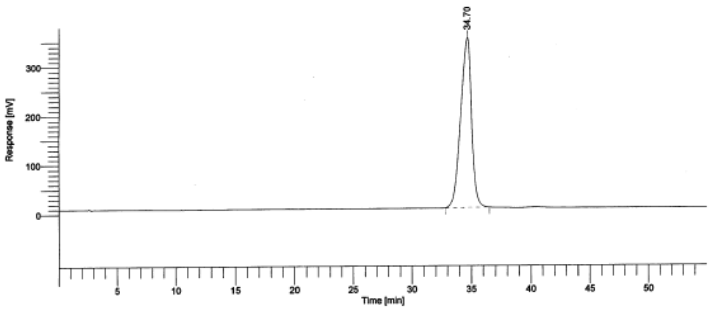

HPLC REPORT

Peak #	Component Name	Time [min]	Area [uV*sec]	Height [uV]	Area [%]	BL	Adjusted Amount
1		34.696	22040175.35	345979.96	100.00	BB	22.0402
			22040175.35	345979.96	100.00		22.0402

Column: Phenomenex Hyperclone 25cm, 4.6mm i.d., 5u, ODS (C18) 120A

Figure 6.1 – Representative HPLC trace (compound 156) for OLED candidates of chapter 2

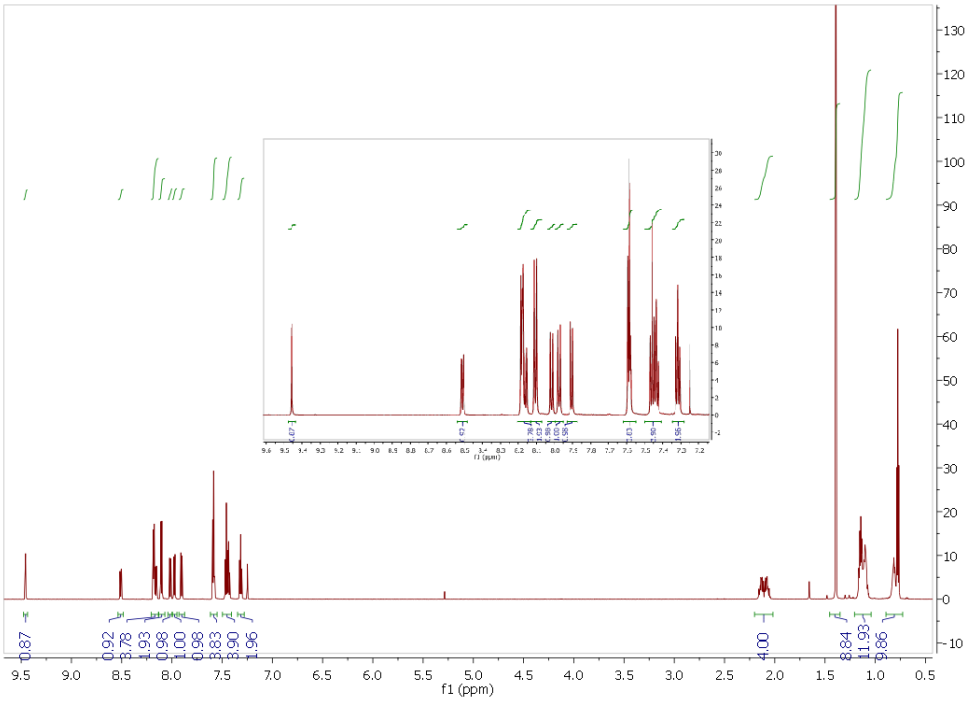

Figure 6.2 – Representative proton NMR spectrum (compound 156) for OLED candidates of chapter 2

6.4 Experimental Details for Chapter 3

180, (5-Bromo-1,3-phenylene)dimethanol

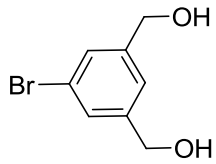

5-Bromoisophthalic acid (**179**) (2.50 g, 0.01 mol) was dissolved in anhydrous THF (20 cm^3) and a borane THF complex (40 cm^3, 40 mmol) was added dropwise. The reaction mixture was stirred at room temperature for 16 h. The reaction mixture was then carefully quenched with HCl (aq) and extracted with DCM (2 x 50 cm^3), washed with $NaHCO_3$ (2 x 30 cm^3) and brine solution. The organic extracts were combined and the solvent removed under reduced pressure. The product **180** was isolated as a white solid (2.04 g, 94%). The NMR data were consistent with the literature.[140] ^{1}H NMR (400 MHz, $CDCl_3$): δ 7.25 (s, 2H), 7.09 (s, 1H), 4.46 (s, 4H).

181, 5-Bromoisophthalaldehyde

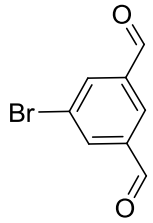

(5-Bromo-1,3-phenylene)dimethanol (**180**) (2.04 g, 9.4 mmol) was dissolved in DCM (40 cm^3) and was added slowly to a mixture of PCC (7.25 g, 33.6 mmol) in DCM (30 cm^3). The reaction mixture was stirred for 1 h at room temperature. After this time, Celite was added to the reaction mixture and the resulting slurry was filtered through a plug of silica gel and washed with DCM. The product **181** was isolated as a white solid (1.73 g, 88%). The NMR data were consistent with the literature.[141] ^{1}H NMR (400 MHz, $CDCl_3$): δ 10.04 (s, 2H), 8.29 (t, *J* = 1.5 Hz, 1H), 8.24 (d, *J* = 1.5 Hz, 2H).

182, 5-Bromoisophthalonitrile

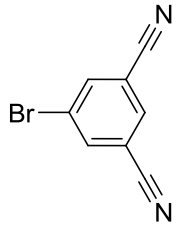

5-Bromoisophthalaldehyde (**181**) (1.70 g, 8.0 mmol) was dissolved in THF (20 cm^3) and aqueous ammonia (60 cm^3) was added followed by iodine (4.47 g, 18.6 mmol). The reaction mixture was stirred for 2 h then poured onto water (100 cm^3) and extracted with ethyl acetate (3 x 50 cm^3) and washed with saturated sodium thiosulfate solution (30 cm^3). The organic extracts were combined and the solvent removed under reduced pressure. The crude product was purified by column chromatography on silica gel using dichloromethane as eluent to give **182** as a white solid (0.81 g, 49%). The NMR data were consistent with the literature.[101] ^{1}H NMR (400 MHz, $CDCl_3$): δ 8.03 (d, *J* = 1.5 Hz, 2H), 7.89 (t, *J* = 1.5 Hz, 1H); ^{13}C NMR (101 MHz, $CDCl_3$) δ 138.73, 133.73, 123.91, 115.64, 115.22.

183; 5,5'-(5-Bromo-1,3-phenylene)bis(1*H*-tetrazole)

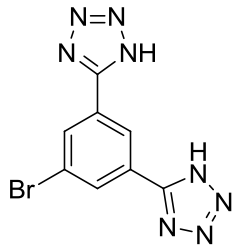

In a flame dried flask under an atmosphere of argon 5-bromoisophthalonitrile (**182**) (0.8 g, 3.9 mmol), ammonium chloride (0.48 g, 9 mmol) and sodium azide (0.60 g, 9 mmol) were added. Anhydrous DMF (30 cm^3) was added and the reaction mixture was heated to reflux for 5 h. After this time the mixture was cooled and poured onto iced water. The solution was then acidified to pH 2 with HCl to precipitate the product. The product was filtered and dried under high vacuum to give **183** which was isolated as a white solid and used without further purification (1.16 g, 100%). The identity of the intermediate was confirmed by NMR spectroscopy. ^{1}H NMR (400 MHz, DMSO-d_6): δ 8.78 (t, *J* = 1.5 Hz, 1H), 8.41 (d, *J* = 1.5 Hz, 2H), 7.95 (s, 2H); ^{13}C NMR (101 MHz, DMSO-d_6): δ 171.97, 162.74, 131.97, 123.60, 99.98.

184; 5,5'-(5-Bromo-1,3-phenylene)bis(2-(4-*tert*-butylphenyl)-1,3,4-oxadiazole)

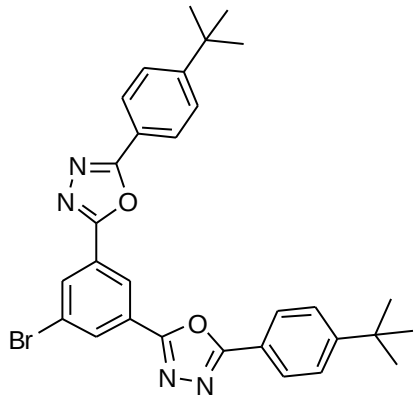

To a flask containing 5,5'-(5-bromo-1,3-phenylene)bis(1*H*-tetrazole) (**183**) (1.1 g, 3.8 mmol) dissolved in pyridine (30 cm^3) was added *tert*-butylbenzoyl chloride (1.83 cm^3, 9.4 mmol). The reaction mixture was heated to reflux for 15 h after which time the reaction mixture was poured onto an ice-water mixture to precipitate a white solid. The product was filtered and dried under high vacuum to give **184** as a white solid (1.59 g, 76%). ^{1}H NMR (400 MHz, $CDCl_3$): δ 8.82 (t, *J* = 1.5 Hz, 1H), 8.48 (d, *J* = 1.5 Hz, 2H), 8.13 (d, *J* = 8.5 Hz, 4H), 7.61 (d, *J* = 8.5 Hz, 4H), 1.41 (s, 9H); ^{13}C NMR (101 MHz, $CDCl_3$): δ 164.45, 161.25, 154.97, 131.20, 126.03, 125.74, 125.21, 122.89, 122.35, 119.51, 34.19, 30.13; MS (ASAP$^+$) 558.2 (100%, M^+); Mp: 203.6 – 204.9 ^{o}C.

177; 2,5,5'-(5-(7-(9*H*-Carbazol-9-yl)-9,9-dihexyl-9*H*-fluoren-2-yl)-1,3-phenylene)bis(2-(4-*tert*-butylphenyl)-1,3,4-oxadiazole)

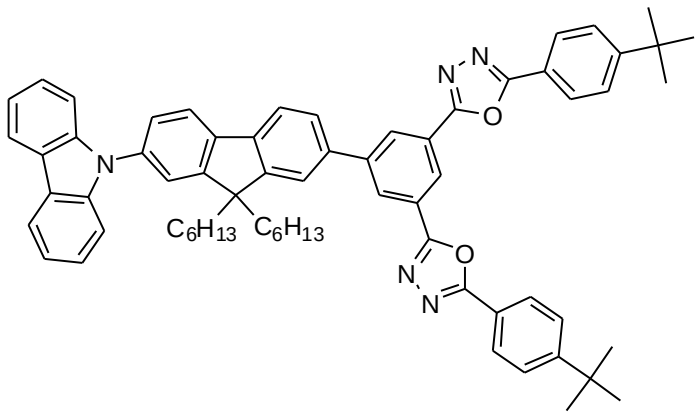

The standard Suzuki-Miyaura cross-coupling procedure was followed using the following quantities: 9-(9,9-dihexyl-7-

(4,4,5,5-tetramethyl-1,3,2-dioxaborolan-2-yl)-9*H*-fluoren-2-yl)-9*H*-carbazole (**139**) (0.34 g, 0.54 mmol), 5,5'-(5-bromo-1,3-phenylene)bis(2-(4-*tert*-butylphenyl)-1,3,4-oxadiazole) (**184**) (0.30 g, 0.54 mmol), [$PdCl_2(PPh_3)_2$], NaOH (60 mg in 10 cm^3) and THF (20 cm^3). The crude product was purified by column chromatography on silica gel using DCM as eluent to afford **177** as a white solid (0.46 g, 87%). ^{1}H NMR (700 MHz, $CDCl_3$): δ 8.83 (s, 1H), 8.66 (d, *J* = 1.5 Hz, 2H), 8.19 (d, *J* = 7.5 Hz, 2H), 8.16 (d, *J* = 8.5 Hz, 4H), 7.99 (d, *J* = 8.5 Hz, 1H), 7.94 (d, *J* = 7.5 Hz, 1H), 7.81 (d, *J* = 7.5 Hz, 1H), 7.76 (s, 1H), 7.64 – 7.57 (m, 6H), 7.50 – 7.41 (m, 4H), 7.32 (t, *J* = 7.5 Hz, 2H), 2.20 – 2.03 (m, 4H), 1.40 (s, 18 2H), 1.22 – 1.07 (m, 12H), 0.88 – 0.74 (m, 10H); ^{13}C NMR (176 MHz, $cdcl_3$) δ 165.26, 163.59, 155.76, 153.00, 152.22, 143.75, 140.99, 140.96, 139.57, 137.83, 136.83, 128.31, 126.99, 126.56, 126.15, 125.91, 125.68, 123.39, 123.35, 121.87, 121.63, 121.16, 120.80, 120.52, 120.37, 119.90, 109.75, 55.77, 40.30, 35.15, 31.50, 31.11, 29.60, 23.98, 22.54, 13.97; HRMS (ASAP$^+$) calcd for $C_{67}H_{69}N_5O_2$: 975.5451. Found: 975.5480; Mp: 166.3 – 166.9 ^oC.

185; 3,6-Bis(4-(5-(4-*tert*-butylphenyl)-1,3,4-oxadiazol-2-yl)phenyl)-9*H*-carbazole

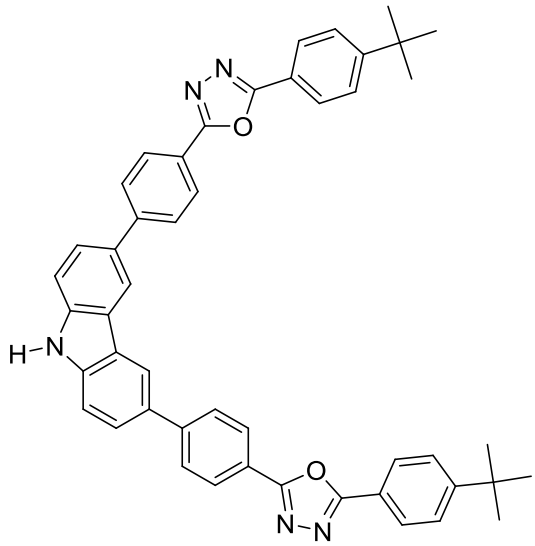

In a flame dried flask under an atmosphere of argon 3,6-dibromo-9*H*-carbazole (**141**) (0.30 g, 0.92 mmol) and 2-(4-*tert*-butylphenyl)-5-(4-(4,4,5,5-tetramethyl-1,3,2-dioxaborolan-2-yl)phenyl)-1,3,4-oxadiazole (**158**) (0.82 g, 2.03 mmol) were combined. To the solid reagents was added anhydrous toluene (50 cm^3) which was heated to 40 °C to achieve full dissolution of the starting materials. To this stirred solution potassium phosphate (1.18 g, 5.5 mmol) in water (10 cm^3) was added. The mixture was degassed for 10 min followed by the addition of [$PdCl_2$(dppf)] (44 mg, 0.06 mmol). The reaction mixture was then heated to 110 °C for 15 h. The reaction was cooled and extracted with diethyl ether and brine solution. The organic extracts were combined and the solvent removed under reduced pressure. The crude product was purified by chromatography on silica gel using dichloromethane with 10% ethyl acetate as eluent. The crude product **185** was isolated as a white solid and used without further purification (0.32 g, 47%). The ^{1}H NMR spectrum was consistent with structure **185**. ^{1}H NMR (400 MHz, $CDCl_3$): δ 8.39 (d, *J* = 1.5 Hz, 2H), 8.23 (s, 1H),

8.19 (d, *J* = 8.5 Hz, 4H), 8.04 (d, *J* = 8.5 Hz, 4H), 7.84 (d, *J* = 8.5 Hz, 4H), 7.72 (dd, *J* = 8.5, 1.5 Hz, 2H), 7.56 – 7.48 (m, 6H), 1.32 (s, 18H)

185; 5,5'-(4,4'-(9-(7-Bromo-9,9-dihexyl-9*H*-fluoren-2-yl)-9*H*-carbazole-3,6-diyl)bis(4,1-phenylene))bis(2-(4-*tert*-butylphenyl)-1,3,4-oxadiazole)

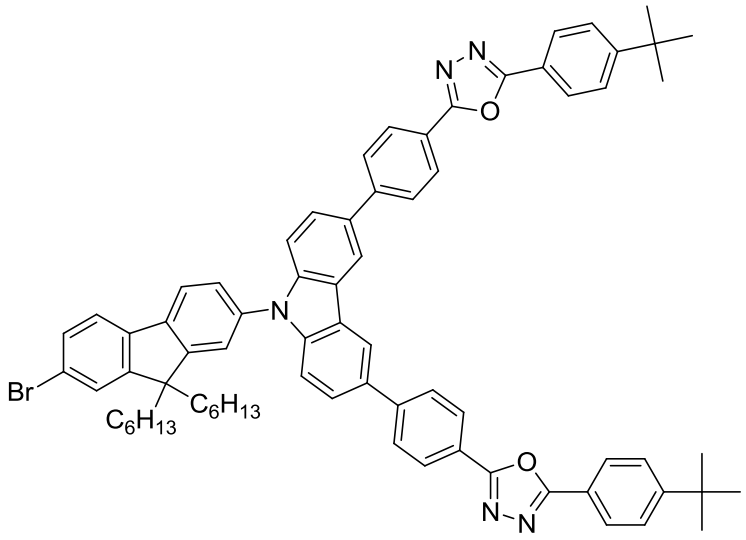

The standard ligand mediated Ullmann cross-coupling procedure was followed using the following quantities: 3,6-bis(4-(5-(4-*tert*-butylphenyl)-1,3,4-oxadiazol-2-yl)phenyl)-9*H*-carbazole (**185**) (0.15 g, 0.21 mmol), 2-bromo-9,9-dihexyl-7-iodo-9*H*-fluorene (**137**) (0.16 g, 0.29 mmol), potassium carbonate (0.06 g, 0.42 mmol), copper iodide (4 mg) and 1,10-phenanthroline (8 mg) and DMF (8 cm^3). The crude product was purified by chromatography on silica gel using dichloromethane with 10% ethyl acetate as eluent. The product **185** was isolated as a white solid (0.12 g, 51%). ^{1}H NMR (400 MHz, $CDCl_3$): δ 8.56 (d, *J* = 2.0 Hz, 2H), 8.29 (d, *J* = 8.5 Hz, 4H), 8.13 (d, *J* = 8.5 Hz, 4H), 7.95 (d, *J* = 8.5 Hz, 4H), 7.80 (dd, *J* = 8.5, 2.0 Hz, 2H), 7.72 – 7.53 (m, 10H), 2.12 – 1.96 (m, 4H), 1.41 (s, 18H), 1.29 – 1.10 (m, 12H), 0.90 – 0.66 (m, 10H); ^{13}C NMR (176 MHz, $CDCl_3$): δ 164.51, 163.23, 151.30, 150.04, 148.42, 143.76, 142.17, 141.34, 140.89, 140.03, 139.13, 137.85, 133.51, 129.67, 129.06, 128.80, 127.22, 127.13, 127.14, 125.25, 125.05, 122.58, 119.42, 118.34, 116.84, 111.62, 111.60, 115.66, 52.22, 43.93, 34.25, 31.82, 31.47, 29.93, 24.42, 22.70, 14.11; MS (MALDI$^+$) 1129.5 (M^+, 100%); Mp: 207.3 – 208.1 ^{o}C.

178; 5,5'-(4,4'-(9-(7-(4-(5-(4-*tert*-Butylphenyl)-1,3,4-oxadiazol-2-yl)phenyl)-9,9-dihexyl-9*H*-fluoren-2-yl)-9*H*-carbazole-3,6-diyl)bis(4,1-phenylene))bis(2-(4-*tert*-butylphenyl)-1,3,4-oxadiazole)

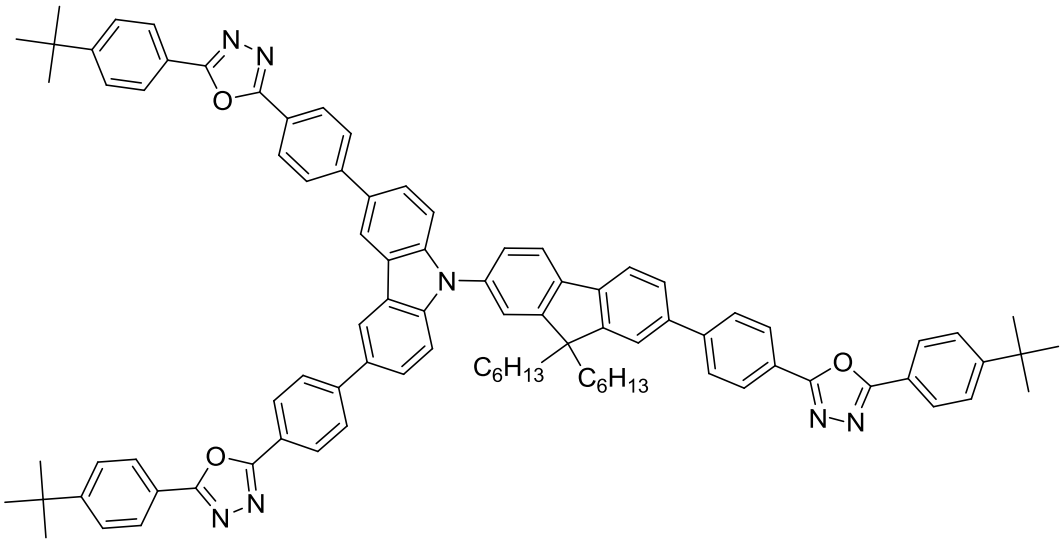

The standard Suzuki-Miyaura cross-coupling procedure was followed using the following quantities: 5,5'-(4,4'-(9-(7-bromo-9,9-dihexyl-9*H*-fluoren-2-yl)-9*H*-carbazole-3,6-diyl)bis(4,1-phenylene))bis(2-(4-*tert*-butylphenyl)-1,3,4-oxadiazole) (**185**) (85 mg, 0.075 mmol), 2-(4-*tert*-butylphenyl)-5-(4-(4,4,5,5-tetramethyl-1,3,2-dioxaborolan-2-yl)phenyl)-1,3,4-oxadiazole (**158**), $[PdCl_2(PPh_3)_2]$ (5 mg), NaOH (6 mg in 2 cm^3 H_2O) and THF (10 cm^3). The crude product was purified by column chromatography on silica gel using 4 : 1 diethyl ether : petroleum ether (b.p. 40 – 60 ^oC) as eluent followed by second purification with dichloromethane with 5% ethyl acetate as eluent. The product **178** was isolated as a white solid (80 mg, 80%). ^1H NMR (700 MHz, $CDCl_3$): δ 8.54 (d, *J* = 1.0 Hz, 2H), 8.26 (d, *J* = 8.5 Hz, 6H), 8.10 (d, *J* = 8.0 Hz, 6H), 8.03 (d, *J* = 8.0 Hz, 1H), 8.01 (d, *J* = 8.0 Hz, 1H), 7.93 (d, *J* = 8.5 Hz, 4H), 7.90 (d, *J* = 7.5 Hz, 1H), 7.87 (d, *J* = 8.5 Hz, 2H), 7.78 (d, *J* = 8.5 Hz, 2H), 7.73 (d, *J* = 7.5 Hz, 1H), 7.68 (s, 1H), 7.65 – 7.60 (m, 3H), 7.60 – 7.55 (m, 8H), 7.53 (d, *J* = 8.5 Hz, 1H), 7.01 (d, *J* = 8.5 Hz, 1H), 2.14 – 2.06 (m, 4H), 1.38 (s, 9H), 1.38 (s, 18H), 1.22 – 1.08 (m, 12H), 0.92 – 0.76 (m, 10H); ^{13}C NMR (176 MHz, $CDCl_3$): δ 164.72, 164.64, 164.41, 164.28, 155.40, 155.32, 153.16, 151.94, 150.96, 144.95, 144.57, 141.51, 140.29, 140.26, 140.08, 139.23, 136.12, 132.38, 128.90, 127.74, 127.70, 127.45, 127.39, 126.80, 126.78, 126.63, 126.46, 126.07, 126.05, 125.97, 125.76, 124.08, 122.19, 121.68, 121.55, 121.25, 121.16, 121.11, 120.46, 119.16, 116.08, 110.56, 60.36, 55.69, 40.30, 35.09, 31.51, 31.12, 29.62, 23.97, 22.54, 14.17, 14.02; MS (MALDI$^+$) 1327.7 (M^+, 100%); Mp: > 350 ^oC.

6.5 Experimental Details for Chapter 4

TCSPC Measurements

The sample is excited by a pulsed laser comprising a Verdi V8 green diode laser which pumps a picosecond Mira 9000 Ti:Sapphire mode-locked tuneable oscillator cavity. This cavity is tuned to 780 nm and produces a stream of pulses with a mean power of 0.7-1.2 W, dependent upon the precise cavity conditions. These pulses are passed through a beta-barium borate crystal aligned on a micrometer support to provide frequency doubling to 390 nm. The mixed 780 nm/390 nm beam is then split at a layered dielectric mirror that reflects the longer wavelength component onto a photodiode to trigger the streak camera start time. The 390nm component is directed through alignment irises and onto the sample. The sample emission is collected through a filter to remove the laser scatter, and focused into a broad bandpass monochromator. The resulting frequency-separated light is directed into the single photon counting detector. The detector is a water-cooled high resolution Hamamatsu E3809U-50 MCP photomultiplier tube for single photon detection attached to the double-monochromator assembly. The computer attached to the detector has a Becker & Hickl SPC-630 Time-Correlated Single-Photon Counting (TCSPC) card, which has a maximum of 4096 channels, with adjustable time window resolution with a minimum of 814 fs. This allows photoluminescence decays to be measured both on ultra-short timescales as well as on longer time domains up to 10 ns not accessible to the streak camera. The laser pulses measured by the system (incorporating the detector response characteristics) have a full width half maximum of 21-23 ps. With deconvolution of the decays, components with lifetimes of several picoseconds can be fitted, although the accuracy and validity of fitting such short lifetime components is at best uncertain.

The TCSPC module builds up a profile of the decay by repeated measurements of the same experiment. The incident laser beam that excites the sample passes through a beam-splitter that passes a small part of the laser pulse to a Becker & Hickl PHD-400N fast photodiode that provides the trigger pulse to the TCSPC card. This trigger pulse stops the charging of a capacitor within the card, which is started when a photon, emitted from the sample through the monochromators to the detector triggers a second pulse. This reverse mode of operation ensures that only real events are counted. The charge stored on the capacitor is read out and binned in the appropriate time channel. The probability of the photon from the sample arriving within a certain time bin is determined by the sample lifetime, and after a large number of repeats, of the order of 106 for an average sample, the profile of the integrated

counts across the time bins represents the decay profile of the sample in the time domain. The laser repetition rate is 76 MHz, and with a low gain preamplifier on the MCP this allows most decay profiles to be collected within a few minutes.

208, 1,4-Bis(hexyloxy)benzene

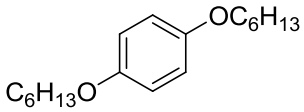

In an oven dried flask hydroquinone **207** (50.0 g, 0.45 mol), potassium hydroxide (70.0 g, 1.25 mol) and ethanol (500 cm^3) were added. This mixture was stirred at room temperature for 30 min, after which time 1-bromohexane (191 cm^3, 1.36 mol) was added dropwise and then heated to 65 °C for 4 h. The reaction mixture was cooled and filtered from the insoluble inorganics. The filtrate was concentrated under reduced pressure. The filtered solid was washed with hexane (2 x 250 cm^3) and the washings combined with the crude product. This was washed with water and extracted with hexane then concentrated. The crude product was recrystallised from methanol to yield **208** as colourless crystals (113.2 g, 90%). The NMR data were consistent with the literature.[114] ^{1}H NMR (400 MHz, $CDCl_3$): δ 6.81 (s, 4H), 3.88 (t, *J* = 6.5 Hz, 4H), 1.78 – 1.67 (m, 4H), 1.49 – 1.26 (m, 12H), 0.92 – 0.85 (t, *J* = 7.0 Hz 6H).

209, 1,4-Bis(hexyloxy)-2,5-diiodobenzene

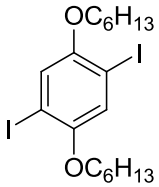

In a flame dried flask 1,4-bis(hexyloxy)benzene **208** (5.00 g, 18.0 mmol) was added to a mixture of glacial acetic acid (100 cm^3), conc. sulfuric acid (2 cm^3) and water (5 cm^3). To this stirred solution potassium iodate (1.92 g, 9.0 mmol) and iodine (4.79 g, 18.9 mmol) were added. The reaction mixture was heated to reflux for 6 h then cooled. Water (50 cm^3) was added and the mixture was extracted with DCM and the organic extracts washed with water. The crude product was purified by column chromatography with 9:1 petroleum ether (b.p. 40 – 60 ^oC) : ethyl acetate as eluent followed by recrystallisation from methanol to give **209** as white crystals (3.03 g, 32%). The NMR data were consistent with the literature.[113] ^{1}H NMR (400 MHz, $CDCl_3$): δ 7.19 (s, 2H), 3.95 (t, *J* = 6.5 Hz, 4H), 1.82 (m, 4H), 1.59 – 1.46 (m, 6H), 1.44 – 1.31 (m, 8H), 1.03 – 0.86 (m, 6H).

210; 4-(2,5-Bis(hexyloxy)-4-iodophenyl)-2-methylbut-3-yn-2-ol

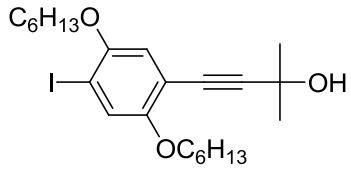

The standard Sonogashira cross-coupling procedure was followed using the following quantities: 1,4-bis(hexyloxy)-2,5-diiodobenzene **209** (5.00 g, 9.43 mmol),), 2-methylbut-3-yn-2-ol (0.91 cm^3, 9.43 mmol), [$PdCl_2(PPh_3)_2$] (0.3 g), copper iodide (0.1 g) and triethylamine (100 cm^3). The crude product was purified by column chromatography using dichloromethane as eluent to yield **210** as a pale yellow solid (2.32 g, 51%). The NMR data were consistent with the literature.[113] ^{1}H NMR (400 MHz, $CDCl_3$): δ 7.27 (s, 1H), 6.81 (s, 1H), 3.94 (t, *J* = 6.5 Hz, 4H), 2.12 (s, 1H), 1.90 – 1.71 (m, 5H), 1.64 (s, 6H), 1.58 – 1.43 (m,4H), 1.43 – 1.26 (m, 8H), 1.06 – 0.83 (m, 6H).

211; 4-(2,5-bis(hexyloxy)-4-((trimethylsilyl)ethynyl)phenyl)-2-methylbut-3-yn-2-ol

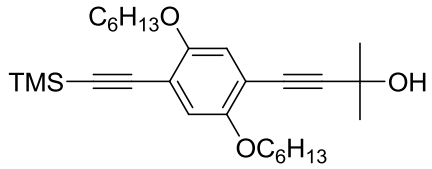

In a flame dried flask under an atmosphere of argon 4-(2,5-bis(hexyloxy)-4-iodophenyl)-2-methylbut-3-yn-2-ol **210** (2.32 g, 4.77 mmol) is dissolved in THF (20 cm^3). To this stirred solution [$PdCl_2(PPh_3)_2$] (0.1 g), copper iodide (0.1 g) and triethylamine (50 cm^3) were added. The mixture was degassed for 20 min after which time trimethylsilyl acetylene (0.98 g, 10 mmol) was added. The reaction mixture was stoppered and stirred at room temperature for 1 h followed by stirring at 50 °C for 1 h. . The solvent was then removed under vacuum and the crude oil purified by column chromatography using DCM as eluent to yield **211** as a pale yellow solid (2.02 g, 93%). The NMR data were consistent with the literature.[113] ^{1}H NMR (400 MHz, $CDCl_3$): δ 6.91 (s, 1H), 6.86 (s, 1H), 3.95 (t, *J* = 6.5Hz, 4H), 2.07 (s, 1H), 1.89 – 1.71 (m, 4H), 1.64 (s, 6H), 1.59 – 1.43 (m, 4H), 1.43 – 1.27 (m, 8H), 0.92 (m, 6H), 0.27 (s, 9H).

212, ((4-Ethynyl-2,5-bis(hexyloxy)phenyl)ethynyl)trimethylsilane

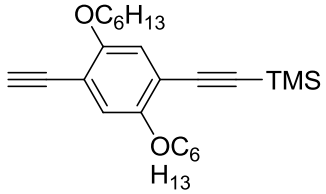

4-(2,5-Bis(hexyloxy)-4-((trimethylsilyl)ethynyl)phenyl)-2-methylbut-3-yn-2-ol **211** (1.39 g, 3.1 mmol) was dissolved in anhydrous toluene (50 cm^3) to which powdered sodium hydroxide (0.73 g) was added. The reaction mixture was heated to 100 °C for 3 h. The solvent was removed and the crude oil was purified by column chromatography using 4:1 (v/v) petroleum ether (b.p. 40 – 60 ^{o}C) : DCM as eluent to yield **212** as a yellow solid (0.62 g, 51%). The NMR data were consistent with the literature.[113] ^{1}H NMR (400 MHz, $CDCl_3$) δ 6.91 (s, 2H), 4.00 – 3.89 (m, 4H), 3.32 (s, 1H), 2.17 (s, 6H), 1.85 – 1.73 (m, 4H), 1.56 – 1.40 (m, 4H), 1.40 – 1.27 (m, 8H), 0.94 – 0.84 (m, 6H), 0.25 (s, 9H).

213, 4-Bromo-*N*,*N*-di*p*-tolylbenzenamine

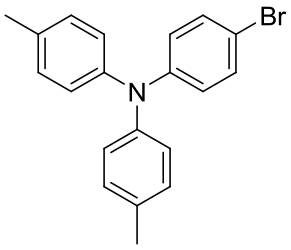

The standard Buchwald-Hartwig amination procdure A was followed using the following quantities: di-*p*-tolylamine **131** (4.71 g, 23.9 mmol), 1-bromo-4-iodobenzene (7.43 g, 26.3 mmol), sodium *tert*-butoxide (3.21 g, 33.4 mmol), [$Pd_2(dba)_3$] (0.22 g, 1 mol %), dppf (0.39 g, 3 mol %) and toluene (100 cm^3). The crude product purified by column chromatography with 1 : 10 DCM : petroleum ether (b.p. 40 – 60 °C as eluent. The product was recrystallised from hexane to yield white crystals of **213** (4.50 g, 54%). The NMR data were consistent with the literature.[142] ^{1}H NMR (400 MHz, $CDCl_3$): δ 7.28 (d, *J* = 9.0 Hz, 2H), 7.08 (d, *J* = 8.0 Hz, 4H), 6.98 (d, *J* = 8.0 Hz, 4H), 6.90 (d, *J* = 9.0 Hz, 2H), 2.32 (s, 6H).

214, 4-Methyl-*N*-*p*-tolyl-*N*-(4-((trimethylsilyl)ethynyl)phenyl)benzenamine

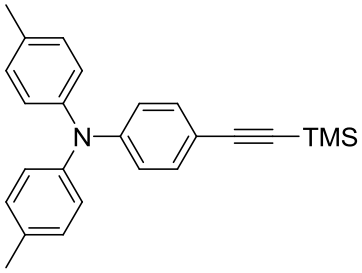

The standard Sonogashira cross-coupling procedure was followed using the following quantities: 4-bromo-*N*,*N*-di*p*-tolylbenzenamine **213** (2.00 g, 5.7 mmol), trimethylsilyl acetylene (0.61 g, 6.3 mmol), copper iodide (27 mg), [$PdCl_2(PPh_3)_2$] (200 mg) and triethylamine (75 cm^3). The resulting oil was purified by column chromatography using 9:1 petroleum ether (b.p. 40 – 60 ^{o}C): DCM as eluent to afford **214** as a yellow solid (1.2 g, 56%). The NMR data were consistent with the literature.[142] ^{1}H NMR (400 MHz, $CDCl_3$): δ 7.30 (d, *J* = 9.0 Hz, 2H), 7.10 (d, *J* = 8.5 Hz, 4H), 7.01 (d, *J* = 8.5 Hz, 4H), 6.92 (d, *J* = 9.0 Hz, 2H), 2.35 (s, 6H), 0.27 (s, 9H).

215, 4-Ethynyl-*N*,*N*-di*p*-tolylbenzenamine

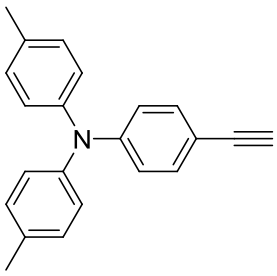

4-Methyl-*N*–*p*–tolyl-*N*-(4-((trimethylsilyl)ethynyl)phenyl) benzenamine **214** (1.18 g, 3.2 mmol) was dissolved in anhydrous THF (20 cm^3). To this solution methanol (60 cm^3) was added followed by potassium carbonate (1.76 g, 12.7 mmol). The reaction mixture was then stirred at room temperature for 2 h. The mixture was extracted with DCM and washed with water. The solvent was removed to leave the product **215** as a yellow oil which solidified on standing (1.23 g, 99%). The NMR data were

consistent with the literature.[143] ^{1}H NMR (400 MHz, $CDCl_3$): δ 7.28 (d, *J* = 9.0 Hz, 2H), 7.07 (d, *J* = 9.0 Hz, 4H), 6.99 (d, *J* = 9.0 Hz, 4H), 6.90 (d, *J* = 9.0 Hz, 2H), 2.31 (s, 6H).

203, 4-((4-(5-(4-*tert*-Butylphenyl)-1,3,4-oxadiazol-2-yl)phenyl)ethynyl)-*N*,*N*-di*p*-tolylbenzenamine

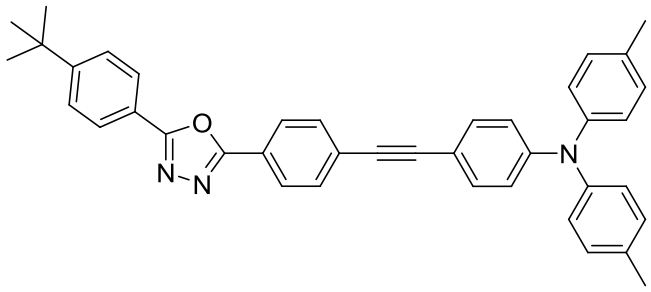

The general Sonogashira cross-coupling procedure was followed using the following quantities: 2-(4-*tert*-butylphenyl)-5-(4-iodophenyl)-1,3,4-oxadiazole **150** (0.20 g, 0.49 mmol) and 4-ethynyl-N,N-di*p*-tolylbenzenamine **217** (0.16 g, 0.54 mmol), [$Pd(PPh_3)_4$] (28 mg), THF (20 cm^3) and triethylamine (10 cm^3). The crude product was purified by column chromatography on silica gel using DCM with 5% ethyl acetate as eluent to yield **203** as a pale yellow solid (0.30 g, 92%). ^{1}H NMR (700 MHz, $CDCl_3$): δ 8.09 (d, *J* = 8.5 Hz, 2H), 8.06 (d, *J* = 8.5 Hz, 2H), 7.63 (d, *J* = 8.5 Hz, 2H), 7.55 (d, *J* = 8.5 Hz, 2H), 7.35 (d, *J* = 9.0 Hz, 2H), 7.09 (d, *J* = 8.5 Hz, 4H), 7.02 (d, *J* = 8.5 Hz, 4H), 6.94 (d, *J* = 9.0 Hz, 2H), 2.32 (s, 6H), 1.37 (s, 9H); ^{13}C NMR (176 MHz, $CDCl_3$): δ 164.70, 164.03, 155.39, 148.75, 144.48, 133.53, 132.56, 131.87, 130.05, 127.25, 126.78, 126.70, 126.04, 125.38, 122.82, 121.03, 120.67, 114.07, 93.18, 87.72, 35.09, 31.11, 20.85; HRMS ($ASAP^+$) calcd for $C_{40}H_{36}N_3O$: 574.2858. Found: 574.2874; Mp: 94.3 – 96.2 °C.

217, 4-(4-(5-(4-*Tert*-butylphenyl)-1,3,4-oxadiazol-2-yl)phenyl)-2-methylbut-3-yn-2-ol

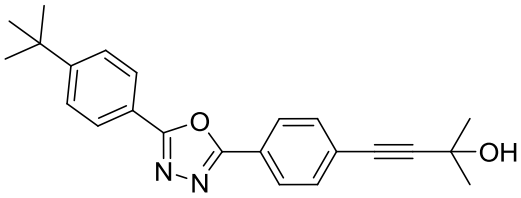

The standard Sonogashira cross-coupling procedure was followed using the following quantities: 2-(4-bromophenyl)-5-(4-*tert*-butylphenyl)-1,3,4-oxadiazole **150** (1.00 g, 2.3 mmol), 2-methylbut-3-yn-2-ol (0.33 cm^3, 3.4 mmol), [$PdCl_2(PPh_3)_2$] (58 mg), copper iodide (28 mg) and triethylamine (20 cm^3). The resulting oil was purified by column chromatography using 9:1 petroleum ether 40-60 °C : ethyl acetate; 7:1 petroleum ether (b.p. 40 – 60 °C) : ethyl acetate as eluent. The product **217** was isolated as a pale yellow solid (0.98 g, 98%). The NMR data were consistent with the literature.[109] ^{1}H NMR (400 MHz, $CDCl_3$): δ 8.12 – 8.02 (m, 4H), 7.56 (m, 4H), 1.98 (s, 1H), 1.65 (s, 6H), 1.37 (s, 9H).

218, 2-(4-*Tert*-butylphenyl)-5-(4-ethynylphenyl)-1,3,4-oxadiazole

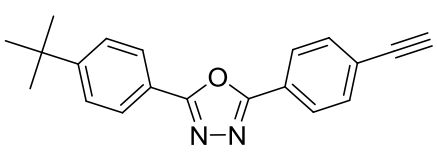

4-(4-(5-(4-*tert*-butylphenyl)-1,3,4-oxadiazol-2-yl)phenyl)-2-methylbut-3-yn-2-ol **217** (0.6 g, 1.66 mmol) was dissolved in toluene (70 cm^3). To this stirred solution sodium hydroxide (0.1 g) was added and the mixture was stirred at 130 °C under argon for 40 min. The reaction mixture was cooled to room temperature and the solvent evaporated. The crude product was purified by column chromatography using 9:1 petroleum ether (b.p. 40 – 60 ^oC) : ethyl acetate as eluent. The resulting solid was recrystallised from an ethanol-water mixture to give **218**as pale yellow crystals (0.33 g, 66%). The NMR data were consistent with the literature.[109] ^1H NMR (400 MHz, $CDCl_3$): δ 8.10 (d, *J* = 8.5 Hz, 2H), 8.06 (d, *J* = 8.5 Hz, 2H), 7.65 (d, *J* = 8.5 Hz, 2H), 7.55 (d, *J* = 8.5 Hz, 2H), 3.25 (s, 1H), 1.37 (s 9H).

216, 2-(4-*Tert*-butylphenyl)-5-(4-iodophenyl)-1,3,4-oxadiazole

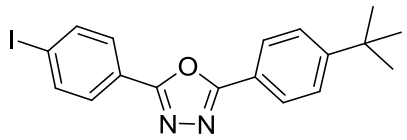

In a flame dried flask under an atmosphere of argon 5-(4-iodophenyl)-1H-tetrazole (3.00 g, 11.0 mmol) was dissolved in pyridine (70 cm^3). To this stirred solution *tert*-butylbenzoyl chloride (4.3 cm^3, 22.0 mmol) was added dropwise. The reaction mixture was heated to reflux for 15 h. The reaction mixture was allowed to cool and the solution was poured onto water, precipitating the product. The solid was filtered, dried and recrystallised from acetonitrile to yield **216** as a white solid (2.89 g, 65%). The NMR data were consistent with the literature.[109] ^1H NMR (400 MHz, $CDCl_3$): δ 8.08 – 8.02 (m, 2H), 7.92 – 7.83 (m, 4H), 7.58 – 7.53 (m, 2H), 1.37 (s, 9H).

220, 2-(4-((2,5-Bis(hexyloxy)-4-((trimethylsilyl)ethynyl)phenyl)ethynyl)phenyl)-5-(4-*tert*-butylphenyl)-1,3,4-oxadiazole

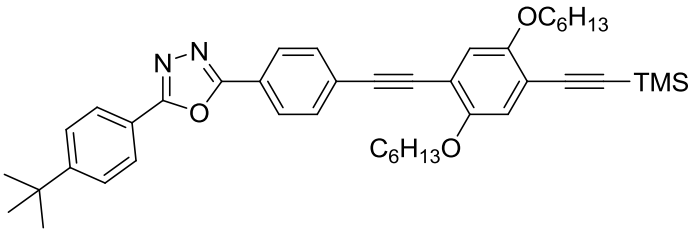

The standard Sonogashira cross-coupling procedure was followed using the following quantities: 2-(4-*tert*-butylphenyl)-5-(4-iodophenyl)-1,3,4-oxadiazole **216** (0.34 g, 0.83 mmol), ((4-ethynyl-2,5-bis(hexyloxy)phenyl)ethynyl)trimethylsilane **212** (0.30 g, 0.75 mmol), copper iodide (20 mg), [$Pd(PPh_3)_4$] (60 mg) and triethylamine (30 cm^3). The resulting solid was purified by column chromatography using 9 : 1 (v/v) petroleum ether (b.p. 40 – 60 °C) : ethyl acetate as eluent to yield **220** as a yellow solid (0.43 g, 85%). ^1H NMR (400

MHz, $CDCl_3$): δ 8.12 (d, *J* = 8.5 Hz, 2H), 8.06 (d, *J* = 8.5 Hz, 2H), 7.66 (d, *J* = 8.5 Hz, 2H), 7.55 (d, *J* = 8.5 Hz, 2H), 6.98 (s, 1H), 6.96 (s, 1H), 4.00 (m, 4H), 1.89 – 1.77 (m, 4H), 1.60 – 1.46 (m, 4H), 1.43 – 1.29 (m, 16H), 0.98 – 0.83 (m, 6H), 0.27 (s, 9H); ^{13}C NMR (101 MHz, $CDCl_3$): δ 155.54, 154.22, 154.16, 153.72, 132.14, 126.88, 126.81, 126.15, 123.42, 122.91, 121.02, 117.28, 116.96, 113.56, 112.57, 101.08, 94.02, 89.01, 69.61, 69.59, 35.16, 31.67, 31.64, 31.18, 29.35, 29.33, 25.79, 25.77, 22.70, 14.13, 14.10, 0.00; HRMS (ASAP$^+$) calcd for $C_{43}H_{55}N_2O_3Si$: 675.3982. Found: 675.3967; Mp: 121.4 – 122.9 ^{o}C.

222, 2-(4-*Tert*-butylphenyl)-5-(4-((4-ethynyl-2,5-bis(hexyloxy)phenyl)ethynyl)phenyl)-1,3,4-oxadiazole

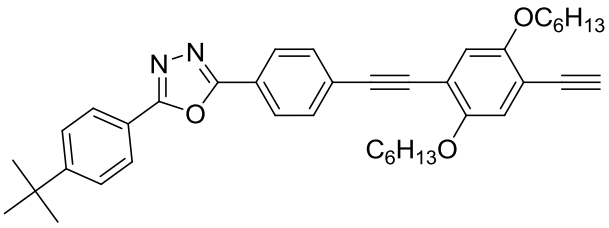

2-(4-((2,5-Bis(hexyloxy)-4-((trimethylsilyl)ethynyl)phenyl)ethynyl)phenyl)-5-(4-*tert*-butylphenyl)-1,3,4-oxadiazole **220** (0.43 g, 0.64 mmol) was dissolved in THF (20 cm^3) and methanol (20 cm^3). To this solution potassium carbonate (0.28 g, 2.0 mmol) was added and the reaction mixture stirred at room temperature for 2 h. The reaction mixture was extracted into DCM (2 x 50 cm^3) and the organic layers were combined and evaporated to dryness to give **222** was as a yellow solid (0.40 g, 100%). ^{1}H NMR (400 MHz, $CDCl_3$): δ 8.12 (d, *J* = 8.5 Hz, 2H), 8.06 (d, *J* = 8.5 Hz, 2H), 7.67 (d, *J* = 8.5 Hz, 2H), 7.55 (d, *J* = 8.5 Hz, 2H), 7.01 (s, 1H), 6.99 (s, 1H), 4.01 (m, 4H), 3.36 (s, 1H), 1.91 – 1.76 (m, 4H), 1.60 – 1.43 (m, 4H), 1.42 – 1.26 (m, 15H), 0.94 – 0.86 (m, 6H);); ^{13}C NMR (101 MHz, $CDCl_3$): δ 155.54, 154.22, 154.18, 153.72, 132.14, 126.88, 126.79, 126.17, 123.42, 122.90, 121.02, 117.28, 116.96, 113.56, 112.57, 101.01, 94.03, 89.01, 69.58, 69.59, 35.14, 31.67, 31.68, 31.18, 29.35, 29.33, 25.79, 25.77, 22.72, 14.13, 14.11 MS (ASAP$^+$) 602.80 (M^+, 100%); Mp: 114.3 – 116.7 ^{o}C.

The standard Sonogashira cross-coupling procedure was followed using the following quantities: 4-ethynyl-N,N-di*p*-tolylbenzenamine **215** (1.20 g, 4.0 mmol), 1,4-bis(hexyloxy)-2,5-diiodobenzene **209** (4.28 g, 8.1 mmol), [$Pd(PPh_3)_4$] (230 mg), copper iodide (20 mg) and triethylamine (80 cm^3). The resulting oil was purified by column chromatography using petroleum ether 40-60 °C; 7:3 petroleum ether (b.p. 40 – 60 ^{o}C) : DCM as eluent.

223, 4-((2,5-Bis(hexyloxy)-4-iodophenyl)ethynyl)-*N*,*N*-di*p*-tolylbenzenamine

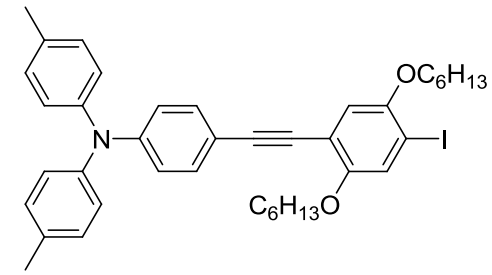

The first fraction **223** was isolated as a pale yellow oil (1.50 g, 53%). ^{1}H NMR (400 MHz, $CDCl_3$): δ 7.33 (d, *J* = 8.5 Hz, 2H), 7.28 (s, 1H), 7.09 (d, *J* = 8.0 Hz, 4H), 7.01 (d, *J* = 8.0 Hz, 4H), 6.94 (d, *J* = 8.5 Hz, 2H), 6.89 (s, 1H), 4.05 – 3.89 (m, 4H), 2.33 (s, 6H), 1.92 – 1.71 (m, 4H), 1.61 – 1.42 (m, 4H), 1.42 – 1.22 (m, 8H), 0.96 – 0.80 (m, 6H); ^{13}C NMR (101 MHz, $CDCl_3$): δ 154.21, 153.04, 151.88, 148.31, 144.67, 133.30, 132.36, 130.02, 125.23, 123.98, 120.99, 115.87, 115.13, 114.29, 94.85, 86.73, 84.48, 70.10, 69.99, 31.57, 31.51, 29.30, 29.17, 25.76, 25.69, 22.62, 22.61, 20.86, 14.04; MS (ASAP$^+$) 699.1 (M^+, 45%), 573.1 (100%).

224, 4,4'-(2,5-Bis(hexyloxy)-1,4-phenylene)bis(ethyne-2,1-diyl)bis(*N*,*N*-di*p*-tolylaniline)

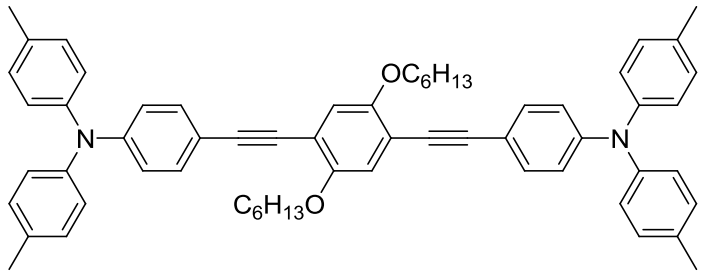

A second fraction **224** was obtained as yellow crystals (0.25 g, 14%). ^{1}H NMR (400 MHz, $CDCl_3$): δ 7.35 (d, *J* = 9.0 Hz, 4H), 7.14 – 7.08 (m, 8H), 7.07 – 7.01 (m, 8H), 6.99 (s, 2H), 6.96 (d, *J* = 9.0 Hz, 4H), 4.03 (t, *J* = 6.5 Hz, 4H), 2.35 (s, 12H), 1.90 – 1.78 (m, 4H), 1.61 – 1.49 (m, 8H), 1.36 (d, *J* = 3.6 Hz, 1H), 0.90 (t, *J* = 7.1 Hz, 6H); ^{13}C NMR (101 MHz, $CDCl_3$): δ 152.49, 147.22, 143.69, 132.27, 131.38, 129.01, 124.22, 120.01, 115.84, 114.32, 113.01, 94.33, 84.06, 68.66, 30.62, 28.35, 24.74, 21.65, 19.87, 13.07; HRMS (ES$^+$) calcd for $C_{62}H_{64}N_2O_2$: 869.4968. Found: 868.4930; Mp: 210.1 – 212.0 ^{o}C.

203, 4-((4-((4-(5-(4-*Tert*-butylphenyl)-1,3,4-oxadiazol-2-yl)phenyl)ethynyl)-2,5-bis(hexyloxy)phenyl)ethynyl)-*N*,*N*-di*p*-tolylbenzenamine

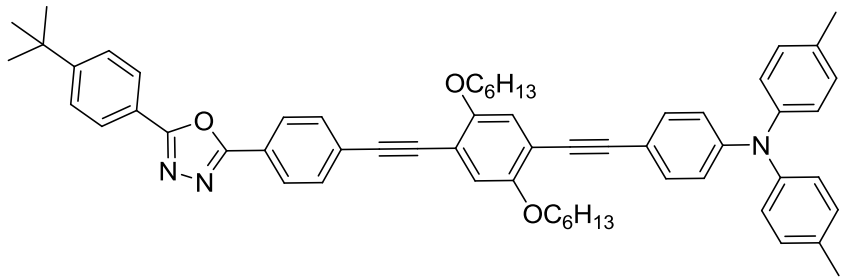

The general Sonogashira cross-coupling procedure was followed using the following

quantities: 2-(4-*tert*-butylphenyl)-5-(4-ethynylphenyl)-1,3,4-oxadiazole **218** (0.05 g, 0.17 mmol), 4-((2,5-bis(hexyloxy)-4-iodophenyl)ethynyl)-*N*,*N*-di*p*-tolylbenzenamine **223** (0.12 g, 0.17 mmol), $[PdCl_2(PPh_3)_2]$ (20 mg), copper iodide (20 mg) and triethylamine (20 cm^3). The crude product was purified by column chromatography using DCM as eluent followed by recrystallisation from acetonitrile to give **203** as yellow crystals (71 mg, 47%). ^{1}H NMR (400 MHz, $CDCl_3$): δ 8.12 (d, *J* = 8.5 Hz, 2H), 8.07 (d, *J* = 9.0 Hz, 2H), 7.67 (d, *J* = 8.5 Hz, 2H), 7.56 (d, *J* = 9.0 Hz, 2H), 7.34 (d, *J* = 9.0 Hz, 2H), 7.12 – 7.06 (m, 4H), 7.04 – 6.99 (m, 6H), 6.94 (d, *J* = 9.0 Hz, 2H), 4.03 (m, 4H), 2.32 (s, 6H), 1.91 – 1.77 (m, 4H), 1.56 (m, 4H), 1.43 – 1.29 (m, 120H), 0.96 – 0.82 (m, 6H); ^{13}C NMR (101 MHz, $CDCl_3$): δ 144.64, 133.36, 132.44, 132.07, 130.03, 126.83, 126.75, 126.10, 125.28, 120.90, 69.71, 69.56, 35.11, 31.60, 31.13, 29.35, 29.32, 25.78, 25.73, 22.66, 22.65, 20.86, 14.06; HRMS (ES^+) calcd for $C_{60}H_{63}N_3O_3$: 873.4869. Found: 873.4824; Mp: 141.6 – 142.2 °C

204, 4-((4-((4-((4-(5-(4-*Tert*-butylphenyl)-1,3,4-oxadiazol-2-yl)phenyl)ethynyl)-2,5-bis(hexyloxy)phenyl)ethynyl)-2,5-bis(hexyloxy)phenyl)ethynyl)-*N*,*N*-di*p*-tolylbenzenamine

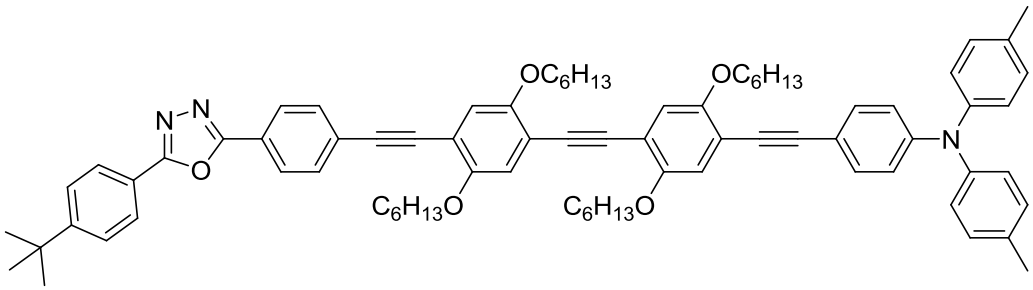

The standard Sonogashira cross-coupling procedure was followed using the following quantities: 2-(4-((2,5-bis(hexyloxy)-4-iodophenyl)ethynyl)phenyl)-5-(4-*tert*-butylphenyl)-1,3,4-oxadiazole **222** (0.062 g, 0.1 mmol), 4-((2,5-bis(hexyloxy)-4-iodophenyl)ethynyl)-*N*,*N*-di*p*-tolylbenzenamine **223** (0.071 g, 0.1 mmol), $[Pd(PPh_3)_4]$ (5 mg), CuI (5 mg), triethylamine (10 cm^3) and THF (15 cm^3). The crude product was purified by column chromatography on silica gel using petroleum ether (b.p. 40 – 60 °C) and 10% ethyl acetate as eluent to give **204** as a yellow solid (60 mg, 50%). ^{1}H NMR (500 MHz, $CDCl_3$); δ 8.14 (d, *J* = 8.5 Hz, 2H), 8.08 (d, *J* = 8.5 Hz, 2H), 7.69 (d, *J* = 8.5 Hz, 2H), 7.57 (d, *J* = 8.5 Hz, 2H), 7.34 (d, *J* = 9.0 Hz, 2H), 7.12 – 6.98 (m, 12H), 6.95 (d, *J* = 9.0 Hz, 2H), 4.09 – 3.98 (m, 8H), 2.33 (s, 6H), 1.92 – 1.78 (m, 8H), 1.59 – 1.49 (m, 8H), 1.39 (m, 21H), 0.99 – 0.80 (m, 12H); ^{13}C NMR (126 MHz, $CDCl_3$): δ 207.25, 165.03, 164.23, 155.71, 154.04, 153.81, 153.67, 153.65, 148.53, 144.87, 133.55, 132.63, 132.32, 130.24, 127.17, 127.05, 126.99, 126.33, 125.47, 123.50, 121.21, 121.16, 117.41, 117.29, 117.19, 117.05, 115.36, 115.30, 115.00, 113.71, 113.31, 109.98, 108.61, 108.56, 106.07, 95.94, 94.22,

92.26, 91.36, 89.40, 85.19, 69.98, 69.88, 69.87, 69.76, 35.36, 31.86, 31.84, 31.36, 31.18, 29.58, 29.55, 29.51, 26.01, 25.97, 25.92, 22.89, 22.87, 21.10, 14.30; HRMS (ES^+), calcd for $C_{80}H_{91}N_3O_5$: 1173.6959, found: 1173; Mp: 110.3 – 112.0 ^oC.

225, 4-((4-((4-Ethynyl-2,5-bis(hexyloxy)phenyl)ethynyl)-2,5-bis(hexyloxy)phenyl)ethynyl)-*N*,*N*-di*p*-tolylbenzenamine

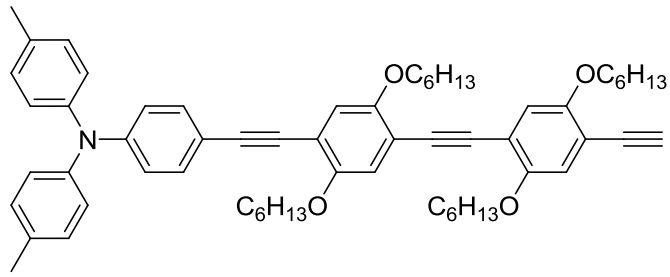

The standard Sonogashira cross-coupling procedure was followed using the following quantities: 4-((2,5-bis(hexyloxy)-4-iodophenyl)ethynyl)-*N*,*N*-di*p*-tolylbenzenamine **223** (0.44 g, 0.63 mmol), ((4-ethynyl-2,5-bis(hexyloxy)phenyl)ethynyl)trimethylsilane **212** (0.30 g, 0.75 mmol), [$Pd(PPh_3)_4$] (60 mg), copper iodide (30 mg), triethylamine (20 cm^3) and THF (10 cm^3). The crude solid was purified by column chromatography in 7 : 3 (v/v) petroleum ether 40 – 60 °C : DCM to yield the product as a yellow solid (0.53 g, 87 %). ^1H NMR (500 MHz, $CDCl_3$): δ 7.36 – 7.31 (m, 2H), 7.11 – 7.07 (m, 4H), 7.04 – 7.00 (m, 4H), 6.98 (m, 2H), 6.97 – 6.91 (m, 4H), 4.06 – 3.95 (m, 8H), 2.33 (s, 6H), 1.93 – 1.74 (m, 8H), 1.56 – 1.43 (m, 8H), 1.42 – 1.28 (m, 16H), 1.00 – 0.82 (m, 12H), 0.27 (s, 9H), ^{13}C NMR (126 MHz, $CDCl_3$): δ 154.38, 153.77, 153.64, 153.53, 148.53, 144.89, 133.54, 132.64, 130.25, 125.48, 121.18, 117.62, 117.41, 117.21, 117.06, 115.41, 114.88, 113.81, 113.76, 101.46, 100.27, 95.88, 91.90, 91.41, 85.21, 69.90, 31.87, 31.86, 31.85, 29.58, 29.51, 25.97, 25.90, 22.89, 21.11, 14.30, 0.22; MS ($MALDI^+$) 969.6 (M+, 100%); Mp: 101.0 – 102.6 ^oC. The product 4-((4-((2,5-Bis(hexyloxy)-4-((trimethylsilyl)ethynyl)phenyl)ethynyl)-2,5-bis(hexyloxy)phenyl)ethynyl)-*N*,*N*-di*p*-tolylbenzenamine (0.49 g, 0.5 mmol) was dissolved in a mixture of THF (20 cm^3) and methanol (20 cm^3). To this solution potassium carbonate (0.28 g, 2.0 mmol) was added and the reaction mixture stirred at room temperature for 2 h. The reaction mixture was extracted into DCM (2 x 50 cm^3) and the organic layers were evaporated to dryness to yield **225** as a yellow solid (0.45 g, 100%). ^1H NMR (400 MHz, $CDCl_3$): δ 7.37 – 7.31 (m, 2H), 7.13 – 6.92 (m, 14H), 4.09 – 3.94 (m, 8H), 3.35 (s, 1H), 2.33 (s, 6H), 1.94 – 1.73 (m, 8H), 1.59 – 1.44 (m, 8H), 1.44 – 1.24 (m, 16H), 0.97 – 0.83 (m, 12H); ^{13}C NMR (101 MHz, $CDCl_3$): δ 144.66, 133.32, 132.40, 130.01, 125.25, 120.95, 117.98, 117.04, 113.52, 69.68, 69.66, 31.61, 31.54, 29.35, 29.28, 29.14, 25.73, 25.66, 25.61, 22.63, 22.59, 20.86, 14.02; MS ($MALDI^+$) 897.4 (M^+, 100%); Mp: 63.5 – 64.3 ^oC.

226 2-(4-((2,5-Bis(hexyloxy)-4-iodophenyl)ethynyl)phenyl)-5-(4-*tert*-butylphenyl)-1,3,4-oxadiazole

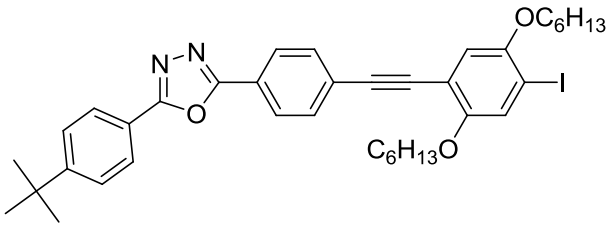

The standard Sonogashira cross-coupling procedure was followed using the following quantities: 2-(4-*tert*-butylphenyl)-5-(4-ethynylphenyl)-1,3,4-oxadiazole **218** (0.15 g, 0.49 mmol), 1,4-bis(hexyloxy)-2,5-diiodobenzene **209** (0.66 g, 1.2 mmol), [$Pd(PPh_3)_4$] (5 mg), CuI (5 mg), triethylamine (10 cm^3) and THF (15 cm^3). The crude product was purified by column chromatography on silica gel using 9 : 1 petroleum ether : ethyl acetate as eluent to give **226** as a pale yellow solid (0.20 g, 58%). ^{1}H NMR (400 MHz, $CDCl_3$): δ 8.12 (d, *J* = 8.5 Hz, 2H), 8.07 (d, *J* = 8.5 Hz, 2H), 7.67 (d, *J* = 8.5 Hz, 2H), 7.56 (d, *J* = 8.5 Hz, 2H), 7.33 (s, 1H), 6.93 (s, 1H), 4.00 (m, 4H), 1.91 – 1.76 (m, 4H), 1.58 – 1.43 (m, 4H), 1.43 – 1.29 (m, 17H), 0.99 – 0.82 (m, 6H); ^{13}C NMR (126 MHz, $CDCl_3$): δ 164.52, 153.31, 151.24 147.34, 142.22, 132.81, 127.15, 127.02 125.81, 125.63, 125.50 122.71, 120.31, 122.72, 111.52, 95.94, 86.31, 84.22, 67.09, 67.91, 34.22, 31.85, 31.34, 28.90, 25.61, 22.71, 22.81, 14.30; MS (ASAP$^+$) 704.2 (M^+, 100%); Mp: 147.5 – 148.2 °C.

205, 4-((4-((4-((4-((4-(5-(4-*tert*-Butylphenyl)-1,3,4-oxadiazol-2-yl)phenyl)ethynyl)-2,5-bis(hexyloxy)phenyl)ethynyl)-2,5-bis(hexyloxy)phenyl)ethynyl)-2,5-bis(hexyloxy)phenyl)ethynyl)-*N*,*N*-di*p*-tolylbenzenamine

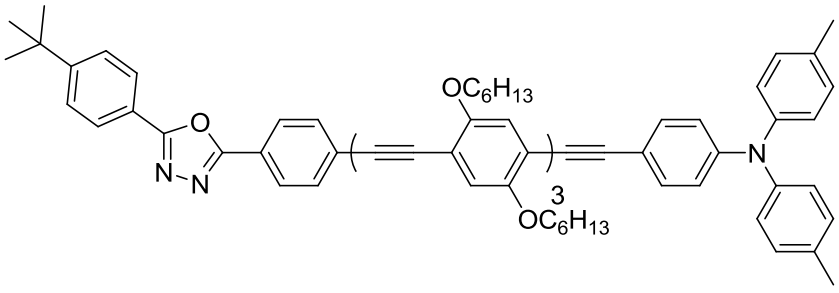

The standard Sonogashira cross-coupling procedure was followed using the following quantities: 4-((4-((4-ethynyl-2,5-bis(hexyloxy)phenyl)ethynyl)-2,5-bis(hexyloxy)phenyl)ethynyl)-*N*,*N*-di*p*-tolylbenzenamine **225** (0.13 g, 0.14 mmol), 2-(4-((2,5-bis(hexyloxy)-4-iodophenyl)ethynyl)phenyl)-5-(4-*tert*-butylphenyl)-1,3,4-oxadiazole **226** (0.10 g, 0.14 mmol), [$PdCl_2(PPh_3)_2$] (20 mg), copper iodide (20 mg), triethylamine (20 cm^3) and THF (20 cm^3). The crude product was purified by column chromatography using 7 : 3 (v/v) petroleum ether (b.p. 40 – 60 °C) : ethyl acetate as eluent to yield **204** as a yellow solid (87 mg, 22%). ^{1}H NMR (500 MHz, $CDCl_3$): δ 8.14 (d, *J* = 8.5 Hz, 2H), 8.09 (d, *J* = 8.5 Hz, 2H), 7.70 (d, *J* = 8.5 Hz, 2H), 7.57 (d, *J*

= 8.5 Hz, 2H), 7.35 (d, *J* = 9.0 Hz, 2H), 7.13 – 6.98 (m, 14H), 6.95 (d, *J* = 8.5 Hz, 2H), 4.10 – 3.99 (m, 12H), 2.34 (s, 6H), 1.95 – 1.77 (m, 12H), 1.58 – 1.49 (m, 12H), 1.45 – 1.31 (m, 33H), 0.97 – 0.85 (m, 18H); ^{13}C NMR (126 MHz, $CDCl_3$): δ 165.04, 164.23, 155.72, 154.04, 153.77, 153.75, 153.68, 153.64, 148.52, 144.87, 133.55, 132.64, 132.33, 130.25, 127.16, 127.05, 127.00, 126.34, 125.47, 123.51, 121.21, 121.16, 117.45, 117.38, 117.25, 117.18, 117.04, 115.38, 115.21, 114.87, 114.73, 114.23, 113.81, 113.40, 95.90, 94.27, 92.19, 92.01, 91.59, 91.50, 89.38, 85.21, 69.96, 69.90, 69.88, 69.85, 69.75, 35.37, 31.88, 31.87, 31.85, 31.37, 29.59, 29.54, 29.52, 29.51, 26.02, 25.98, 25.94, 25.92, 22.90, 21.11, 14.31; MS (MALDI$^+$) 1474.7 (100%); Mp: 105.5 – 107.2 ^{o}C.

The standard Sonogashira cross-coupling procedure was followed using the following quantities: 2-(4-*tert*-butylphenyl)-5-(4-((4-ethynyl-2,5-bis(hexyloxy)phenyl)ethynyl)phenyl)-1,3,4-oxadiazole **222** (0.34 g, 0.56 mmol), 1,4-bis(hexyloxy)-2,5-diiodobenzene **209** (0.74 g, 1.4 mmol), [$Pd(PPh_3)_4$] (20 mg), CuI (10 mg), Et_3N (5 cm^3), THF (10 cm^3). The crude product was purified by column chromatography using 9 : 1 (v/v) petroleum ether (b.p. 40 – 60 ^{o}C) : ethyl acetate as eluent.

228, 2-(4-((4-((2,5-Bis(hexyloxy)-4-iodophenyl)ethynyl)-2,5-bis(hexyloxy)phenyl)ethynyl)phenyl)-5-(4-*tert*-butylphenyl)-1,3,4-oxadiazole

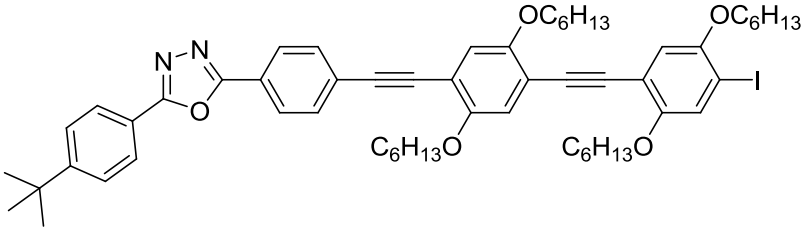

The first fraction was **228** isolated as a yellow solid (0.30 g, 54%). ^{1}H NMR (500 MHz, $CDCl_3$): δ 8.14 (d, *J* = 8.5 Hz, 2H), 8.08 (d, *J* = 8.5 Hz, 2H), 7.69 (d, *J* = 8.5 Hz, 2H), 7.57 (d, *J* = 8.5 Hz, 2H), 7.32 (s, 1H), 7.27 (s, 1H), 7.04 (m, 2H), 6.92 (s, 1H), 4.08 – 3.94 (m, 4H), 1.92 – 1.79 (m, 4H), 1.61 – 1.45 (m, 4H), 1.43 – 1.28 (m, 17H), 0.97 – 0.85 (m, 6H). ^{13}C NMR (126 MHz, $CDCl_3$): δ 165.04, 164.22, 155.72, 154.44, 154.03, 153.67, 152.06, 138.57, 135.16, 135.11, 135.06, 132.32, 130.04, 128.46, 127.86, 127.82, 127.78, 127.13, 127.05, 126.99, 126.34, 124.22, 123.53, 121.20, 117.25, 117.17, 116.35, 115.08, 114.02, 113.45, 94.26, 91.63, 90.88, 89.33, 87.96, 70.30, 70.20, 69.93, 69.77, 35.36, 31.84, 31.75, 31.37, 31.19, 29.55, 29.50, 29.48, 29.41, 26.01, 25.91, 25.88, 22.90, 22.89, 22.88, 22.85, 14.30; MS (MALDI$^+$) 1004.3 (M^+, 100%); Mp: 85.1 – 87.3 ^{o}C.

227, OXD-(OPE)$_3$-OXD

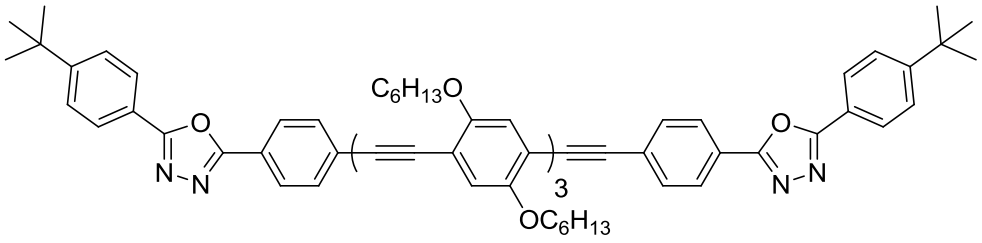

The second fraction **227** was isolated as a yellow solid (0.10 g, 24%). ^{1}H NMR (500 MHz, $CDCl_3$): δ 8.17 – 8.12 (m, 4H), 8.09 (d, *J* = 8.5 Hz, 4H), 7.72 – 7.66 (m, 4H), 7.57 (d, *J* = 8.5 Hz, 4H), 7.41 – 7.36 (m, 1H), 7.34 – 7.28 (m, 2H), 7.07 – 7.01 (m, 2H), 4.12 – 3.99 (m, 6H), 1.96 – 1.79 (m, 6H), 1.63 - 1.48 (m, 6H), 1.47 – 1.30 (m, 30H), 1.00 – 0.85 (m, 12H). ^{13}C NMR (126 MHz, $CDCl_3$): δ 210.22, 208.98, 207.28, 165.06, 164.20, 155.74, 154.01, 134.39, 134.24, 132.36, 127.05, 127.01, 126.34, 123.61, 121.19, 117.02, 114.09, 94.55, 89.15, 69.84, 35.37, 31.84, 31.78, 31.37, 31.20, 29.52, 26.01, 22.91, 14.32; MS (MALDI$^+$) 1479.7 (M^+, 100%); Mp: 85.2 – 89.3 ^{o}C.

206, 4-((4-((4-((4-((4-((4-(5-(4-*Tert*-butylphenyl)-1,3,4-oxadiazol-2-yl)phenyl)ethynyl)-2,5-bis(hexyloxy)phenyl)ethynyl)-2,5-bis(hexyloxy)phenyl)ethynyl)-2,5-bis(hexyloxy)phenyl)ethynyl)-2,5-bis(hexyloxy)phenyl)ethynyl)-*N*,*N*-di*p*-tolylbenzenamine

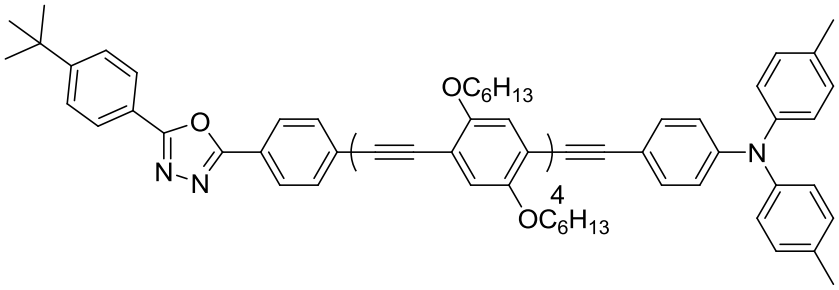

The standard Sonogashira cross-coupling procedure was followed using the following quantities: 4-((4-((4-ethynyl-2,5-bis(hexyloxy)phenyl)ethynyl)-2,5-bis(hexyloxy)phenyl)ethynyl)-*N*,*N*-di*p*-tolylbenzenamine **225** (0.09 g, 0.10 mmol), 2-(4-((4-((2,5-bis(hexyloxy)-4-iodophenyl)ethynyl)-2,5-bis(hexyloxy)phenyl)ethynyl)phenyl)-5-(4-*tert*-butylphenyl)-1,3,4-oxadiazole **228** (0.10 g, 0.10 mmol), $[PdCl_2(PPh_3)_2]$ (20 mg), copper iodide (20 mg), triethylamine (20 cm^3) and THF (20 cm^3). The crude product was purified by column chromatography using DCM as eluent to yield **206** as a yellow solid (0.17 g, 85%). ^{1}H NMR (500 MHz, $CDCl_3$): δ 8.14 (d, *J* = 7.5 Hz, 2H), 8.08 (d, *J* = 7.5 Hz, 2H), 7.69 (d, *J* = 7.5 Hz, 3H), 7.57 (d, *J* = 7.5 Hz, 3H), 7.34 (d, *J* = 7.5 Hz, 3H), 7.10 (d, *J* = 8.0 Hz, 4H), 7.07 – 6.97 (m, 9H), 6.95 (d, *J* = 8.0 Hz, 2H), 4.10 – 3.98 (m, 16H), 2.33 (s, 6H), 1.94 – 1.80 (m, 16H), 1.67 – 1.47 (m, 16H), 1.39 (s, 9H), 1.38 – 1.28 (m, 32H), 0.89 (m, 24H); ^{13}C NMR (126 MHz, $CDCl_3$): δ 165.03, 164.22, 158.06, 155.71, 154.07, 153.72, 148.52,

147.98, 144.88, 133.53, 132.62, 132.31, 130.24, 127.05, 126.98, 126.32, 125.46, 121.18, 117.48, 117.34, 117.25, 117.13, 115.43, 114.91, 114.73, 114.41, 113.91, 113.45, 109.99, 95.85, 94.26, 92.17, 91.92, 85.22, 70.00, 69.91, 69.79, 35.35, 31.86, 31.36, 29.55, 26.00, 25.97, 25.92, 22.88, 21.09, 14.28; MS (MALDI$^+$) 1774.7 (M^+, 20%) 1139.5 (100%); Mp: 138.6 – 139.7 ^{o}C.

229, 1,2-Bis(4-((4-(5-(4-*tert*-butylphenyl)-1,3,4-oxadiazol-2-yl)phenyl)ethynyl)-2,5-bis(hexyloxy)phenyl)ethyne

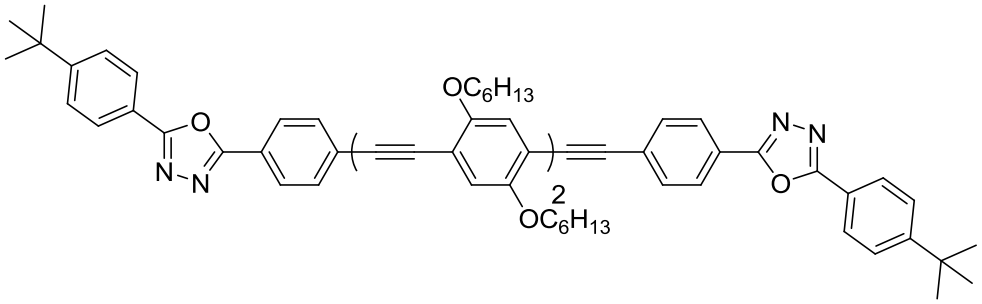

The standard Sonogashira cross-coupling procedure was followed using the following quantities: 2-(4-((4-((2,5-bis(hexyloxy)-4-iodophenyl)ethynyl)-2,5-bis(hexyloxy)phenyl)ethynyl)phenyl)-5-(4-*tert*-butylphenyl)-1,3,4-oxadiazole **228** (0.085 g, 0.11 mmol), 2-(4-*tert*-butylphenyl)-5-(4-ethynylphenyl)-1,3,4-oxadiazole **218** (0.032 g, 0.085 mmol), [$Pd(PPh_3)_4$] (5 mg), CuI (5 mg), triethylamine (10 cm^3) and THF (15 cm^3). The crude product was purified by column chromatography on silica gel using dichloromethane and 5% ethyl acetate as eluent to yield **229** as a yellow solid (91 mg, 72%). ^{1}H NMR (400 MHz, $CDCl_3$): δ 8.13 (d, *J* = 8.5 Hz, 4H), 8.08 (d, *J* = 8.5 Hz, 4H), 7.68 (d, *J* = 8.5 Hz, 4H), 7.56 (d, *J* = 8.5 Hz, 4H), 7.04 (s, 4H), 4.06 (m, 8H), 1.94 – 1.80 (m, 8H), 1.58 (s, 8H), 1.38 (s, 18H), 1.35 (s, 20H), 0.96 – 0.85 (m, 12H); ^{13}C NMR (101 MHz, $CDCl_3$): δ 165.21, 163.82, 163.00, 154.49, 152.83, 152.52, 131.10, 125.90, 125.83, 125.77, 125.11, 122.57, 122.42, 122.33, 120.00, 116.06, 116.01, 113.80, 112.35, 109.29, 99.99, 93.10, 90.73, 88.11, 68.75, 68.57, 34.14, 30.64, 30.62, 30.14, 28.33, 28.29, 24.79, 24.70, 21.68, 13.08; MS (MALDI$^+$) 1179.3 (M^+, 100%); Mp: 207.5 – 209.1 ^{o}C

234, (4-Bromophenyl)trimethylsilane

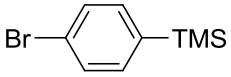

In a flame dried flask under an atmosphere of argon 1,4-dibromobenzene **233** (5.00 g, 0.021 mol) was dissolved in diethyl ether (50 cm^3) and cooled to -78 ^{o}C. nBuLi (2.5 M, 9.3 cm^3) was added to the solution dropwise, the reaction mixture was then stirred for 30 minutes before TMSCl (3.2 cm^3, 0.025 mol) was added dropwise. The reaction mixture was then stirred for 2 h and allowed to warm to room temperature before being poured onto water (50 cm^3) and extracted with diethyl ether (2 x 50

cm^3). The organic extracts were combined and the solvent removed under reduced pressure. The product **234** was isolated as a colourless oil (4.22 g, 88%). The NMR data were consistent with the literature. ^{1}H NMR (400 MHz, $CDCl_3$) δ 7.51 – 7.45 (m, 1H), 7.42 – 7.34 (m, 1H), 0.26 (s, 4H).[144]

235, Trimethyl(4-(4,4,5,5-Tetramethyl-1,3,2-dioxaborolan-2-yl)phenyl)silane

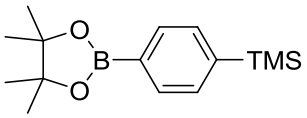

The standard Miyaura-borylation procedure was followed using the following quantities: (4-bromophenyl)trimethylsilane **234** (4.20 g, 0.018 mol), B_2pin_2 (8.84 g, 0.035 mol), [$PdCl_2$(dppf)] (0.19 g, 0.26 mmol), KOAc (5.14 g, 0.050 mol) and DMF (10 cm^3). The crude product was purified by column chromatography using dichloromethane as eluent to yield **235** as a white solid (4.75 g, 96%). ^{1}H NMR (400 MHz, $CDCl_3$): δ 7.82-7.76 (m, 2H), 7.56-7.51 (m, 2H), 1.34 (s, 12H), 0.27 (s, 9H). 19B NMR (128 MHz) δ 31.01. ^{13}C NMR (100 MHz, CDCl3): δ 145.5, 135.1, 133.9, 85.0, 26.1, 0.0. MS (MALDI$^+$) 261.1 ([M-CH_3]$^+$, 100); Mp: 119.9 - 120.3 °C.

236, *N*,*N*-Di-*p*-tolyl-4'-(trimethylsilyl)biphenyl-4-amine

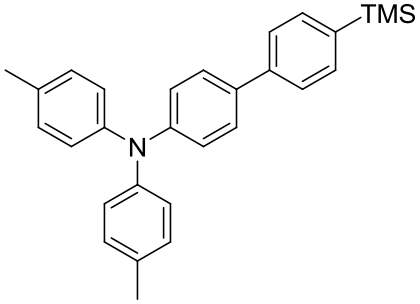

The standard Suzuki-Miyaura cross-coupling procedure was followed using the following quantities: 4-bromo-*N*,*N*-di-*p*-tolylaniline **213** (1.00 g, 2.84 mmol), trimethyl(4-(4,4,5,5-tetramethyl-1,3,2-dioxaborolan-2-yl)phenyl)silane **235** (0.86 g, 3.1 mmol), [$PdCl_2(PPh_3)_2$] (0.10 g, 0.14 mmol), NaOH (0.23 g in 10 cm^3 H_2O), THF (20 cm^3). The crude product was purified by column chromatography using 4 : 1 (v/v) petroleum ether : dichloromethane to yield **236** as a white solid (0.93 g, 78%). ^{1}H NMR (500 MHz, $CDCl_3$): δ 7.60 – 7.52 (m, 4H), 7.44 (d, *J* = 8.5 Hz, 2H), 7.11 – 7.01 (m, 10H), 2.33 (s, 6H), 0.30 (s, 9H); ^{13}C NMR (126 MHz, $CDCl_3$): δ 147.89, 145.44, 141.42, 138.59, 134.23, 133.99, 132.86, 130.13, 127.82, 126.14, 124.99, 122.72, 21.06, 0.01; HRMS (ASAP$^+$) calcd for $C_{29}H_{32}NSi$: 422.2304. Found: 422.2311; Mp: 56.6 – 58.0 ^{o}C.

237, 4'-Iodo-*N*,*N*-di-*p*-tolylbiphenyl-4-amine

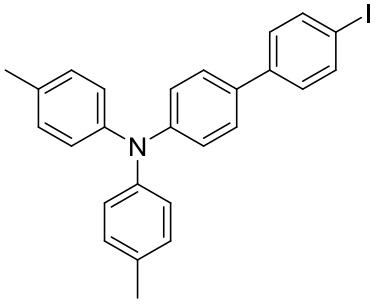

N,*N*-Di-*p*-tolyl-4'-(trimethylsilyl)biphenyl-4-amine **236** (0.50 g, 1.19 mmol) was dissolved in DCM (30 cm^3). To this stirred solution 1 M iodine monochloride (1.19 cm^3, 1.19 mmol) was

added dropwise and the reaction mixture was stirred for 2 h. The reaction mixture was then poured onto water and extracted with DCM (2 x 30 cm^3). The organic extracts were combined and the solvent removed under reduced pressure to give **237** as a white solid (0.57 g, 100%).^{1}H NMR (400 MHz, $CDCl_3$): δ 7.65 (d, *J* = 8.5 Hz, 2H), 7.31 (d, *J* = 8.5 Hz, 2H), 7.22 (d, *J* = 8.5 Hz, 2H), 7.05 – 6.93 (m, 10H), 2.26 (s, 6H); ^{13}C NMR (126 MHz, $CDCl_3$): δ 148.25, 145.28, 140.51, 139.79, 138.23, 137.96, 133.06, 132.85, 130.17, 128.92, 128.61, 127.55, 125.07, 122.60, 93.74, 92.24, 21.08; HRMS (ASAP$^+$) calcd for $C_{26}H_{22}N^{127}I$: 475.0797. Found: 475.0806; Mp: 149.9 – 151.3 ^{o}C.

231, DPA-(Ph)$_3$-OXD

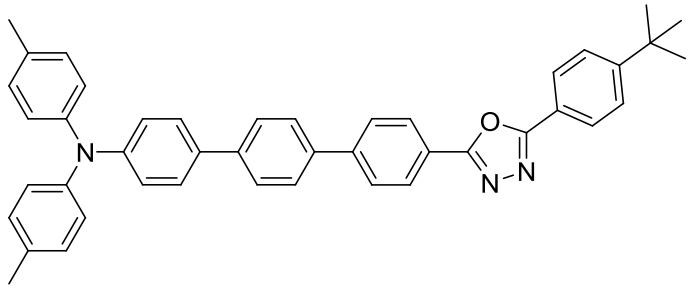

The standard Suzuki-Miyaura cross-coupling procedure was followed using the following quantities: 4'-iodo-*N*,*N*-di-*p*-tolylbiphenyl-4-amine **237** (0.20 g, 0.42 mmol), 2-(4-*tert*-butylphenyl)-5-(4-(4,4,5,5-tetramethyl-1,3,2-dioxaborolan-2-yl)phenyl)-1,3,4-oxadiazole **158** (0.20 g, 0.5 mmol), [$PdCl_2(PPh_3)_2$] (15 mg), NaOH (50 mg in 5 cm^3 H_2O) and THF (20 cm^3). The mixture was cooled, poured onto water and extracted with diethyl ether (2 x 50 cm^3). The organic extracts were combined and the solvent removed under reduced pressure. The crude product was purified by column chromatography using 7:3 (v/v) petroleum ether (b.p. 40 – 60 ^{o}C) : diethyl ether as eluent to yield **231** as a yellow solid (0.15 g, 57%). ^{1}H NMR (400 MHz, $CDCl_3$): δ 8.15 (d, *J* = 8.5 Hz, 2H), 8.02 (d, *J* = 8.5 Hz, 2H), 7.74 (d, *J* = 8.5 Hz, 2H), 7.63 (q, *J* = 8.5 Hz, 4H), 7.50 (d, *J* = 8.5 Hz, 2H), 7.43 (d, *J* = 8.5 Hz, 2H), 7.08 – 6.95 (m, 8H), 2.26 (s, 6H), 1.31 (s, 9H); ^{13}C NMR (126 MHz, $CDCl_3$): δ 164.90, 164.55, 155.57, 148.16, 145.35, 144.15, 140.86, 138.13, 133.28, 133.02, 130.17, 127.72, 127.67, 127.62, 127.26, 127.02, 126.30, 125.06, 122.92, 122.69, 121.38, 35.35, 31.37, 21.07; HRMS (ASAP$^+$) calcd for $C_{44}H_{39}N_3O$: 625.3093. Found: 625.3083; Mp: 109.9 – 110.4 ^{o}C.

239, 1,4-Dibromo-2,5-dimethylbenzene

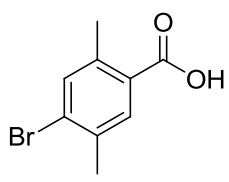

In a flame dried flask under an atmosphere of argon 1,4-dibromo-2,5-dimethylbenzene **238** (5.00 g, 0.020 mol) was dissolved in diethyl ether (130 cm^3). The stirred solution was cooled to -78 ^{o}C and 2.5 M *n*-butyl

lithium (9.1 cm^3, 0.023 mol) was added while maintaining the temperature at -78 ^oC; the reaction was then stirred for 30 min and then allowed to warm to room temperature. The reaction mixture was then cooled a second time to -78 ^oC and an excess of solid CO_2 was added. The mixture was then allowed to slowly reach room temperature and was stirred for a further 15 h. The reaction was quenched with water, washed with dilute HCl and extracted with diethyl ether. The solvent from the combined organic extracts was removed under reduced pressure and the solid was triturated with hot hexane to give **239** as a white solid (3.53 g, 82%). The melting point was consistent with the literature.[145] ^1H NMR (400 MHz, $CDCl_3$): δ 7.92 (s, 1H), 7.47 (s, 1H), 2.58 (s, 3H), 2.41 (s, 3H). Mp: 170.9 – 172.1 ^oC (lit Mp: 171.5-172.5 ^oC).

241, 2-(4-Bromo-2,5-dimethylphenyl)-5-(4-*tert*-butylphenyl)-1,3,4-oxadiazole

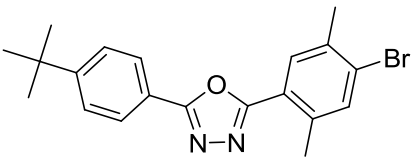

1,4-Dibromo-2,5-dimethylbenzene (1 g, 4.4 mmol) was dissolved in anhydrous DCM (20 cm^3). To this stirred solution thionyl chloride (0.96 cm^3, 13.1 mmol) was added. This stirred solution was heated to reflux for 2 h after which time the reaction mixture was cooled and the solvent and excess thionyl chloride were removed under reduced pressure. The product **240** was isolated as a white low melting point solid and its identity confirmed by ^1H NMR, (1.09 g, 100%). ^1H NMR (400 MHz, $CDCl_3$): δ 8.05 (s, 1H), 7.49 (s, 1H), 2.50 (s, 3H), 2.46 – 2.43 (m, 3H). 4-Bromo-2,5-dimethylbenzoyl chloride **240** (1.00 g, 4.04 mmol) and 5-(4-*tert*-butylphenyl)-1*H*-tetrazole **150** (0.90 g, 4.44 mmol) were dissolved in pyridine (20 cm^3). The stirred mixture was heated to reflux for 4 h after which time the reaction was cooled and poured onto water. The mixture was extracted with DCM and washed with brine. The solvent was removed from the combined organic extracts and the crude product was recrystallised from acetonitrile to afford **241**. as white needles (0.87 g, 56%). ^1H NMR (400 MHz, $CDCl_3$): δ 8.06 (d, *J* = 9.0 Hz, 2H), 7.90 (s, 1H), 7.59 – 7.54 (m, 3H), 2.70 (s, 3H), 2.46 (s, 3H), 1.38 (s, 9H); ^{13}C NMR (126 MHz, $CDCl_3$) δ 164.59, 164.37, 155.67, 137.47, 136.17, 135.63, 130.88, 128.34, 127.04, 126.34, 122.40, 121.23, 35.36, 31.37, 22.60, 21.56; HRMS ($ASAP^+$) calcd for $C_{20}H_{21}N_2O^{79}Br$: 384.0837. Found: 384.0834; Mp: 152.6 – 153.3 ^oC.

242, 2-(4-*Tert*-butylphenyl)-5-(2,2',5,5'-tetramethyl-4'-(trimethylsilyl)biphenyl-4-yl)-1,3,4-oxadiazole

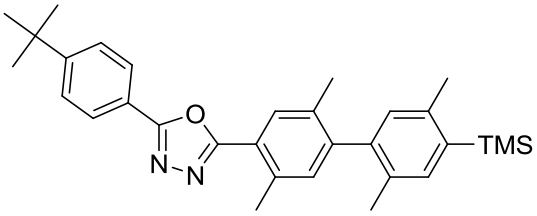

The standard Suzuki-Miyaura cross-coupling procedure was followed using the following quantities: 2-(4-bromo-2,5-dimethylphenyl)-5-(4-*tert*-butylphenyl)-1,3,4-oxadiazole **241** (0.42 g, 1.25 mmol), (2,5-dimethyl-4-(4,4,5,5-tetramethyl-1,3,2-dioxaborolan-2-yl)phenyl)trimethylsilane **246** (0.32 g, 1.25 mmol), $[PdCl_2(PPh_3)_2]$ (10 mg), NaOH (0.1 g in 5 cm^3 H_2O) and THF (15 cm^3). The crude product was purified by column chromatography on silica gel using petroleum ether (b.p. 40 – 60 ^oC) with 10% ethyl acetate as eluent to yield **242** as a white solid (0.36 g, 60%). ^1H NMR (400 MHz, $CDCl_3$): δ 8.11 (d, *J* = 9.0 Hz, 2H), 7.96 (s, 1H), 7.59 (d, *J* = 9.0 Hz, 2H), 7.36 (s, 1H), 7.14 (s, 1H), 6.93 (s, 1H), 2.74 (s, 3H), 2.47 (s, 3H), 2.16 (s, 3H), 2.08 (s, 3H), 1.40 (s, 9H), 0.39 (s, 9H); ^{13}C NMR (126 MHz, $CDCl_3$): δ 165.09, 164.45, 155.47, 145.10, 141.43, 140.89, 137.75, 136.32, 135.52, 134.20, 132.97, 131.75, 130.44, 130.43, 127.02, 126.32, 122.00, 121.50, 35.35, 31.41, 22.71, 21.83, 19.63, 19.54, 0.22; MS ($ASAP^+$) 482.3 (M^+, 100%); HRMS (ASAP+), calcd for $C_{31}H_{39}N_2OSi$: 483.2832, found: 483.2827; Mp: 157.0 – 157.8 ^oC.

243, 2-(4-*tert*-Butylphenyl)-5-(4'-iodo-2,2',5,5'-tetramethylbiphenyl-4-yl)-1,3,4-oxadiazole

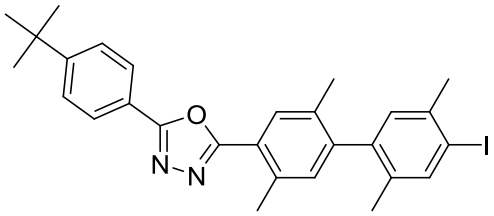

2-(4-*tert*-Butylphenyl)-5-(2,2',5,5'-tetramethyl-4'-(trimethylsilyl)biphenyl-4-yl)-1,3,4-oxadiazole **242** (0.2 g, 0.41 mmol) was dissolved in dichloromethane (20 cm^3). To this stirred solution 1 M iodine monochloride (0.55 cm^3, 0.55 mmol) was added. The orange solution was stirred at room temperature for 3 h after which time it was poured onto water and washed with sodium thiosulfate solution and brine. The solvent was removed from the combined organic extracts yielding **243** as a white solid (0.22 g, 99%). ^1H NMR (500 MHz, $CDCl_3$): δ 8.10 (d, *J* = 8.5 Hz, 2H), 7.96 (s, 1H), 7.77 (s, 1H), 7.58 (d, *J* = 8.5 Hz, 2H), 7.09 (s, 1H), 7.00 (s, 1H), 2.74 (s, 3H), 2.44 (s, 3H), 2.13 (s, 3H), 2.02 (s, 3H), 1.40 (s, 9H); ^{13}C NMR (126 MHz, $CDCl_3$): δ 164.94, 164.51, 155.54, 143.95, 140.25, 138.88, 135.69, 135.24, 132.79, 130.53, 130.22, 127.02, 126.33, 121.42, 35.36, 31.39, 31.20, 27.69, 21.80, 19.52, 19.00; HRMS ($ASAP^+$), calcd for $C_{28}H_{30}N_2OI$: 537.1403, found: 537.1425; Mp: 79.0 – 80.6 ^oC.

246, (2,5-Dimethyl-4-(4,4,5,5-tetramethyl-1,3,2-dioxaborolan-2-yl)phenyl)trimethylsilane

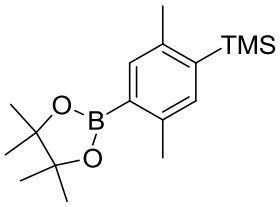

In a flame dried flask under an atmosphere of argon 1,4-dibromo-*p*-xylene **238** (5.0 g, 18.9mmol) was dissolved in anhydrous THF (100 cm^3) and cooled to -78 ^oC . To this stirred solution *n*-butyl lithium (8.3 mL, 20.8 mmol) was added dropwise, the reaction mixture was then stirred for 45 min followed by the addition of trimethylsilyl chloride (2.9 cm^3, 22.7 mmol). The reaction mixture was then slowly allowed to warm to room temperature and stirred for a further 15 h, after which it was poured onto water and extracted with diethyl ether. The solvent was removed from the combined organic extracts and the crude product **245** was isolated as a colourless oil. The colourless oil, (4-bromo-2,5-dimethylphenyl)trimethylsilane (2.0 g, 7.77 mmol), $B_2(pin)_2$ (7.90 g, 31.0 mmol) and potassium acetate (4.58 g, 46.6 mmol) were dissolved in DMF (50 cm^3). The stirred solution was degassed for 10 min with argon followed by the addition of [$PdCl_2$(dppf)] (170 mg, 3 mol%). The reaction mixture was then heated to 80 ^oC for 15 h. After the mixture was cooled the solvent was removed under reduced pressure and the crude residue was purified by column chromatography on silica gel with petroleum ether (b.p. 40 – 60 ^oC) as eluent to yield **246** as a white solid (1.09 g, 46%). ^1H NMR (400 MHz, $CDCl_3$): δ 7.56 (s, 1H), 7.27 (s, 1H), 2.52 (s, 3H), 2.43 (s, 3H), 1.35 (s, 12H), 0.33 (s, 9H); ^{13}C NMR (126 MHz, $CDCl_3$): δ 141.77, 141.06, 139.71, 137.02, 136.10, 83.59, 25.11, 22.51, 22.04, 0.02; HRMS (ASAP$^+$) calcd for $C_{17}H_{29}{}^{10}BOSi$: 303.2066. Found: 303.2054; Mp: 108.4 – 112.0 ^oC.

252, 2,5-Dimethyl-*N*-*p*-tolylbenzenamine,

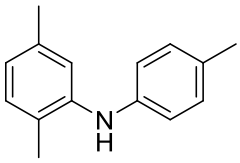

The standard Buchwald-Hartwig amination procedure B was followed using the following quantities: 4-iodotoluene (5.45 g, 25 mmol), 2,5-dimethylaniline (2.00 g, 10 mmol), 10% Pd/C (212 mg, 0.5 mmol), sodium *tert*-butoxide (2.40 g, mmol), dppf (0.17 g, 0.3 mmol) and mesitylene (10 cm^3). The crude product was purified by column chromatography on silica gel with petroleum ether and 5% dichloromethane as eluent to yield **252** as a pale yellow solid (2.53 g, 96%). The NMR data were consistent with the literature.[146] ^1H NMR (400 MHz, $CDCl_3$): δ 7.11 – 7.02 (m, 3H), 6.99 (s, 1H), 6.91 (d, *J* = 8.5 Hz, 2H), 6.70 (d, *J* = 7.5 Hz, 1H), 5.26 (s, 1H), 2.30 (s, 3H), 2.25 (s, 3H), 2.20 (s, 3H); ^{13}C NMR (126 MHz, $CDCl_3$): δ 142.16, 141.49, 136.75, 131.00, 130.61, 130.16, 124.34, 122.21, 118.96, 118.30, 21.56, 21.01, 17.77; MS (ASAP$^+$) 211.4 (M^+, 100%); Mp: 51.6 – 52.0 ^oC.

253, 2,5-Dimethyl-*N*,*N*-di*p*-tolylbenzenamine

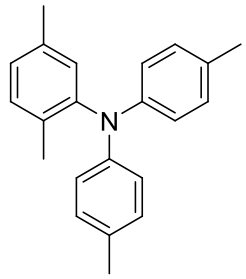

The standard Buchwald-Hartwig amination procedure B was followed using the following quantities: 4-bromotoluene (0.97 g, 5.7 mmol), 2,5-dimethyl-*N*-*p*-tolylbenzenamine **252** (1.00 g, 4.7 mmol), 10% Pd/C (100 mg, 0.1 mmol), sodium *tert*-butoxide (0.68 g, 7.1 mmol), dppf (78 mg, 0.2 mmol) and mesitylene (10 cm^3). The crude product was purified by column chromatography on silica gel with petroleum ether (b.p. 40 – 60^oC) and 5% dichloromethane as eluent to yield **253** as a colourless oil (1.24 g, 88%). ^1H NMR (400 MHz, $CDCl_3$): δ 7.30 (s, 1H), 6.92 (d, *J* = 8.5 Hz, 4H), 6.88 (s, 1H), 6.74 (d, *J* = 8.5 Hz, 4H), 2.20 (s, 6H), 2.19 (s, 3H), 1.86 (s, 3H); ^{13}C NMR (101 MHz, $CDCl_3$): δ 145.11, 145.01, 136.56, 135.44, 134.90, 131.17, 130.88, 129.62, 121.65, 121.02, 22.32, 20.64, 17.96; HRMS ($ASAP^+$) calcd for $C_{22}H_{23}N$: 301.1830. Found: 301.1849.

247, 4-Bromo-2,5-dimethyl-*N*,*N*-di*p*-tolylbenzenamine

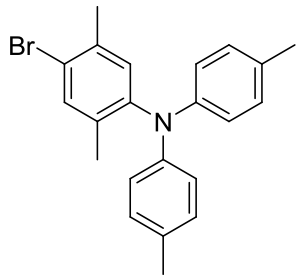

2,5-Dimethyl-*N*,*N*-di*p*-tolylbenzenamine **253** (0.80 g, 2.7 mmol) was dissolved in dichloromethane (30 cm^3), degassed and cooled to 0 ^oC. To this stirred solution *N*-bromosuccinimide (0.47 g, 2.9 mmol) was added and the reaction mixture was stirred in the dark for 1.5 h after which time water was added and the reaction mixture extracted with dichloromethane. The combined organic extracts were dried and the solvent removed under reduced pressure to give **247** as a colourless oil (1.04 g, 100%). ^1H NMR (400 MHz, $CDCl_3$): δ 7.39 (s, 1H), 7.02 (d, *J* = 8.0 Hz, 4H), 6.97 (s, 1H), 6.84 (d, *J* = 8.0 Hz, 4H), 2.29 (s, 6H), 2.29 (s, 3H), 1.95 (s, 3H); MS (ASAP+) 379.1 (M+, 100%), 211.1 (43); ^{13}C NMR (101 MHz, $CDCl_3$) δ 144.05, 144.04, 135.54, 134.42, 133.86, 130.15, 129.85, 128.60, 120.60, 120.00, 21.33, 19.64, 16.96; HRMS ($ASAP^+$), calcd for $C_{22}H_{22}N^{79}Br$: 379.0936, found: 379.0934.

254, 2,5-Dimethyl-4-(4,4,5,5-tetramethyl-1,3,2-dioxaborolan-2-yl)-*N*,*N*-di*p*-tolylbenzenamine

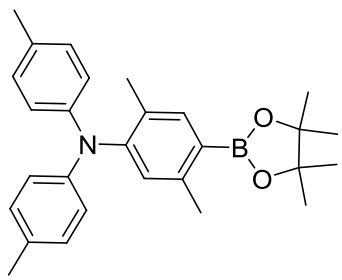

In a flame dried flask under an atmosphere of argon 4-bromo-2,5-dimethyl-*N*,*N*-di*p*-tolylbenzenamine **247** (0.85 g, 2.20 mmol) was dissolved in diethyl ether (80 cm^3) and cooled to -78 ^oC. To this stirred solution 2.5 M *n*-butyl lithium (2.37 cm^3, 5.9 mmol)

was added dropwise and the solution was then stirred at -78 °C for 40 min. The mixture was then allowed to warm to room temperature for 20 min and then cooled again to -78 °C. To the stirred yellow solution 2-isopropoxy-4,4,5,5-tetramethyl-1,3,2-dioxaborolane (1.47 cm^3, 7.2 mmol) was added dropwise. The reaction mixture was then allowed to warm slowly to room temperature and was stirred overnight. The reaction was quenched with dilute HCl (20 cm^3) and extracted with diethyl ether. The combined organic extracts were dried and the solvent removed under reduced pressure. The crude product was purified by column chromatography on silica gel with petroleum ether (b.p. 40 – 60 °C) with 5% DCM as eluent to yield **254** as a colourless viscous oil (0.44 g, 45%). ^{1}H NMR (400 MHz, $CDCl_3$): δ 7.61 (s, 1H), 6.99 (d, *J* = 8.0 Hz, 4H), 6.88 (s, 1H), 6.84 (d, *J* = 8.0 Hz, 4H), 2.42 (s, 3H), 2.28 (s, 6H), 1.95 (s, 3H), 1.35 (s, 12H); ^{13}C NMR (126 MHz, $CDCl_3$): δ 148.37, 145.51, 144.17, 139.63, 132.03, 130.97, 130.18, 129.78, 122.16, 83.59, 25.18, 25.08, 21.93, 20.96, 18.40; HRMS (ASAP$^+$) calcd for $C_{28}H_{34}{}^{10}BNO_2$: 426.2719. Found: 426.2721.

230, DPA-(*p*-xylene)$_3$-OXD

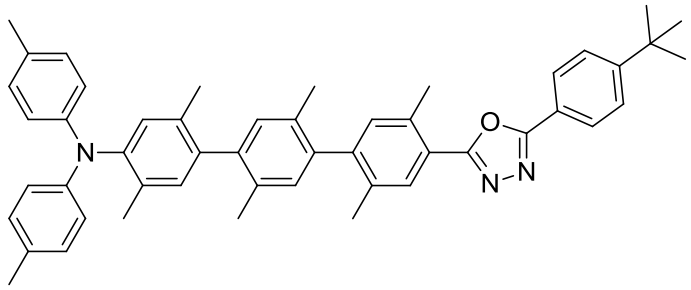

The standard Suzuki-Miyaura cross-coupling procedure was followed using the following quantities: 2,5-dimethyl-4-(4,4,5,5-tetramethyl-1,3,2-dioxaborolan-2-yl)-*N*,*N*-di-*p*-tolylbenzenamine **254** (0.14 g, 0.33 mmol), 2-(4-*tert*-butylphenyl)-5-(4'-iodo-2,2',5,5'-tetramethylbiphenyl-4-yl)-1,3,4-oxadiazole **230** (0.10 g, 0.19 mmol), [$PdCl_2(PPh_3)_2$] (7 mg, 5 mol%), NaOH (50 mg in 5 cm^3 H_2O) and THF (15 cm^3). The crude product was purified by column chromatography on silica gel using 8 : 2 (v/v) petroleum ether (b.p. 40 – 60 °C) : diethyl ether as eluent to yield **230** as a white solid (0.11 g, 82%). ^{1}H NMR (400 MHz, $CDCl_3$): δ 8.10 (d, *J* = 8.5 Hz, 2H), 7.98 (s, 1H), 7.58 (d, *J* = 8.5 Hz, 2H), 7.21 (s, 1H), 7.11 – 6.98 (m, 8H), 6.92 (d, *J* = 8.5 Hz, 4H), 2.76 (s, 3H), 2.30 (s, 6H), 2.20 (m, 3H), 2.11 (s, 3H), 2.08 (s, 3H), 2.05 – 1.97 (m, 6H), 1.39 (s, 9H); ^{13}C NMR (126 MHz, Acetone): δ 165.73, 165.13, 164.81, 156.37, 155.18, 146.72, 146.59, 145.85, 144.02, 141.79, 141.09, 140.58, 140.32, 140.19, 138.87, 136.46, 135.98, 135.90, 135.57, 135.26, 135.12, 134.21, 134.00, 133.91, 133.61, 133.50, 132.17, 132.03, 131.69, 131.61, 131.39, 130.81, 129.96, 127.82, 127.42, 126.76, 123.26, 123.18, 122.71, 122.64, 117.10, 35.99, 22.00, 21.94, 21.71, 21.01, 20.31, 20.02, 19.95, 19.82, 19.75, 19.33, 18.66; HRMS (ASAP$^+$) calcd for $C_{50}C_{51}N_3O$: 709.4032. Found: 709.4027; Mp: 140.3 – 141.5 °C.

256, 2,5-Diphenyl-1,4-dimethylbenzene

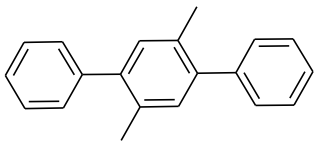

To a flame dried flask under an atmosphere of argon 1,4-dibromo-2,5-dimethylbenzene (1.5 g, 5.68 mmol), phenylboronic acid (1.52 g, 12.47 mmol), potassium carbonate (3.93 g, 28.44 mmol), *tetra*-*n*-butylammonium bromide (3.66 g, 11.35 mmol) and palladium (II) acetate (2.5 mg, 0.2 mol%) were added. Separately, deionised water (12.5 cm^3) was degassed with argon for 15 min after which time the water was added to the solid reagents and the mixture was heated to 70 ^oC with vigorous stirring. After 2 h the reaction mixture was cooled, washed with water and extracted with toluene. The organic extracts were combined and the solvent removed under reduced pressure. The resulting solid was recrystallised from cyclohexane to yield **256** as a white solid (1.00 g, 68%) The NMR data were consistent with the literature.[147] ^1H NMR (400 MHz, $CDCl_3$): δ 7.46 – 7.32 (m, 10H), 7.16 (s, 2H), 2.28 (s, 6H).

257, 2,5-Diphenyl-1,4-dibenzoic acid

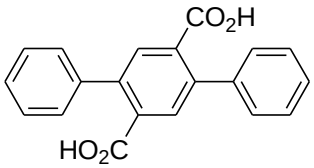

In a flask under an atmosphere of argon 2,5-diphenyl-1,4-dimethylbenzene **256** (1.00 g, 3.87 mmol) was dissolved in pyridine (30 cm^3) and water (3 cm^3). To this stirred solution $KMnO_4$ (3.0 g) was added. The reaction mixture was heated to reflux for 2 h under argon. During this time at 0.5 h intervals additional $KMnO_4$ (1.5 g) and water (5 cm^3) were added. The reaction mixture was then stirred at reflux for a further 4 h, then water (35 cm^3) was added and the mixture refluxed overnight. The resulting hot slurry was filtered through a plug of Celite and washed with hot water. The filtrate was concentrated and acidified with conc. HCl. The resulting product was dried in an oven for 15 hours yielding **257** as a white solid (1.17 g, 95%). The NMR data were consistent with the literature.[147] ^1H NMR (400 MHz, acetone-d_6): δ 7.71 (s, 2H), 7.39 – 7.23 (m, 10H).

258, Indenofluorene-11,12-dione

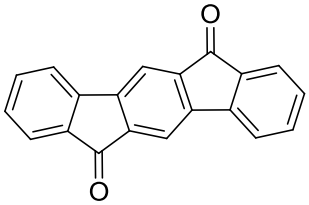

2,5-Diphenyl-1,4-dibenzoic acid **257** (1.5 g, 3.5 mmol) was dissolved in conc. sulfuric acid (80 mL). The mixture was stirred at room temperature for 2 h and then poured onto ice. The purple precipitate was filtered and washed with water. The solid was then stirred in potassium carbonate solution for 3 h, filtered and dried in an oven at 80 ^oC overnight. The product **258** was isolated as a deep purple solid (0.87 g, 89%). The NMR data

were consistent with the literature.[147] ^{1}H NMR (400 MHz, $CDCl_3$): δ 7.82 (s, 2H), 7.70 (d, *J* = 7.5 Hz, 2H), 7.60 – 7.54 (m, 4H), 7.39 – 7.31 (m, 2H).

259, Indenofluorene

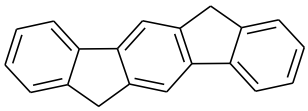

Indenofluorene-11,12-dione **258** (0.87 g, 3.1 mmol) was dissolved in diethylene glycol (100 mL), to which potassium hydroxide (5.00 g, 89.2 mmol) and hydrazine monohydrate (5 mL, 100 mmol) were added. The reaction mixture was heated to 180 °C for 20 h with stirring. The hot solution was then poured onto a mixture of ice and HCl. The white precipitate was filtered and dried to give **259** (0.59 g, 75%). The NMR data were consistent with the literature. [119] ^{1}H NMR (400 MHz, $CDCl_3$): δ 7.95 (s, 2H), 7.81 (d, *J* = 7.5 Hz, 2H), 7.56 (d, *J* = 7.5 Hz, 2H), 7.39 (t, *J* = 7.5 Hz, 2H), 7.30 (m, 2H), 3.98 (s, 4H).

260, 11,11,12,12-Tetrahexylindenofluorene

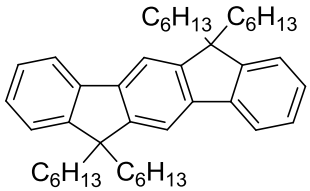

In a flame dried flask under an atmosphere of argon indenofluorene **259** (1.0 g, 11.8 mmol) and anhydrous THF (50 mL) were cooled to -78 °C. To this stirred suspension *n*-butyl lithium (4.5 mL, 3.93 mmol) was added dropwise and the reaction mixture stirred for 30 min at 0 °C after which time 1-bromohexane (1.5 cm^3, 11.5 mmol) was added at 0 °C. After stirring for 4 h a second portion of *n*-butyl lithium (4.5 cm^3, 3.93 mmol) was added with 30 min of stirring at 0 °C, followed by 1-bromohexane (1.5 cm^3, 11.5 mmol). The reaction mixture was then stirred for 12 h at room temperature. The reaction mixture was then quenched with aqueous ammonium chloride solution (20 cm^3) and extracted with diethyl ether (2x 30 cm^3). The combined organic extracts were dried and the solvent removed under reduced pressure. The crude product was purified by column chromatography on silica gel using petroleum ether (b.p. 40 – 60 °C) as eluent to yield **260** as a pale yellow solid (0.73 g, 31%). The NMR data were consistent with the literature. [119] ^{1}H NMR (400 MHz, $CDCl_3$): δ 7.79 – 7.73 (m, 2H), 7.65 – 7.62 (m, 2H), 7.39 – 7.29 (m, 6H), 2.10 – 1.97 (m, 8H), 1.17 – 0.87 (m, 26H), 0.81 – 0.58 (m, 18H).

261, 2,9-Dibromo-11,11,12,12-tetrahexylindenofluorene

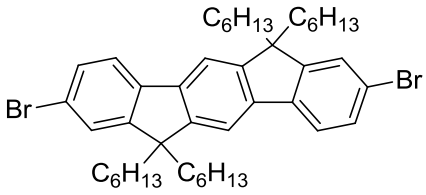

A solution of 11,11,12,12-tetrahexylindenofluorene **260** (1.13 g, 2.0 mmol) in chloroform (30 cm^3) was cooled to 0 °C. To this stirred solution $FeCl_3$ (8 mg) and bromine (0.11 cm^3, 2.2 mmol) were added dropwise. The solution was allowed to warm to room temperature and was stirred for 3 h in the dark. The reaction mixture was then poured onto water and washed with sodium thiosulphate. The solution was extracted with chloroform (2 x 30 cm^3) and the solvent was removed from the combined organic extracts under reduced pressure. The product **261** was isolated as a white solid (1.36 g, 91%). The NMR data were consistent with the literature. [119] ^{1}H NMR (400 MHz, $CDCl_3$): δ 7.59 (d, *J* = 8.5 Hz, 2H), 7.55 (s, 2H), 7.48 – 7.44 (m, 4H), 1.98 (m, 8H), 1.18 – 0.92 (m, 24H), 0.76 – 0.50 (m, 20H).

262, 2-Bromo-9-cyano-11,11,12,12-tetrahexylindenofluorene

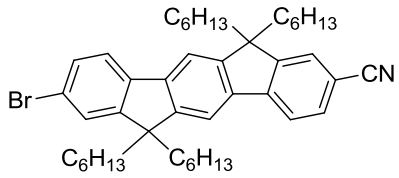

In a flame dried flask under an atmosphere of argon 2,9-dibromo-11,11,12,12-tetrahexylindenofluorene **261** (0.50 g, 0.67 mmol) was dissolved in DMF (5 cm^3) and copper cyanide (57 mg, 0.63 mmol) was added. The reaction mixture was then heated to reflux for 20 h. The reaction mixture was then poured onto aqueous iron(III) chloride solution (5.00 g in 2 cm^3 HCl and 8 cm^3 water) and stirred at 90 °C for 30 min. The mixture was then extracted with toluene (3 x 50 cm^3) and the combined organic layers were then washed with 5 M HCl until the dark colour disappeared, followed by water (3 x 50 cm^3). The solvent was removed from the organic layers under reduced pressure and the crude product was purified by column chromatography using petroleum ether 40-60 °C to 7 : 3 (v/v) petroleum ether (b.p. 40-60 °C) : dichloromethane as eluent to yield **262** as a pale yellow solid (0.23 g, 50%). ^{1}H NMR (400 MHz, $CDCl_3$) δ 7.80 (d, *J* = 8.0 Hz, 1H), 7.69 – 7.57 (m, 5H), 7.51 – 7.46 (m, 1H), 7.35 – 7.31 (m, 1H), 2.09 – 1.95 (m, 8H), 1.16 – 0.94 (m, 24H), 0.73 (m, 8H), 0.65 – 0.51 (m, 12H); ^{13}C NMR (126 MHz, $CDCl_3$) δ 153.70, 151.98, 151.33, 150.42, 146.11, 141.66, 140.07, 139.13, 131.48, 130.24, 126.60, 126.45, 121.62, 121.42, 120.28, 120.22, 115.18, 114.33, 109.70, 55.43, 55.41, 40.72, 40.55, 31.70, 31.68, 29.80, 29.75, 23.90, 22.72, 22.69, 14.18, 14.16; HRMS ($ASAP^+$) calcd for $C_{45}H_{60}N^{79}Br$: 693.3909. Found: 693.3884; Mp: 142.3 – 150.0 °C.

263, 5-(8-Bromo-6,6,12,12-tetrahexyl-6,12-dihydroindeno[1,2-b]fluoren-2-yl)-1*H*-tetrazole

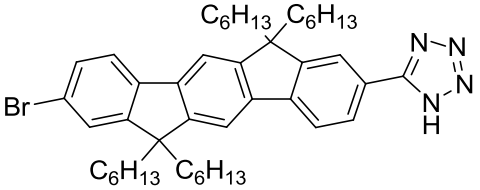

2-Bromo-9-cyano-11,11,12,12-tetrahexylindenofluorene **262** (0.16 g, 0.22 mmol),

sodium azide (29 mg, 0.45 mmol) and ammonium chloride (24 mg, 0.45 mmol) were dissolved in anhydrous DMF (5 cm^3) and heated to reflux for 48 h. The reaction mixture was cooled, poured onto water and extracted with DCM. The combined organic extracts were washed with water and the solvent removed under reduced pressure. The crude product was purified by column chromatography on silica gel using 9 : 1 DCM : ethyl acetate as eluent. The product was isolated as a white solid (90 mg, 56%). The identity of the product **263** was confirmed by NMR spectroscopy and MS; however an unidentified inseparable impurity remained (75% by ^{1}H NMR), to be removed at a later stage in the synthesis. ^{1}H NMR (700 MHz, DMSO-d_6) δ 8.09 – 7.99 (m, 3H), 7.93 (m, 2H), 7.81 (d, *J* = 8.0 Hz, 1H), 7.65 (d, *J* = 1.5 Hz, 1H), 7.50 (dd, *J* = 8.0, 1.5 Hz, 1H), 2.14 – 1.99 (m, 8H), 1.02 – 0.82 (m, 24H), 0.66 – 0.56 (m, 12H), 0.55 – 0.40 (m, 1H); ^{13}C NMR (176 MHz, DMSO-d_6) δ 153.60, 151.88, 150.97, 150.89, 150.66, 150.26, 150.03, 141.77, 141.18, 140.56, 139.95, 130.27, 126.50, 126.34, 122.26, 121.13, 120.80, 115.35, 115.01, 55.33, 55.16, 55.12, 54.82, 31.33, 31.30, 29.21, 29.19, 23.74, 23.69, 22.65, 22.19, 22.18, 14.16, 14.13; HRMS (ASAP$^+$) calcd for $C_{45}H_{62}N_4{}^{79}Br$: 737.4158. Found: 737.4173.

264, 2-(8-Bromo-6,6,12,12-tetrahexyl-6,12-dihydroindeno[1,2-b]fluoren-2-yl)-5-(4-*tert*-butylphenyl)-1,3,4-oxadiazole

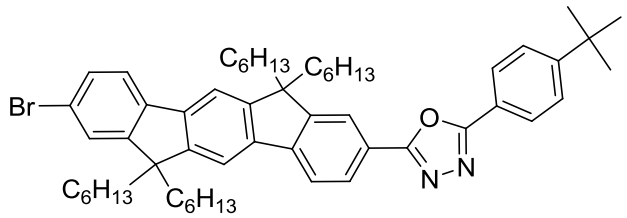

5-(8-Bromo-6,6,12,12-tetrahexyl-6,12-dihydroindeno[1,2-b]fluoren-2-yl)-1H-tetrazole **263** (0.18 g, 0.24 mmol) was dissolved in pyridine (5 cm^3) and 4-*tert*-butylbenzoyl chloride (0.095 cm^3, 0.49 mmol) was added dropwise. The reaction mixture was heated to reflux for 20 h. The product was isolated as a pale yellow solid The reaction mixture was cooled, poured onto water and extracted with DCM. The combined organic extracts were washed with water and the solvent removed under reduced pressure. The crude product was purified by column chromatography on silica gel using 9 : 1 DCM : ethyl acetate as eluent. The desired product was inseparable from the debrominated impurity. The identity of **264** was confirmed by mass spectrometry and the purity judged to be 85% by ^{1}H NMR. ^{1}H NMR (400 MHz, $CDCl_3$) δ 8.18 – 8.09 (m, 4H), 7.88 (d, *J* = 8.5 Hz, 1H), 7.64 (m, 3H), 7.58 (d, *J* = 8.5 Hz, 2H), 7.51 – 7.46 (m, 2H), 2.22 – 1.94 (m, 8H), 1.39 (s, 9H), 1.15 – 0.94 (m, 24H), 0.78 – 0.57 (m, 20H); MS (MALDI$^+$) 871.4 (50%, M^+), 825.5 (20%), 791.5 (100%).

232, 8-(5-(4-*tert*-Butylphenyl)-1,3,4-oxadiazol-2-yl)-6,6,12,12-tetrahexyl-*N*,*N*-di*p*-tolyl-6,12-

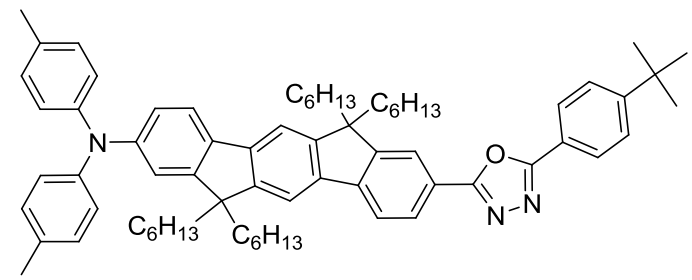

dihydroindeno[1,2-b]fluoren-2-amine

The standard Buchwald-Hartwig cross-coupling procedure was followed using the following quantities: 2-(8-bromo-6,6,12,12-tetrahexyl-6,12-dihydroindeno[1,2-b]fluoren-2-yl)-5-(4-*tert*-butylphenyl)-1,3,4-oxadiazole **264** (80mg, 0.09 mmol), di-*p*-tolylamine (24 mg, 0.12 mmol), $[Pd_2(dba)_3]$ (3.0 mg, 0.003 mmol), dppf (2.3 mg, 0.004 mmol), NaO^tBu (13 mg, 0.14 mmol) and toluene (5 cm^3). The identity of the product **232** was confirmed by NMR but it remained inseparable from an impurity in a variety of solvent systems (petroleum ether (b.p. 40 – 60 ^oC) and 10% diethyl ether (R_f product: 0.5, R_f impurity 0.5); petroleum ether (b.p. 40 – 60 ^oC) and 5% acetone (R_f product: 0.4, R_f impurity 0.4); carbon disulfide and 10% dichloromethane (R_f product: 0.3, R_f impurity 0.3)). ^1H NMR (700 MHz, $CDCl_3$) δ 8.11 (m, 4H), 7.88 – 7.82 (m, 1H), 7.69 – 7.64 (m, 1H), 7.63 – 7.51 (m, 5H), 7.35 – 7.31 (m, 1H), 7.12 – 6.94 (m, 8H), 2.32 (s, 6H), 2.15 – 1.83 (m, 6H), 1.38 (d, *J* = 1.2 Hz, 9H), 1.13 – 0.96 (m, 20H), 0.92 – 0.55 (m, 24H). ^{13}C NMR (176 MHz, $CDCl_3$) δ 165.20, 165.10, 164.48, 164.40, 155.21, 155.14, 153.11, 151.93, 151.06, 150.09, 144.88, 140.71, 139.69, 139.58, 132.84, 129.73, 127.06, 126.78, 126.77, 126.01, 125.99, 123.96, 123.23, 122.03, 121.30, 121.25, 121.19, 120.63, 119.96, 119.64, 114.58, 114.01, 55.17, 55.07, 54.71, 40.62, 40.53, 40.46, 35.07, 31.52, 31.48, 31.13, 29.64, 29.60, 23.74, 22.50, 20.76, 14.00, 13.93; MS (MALDI$^+$) 985.5 (100%, M^+).

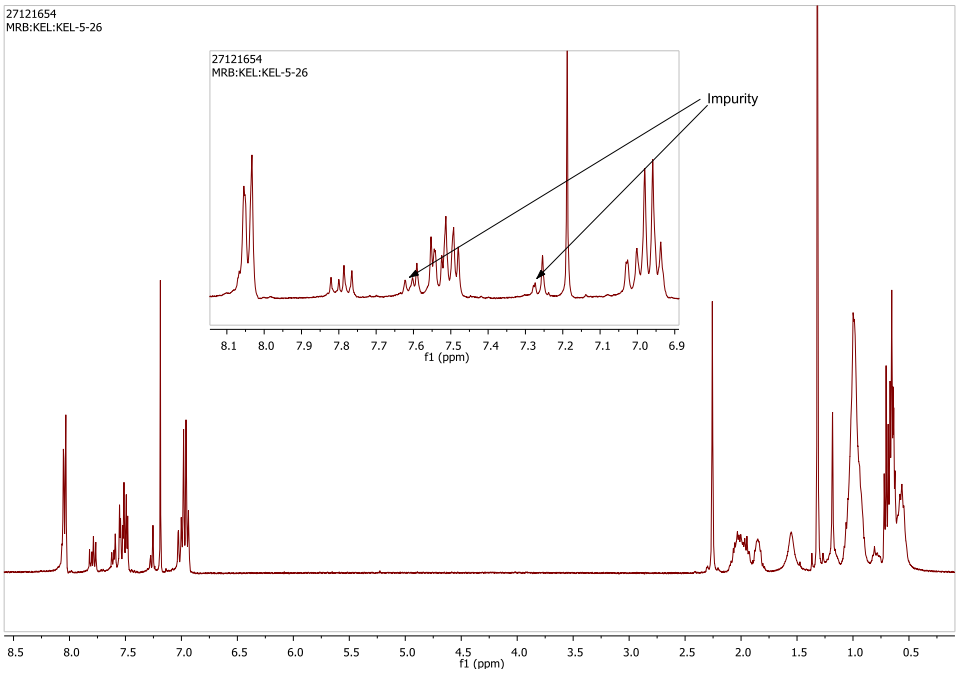

Figure 6.2 – ^1H NMR spectrum of 232 with expansion of aromatic region inset showing impurity peaks

6.6 Experimental procedures for chapter 5

Both the nanosecond and femtosecond time resolved spectroscopy studies described were

carried out at the EPFL, Switzerland with assistance from Dr. Mateusz Wielopolski.

Nanosecond Flash Photolysis

The Nanosecond laser flash photolysis technique was applied to dye-sensitised, 8 µm-thick, transparent TiO_2 mesoporous films deposited on normal flint glass. Pulsed excitation (λ= 505 nm, 7 ns pulse duration, 30 Hz repetition rate) was carried out by a Powerlite 7030 frequency-doubled Q-switched Nd:YAG laser (Continuum, Santa Clara, California, USA). The laser beam output was expanded by a planoconcave lens to irradiate a large cross-section of the sample, whose surface was kept at a 30° angle to the excitation beam. The laser fluence on the sample was kept at a low level (30 µJ cm^{-2} per pulse) to ensure that, on average, less than one electron is injected per nanocrystalline TiO_2 particle on pulsed irradiation. The probe light, produced by a continuous wave xenon arc lamp, was first passed through a monochromator tuned at 420 nm, various optical elements, the sample, and then through a second monochromator, before being detected by a fast photomultiplier tube (Hamamatsu, R9110). Data waves were recorded on a DSA 602A digital signal analyser (Tektronix, Beaverton, Oregon, USA). Satisfactory signal-to-noise ratios were typically obtained by averaging over 1,500 laser shots.

Femtosecond Transient Absorption.

Time-resolved transient absorption measurements by the pump-probe technique used a compact CPA-2001, 1 kHz, Ti:Sapphire-amplified femtosecond laser (Clark-MXR), with a pulse width of about 120 fs and a pulse energy of 1 mJ at a central wavelength of 775 nm. The output beam was split into two parts for pumping a double-stage noncollinear optical parametric amplifier (NOPA) and to produce a white light continuum in a sapphire plate or 387 nm UV light by second harmonic generation of the CPA output in a thin BBO crystal. The NOPAs was pumped by 200 *µJ* pulses at a central wavelength of 775 nm and the excitation wavelength was tuned to 400 nm to generate pulses of approximately 10 *µJ*. The output pulses of the NOPAs were compressed in a SF10-glass prism pair compressor down to a duration of less than 50 fs (fwhm). Iris diaphragms were used to decrease the pulse energy down to a few microjoules for the pump and to less than 1 *µJ* for the probe beam. Transient spectra were measured using a white light continuum (WLC) for probing. The latter was generated from pulses (energy <10 *µJ)* focused into a 2 mm thick sapphire plate. The monofilament white beam was collimated using a 90° off-axis paraboloid mirror and steered to the sample using only reflective optics. A smooth monotonic spectral

distribution between 480 and 720 nm was obtained by controlling the pump energy with an iris and a variable density filter. The polarization between the pump and probe beams was controlled using a coherent zero-order half waveplate, and experiments were carried out at the magic angle (54.7°) configuration. Pump and probe beams were directed parallel to each other toward a 60° off-axis paraboloid mirror that focused them into the sample. A broadband membrane-beam splitter was placed before the sample to split the probe beam into reference and signal arms. Both were collected by a lens system and directed into two Andor Shamrock 163 imaging spectrographs. The absorbance change was calculated using the ratio between data obtained with and without the pump pulses reaching the sample and corrected for fluctuations in the WLC intensity using the reference beam spectra.

Procedure for Fabrication of DSSCs

Double layered films, consisted of an 8 µm thick transparent layer of 20 nm-sized TiO_2 covered with a 5 µm thick scattering layer of 400 nm sized TiO_2 particles, were screen-printed on the fluorine doped SnO_2 (FTO) conducting glass electrode. The porosity was evaluated as 67% for the 20 nm TiO_2 transparent layer and 42% for the scattering layer, determined from BET (Brunauer Emmett-Teller theory) measurements. After sintering at 500 °C and cooling to 80 °C, the sintered TiO_2 electrodes were sensitised by overnight dipping in the respective dye solutions (0.2 mM of the dye in *t*BuOH/MeCN 1:1 mixture), and then assembled using a thermally platinised FTO/glass counter electrode. The working and counter electrodes were separated by a 25 µm thick hot melt ring (Surlyn, DuPont) and sealed by heating. The cell's internal space was filled with electrolyte using a vacuum pump. The electrolyte-injecting hole on the thermally platinised FTO glass counter electrode was finally sealed with a Surlyn sheet and a thin glass cover by heating.

283, 7-Bromo-9,9-dihexyl-*N*,*N*-diphenyl-9*H*-fluoren-2-amine

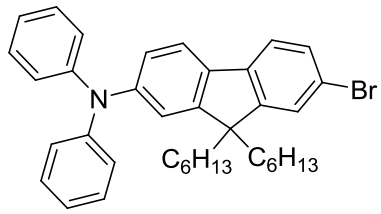

The general Buchwald-Hartwig amination procedure B was followed using the following quantities: diphenylamine (1.00 g, 5.9 mmol), 2,7-dibromo-9*H*-fluorene **55** (3.49 g, 7.0 mmol), NaO^tBu (0.85 g, 8.85 mmol), mesitylene (6 cm^3), 10% Pd/C (0.13 g, 0.12 mmol) and dppf (0.10 g, 0.18 mmol). The crude product was purified by column chromatography on silica gel using petroleum ether (b.p. 40 – 60 °C) with 20% dichloromethane as eluent to yield **283** as a colourless oil (1.0 g, 29%). The NMR data were consistent with the literature.[148] ^1H NMR (400 MHz, $CDCl_3$) δ 7.52 (d,

J = 8.0 Hz, 1H), 7.49 – 7.39 (m, 3H), 7.29 – 7.20 (m, 4H), 7.15 – 7.07 (m, 1H), 7.06 – 6.97 (m, 1H), 1.88 – 1.78 (m, 4H), 1.21 – 0.97 (m, 12H), 0.81 (t, *J* = 7.0 Hz, 6H), 0.70 – 0.57 (m, 4H).

284, 4-(4,4,5,5-Tetramethyl-1,3,2-dioxaborolan-2-yl)benzonitrile

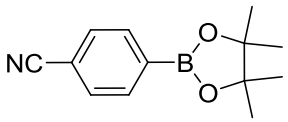

The general Miyaura borylation procedure was followed using the following quantities: 4-bromobenzonitrile (3.00 g, 16.0 mmol), B_2pin_2 (5.84 g, 23 mmol), KOAc (2.51 g, 25.6 mmol) and [$PdCl_2$(dppf)] (0.23 g, 0.32 mmol). The crude product was purified by column chromatography on silica gel using 1 : 1 (v/v) DCM : petroleum ether (b.p. 40 – 60 ^{o}C) as eluent to yield **284** as a pale green solid (2.85 g, 78%). The NMR data were consistent with the literature.[149] ^{1}H NMR (400 MHz, $CDCl_3$) δ 7.88 (d, *J* = 8.5 Hz, 2H), 7.64 (d, *J* = 8.5 Hz, 2H), 1.35 (s, 12H).

285, 4-(7-(Diphenylamino)-9,9-dihexyl-9*H*-fluoren-2-yl)benzonitrile

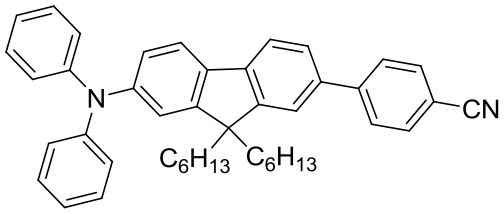

The general Suzuki-Miyaura cross-coupling procedure was followed using the following quantities: 7-bromo-9,9-dihexyl-*N*,*N*-diphenyl-9*H*-fluoren-2-amine **283** (0.95 g, 1.64 mmol), 4-(4,4,5,5-tetramethyl-1,3,2-dioxaborolan-2-yl)benzonitrile **284** (0.41 g, 1.9 mmol), NaOH (0.05 g in 5 cm^3). The crude product was purified by column chromatography using 1:1 (v/v) dichloromethane : petroleum ether (b.p. 40 – 60 ^{o}C) as eluent to yield **285** as a yellow solid (0.71 g, 72%). ^{1}H NMR (400 MHz, $CDCl_3$) δ 7.75 (d, *J* = 1.0 Hz, 4H), 7.69 (dd, *J* = 8.0, 1.0 Hz, 1H), 7.59 (d, *J* = 8.0 Hz, 1H), 7.55 (dd, *J* = 8.0, 1.5 Hz, 1H), 7.49 (d, *J* = 1.5 Hz, 1H), 7.29 – 7.21 (m, 4H), 7.17 – 7.09 (m, 5H), 7.06 – 6.99 (m, 3H), 1.99 – 1.76 (m, 4H), 1.20 – 0.99 (m, 12H), 0.79 (t, *J* = 7.0 Hz, 6H), 0.74 – 0.56 (m, 4H); ^{13}C NMR (101 MHz, $CDCl_3$) δ 151.49, 150.67, 146.89, 146.68, 145.18, 140.74, 135.97, 134.21, 131.56, 128.21, 126.61, 125.22, 122.97, 122.41, 121.69, 120.26, 119.73, 118.61, 118.15, 118.07, 109.36, 54.25, 39.24, 30.50, 28.61, 22.80, 21.55, 13.04; HRMS (ASAP^{+}), calcd for $C_{44}H_{46}N_4$: 602.3661, found: 602.3651; Mp 51.2 – 52.3 ^{o}C.

286, 7-(4-(1*H*-Tetrazol-5-yl)phenyl)-9,9-dihexyl-*N*,*N*-diphenyl-9*H*-fluoren-2-amine

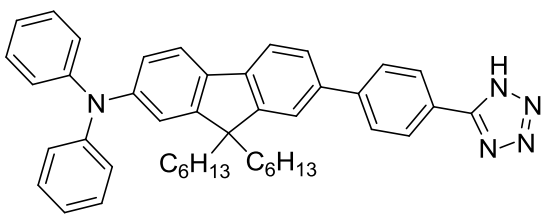

4-(7-(Diphenylamino)-9,9-dihexyl-9*H*-fluoren-2-yl)benzonitrile **285** (0.6 g, 1.00 mmol) was dissolved in anhydrous DMF (25 cm^3). To this stirred solution ammonium chloride (64 mg,

1.2 mmol) and sodium azide (78 mg, 1.2 mmol) were added and the reaction mixture heated to reflux for 24 h. The reaction mixture was then poured onto water and extracted with ethyl acetate. The organic layers were combined and the solvent removed under reduced pressure. The crude product was purified by column chromatography with dichloromethane and 10% ethyl acetate as eluent to yield **286** as a pale yellow solid (0.375 g, 57%). ^{1}H NMR (400 MHz, acetone-d_6) δ: 8.10 (d, *J* = 8.5 Hz, 2H), 7.86 (d, *J* = 8.5 Hz, 2H), 7.78 – 7.69 (m, 2H), 7.67 – 7.60 (m, 2H), 7.18 (dd, *J* = 8.5, 7.5 Hz, 4H), 7.08 (d, *J* = 2.0 Hz, 1H), 7.02 – 6.87 (m, 7H), 2.05 – 1.75 (m, 4H), 1.06 – 0.89 (m, 12H), 0.71 – 0.50 (m, 10H). ^{13}C NMR (101 MHz, acetone-d_6) δ: 153.38, 152.45, 148.92, 148.48, 146.14, 144.87, 142.08, 138.75, 138.19, 136.83, 130.19, 128.52, 128.47, 126.94, 124.64, 124.43, 123.63, 122.15, 121.74, 120.61, 120.21, 56.11, 40.79, 32.23, 24.62, 23.15, 14.26; MS (ASAP$^+$) 645.2 (30%, M$^+$), 602.2 (100%); Mp: 187.2 – 189.0 ^{o}C.

291, 2-(4-Bromophenyl)-5-*p*-tolyl-1,3,4-oxadiazole

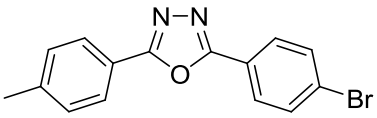

5-*p*-Tolyl-1*H*-tetrazole **290** (5.45 g, 33.0 mmol) was dissolved in pyridine (50 cm^3), to this stirred solution 4-bromobenzoyl chloride (7.84 g, 36.0 mmol) and heated to reflux for 72 h. The reaction mixture was cooled and poured onto water to precipitate **291** which was filtered, dried and isolated as a white solid (6.12 g, 57%). ^{1}H NMR (400 MHz, $CDCl_3$) δ 8.05 – 7.92 (m, 4H), 7.68 (m, 2H), 7.36 – 7.31 (m, 2H), 2.45 (s, 3H). ^{13}C NMR (101 MHz, $CDCl_3$) δ 164.93, 163.64, 142.50, 132.41, 129.83, 128.28, 126.94, 126.29, 122.96, 120.96, 21.68. MS (ASAP+) 314 (85%, M+), 179 (100), 119 (45); HRMS (ASAP$^+$) calcd for $C_{15}H_{12}N_2OBr$: 315.0133. Found: 315.0150; Mp: 205.0 – 206.2 ^{o}C.

292, 2-(4-(Bromomethyl)phenyl)-5-(4-bromophenyl)-1,3,4-oxadiazole

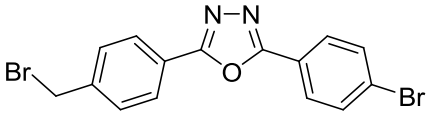

2-(4-Bromophenyl)-5-*p*-tolyl-1,3,4-oxadiazole **291** (2.00 g, 6.3 mmol) was dissolved in 1,2-dichloroethane (50 cm^3) to which *N*-bromosuccinimide (1.07 g, 6.0 mmol) and benzoyl peroxide (0.30 g, 1.2 mmol) were added. The reaction mixture was heated to 70 ^{o}C for 15 h. The reaction mixture was cooled and the solvent removed under reduced pressure. The crude product was purified by column chromatography using petroleum ether and then petroleum ether and 50% ethyl acetate as eluents. The product was further purified by recrystallisation from acetonitrile and **292 was** isolated as a white solid (1.12 g, 48%). ^{1}H NMR (400 MHz, $CDCl_3$) δ 8.12 (d, *J* = 8.5 Hz, 2H), 8.01 (d, *J* = 9.0 Hz, 2H), 7.69 (d, *J* = 9.0 Hz, 2H), 7.57 (d, *J* = 8.5 Hz, 2H), 4.54 (s, 2H); ^{13}C NMR (176 MHz, $cdcl_3$) δ 164.25, 163.98, 141.62, 132.45,

129.77, 128.32, 127.37, 126.53, 123.60, 122.71, 32.15; HRMS (ASAP$^+$), for $C_{15}H_{10}Br_2N_2O$ calcd: 391.9160. Found: 391.9171; Mp 184.2 – 186.7 ^oC.

293, 4-(5-(4-(4,4,5,5-Tetramethyl-1,3,2-dioxaborolan-2-yl)phenyl)-1,3,4-oxadiazol-2-yl)benzyl acetate

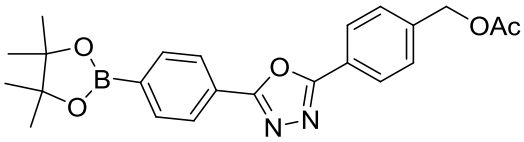

The general Miyaura borylation procedure was followed using the following quantities: 2-(4-(bromomethyl)phenyl)-5-(4-bromophenyl)-1,3,4-oxadiazole **292** (0.50 g, 1.6 mmol), B_2Pin_2 (1.02 g, 4 mmol), potassium acetate (0.31 g, 3.2 mmol) and [$PdCl_2$(dppf)] (35 mg, 0.5 mmol). The crude product was purified by column chromatography on silica gel using petroleum ether (b.p. 40 – 60 ^oC) with 10 then 30% ethyl acetate as eluent to yield **293** as a white solid (0.26 g, 36%). ^1H NMR (400 MHz, $CDCl_3$) δ 8.14 (m, 4H), 7.97 (d, *J* = 8.5 Hz, 2H), 7.52 (d, *J* = 8.5 Hz, 2H), 5.19 (s, 2H), 1.38 (s, 12H); ^{13}C NMR (101 MHz, $CDCl_3$) δ 170.63, 164.70, 164.37, 139.86, 135.32, 128.53, 127.20, 125.98, 123.70, 84.24, 65.49, 24.89, 20.89; HRMS (ASAP$^+$), for $C_{23}H_{26}N_2O_5{}^{10}B$ calcd: 420.1971, found: 420.1964; Mp: 168.1 – 169.4 ^oC.

278, (4-(5-(4-(7-(Diphenylamino)-9,9-dihexyl-9*H*-fluoren-2-yl)phenyl)-1,3,4-oxadiazol-2-yl)phenyl)methanol

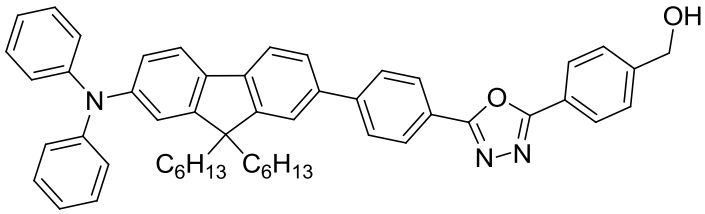

The general Suzuki-Miyaura procedure was followed using the following quantities: 4-(5-(4-(4,4,5,5-tetramethyl-1,3,2-dioxaborolan-2-yl)phenyl)-1,3,4-oxadiazol-2-yl)benzyl acetate **293** (0.10 g, 0.24 mmol), 7-bromo-9,9-dihexyl-*N*,*N*-diphenyl-9*H*-fluoren-2-amine **283** (0.14 g, 0.25 mmol), sodium hydroxide (0.02 g, 0.57 mmol), H_2O (5 cm^3) and [$PdCl_2(PPh_3)_2$] (0.01 g, 0.01 mmol). The crude product was purified by column chromatography on silica gel using 1 : 1 (v/v) petroleum ether (b.p. 40 – 60 ^oC) : diethyl ether as eluent. The product **278** was isolated as a yellow solid (0.14 g, 76%). ^1H NMR (600 MHz, $CDCl_3$) δ 8.23 (d, *J* = 8.5 Hz, 2H), 8.17 (d, *J* = 8.5 Hz, 2H), 7.83 (d, *J* = 8.5 Hz, 2H), 7.70 (d, *J* = 8.0 Hz, 1H), 7.62 (dd, *J* = 8.0, 1.7 Hz, 1H), 7.60 (d, *J* = 8.0 Hz, 1H), 7.58 – 7.54 (m, 3H), 7.28 – 7.23 (m, 4H), 7.16 – 7.11 (m, 5H), 7.06 – 6.99 (m, 3H), 4.83 (s, 2H), 1.99 – 1.80 (m, 4H), 1.19 – 1.00 (m, 12H), 0.79 (t, *J* = 7.0 Hz, 6H), 0.77 – 0.65 (m, 4H); ^{13}C NMR (151 MHz, $CDCl_3$) δ 164.55, 164.39, 152.45, 151.55, 147.91, 147.45, 145.00, 144.70, 141.24, 137.67, 135.49, 129.15,

127.58, 127.34, 127.24, 127.15, 126.08, 123.87, 123.45, 123.14, 122.56, 122.23, 121.18, 120.59, 119.49, 119.20, 64.70, 55.21, 53.38, 40.22, 31.47, 30.89, 29.58, 24.83, 23.78, 22.52, 14.00; HRMS (ASAP$^+$), calcd for $C_{52}H_{53}N_3O_2$: 751.4138, found: 751.4161; Mp: 73.9 – 76.6 ^{o}C.

295, 3,4-Bis(benzyloxy)benzonitrile

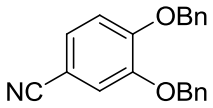

A mixture of 3,4-dihydroxybenzonitrile **294** (3.00 g, 0.022 mol), potassium carbonate (12.16 g, 0.088 mol) and benzyl bromide (6.53 cm^3, 0.055 mol) in anhydrous DMF (40 cm^3) was heated to 120 ^{o}C for 20 h. After cooling, the reaction mixture was poured onto water (100 cm^3) and extracted with diethyl ether (3 x 50 cm^3). The organic solvent was removed under reduced pressure. The crude solid was washed with hexane to yield **295** as a white solid (7.13 g, 100%). The NMR data were consistent with the literature.[56] ^{1}H NMR (400 MHz, $CDCl_3$) δ 7.47 – 7.30 (m, 10H), 7.22 (dd, *J* = 8.5, 2.0, Hz, 1H), 7.14 (d, *J* = 2.0 Hz, 1H), 6.94 (d, *J* = 8.5 Hz, 1H), 5.22 (s, 2H), 5.17 (s, 2H).

296, 5-(3,4-Bis(benzyloxy)phenyl)-1*H*-tetrazole

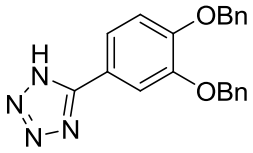

A mixture of 3,4-bis(benzyloxy)benzonitrile **295** (4.00 g, 0.013 mol), ammonium chloride (0.81 g, 0.015 mol) and sodium azide (0.99 g, 0.015 mol) in anhydrous DMF was heated to reflux for 20 h. The reaction mixture was cooled, poured onto an ice-water mixture and acidified to pH 2 with hydrochloric acid. The white precipitate was filtered and dried to yield the product **296** (3.26 g, 75%). The NMR data were consistent with the literature.[56] ^{1}H NMR (400 MHz, DMSO-d_6) δ 7.71 (d, *J* = 2.0 Hz, 1H), 7.58 (dd, *J* = 8.5, 2.0 Hz, 1H), 7.51 – 7.43 (m, 4H), 7.41 – 7.35 (m, 4H), 7.34 – 7.23 (m, 3H), 5.21 (s, 2H), 5.20 (s, 2H).

297, 2-(3,4-Bis(benzyloxy)phenyl)-5-(4-bromophenyl)-1,3,4-oxadiazole

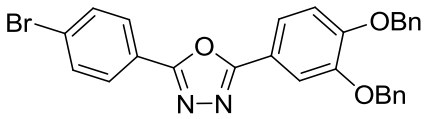

5-(3,4-Bis(benzyloxy)phenyl)-1*H*-tetrazole **296** (0.50 g, 1.4 mmol) was dissolved in anhydrous pyridine (20 cm^3). To this stirred solution 4-brombenzoyl chloride (0.46 g, 2.1 mmol) was added. The reaction was heated to reflux for 15 h, then poured onto water and extracted with ethyl acetate. The organic layer was separated, dried ($MgSO_4$) and evaporated. The crude product was purified by column chromatography on silica gel using 1 : 1 (v/v) dichloromethane : ethyl acetate as eluent to yield **297** as a white solid (0.18 g, 24%). ^{1}H NMR (600 MHz, $CDCl_3$) δ 7.97 (d, *J* = 8.5 Hz, 2H), 7.74 (d, *J* = 2.0 Hz, 1H), 7.70 – 7.62 (m, 3H), 7.50 (d, *J* = 7.5 Hz, 2H), 7.46 (d, *J* = 7.5 Hz, 2H), 7.41 – 7.36 (m, 4H), 7.36 – 7.30 (m, 2H), 7.04 (d, *J* = 8.5

Hz, 1H), 5.26 (s, 2H), 5.25 (s, 2H); ^{13}C NMR (151 MHz, $CDCl_3$) δ 164.59, 163.49, 152.06, 149.14, 136.60, 136.44, 132.37, 128.60, 128.56, 128.20, 128.05, 128.03, 127.42, 127.16, 126.21, 122.93, 120.95, 116.69, 114.29, 113.02, 71.41, 70.99; HRMS (ASAP+), calcd for $C_{52}H_{50}N_4O$: 746.3985, found: 746.3962; Mp: 159.9 – 162.0 ^{o}C.

298, 2-(3,4-Bis(benzyloxy)phenyl)-5-(4-(4,4,5,5-tetramethyl-1,3,2-dioxaborolan-2-yl)phenyl)-1,3,4-oxadiazole

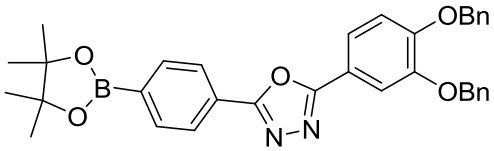

The general Miyaura borylation procedure was followed using the following quantities: 2-(3,4-bis(benzyloxy)phenyl)-5-(4-bromophenyl)-1,3,4-oxadiazole **297** (0.12 g, 0.22 mmol), B_2pin_2 (74 mg, 0.29 mmol), [$PdCl_2$(dppf)] (5 mg, 0.007 mmol) and KOAc (43 mg, 0.44 mmol). The crude product was purified by column chromatography on silica gel using 5 : 1 (v/v) dichloromethane : ethyl acetate as eluent to yield **298** as a white solid (0.42 g, 34%). ^{1}H NMR (400 MHz, $CDCl_3$) δ 8.10 (d, *J* = 8.5 Hz, 2H), 7.96 (d, *J* = 8.5 Hz, 2H), 7.76 (d, *J* = 2.0 Hz, 1H), 7.68 (dd, *J* = 8.5, 2.0 Hz, 1H), 7.55 – 7.50 (m, 2H), 7.49 – 7.44 (m, 2H), 7.43 – 7.36 (m, 4H), 7.37 – 7.30 (m, 2H), 7.05 (d, *J* = 8.5 Hz, 1H), 5.28 (s, 2H), 5.26 (s, 2H), 1.38 (s, 12H); ^{13}C NMR (101 MHz, $CDCl_3$) δ 192.02, 164.54, 164.25, 163.78, 151.99, 149.15, 136.69, 136.52, 135.28, 128.60, 128.57, 128.04, 128.03, 127.45, 127.19, 126.17, 125.86, 121.00, 116.94, 114.37, 113.12, 99.98, 84.23, 71.46, 71.04, 24.90; HRMS (ASAP$^+$) calcd for $C_{34}H_{34}BN_2O_5$: 560.2597. Found: 560.2581; Mp: 57.2 – 59.9 ^{o}C.

299, 7-(4-(5-(3,4-Bis(benzyloxy)phenyl)-1,3,4-oxadiazol-2-yl)phenyl)-9,9-dihexyl-*N*,*N*-diphenyl-9*H*-fluoren-2-amine

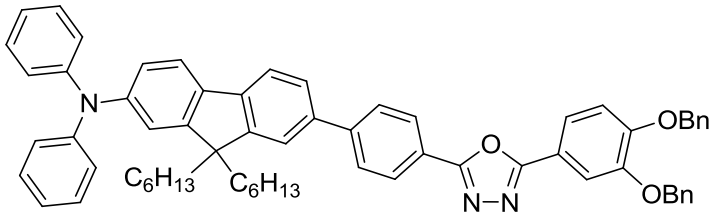

The standard Suzuki-Miyaura cross-coupling procedure was followed using the following quantities: 2-(3,4-bis(benzyloxy)phenyl)-5-(4-(4,4,5,5-tetramethyl-1,3,2-dioxaborolan-2-yl)phenyl)-1,3,4-oxadiazole **298** (0.20 g, 0.36 mmol), 7-bromo-9,9-dihexyl-*N*,*N*-diphenyl-9*H*-fluoren-2-amine **283** (0.23 g, 0.39 mmol), sodium hydroxide (36 mg, 0.9 mmol) in 5 cm^3 H_2O and [$PdCl_2(PPh_3)_2$] (13 mg, 0.02 mmol) in THF (10 cm^3). The crude product was purified by column chromatography on silica gel using dichloromethane and 5% ethyl acetate as eluent to yield **299** as a yellow solid (0.33 g, 98%). ^{1}H NMR (700 MHz, $CDCl_3$) δ 8.11 (d, *J* = 8.5 Hz, 2H), 7.74 (d, *J* = 8.5 Hz, 2H), 7.71 (d, *J* = 2.0 Hz, 1H),

7.64 – 7.61 (m, 2H), 7.54 (dd, *J* = 8.0, 1.5 Hz, 1H), 7.52 (d, *J* = 8.0 Hz, 1H), 7.49 (d, *J* = 1.5 Hz, 1H), 7.45 (d, *J* = 7.5 Hz, 2H), 7.40 (d, *J* = 7.5 Hz, 2H), 7.35 – 7.30 (m, 4H), 7.28 – 7.24 (m, 2H), 7.21 – 7.16 (m, 4H), 7.08 – 7.05 (m, 5H), 7.00 – 6.93 (m, 4H), 5.21 (s, 2H), 5.19 (s, 2H), 1.94 – 1.76 (m, 4H), 1.13 – 0.92 (m, 12H), 0.72 (t, *J* = 7.5 Hz, 6H), 0.69 – 0.57 (m, 4H); ^{13}C NMR (176 MHz, $CDCl_3$) δ 164.36, 164.21, 152.45, 151.90, 151.54, 149.12, 147.92, 147.44, 144.82, 141.20, 137.72, 136.66, 136.50, 135.51, 129.15, 128.59, 128.56, 128.02, 127.54, 127.45, 127.24, 127.16, 126.07, 123.87, 123.47, 122.56, 122.36, 121.18, 120.89, 120.58, 119.49, 119.21, 117.02, 114.33, 113.03, 71.40, 71.00, 55.21, 40.23, 31.48, 29.59, 23.78, 22.52, 14.00; HRMS (ASAP$^+$), calcd for $C_{65}H_{63}N_3O_3$: 934.4948, Found: 934.4962; Mp: 67.2 – 70.5 ^{o}C.

300a, 4-(1*H*-Tetrazol-5-yl)benzoic acid

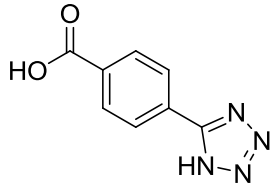

4-Cyanobenzoyl chloride (3.00 g, 20 mmol) was dissolved in DMF (30 cm^3) and ammonium chloride (1.31 g, 24 mmol) and sodium azide (1.59 g, 24 mmol) were added. The reaction mixture was heated to reflux and stirred for 72 h. The mixture was cooled and poured onto an ice and water mixture and acidified to pH 2 with HCl. The precipitate was filtered and dried. The product **300** was isolated as a white solid (3.46 g, 91%). The NMR data were consistent with the literature.[150] ^{1}H NMR (400 MHz, DMSO) δ 13.30 (s, 1H), 8.25 – 8.09 (m, 4H). MS (ASAP$^+$) 190 (20%, M^+), 162 (60), 145 (100).

300b, Ethyl 4-(1*H*-tetrazol-5-yl)benzoate

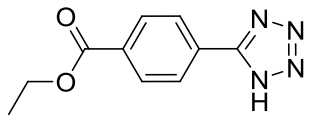

4-Cyanobenzoic acid (3.12 g, 21 mmol) was dissolved in a 1:1 mixture of dichloromethane : ethanol (60 cm^3) and cooled to 0 ^{o}C in an ice bath. To this stirred solution DMAP (2.82 g, 23 mmol) and DCC (4.77 g, 23 mmol) were added. The reaction mixture was stirred for 3 h after which time the solvent was removed under reduced pressure. The crude product was purified by column chromatography on silica gel using dichloromethane as eluent to yield Ethyl 4-cyanobenzoate as a white solid (3.10 g, 84%). The NMR data were consistent with the literature.[151] ^{1}H NMR (400 MHz, $CDCl_3$) 8.14 (d, *J* = 8.0 Hz, 2H), 7.74 (d, *J* = 8.0 Hz, 2H), 4.41 (q, *J* = 7.0 Hz, 2H), 1.41 (t, *J* = 7.0 Hz, 3H); ^{13}C NMR (101 MHz, $CDCl_3$) δ 164.96, 134.30, 132.19, 130.07, 118.03, 116.28, 61.82, 14.24.Ethyl 4-cyanobenzoate (3.00 g, 0.017 mol), sodium azide (1.34 g, 0.021 mol) and ammonium chloride (1.12 g, 0.021 mol) were dissolved in anhydrous DMF (40 cm^3) and heated to reflux for 2 h. After which time the reaction mixture was cooled, poured onto water and

acidified to pH 2 with dilute HCl to precipitate **300b** as a white solid (3.50 g, 94%). The NMR data were consistent with the literature.[151] ^{1}H NMR ($CDCl_3$), δ (ppm): 8.26–8.24 (d, *J* = 8.0 Hz, 2H), 8.22–8.20 (d, *J* = 8.0 Hz, 2H), 4.47–4.41 (q, *J* = 7.0 Hz, 2H), 1.45–1.42 (t, *J* = 7.0 Hz, 3H).

304, *N*'-Benzoyl-4-cyanobenzohydrazide

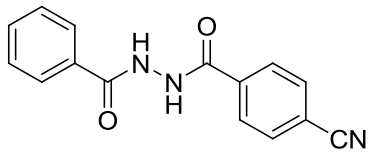

Benzohydrazide **303** (0.17 g, 1.10 mmol), 4-cyanobenzoic acid **302** (0.17 g, 1.1 mmol) and TBTU (0.36 g, 1.10 mmol) were dissolved in anhydrous THF (10 cm^3). To this stirred solution DIPEA (0.39 cm^3, 2.20 mmol) was added. The reaction mixture was stirred at room temperature for 45 min under an atmosphere of argon. After this time the reaction mixture was poured onto brine (100 cm^3), and extracted with ethyl acetate. The organic extracts were combined and the solvent removed under reduced pressure. The crude product was purified by column chromatography on silica gel using ethyl acetate as eluent to yield **304** as a white solid (0.16 g, 56%); ^{1}H NMR (400 MHz, $CDCl_3$) δ 8.25 – 8.17 (m, 2H), 8.09 (dd, *J* = 8.0, 1.5 Hz, 2H), 7.82 – 7.74 (m, 2H), 7.58 – 7.44 (m, 3H); ^{13}C NMR (101 MHz, $CDCl_3$) δ 164.38, 162.06, 131.91, 131.27, 128.24, 126.81, 126.35, 126.13, 122.40, 116.91, 114.19; HRMS (ASAP$^+$) calcd for $C_{15}H_{12}N_3O_2$: 266.0930. Found: 266.0910; Mp: 190.5 – 192.7 ^{o}C.

305, 4-(5-Phenyl-1,3,4-oxadiazol-2-yl)benzonitrile

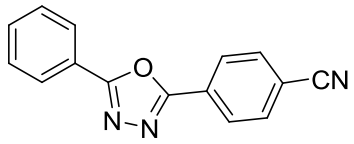

N'-Benzoyl-4-cyanobenzohydrazide **304** (0.16 g, 0.62 mmol) and phosphorus oxychloride (5 cm^3) were heated to reflux for 15 h. After this time the reaction mixture was cooled and the phosphorous oxychloride was removed under reduced pressure. The crude product was purified by column chromatography on silica gel using petroleum ether (b.p. 40 – 60 ^{o}C) with 20% ethyl acetate as eluent to yield **305** as a white solid (0.12 g, 79%). The NMR data were consistent with the literature.[152] ^{1}H NMR (400 MHz, $CDCl_3$) δ 8.27 (d, *J* = 8.5 Hz, 2H), 8.16 (dd, *J* = 8.0, 1.5 Hz, 2H), 7.89 – 7.83 (m, 2H), 7.64 – 7.51 (m, 3H).

307, 4-(5-(4-Bromophenyl)-1,3,4-oxadiazol-2-yl)benzonitrile

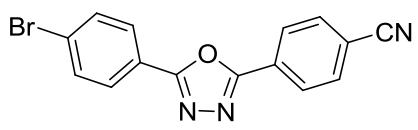

To a stirred solution of 4-cyanobenzoic acid (2.00 g, 0.014 mol), 4-bromobenzohydrazide (2.90 g, 0.014 mol) and TBTU (4.50 g, 0.014 mol) DIPEA (2.44 cm^3, 0.014 mol) were added. The reaction mixture was stirred at room temperature for 24 h. After this time it was poured onto water and extracted with ethyl acetate. The combined organic extracts were

washed with saturated $NaHCO_3$ solution and then 1 M $NaHSO_4$ solution. The solvent was removed from the organic layers under reduced pressure. The crude 4-bromo-*N*'-(4-cyanobenzoyl)benzohydrazide was dissolved in $POCl_3$ and heated to reflux for 12 h. The excess $POCl_3$ was then removed by distillation and the crude product purified by column chromatography on silica gel using chloroform as eluent to yield **307** as a white solid (0.71 g, 16%). ^{1}H NMR (400 MHz, $CDCl_3$): δ 8.20 (d, *J* = 8.5 Hz, 2H), 7.95 (d, *J* = 9.0 Hz, 2H), 7.84 – 7.75 (d, 8.5 Hz, 2H), 7.64 (d, *J* = 9.0 Hz, 2H); ^{13}C NMR (101 MHz, $CDCl_3$): δ 164.68, 163.21, 132.92, 132.62, 128.47, 127.59, 127.38, 127.09, 122.28, 117.82, 115.38; (HRMS ASAP$^+$) calcd for $C_{18}H_8{}^{79}BrN_3O$: 324.9851, Found: 324.9851; Mp: 220.3-221.8 ^{o}C.

308, 4-(5-(4-(4,4,5,5-Tetramethyl-1,3,2-dioxaborolan-2-yl)phenyl)-1,3,4-oxadiazol-2-yl)benzonitrile

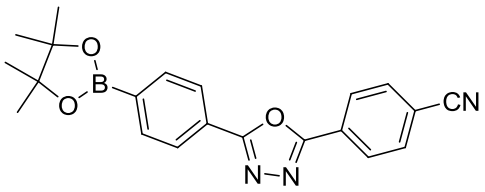

The standard Miyaura borylation procedure was followed using the following quantities: 4-(5-(4-bromophenyl)-1,3,4-oxadiazol-2-yl)benzonitrile **307** (0.30 g, 0.92 mmol), B_2pin_2 (0.30 g, 1.20 mmol), [$PdCl_2$(dppf)] (20 mg, 0.03 mmol), KOAc (0.23 g, 2.3 mmol) and DMF (10 cm^3). The crude product was purified by column chromatography on silica gel using 1 : 1 (v/v) petroleum ether : DCM as eluent to yield **308** as a white solid (0.18 g, 51%). ^{1}H NMR (400 MHz, $CDCl_3$) δ 8.28 (d, *J* = 8.5 Hz, 2H), 8.13 (d, *J* = 8.5 Hz, 2H), 7.97 (d, *J* = 8.5 Hz, 2H), 7.84 (d, *J* = 8.5 Hz, 2H), 1.38 (s, 12H); ^{13}C NMR (101 MHz, $CDCl_3$) δ 165.40, 163.15, 135.42, 132.87, 127.77, 127.40, 126.12, 125.46, 117.88, 115.23, 84.32, 25.02, 24.90. HRMS (ASAP$^+$), calcd for $C_{21}H_{21}{}^{10}BN_3O_2$: 374.1753, Found: 374.1791; Mp: 241.9 – 243.8 ^{o}C.

280, 4-(5-(4-(7-(Diphenylamino)-9,9-dihexyl-9*H*-fluoren-2-yl)phenyl)-1,3,4-oxadiazol-2-yl)benzonitrile

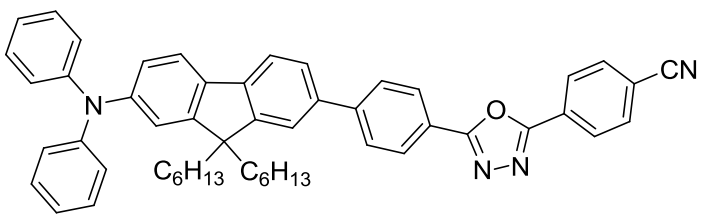

The general Suzuki-Miyaura cross-coupling procedure was followed using the following quantities: 4-(5-(4-(4,4,5,5-tetramethyl-1,3,2-dioxaborolan-2-yl)phenyl)-1,3,4-oxadiazol-2-yl)benzonitrile **308** (0.28 g, 0.75 mmol), 7-bromo-9,9-dihexyl-*N*,*N*-diphenyl-9*H*-fluoren-2-amine **283** (0.48 g, 0.83 mmol), [$PdCl_2(PPh_3)_2$] (25 mg, 0.04 mmol), NaOH (0.08 g in 5 cm^3 H_2O) and THF (10 cm^3). The crude product was purified by column

chromatography on silica gel using 7 : 3 (v/v) petroleum ether : diethyl ether to 1 : 1 (v/v) petroleum ether : diethyl ether as eluent to yield **280** as a yellow solid (0.25 g, 45%). ^{1}H NMR (600 MHz, $CDCl_3$) δ 8.29 (d, *J* = 8.0 Hz, 2H), 8.22 (d, *J* = 8.0 Hz, 2H), 7.84 (t, *J* = 7.5 Hz, 4H), 7.69 (d, *J* = 7.5 Hz, 1H), 7.64 – 7.52 (m, 3H), 7.29 – 7.20 (m, 4H), 7.13 (d, *J* = 7.0 Hz, 5H), 7.02 (m, 3H), 2.00 – 1.80 (m, 4H), 1.19 – 0.94 (m, 12H), 0.78 (t, *J* = 7.0 Hz, 6H), 0.76 – 0.59 (m, 4H); ^{13}C NMR (151 MHz, $CDCl_3$) δ 165.38, 162.98, 152.46, 151.60, 147.89, 147.54, 145.54, 141.42, 137.44, 135.38, 132.87, 129.17, 127.85, 127.69, 127.52, 127.33, 126.12, 123.91, 123.43, 122.61, 121.64, 121.17, 120.63, 119.53, 119.14, 117.90, 115.12, 55.22, 40.22, 31.48, 29.59, 23.78, 22.52, 14.01; HRMS (ASAP^{+}), calcd for $C_{52}H_{50}N_4O$: 746.3985, found: 746.3962; Mp: 167.9 – 168.7 ^{o}C.

281, 4-(5-(4-(7-(Diphenylamino)-9,9-dihexyl-9*H*-fluoren-2-yl)phenyl)-1,3,4-oxadiazol-2-yl)benzoic acid

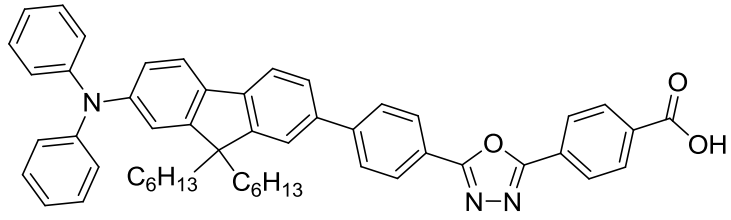

A mixture of 4-(5-(4-(7-(diphenylamino)-9,9-dihexyl-9*H*-fluoren-2-yl)phenyl)-1,3,4-oxadiazol-2-yl)benzonitrile **280** (0.065 mg, 0.09 mmol) and potassium hydroxide (0.13 g, 2.3 mmol) in 3 : 1 ethanol : water solution (10 cm^3) was heated to reflux for 15 h. After this time, when all the solid had dissolved, the pH was altered to pH 3 with dilute hydrochloric acid. The resulting precipitate was filtered, dissolved in dichloromethane and washed with $NaHCO_3$ solution. The organic extracts were combined and the solvent removed under reduced pressure. The crude product was purified by column chromatography on silica gel using dichloromethane and then with dichloromethane and 5% acetic acid as eluent to yield **281** as a yellow solid (38 mg, 57%). ^{1}H NMR (600 MHz, acetone-d_6) δ 8.16 (d, *J* = 8.0 Hz, 2H), 8.10 (d, *J* = 7.0 Hz, 4H), 7.89 (d, *J* = 8.0 Hz, 2H), 7.83 (d, *J* = 7.5 Hz, 2H), 7.76 (d, *J* = 8.0 Hz, 1H), 7.73 (d, *J* = 8.0 Hz, 1H), 7.32 – 7.26 (m, 4H), 7.20 (d, *J* = 2.0 Hz, 1H), 7.13 – 7.07 (m, 4H), 7.07 – 7.00 (m, 3H), 2.18 – 1.88 (m, 4H), 1.18 – 1.04 (m, 12H), 0.77 (t, *J* = 7.0 Hz, 6H), 0.72 (s, 4H); ^{13}C NMR (151 MHz, acetone-d_6) δ 170.96, 166.02, 165.71, 165.43, 152.46, 151.49, 148.00, 147.54, 144.73, 141.13, 137.96, 136.85, 135.92, 133.55, 131.24, 129.68, 129.25, 128.09, 127.61, 126.82, 126.12, 123.71, 123.50, 122.70, 121.33, 120.81, 119.65, 119.30, 55.18, 39.86, 31.30, 23.70, 22.23, 19.51, 13.34; HRMS (ASAP^{+}), calc for $C_{52}H_{52}N_3O_3$: 766.4009, Found: 766.4023; Mp: 129.7 – 132.1 ^{o}C.

309, 4-(5-(4-(7-(Diphenylamino)-9,9-dihexyl-9*H*-fluoren-2-yl)phenyl)-1,3,4-oxadiazol-2-yl)benzaldehyde

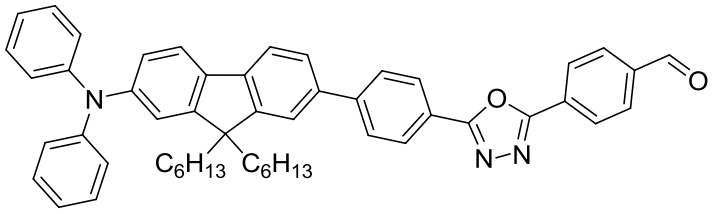

To a solution of (4-(5-(4-(7-(diphenylamino)-9,9-dihexyl-9*H*-fluoren-2-yl)phenyl)-1,3,4-oxadiazol-2-yl)phenyl)methanol **272** (0.15 g, 0.20 mmol) in dichloromethane (5 cm^3) pyridinium chlorochromate (51 mg, 0.24 mmol) in dichloromethane (5 cm^3) was added dropwise. The resulting mixture was stirred at room temperature for 1 h. After this time the reaction mixture was filtered through a Celite plug. The crude product was then purified by column chromatography on silica gel using 1 : 1 (v/v) petroleum ether : diethyl ether as eluent to yield **309** as a yellow solid (89 mg, 60%). ^{1}H NMR (500 MHz, $CDCl_3$) δ 10.08 (s, 1H), 8.31 (d, *J* = 8.0 Hz, 2H), 8.20 (d, *J* = 8.5 Hz, 2H), 8.03 (d, *J* = 8.5 Hz, 2H), 7.80 (d, *J* = 8.5 Hz, 2H), 7.66 (d, *J* = 8.0 Hz, 1H), 7.60 – 7.51 (m, 3H), 7.26 – 7.18 (m, 4H), 7.12 – 7.05 (m, 5H), 7.04 – 6.94 (m, 3H), 1.97 – 1.76 (m, 4H), 1.15 – 0.96 (m, 12H), 0.75 (t, *J* = 7.0 Hz, 6H), 0.72 – 0.62 (m, 4H); ^{13}C NMR (126 MHz, $CDCl_3$) δ 191.46, 165.53, 163.81, 152.72, 151.85, 148.16, 147.77, 145.66, 141.63, 138.42, 137.77, 135.68, 130.51, 129.43, 129.23, 127.93, 127.77, 127.70, 126.38, 124.16, 123.70, 122.86, 122.07, 121.44, 120.89, 119.79, 119.42, 55.48, 40.49, 31.74, 29.85, 24.05, 22.79, 14.28, HRMS ($ASAP^+$), calc for $C_{52}H_{51}N_3O_2$: 749.3981, Found: 749.3961; Mp: 148.3 – 149.9 ^oC.

282, (*E*)-2-Cyano-3-(4-(5-(4-(7-(diphenylamino)-9,9-dihexyl-9*H*-fluoren-2-yl)phenyl)-1,3,4-oxadiazol-2-yl)phenyl)acrylic acid

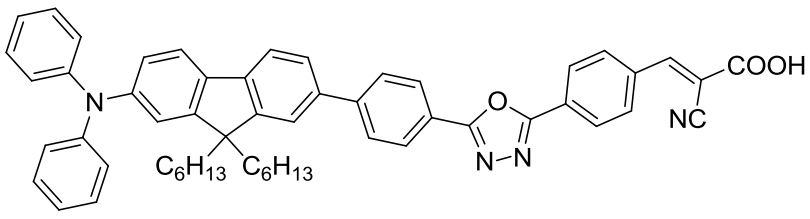

To a solution of 4-(5-(4-(7-(diphenylamino)-9,9-dihexyl-9*H*-fluoren-2-yl)phenyl)-1,3,4-oxadiazol-2-yl)benzaldehyde **309** (46 mg, 0.061 mmol) and ammonium acetate (1 mg, 0.012 mmol) in acetic acid (2 cm^3) was added cyanoacetic acid (15 mg, 0.18 mmol). This stirred mixture was heated to reflux for 15 h after which time it was cooled, poured onto water and filtered. The crude solid was dissolved in dichloromethane and washed with water. The solvent was removed from the combined organic extracts and the crude product purified by column chromatography using dichloromethane – dichloromethane with 20% methanol as eluent to

yield **282** as a yellow solid (25 mg, 50%). ^{1}H NMR (400 MHz, CD_3OD/CS_2): δ 8.27 (m, 4H), 8.20 – 8.12 (m, 3H), 7.96 – 7.87 (m, 2H), 7.74 (d, *J* = 8.5 Hz, 1H), 7.70 – 7.59 (m, 3H), 7.31 – 7.19 (m, 4H), 7.16 – 7.07 (m, 5H), 7.03 (m, 3H), 2.12 – 1.85 (m, 4H), 1.14 (m, 3H), 0.87 – 0.78 (m, 6H), 0.73 (s, 4H); ^{13}C NMR (126 MHz, $CDCl_3$): δ 177.62, 152.67, 151.68, 150.91, 148.14, 147.60, 141.31, 135.68, 129.37, 127.55, 126.38, 124.11, 122.78, 120.87, 119.77, 119.40, 55.42, 40.40, 31.63, 29.93, 29.75, 24.03, 22.68, 14.22; HRMS (ES^+), calc for $C_{55}H_{52}N_4O_3$: 816.4039, Found: 816.4042; IR (THF solution) cm^{-1}; 3372 (O-H), 3502 (O-H), 2217 (C≡N), 1641 (C=O), 1596 (C=N); Mp: 119.3 – 120.0 ^{o}C.

Appendix I: Additional CV scans, absorption and emission spectra for OLED candidates from chapter 2

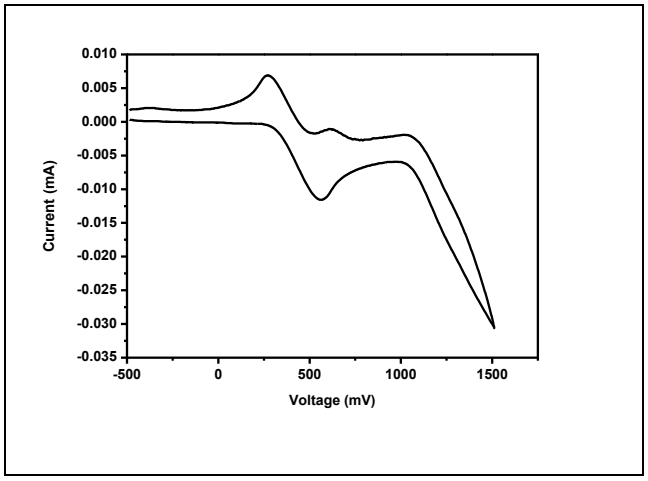

Figure I.I – Cyclic voltammogram showing oxidation waves for **91** in DCM vs ferrocenium/ferrocene couple (FcH^+/FcH = 0.0 V).

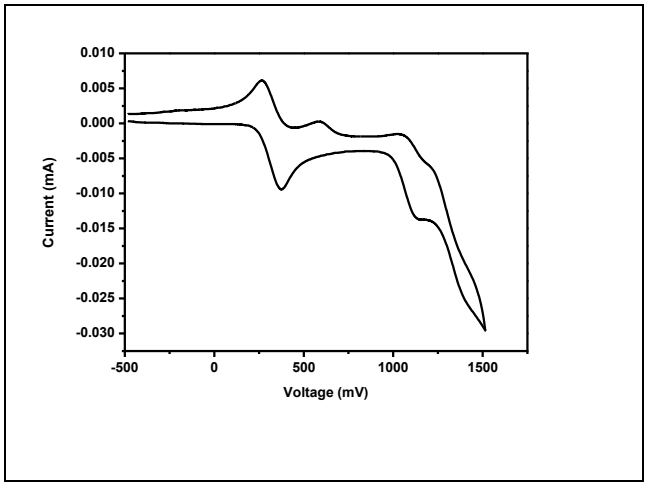

Figure I.II – Cyclic voltammogram showing oxidation waves for **134** in DCM vs ferrocenium/ferrocene couple (FcH^+/FcH = 0.0 V).

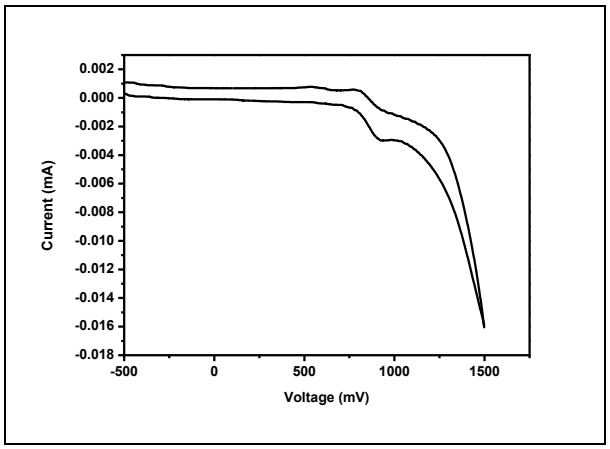

Figure I.III – Cyclic voltammogram showing oxidation waves for **140** in DCM vs ferrocenium/ferrocene couple (FcH^+/FcH = 0.0 V).

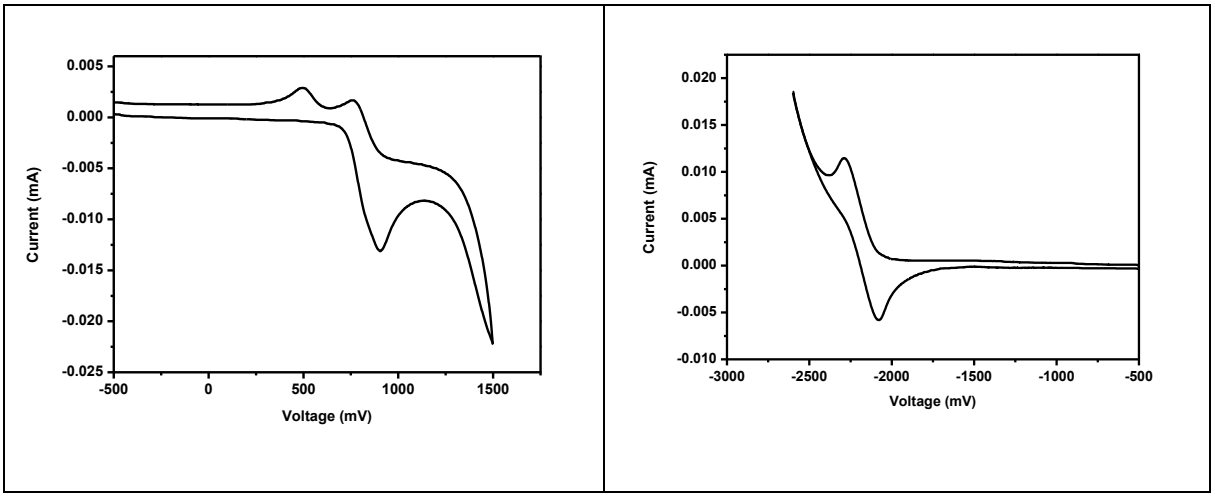

Figure I.IV – Cyclic voltammograms showing oxidation (left: in DCM) and reduction (right: in THF) waves for **156** vs ferrocenium/ferrocene couple (FcH^+/FcH = 0.0 V).

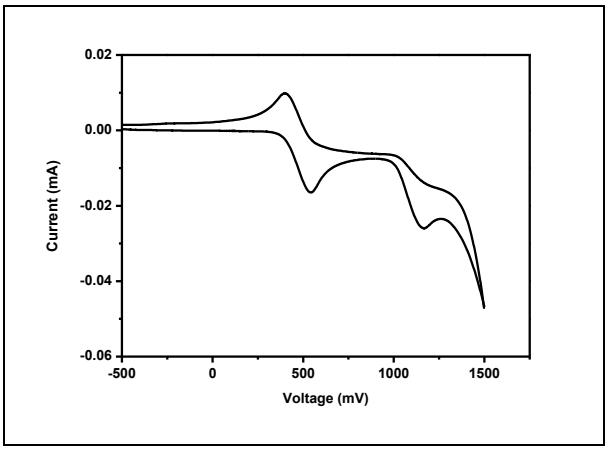

Figure I.V – Cyclic voltammogram showing oxidation waves for **161** in DCM vs ferrocenium/ferrocene couple (FcH^+/FcH = 0.0 V).

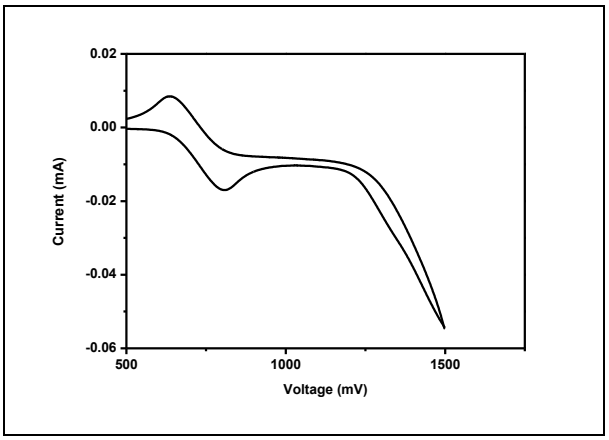

Figure I.VI – Cyclic voltammogram showing oxidation waves for **162** in DCM vs ferrocenium/ferrocene couple (FcH^+/FcH = 0.0 V).

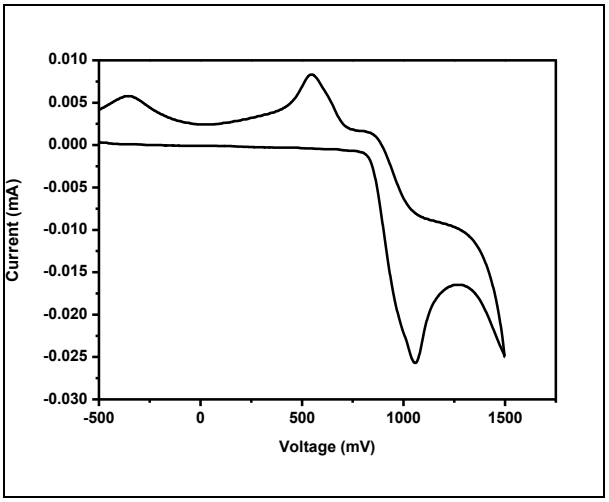

Figure I.VII – Cyclic voltammogram showing oxidation waves for **163** in DCM vs ferrocenium/ferrocene couple (FcH^+/FcH = 0.0 V).

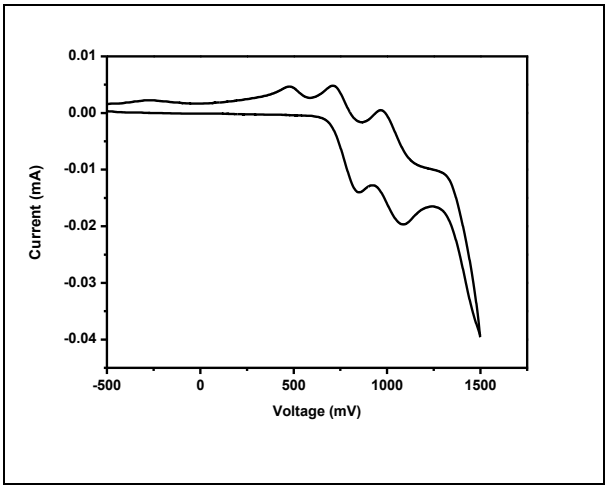

Figure I.VIII – Cyclic voltammogram showing oxidation waves for **165** in DCM vs ferrocenium/ferrocene couple (FcH^+/FcH = 0.0 V).

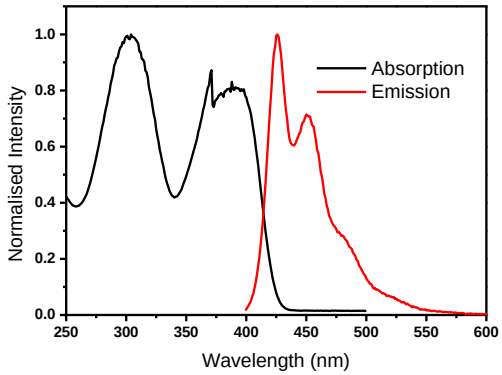

Figure I.IX – Plot of absorption and emission of **91** in cyclohexane solution with emission excitation at 388 nm

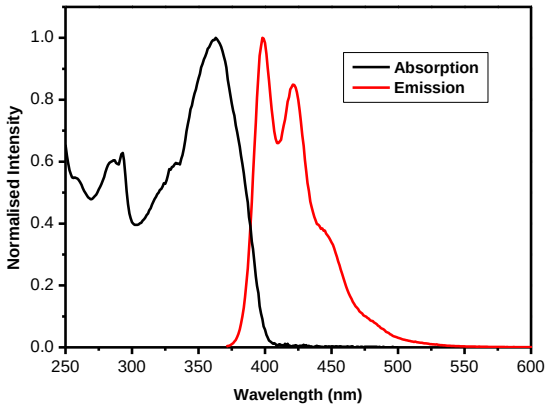

Figure I.X – Absorption and emission spectra of **156** in cyclohexane solution with emission excitation at 363 nm.

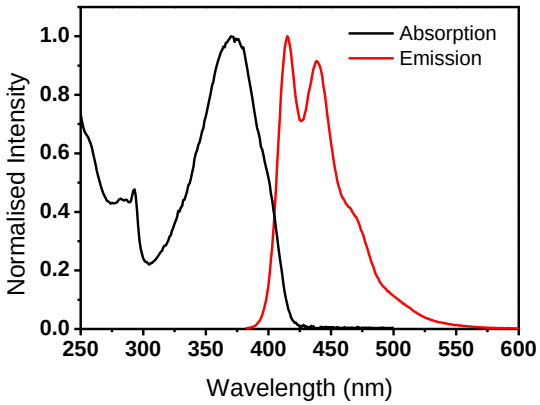

Figure I.XI – Absorption and emission spectra of **157** in cyclohexane solution with emission excitation at 371 nm.

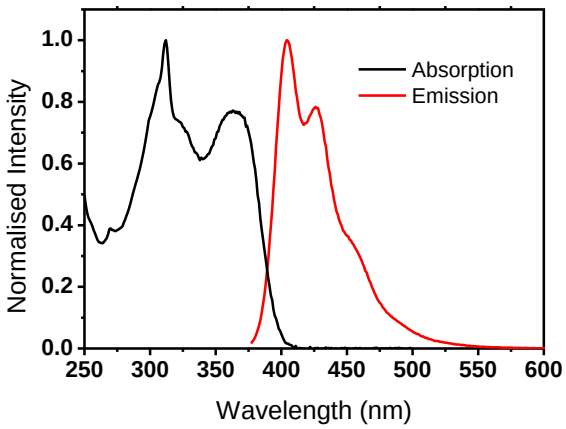

Figure I.XII – Absorption and emission spectra of **161** in cyclohexane solution with emission excitation at 364 nm.

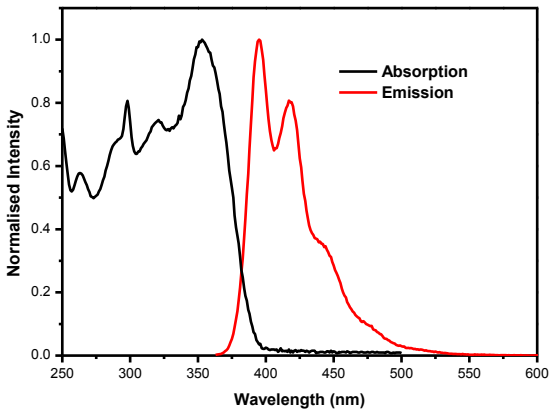

Figure I.XIII – Absorption and emission spectra of **162** in cyclohexane solution with emission excitation at 339 nm.

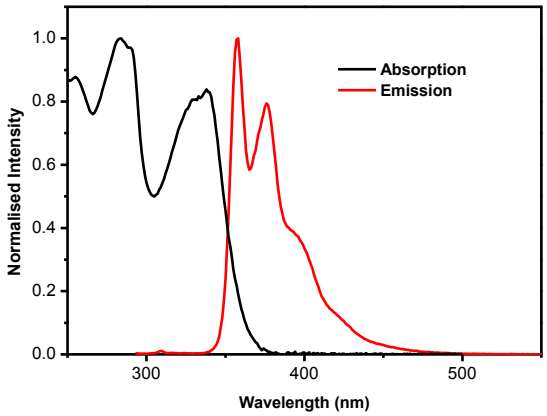

Figure I.XIV – Absorption and emission spectra of **163** in cyclohexane solution with emission excitation at 339 nm.

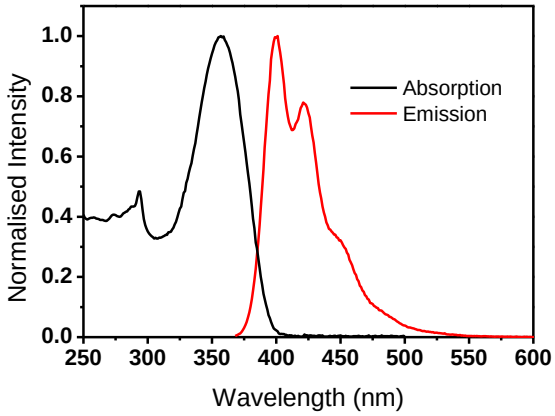

Figure I.XV – Absorption and emission spectra of **165** in cyclohexane solution with excitation at 357 nm.

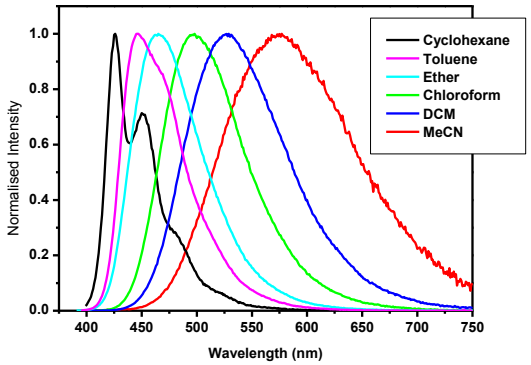

Figure I.XVI – Emission spectra of **134** various solvents

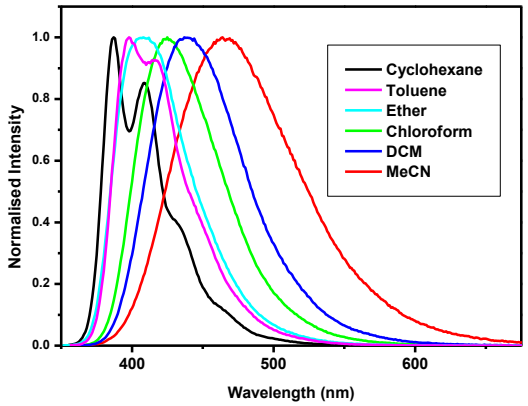

Figure I.XVII – Emission spectra of **140** in various solvents

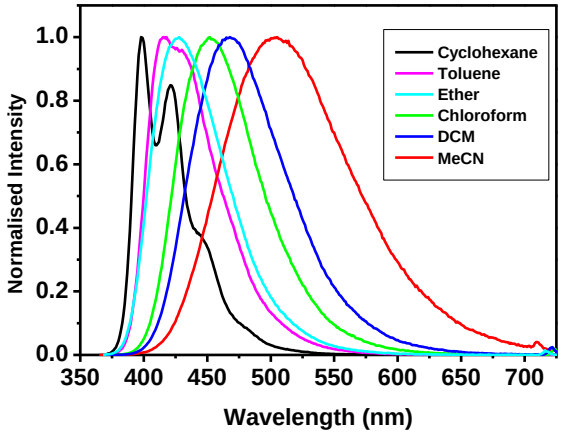

Figure I.XVIII – Emission spectra of **156** in various solvents.

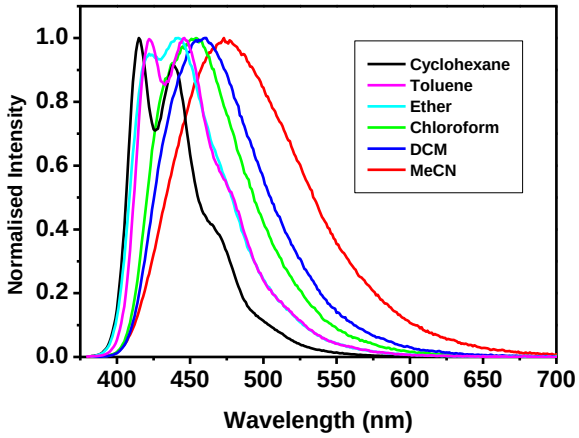

Figure I.XIX – Emission spectra of **157** in various solvents.

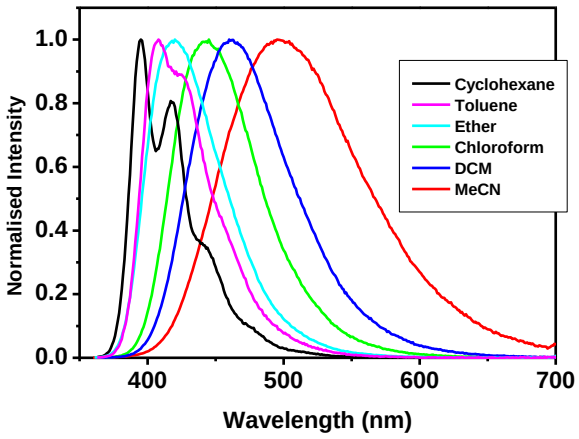

Figure I.XX – Emission spectra of **162** in various solvents.

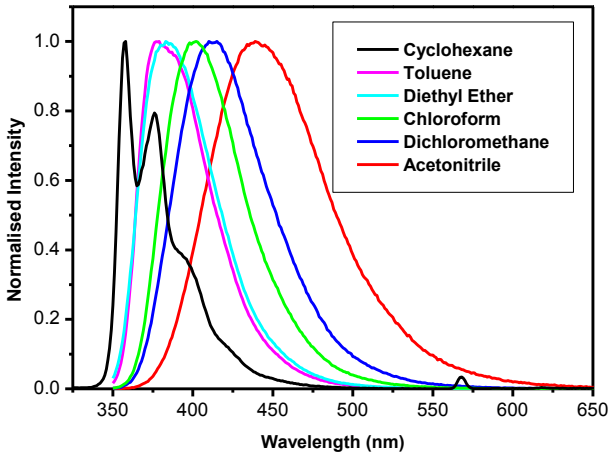

Figure I.XXI – Emission spectra of **163** in various solvents.

Appendix II: Additional absorption and emission spectra and CV scans for molecular wire candidates in chapter 4

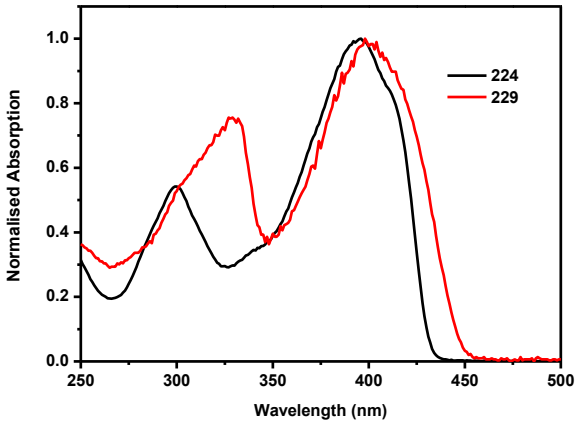

Figure II.I – Normalised absorption spectra

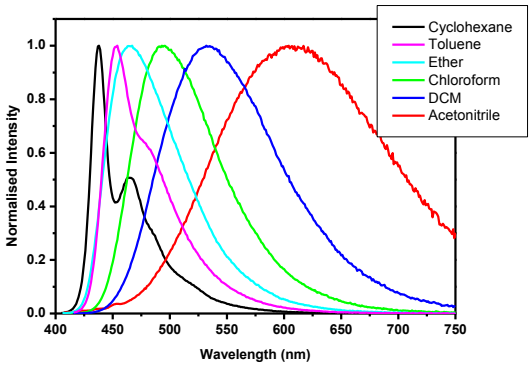

in cyclohexane solution for **224** and **229**

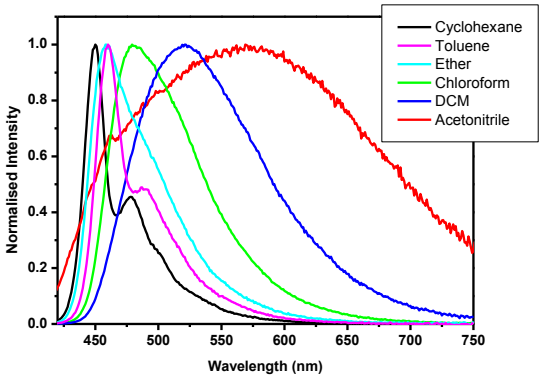

Figure II.II – Normalised emission spectra for **203** (left) and **204** (right) in various solvents

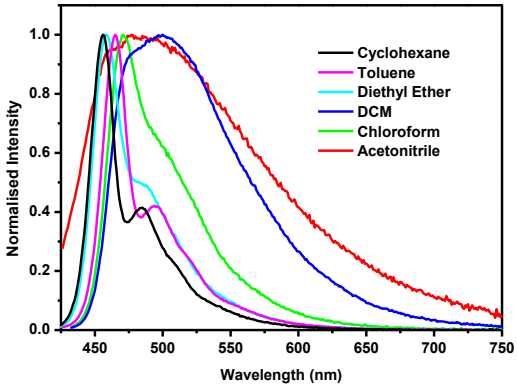

Figure II.III – Normalised emission spectra for **205** in various solvents

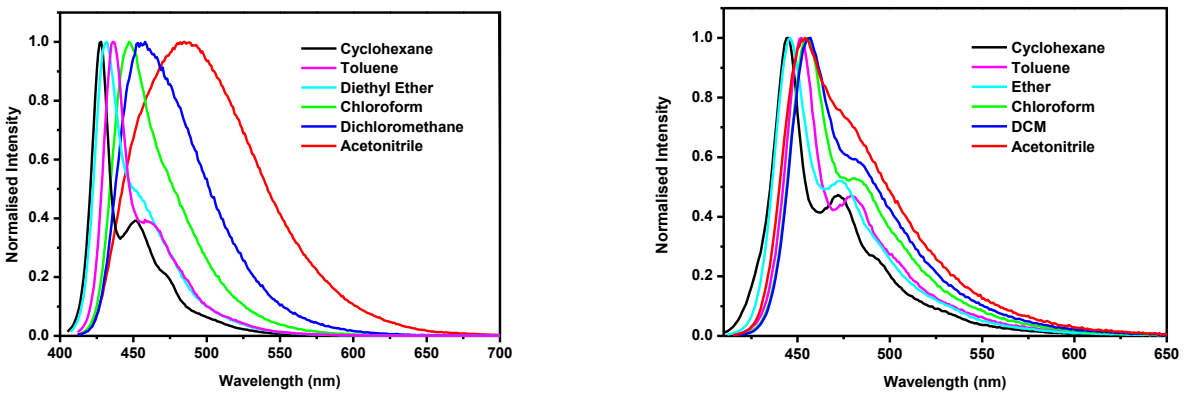

Figure II.IV – Normalised emission spectra for **224** (left) and **229** (right) in various solvents

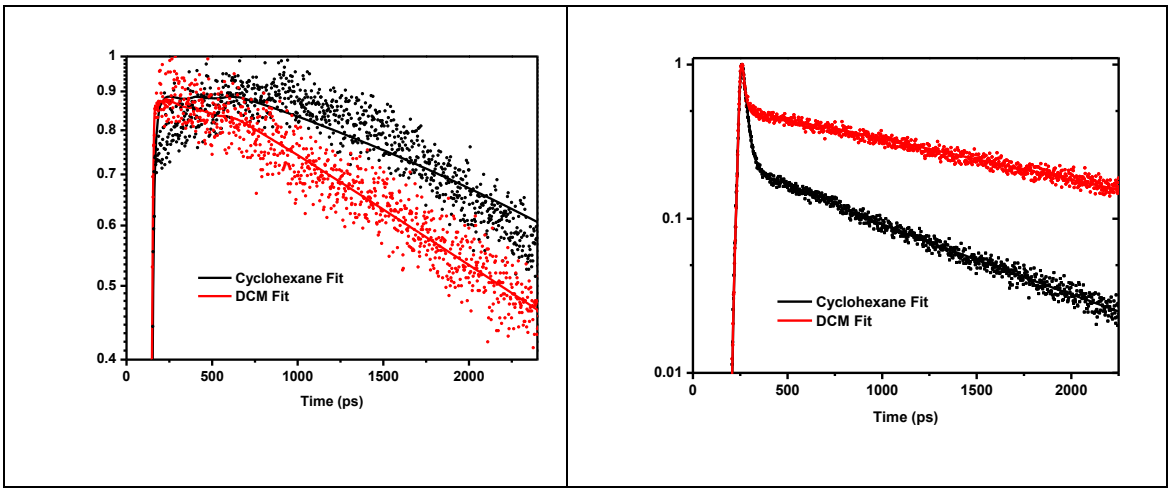

Figure II.V - Luminescence decays recorded at the emission onset of compounds 202 (left) and 204 (right) in cyclohexane and DCM (excitation wavelength: 385 nm)

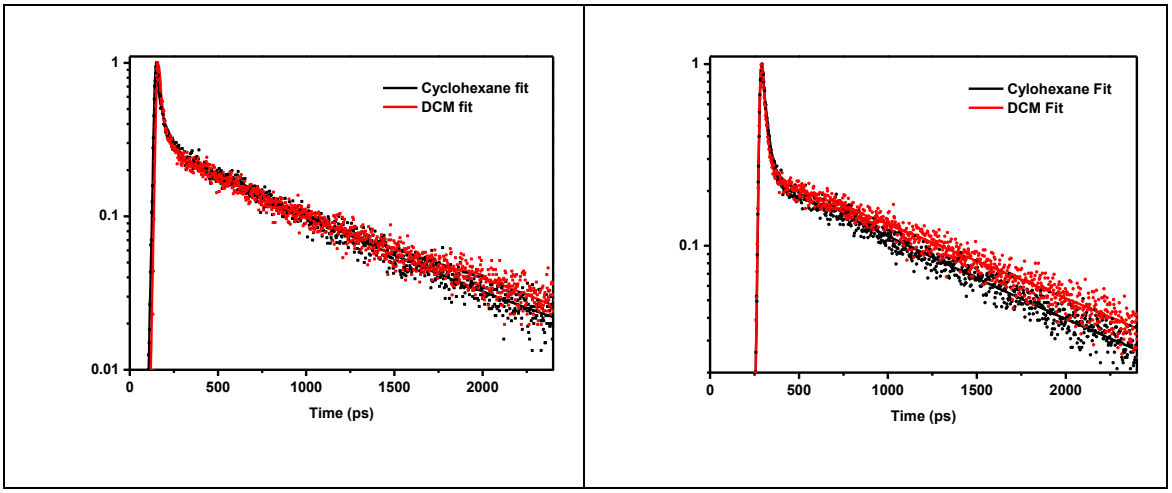

Figure II.VI – Luminescence decays recorded at the emission onset of the compounds 206 (left) and 229 (right) in cyclohexane and DCM (excitation wavelength: 385 nm)

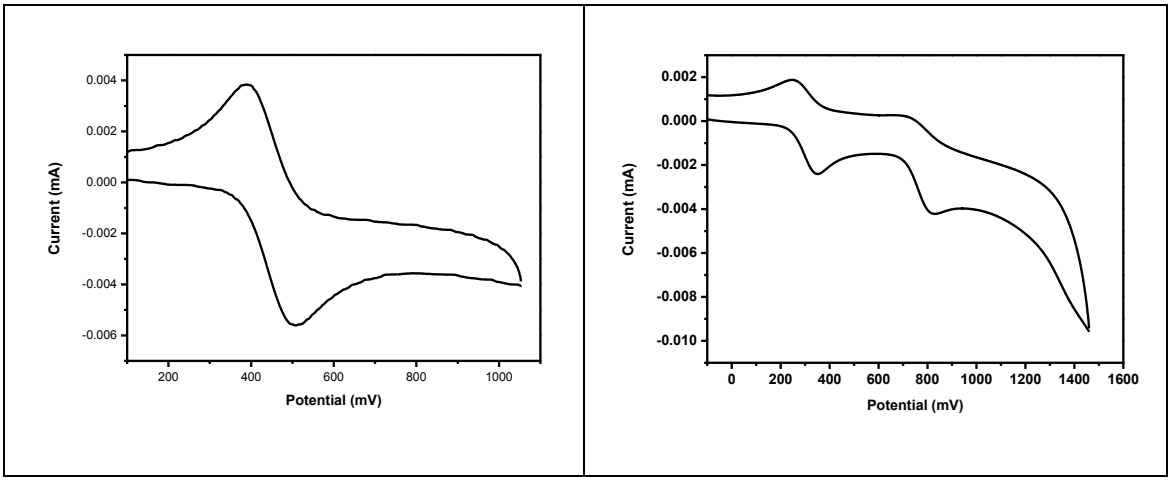

Figure II.VII – Cyclic voltammogram showing oxidation waves for **202** (left) and **203** (right) in DCM vs ferrocenium/ferrocene couple (FcH^+/FcH = 0.0 V).

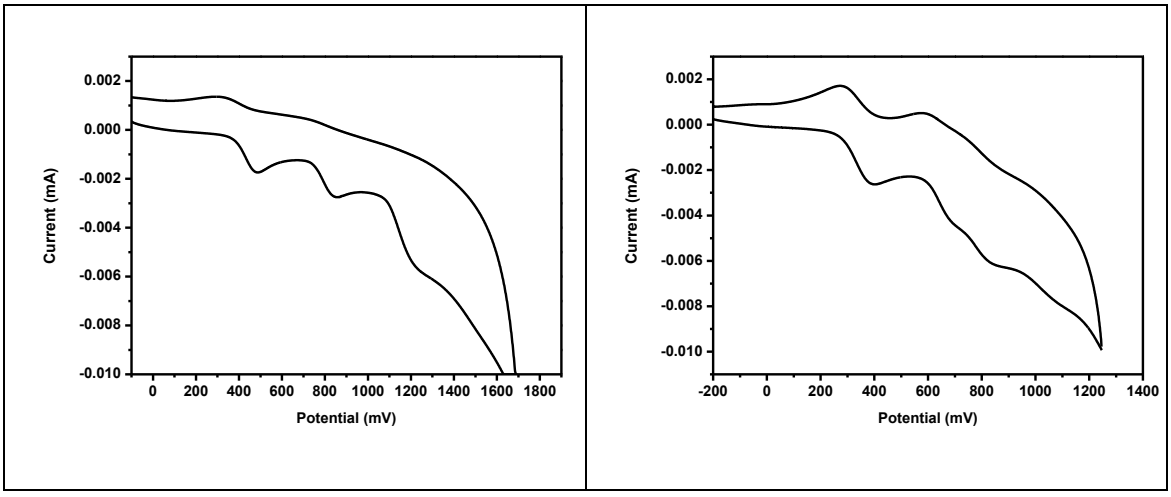

Figure II.VIII – Cyclic voltammogram showing oxidation waves for **204** (left) and **206** (right) in DCM vs ferrocenium/ferrocene couple (FcH^+/FcH = 0.0 V).

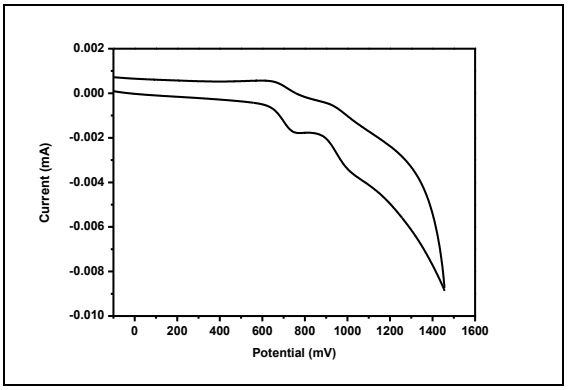

Figure II.IX – Cyclic voltammogram showing oxidation waves for **229** in DCM vs ferrocenium/ferrocene couple (FcH^+/FcH = 0.0 V).

Appendix III: List of Seminars Attended

- 02/03/10: Paul Burn, University of Queensland, “In search of deep blue phosphorescence”
- 04/04/10: Roy Jackson, Monash University, “Metathesis chemistry in organic synthesis”
- 11/03/10: Frieder Jäkle, Rutgers, “Organoborane functionalised conjugated polymers as optoelectronic sensory materials”
- 12/05/10: Dan Nocera, MIT, “Personalised energy for 1 (x 6 billion)”
- 28/09/10: Lars Pålsson, University of Durham, “Time resolved optical spectroscopy”
- 28/09/10: Claude Lapinte, University of Rennes, “Molecular organometallic wires”
- 10/11/10: Martyn Twigg, Johnson Matthey, “Controlling emissions from cars – Chemistry, success and challenges”
- 12/11/10: Michael Bendikov, Welzmann Institute of Science, Israel, “Novel organic electronic materials”
- 23/02/11: Laura Herz, University of Oxford, “Ultraphotoexcitation dynamics in organic/inorganic hybrid materials”
- 27/04/11: Rick Cosstick, University of Liverpool, “Using chemically modified nucleosides to solve biological problems”
- 03/05/11: Michael Willis, University of Oxford, “New reactivity and selectivity in rhodium and palladium catalysts”
- 11/05/11: Peter Skabara, University of Strathclyde, “Complex conjugated architectures – from synthesis through to device applications”
- 11/05/11: Carmen Nicasio, University of Seville, “Carbon-heteroatom bond forming reactions catalysed by copper and nickel complexes”
- 13/05/11: Henri Doucet, University of Rennes, “Palladium catalysed arylations or alkenylations of heteroaromatics *via* C-H bond activation”
- 18/05/11: Randy Thummel, University of Houston, “Designing heterocyclic ligands to help capture the sun”
- 21/06/11: Jacob Israelachvilli, University of California, Santa Barbara, “The search for the hydrophobic interaction potential”

- 12/09/11: Chihaya Adachi, Kyushu University, “A new concept for light emitting materials and devices”
- 09/11/11: Leone Spiccia, Monash University, “Harvesting solar energy in photoelectrochemical solar cells”
- 14/11/11: Jonathon Sessler, University of Texas, “Recent advances in calixpyrrole chemistry”
- 18/11/11: Hon Wai Lam, University of Edinburgh, “Hetero(arenes) as activating groups in asymmetric catalysis”
- 07/12/11: Jianliang Xiao, University of Liverpool, “Metal-organo cooperative catalysis: Asymmetric hydrogenation with achiral metal catalysts”
- 17/01/12: Xile Hu, EPFL, “Catalysts made of earth-abundant elements for making C-C and H-H bonds”
- 31/01/12: Niek Buurma, Cardiff University, “Physical organic chemistry in water”
- 22/02/12: Stephen Faulkner, University of Oxford, “Bimetallic questions: Preparation, study and application of heterometallic complexes containing lanthanides”
- 28/02/12: Peter Scott, University of Warwick, “Chiral metal compounds in catalysis and medicine”
- 13/03/12: Tony Flinn, Onyx, “Chemistry and business - a rollercoaster”
- 13/03/12: Paul Quigley, Shasun, “Aromatic bond formation: An overview”
- 03/04/12: Jean-François Halet, University of Rennes, “An example of conjugated systems containing boron moieties”
- 03/04/12: Todd Marder, University of Durham, “Diethynyrhodacyclopentadienes: A new class of luminescent organometallics”
- 04/04/12: Paul Low, University of Durham, “Twists and turns: The surprising redox chemistry of ruthenium complexes”
- 04/04/12: Véronique Guerchais, University of Rennes, “Synthetic strategies to functionalised luminescent cyclometallated Ir(III) complexes”
- 01/05/12: David Parker, Durham University, “Lanthanide coordination chemistry: Probe, excite, measure, relax”
- 08/05/12: Peter Rutledge, University of Sydney, “Functionalising hydrocarbons using iron catalysis”
- 09/05/12: Etienne Baranoff, University of Birmingham, “Cyclometallated iridium(III) complexes: to OLED materials… and beyond”

Chapter 7: Bibliography

(1) Moore, G. E. *Electronics* **1965**, *38*, 82.
(2) Aviram, A.; Ratner, M. A. *Chem. Phys. Lett.* **1974**, *29*, 277.
(3) Pope, M.; Kallmann, H. P.; Magnante, P. *J. Chem. Phys.* **1963**, *38*, 2042.
(4) Tang, C. W.; VanSlyke, S. A. *Appl. Phys. Lett.* **1987**, *51*, 913.
(5) Hughes, G.; Bryce, M. R. *J. Mater. Chem.* **2005**, *15*, 94.
(6) Kulkarni, A. P.; Tonzola, C. J.; Babel, A.; Jenekhe, S. A. *Chem. Mater.* **2004**, *16*, 4556.
(7) Shirota, Y.; Kageyama, H. *Chem. Rev.* **2007**, *107*, 953.
(8) Mitschke, U.; Bauerle, P. *J. Mater. Chem.* **2000**, *10*, 1471.
(9) Zaumseil, J.; Sirringhaus, H. *Chem. Rev.* **2007**, *107*, 1296.
(10) Meijer, E. J.; de Leeuw, D. M.; Setayesh, S.; van Veenendaal, E.; Huisman, B. H.; Blom, P. W. M.; Hummelen, J. C.; Scherf, U.; Klapwijk, T. M. *Nature Mater.* **2003**, *2*, 678.
(11) Tang, M. L.; Reichardt, A. D.; Miyaki, N.; Stoltenberg, R. M.; Bao, Z. *J. Am. Chem. Soc.* **2008**, *130*, 6064.
(12) Zaumseil, J.; Friend, R. H.; Sirringhaus, H. *Nature Mater.* **2006**, *5*, 69.
(13) Huang, L.-T.; Yen, H.-J.; Chang, C.-W.; Liou, G.-S. *J. Polym. Sci., Part A: Polym. Chem.* **2010**, *48*, 4747.
(14) Hayes, F. N.; Rogers, B. S.; Ott, D. G. *J. Am. Chem. Soc.* **1955**, *77*, 1850.
(15) Huisgen, R.; Sauer, J.; Sturm, H.; Markgraf, J. *Chem. Ber.* **1960**, *93*, 2106.
(16) Lee, J.-H.; Tsai, H.-H.; Leung, M.-K.; Yang, C.-C.; Chao, C.-C. *Appl. Phys. Lett.* **2007**, *90*, 243501.
(17) Lee, T.; Landis, C. A.; Dhar, B. M.; Jung, B. J.; Sun, J.; Sarjeant, A.; Lee, H.-J.; Katz, H. E. *J. Am. Chem. Soc.* **2009**, *131*, 1692.
(18) Kim, S.-K.; Yang, B.; Ma, Y.; Lee, J.-H.; Park, J.-W. *J. Mater. Chem.* **2008**, *18*, 3376.
(19) Wolfe, J. P.; Tomori, H.; Sadighi, J. P.; Yin, J.; Buchwald, S. L. *J. Org. Chem.* **2000**, *65*, 1158.
(20) Borsenberger, P. M.; Pautmeier, L.; Richert, R.; Bassler, H. *J. Chem. Phys.* **1991**, *94*, 8276.
(21) Ge, Z.; Hayakawa, T.; Ando, S.; Ueda, M.; Akiike, T.; Miyamoto, H.; Kajita, T.; Kakimoto, M.-a. *Chem. Mater.* **2008**, *20*, 2532.
(22) Lim, B.; Nah, Y.-C.; Hwang, J.-T.; Ghim, J.; Vak, D.; Yun, J.-M.; Kim, D.-Y. *J. Mater. Chem.* **2009**, *19*, 2380.
(23) O'Brien, D. F.; Burrows, P. E.; Forrest, S. R.; Koene, B. E.; Loy, D. E.; Thompson, M. E. *Adv. Mater.* **1998**, *10*, 1108.
(24) Justin Thomas, K. R.; Lin, J. T.; Tao, Y.-T.; Ko, C.-W. *J. Am. Chem. Soc.* **2001**, *123*, 9404.
(25) Borsche, W. *Justus Liebigs Annalen der Chemie* **1908**, *359*, 49.
(26) Drechsel, E. *Journal für Praktische Chemie* **1888**, *38*, 65.
(27) Sonntag, M.; Strohriegl, P. *Chem. Mater.* **2004**, *16*, 4736.
(28) Strohriegl, P.; Grazulevicius, J. V. *Adv. Mater.* **2002**, *14*, 1439.
(29) Chen, C. H.; Shi, J.; Tang, C. W. *Macromol. Symp.* **1998**, *125*, 1.
(30) Farinola, G. M.; Ragni, R. *Chem. Soc. Rev.* **2011**, *40*, 3467.
(31) Hsu, F.-M.; Chien, C.-H.; Shih, P.-I.; Shu, C.-F. *Chem. Mater.* **2009**, *21*, 1017.
(32) Kim, D.; Coropceanu, V.; Brédas, J.-L. *J. Am. Chem. Soc.* **2011**, *133*, 17895.
(33) Brunner, K.; van Dijken, A.; Börner, H.; Bastiaansen, J. J. A. M.; Kiggen, N. M. M.; Langeveld, B. M. W. *J. Am. Chem. Soc.* **2004**, *126*, 6035.

(34) van Dijken, A.; Bastiaansen, J. J. A. M.; Kiggen, N. M. M.; Langeveld, B. M. W.; Rothe, C.; Monkman, A.; Bach, I.; Stössel, P.; Brunner, K. *J. Am. Chem. Soc.* **2004**, *126*, 7718.
(35) Kawamura, Y.; Yanagida, S.; Forrest, S. R. *J. Appl. Phys.* **2002**, *92*, 87.
(36) Kido, J.; Hongawa, K.; Okuyama, K.; Nagai, K. *Appl. Phys. Lett.* **1993**, *63*, 2627.
(37) Jankus, V.; Monkman, A. P. *Adv. Funct. Mater.* **2011**, *21*, 3350.
(38) Kido, J.; Kimura, M.; Nagai, K. *Science* **1995**, *267*, 1332.
(39) Kido, J.; Shionoya, H.; Nagai, K. *Appl. Phys. Lett.* **1995**, *67*, 2281.
(40) Lin, M.-S.; Chi, L.-C.; Chang, H.-W.; Huang, Y.-H.; Tien, K.-C.; Chen, C.-C.; Chang, C.-H.; Wu, C.-C.; Chaskar, A.; Chou, S.-H.; Ting, H.-C.; Wong, K.-T.; Liu, Y.-H.; Chi, Y. *J. Mater. Chem.* **2012**, *22*, 870.
(41) Hung, W.-Y.; Chi, L.-C.; Chen, W.-J.; Chen, Y.-M.; Chou, S.-H.; Wong, K.-T. *J. Mater. Chem.* **2010**, *20*, 10113.
(42) Boudreault, P.-L. T.; Virkar, A. A.; Bao, Z.; Leclerc, M. *Org. Electron.* **2010**, *11*, 1649.
(43) Fomina, N.; Bradforth, S. E.; Hogen-Esch, T. E. *Macromolecules* **2009**, *42*, 6440.
(44) Fomina, N.; Hogen-Esch, T. E. *Macromolecules* **2008**, *41*, 3765.
(45) Chua, L.-L.; Zaumseil, J.; Chang, J.-F.; Ou, E. C. W.; Ho, P. K. H.; Sirringhaus, H.; Friend, R. H. *Nature* **2005**, *434*, 194.
(46) Kajii, H.; Koiwai, K.; Hirose, Y.; Ohmori, Y. *Org. Electron.* **2010**, *11*, 509.
(47) Chu, Z.; Wang, D.; Zhang, C.; Fan, X.; Tang, Y.; Chen, L.; Zou, D. *Macromol. Rapid Commun.* **2009**, *30*, 1745.
(48) Zou, L.; Liu, Z.; Yan, X.; Liu, Y.; Fu, Y.; Liu, J.; Huang, Z.; Chen, X.; Qin, J. *Eur. J. Org. Chem.* **2009**, *2009*, 5587.
(49) Tao, Y.; Wang, Q.; Yang, C.; Wang, Q.; Zhang, Z.; Zou, T.; Qin, J.; Ma, D. *Angew. Chem. Int. Ed.* **2008**, *47*, 8104.
(50) Lai, M.-Y.; Chen, C.-H.; Huang, W.-S.; Lin, Jiann T.; Ke, T.-H.; Chen, L.-Y.; Tsai, M.-H.; Wu, C.-C. *Angew. Chem. Int. Ed.* **2008**, *47*, 581.
(51) Finlayson, C. E.; Kim, J.-S.; Liddell, M. J.; Friend, R. H.; Jung, S.-H.; Grimsdale, A. C.; Mullen, K. *J. Chem. Phys.* **2008**, *128*, 044703.
(52) Zheng, C.-J.; Ye, J.; Lo, M.-F.; Fung, M.-K.; Ou, X.-M.; Zhang, X.-H.; Lee, C.-S. *Chem. Mater.* **2012**, *24*, 643.
(53) Lee, W.-Y.; Kurosawa, T.; Lin, S.-T.; Higashihara, T.; Ueda, M.; Chen, W.-C. *Chem. Mater.* **2011**, *23*, 4487.
(54) Zheng, Y.; Batsanov, A. S.; Jankus, V.; Dias, F. B.; Bryce, M. R.; Monkman, A. P. *J. Org. Chem.* **2011**, *76*, 8300.
(55) Gong, S.; Chen, Y.; Luo, J.; Yang, C.; Zhong, C.; Qin, J.; Ma, D. *Adv. Funct. Mater.* **2011**, *21*, 1168.
(56) Lin, L.-Y.; Lin, X.-Y.; Lin, F.; Wong, K.-T. *Org. Lett.* **2011**, *13*, 2216.
(57) Zhu, M.; Ye, T.; Li, C.-G.; Cao, X.; Zhong, C.; Ma, D.; Qin, J.; Yang, C. *J. Phys. Chem. C* **2011**, *115*, 17965.
(58) Kamtekar, K. T.; Wang, C.; Bettington, S.; Batsanov, A. S.; Perepichka, I. F.; Bryce, M. R.; Ahn, J. H.; Rabinal, M.; Petty, M. C. *J. Mater. Chem.* **2006**, *16*, 3823.
(59) Pearson, C.; Ahn, J. H.; Mabrook, M. F.; Zeze, D. A.; Petty, M. C.; Kamtekar, K. T.; Wang, C.; Bryce, M. R.; Dimitrakis, P.; Tsoukalas, D. *Appl. Phys. Lett.* **2007**, *91*, 123506.
(60) Vail, S. A.; Schuster, D. I.; Guldi, D. M.; Isosomppi, M.; Tkachenko, N.; Lemmetyinen, H.; Palkar, A.; Echegoyen, L.; Chen, X.; Zhang, J. Z. H. *J. Phys. Chem. B* **2006**, *110*, 14155.
(61) Atienza-Castellanos, C.; Wielopolski, M.; Guldi, D. M.; van der Pol, C.; Bryce, M. R.; Filippone, S.; Martin, N. *Chem. Commun.* **2007**, 5164.
(62) Figueira-Duarte, T. M.; Rio, Y.; Listorti, A.; Delavaux-Nicot, B.; Holler, M.; Marchioni, F.; Ceroni, P.; Armaroli, N.; Nierengarten, J.-F. *New J. Chem.* **2008**, *32*, 54.

(63) Allemand, P. M.; Koch, A.; Wudl, F.; Rubin, Y.; Diederich, F.; Alvarez, M. M.; Anz, S. J.; Whetten, R. L. *J. Am. Chem. Soc.* **1991**, *113*, 1050.
(64) Wudl, F. *Acc. Chem. Res.* **1992**, *25*, 157.
(65) Sun, Y.; Welch, G. C.; Leong, W. L.; Takacs, C. J.; Bazan, G. C.; Heeger, A. J. *Nature Mater.* **2012**, *11*, 44.
(66) Zhu, Y.; Kulkarni, A. P.; Wu, P.-T.; Jenekhe, S. A. *Chem. Mater.* **2008**, *20*, 4200.
(67) Moss, K. C.; Bourdakos, K. N.; Bhalla, V.; Kamtekar, K. T.; Bryce, M. R.; Fox, M. A.; Vaughan, H. L.; Dias, F. B.; Monkman, A. P. *J. Org. Chem.* **2010**, *75*, 6771.
(68) Nicholas J. Turro, V. R., J. C. Scaiano *Principles of Molecular Photochemistry*; University Science Books.
(69) Cao, Y.; Parker, I. D.; Yu, G.; Zhang, C.; Heeger, A. J. *Nature* **1999**, *397*, 414.
(70) Segal, M.; Singh, M.; Rivoire, K.; Difley, S.; Van Voorhis, T.; Baldo, M. A. *Nature Mater.* **2007**, *6*, 374.
(71) Yang, Y.; Cohn, P.; Dyer, A. L.; Eom, S.-H.; Reynolds, J. R.; Castellano, R. K.; Xue, J. *Chem. Mater.* **2010**, *22*, 3580.
(72) Tong, Q.-X.; Lai, S.-L.; Chan, M.-Y.; Zhou, Y.-C.; Kwong, H.-L.; Lee, C.-S.; Lee, S.-T. *Chem. Mater.* **2008**, *20*, 6310.
(73) Lee, M.-T.; Chen, H.-H.; Liao, C.-H.; Tsai, C.-H.; Chen, C. H. *Appl. Phys. Lett.* **2004**, *85*, 3301.
(74) Cho, I.; Kim, S. H.; Kim, J. H.; Park, S.; Park, S. Y. *J. Mater. Chem.* **2012**, *22*, 123.
(75) Zhen, C.-G.; Chen, Z.-K.; Liu, Q.-D.; Dai, Y.-F.; Shin, R. Y. C.; Chang, S.-Y.; Kieffer, J. *Adv. Mater.* **2009**, *21*, 2425.
(76) Chen, C.-T.; Wei, Y.; Lin, J.-S.; Moturu, M. V. R. K.; Chao, W.-S.; Tao, Y.-T.; Chien, C.-H. *J. Am. Chem. Soc.* **2006**, *128*, 10992.
(77) Lin, S.-L.; Chan, L.-H.; Lee, R.-H.; Yen, M.-Y.; Kuo, W.-J.; Chen, C.-T.; Jeng, R.-J. *Adv. Mater.* **2008**, *20*, 3947.
(78) Hancock, J. M.; Gifford, A. P.; Zhu, Y.; Lou, Y.; Jenekhe, S. A. *Chem. Mater.* **2006**, *18*, 4924.
(79) Huang, J.; Su, J.-H.; Li, X.; Lam, M.-K.; Fung, K.-M.; Fan, H.-H.; Cheah, K.-W.; Chen, C. H.; Tian, H. *J. Mater. Chem.* **2011**, *21*, 2957.
(80) Lei, T.; Luo, J.; Wang, L.; Ma, Y.; Wang, J.; Cao, Y.; Pei, J. *New J. Chem.* **2010**, *34*, 699.
(81) Jacob, J.; Zhang, J.; Grimsdale, A. C.; Müllen, K.; Gaal, M.; List, E. J. W. *Macromolecules* **2003**, *36*, 8240.
(82) Tavasli, M.; Bettington, S.; Bryce, M. R.; Attar, H. A. A.; Dias, F. B.; King, S.; Monkman, A. P. *J. Mater. Chem.* **2005**, *15*, 4963.
(83) Geng, Y.; Trajkovska, A.; Katsis, D.; Ou, J. J.; Culligan, S. W.; Chen, S. H. *J. Am. Chem. Soc.* **2002**, *124*, 8337.
(84) Promarak, V.; Punkvuang, A.; Sudyoadsuk, T.; Jungsuttiwong, S.; Saengsuwan, S.; Keawin, T.; Sirithip, K. *Tetrahedron* **2007**, *63*, 8881.
(85) Tao, Y.; Wang, Q.; Yang, C.; Zhong, C.; Zhang, K.; Qin, J.; Ma, D. *Adv. Funct. Mater.* **2010**, *20*, 304.
(86) Lakowicz, J. R. In *Principles of Fluorescence Spectroscopy*; 3rd ed.; Lakowicz, J. R., Ed.; Springer: 2006, p 208.
(87) Pålsson, L. O.; Monkman, A. P. *Adv. Mater.* **2002**, *14*, 757.
(88) *US Energy Information Administration*, www.eia.gov.
(89) Wu, H.; Ying, L.; Yang, W.; Cao, Y. *Chem. Soc. Rev.* **2009**, *38*, 3391.
(90) Kamtekar, K. T.; Monkman, A. P.; Bryce, M. R. *Adv. Mater.* **2010**, *22*, 572.
(91) Sasabe, H.; Takamatsu, J.-i.; Motoyama, T.; Watanabe, S.; Wagenblast, G.; Langer, N.; Molt, O.; Fuchs, E.; Lennartz, C.; Kido, J. *Adv. Mater.* **2010**, *22*, 5003.
(92) Pearson, C.; Cadd, D. H.; Petty, M. C.; Hua, Y. L. *J. Appl. Phys.* **2009**, *106*, 064516.

(93) Alam, M. M.; Jenekhe, S. A. *Macromol. Rapid Commun.* **2006**, *27*, 2053.
(94) Xu, Y.; Peng, J.; Jiang, J.; Xu, W.; Yang, W.; Cao, Y. *Appl. Phys. Lett.* **2005**, *87*, 193502.
(95) Brovelli, S.; Meinardi, F.; Winroth, G.; Fenwick, O.; Sforazzini, G.; Frampton, M. J.; Zalewski, L.; Levitt, J. A.; Marinello, F.; Schiavuta, P.; Suhling, K.; Anderson, H. L.; Cacialli, F. *Adv. Funct. Mater.* **2010**, *20*, 272.
(96) Grice, A. W.; Tajbakhsh, A.; Burn, P. L.; Bradley, D. D. C. *Adv. Mater.* **1997**, *9*, 1174.
(97) Brown, A. R.; Bradley, D. D. C.; Burroughes, J. H.; Friend, R. H.; Greenham, N. C.; Burn, P. L.; Holmes, A. B.; Kraft, A. *Appl. Phys. Lett.* **1992**, *61*, 2793.
(98) Ahn, J. H.; Wang, C.; Pearson, C.; Bryce, M. R.; Petty, M. C. *Appl. Phys. Lett.* **2004**, *85*, 1283.
(99) Oyston, S.; Wang, C.; Hughes, G.; Batsanov, A. S.; Perepichka, I. F.; Bryce, M. R.; Ahn, J. H.; Pearson, C.; Petty, M. C. *J. Mater. Chem.* **2005**, *15*, 194.
(100) Oyston, S.; Wang, C.; Perepichka, I. F.; Batsanov, A. S.; Bryce, M. R.; Ahn, J. H.; Petty, M. C. *J. Mater. Chem.* **2005**, *15*, 5164.
(101) Doyle, T. J.; Haseltine, J. *J. Heterocycl. Chem.* **1994**, *31*, 1417.
(102) James;, D. K.; Tour, J. M. *Top. Curr. Chem.* **2005**, *257*, 33.
(103) Weiss;, E. A.; Wasielewski;, M. R.; Ratner, M. A. *Top. Curr. Chem.* **2005**, *257*, 103.
(104) Zhou, G.; Baumgarten, M.; Müllen, K. *J. Am. Chem. Soc.* **2007**, *129*, 12211.
(105) Hanss, D.; Wenger, O. S. *Inorg. Chem.* **2008**, *47*, 9081.
(106) Hagberg, D. P.; Yum, J.-H.; Lee, H.; De Angelis, F.; Marinado, T.; Karlsson, K. M.; Humphry-Baker, R.; Sun, L.; Hagfeldt, A.; Grätzel, M.; Nazeeruddin, M. K. *J. Am. Chem. Soc.* **2008**, *130*, 6259.
(107) Tsai, M.-S.; Hsu, Y.-C.; Lin, J. T.; Chen, H.-C.; Hsu, C.-P. *J. Phys. Chem. C* **2007**, *111*, 18785.
(108) Dias, F. B.; Pollock, S.; Hedley, G.; Pålsson, L.-O.; Monkman, A.; Perepichka, I. I.; Perepichka, I. F.; Tavasli, M.; Bryce, M. R. *J. Phys. Chem. B* **2006**, *110*, 19329.
(109) Wang, C.; Pålsson, L.-O.; Batsanov, A. S.; Bryce, M. R. *J. Am. Chem. Soc.* **2006**, *128*, 3789.
(110) Pålsson, L.-O.; Wang, C.; Batsanov, A. S.; King, S. M.; Beeby, A.; Monkman, A. P.; Bryce, M. R. *Chem. Eur. J.* **2010**, *16*, 1470.
(111) Atienza, C.; Insuasty, B.; Seoane, C.; Martin, N.; Ramey, J.; Rahman, G. M. A.; Guldi, D. M. *J. Mater. Chem.* **2005**, *15*, 124.
(112) Liu, K.; Li, G.; Wang, X.; Wang, F. *J. Phys. Chem. C* **2008**, *112*, 4342.
(113) Wang, C.; Batsanov, A. S.; Bryce, M. R. *J. Org. Chem.* **2005**, *71*, 108.
(114) Kil Choi, M.; Lim Kim, H.; Hack Suh, D. *J. Appl. Polym. Sci.* **2006**, *101*, 1228.
(115) Hay, A. S. *J. Org. Chem.* **1962**, *27*, 3320.
(116) Siemsen, P.; Livingston, R. C.; Diederich, F. *Angew. Chem. Int. Ed.* **2000**, *39*, 2632.
(117) Elangovan, A.; Wang, Y.-H.; Ho, T.-I. *Org. Lett.* **2003**, *5*, 1841.
(118) Monguchi, Y.; Kitamoto, K.; Ikawa, T.; Maegawa, T.; Sajiki, H. *Adv. Synth. Catal.* **2008**, *350*, 2767.
(119) Zheng, Q.; Jung, B. J.; Sun, J.; Katz, H. E. *J. Am. Chem. Soc.* **2010**, *132*, 5394.
(120) Hagfeldt, A.; Grätzel, M. *Acc. Chem. Res.* **2000**, *33*, 269.
(121) Grätzel, M. *J. Photochem. Photobiol. C: Photochem. Rev.* **2003**, *4*, 145.
(122) Hagfeldt, A.; Boschloo, G.; Sun, L.; Kloo, L.; Pettersson, H. *Chem. Rev.* **2010**, *110*, 6595.
(123) O'Regan, B.; Gratzel, M. *Nature* **1991**, *353*, 737.
(124) Listorti, A.; O'Regan, B.; Durrant, J. R. *Chem. Mater.* **2011**, *23*, 3381.
(125) Baheti, A.; Tyagi, P.; Thomas, K. R. J.; Hsu, Y.-C.; Lin, J. T. s. *J. Phys. Chem. C* **2009**, *113*, 8541.
(126) Albinsson, B.; Mårtensson, J. *J. Photochem. Photobiol. C: Photochem. Rev.* **2008**, *9*, 138.

(127) Yen, Y.-S.; Hsu, Y.-C.; Lin, J. T.; Chang, C.-W.; Hsu, C.-P.; Yin, D.-J. *J. Phys. Chem. C* **2008**, *112*, 12557.
(128) *Laboratory of Photonics and Interfaces - EPFL*, http://lpi.epfl.ch/.
(129) Horiuchi, T.; Miura, H.; Sumioka, K.; Uchida, S. *J. Am. Chem. Soc.* **2004**, *126*, 12218.
(130) Lin, J. T.; Chen, P.-C.; Yen, Y.-S.; Hsu, Y.-C.; Chou, H.-H.; Yeh, M.-C. P. *Org. Lett.* **2008**, *11*, 97.
(131) Yella, A.; Lee, H.-W.; Tsao, H. N.; Yi, C.; Chandiran, A. K.; Nazeeruddin, M. K.; Diau, E. W.-G.; Yeh, C.-Y.; Zakeeruddin, S. M.; Grätzel, M. *Science* **2011**, *334*, 629.
(132) Srinivas, K.; Sivakumar, G.; Ramesh Kumar, C.; Ananth Reddy, M.; Bhanuprakash, K.; Rao, V. J.; Chen, C.-W.; Hsu, Y.-C.; Lin, J. T. *Synth. Met.* **2011**, *161*, 1671.
(133) Manzhos, S.; Segawa, H.; Yamashita, K. *Chem. Phys. Lett.* **2011**, *504*, 230.
(134) Perepichka, I. I.; Perepichka, I. F.; Bryce, M. R.; Palsson, L.-O. *Chem. Commun.* **2005**, 3397.
(135) Ku, C.-H.; Kuo, C.-H.; Chen, C.-Y.; Leung, M.-K.; Hsieh, K.-H. *J. Mater. Chem.* **2008**, *18*, 1296.
(136) Holzapfel, M.; Lambert, C. *J. Phys. Chem. C* **2007**, *112*, 1227.
(137) Mudadu, M. S.; Singh, A. N.; Thummel, R. P. *J. Org. Chem.* **2008**, *73*, 6513.
(138) Hou, S.; Chan, W. K. *Macromolecules* **2001**, *35*, 850.
(139) Wong, K.-T.; Ku, S.-Y.; Cheng, Y.-M.; Lin, X.-Y.; Hung, Y.-Y.; Pu, S.-C.; Chou, P.-T.; Lee, G.-H.; Peng, S.-M. *J. Org. Chem.* **2005**, *71*, 456.
(140) Sherrod, S. A.; Da Costa, R. L.; Barnes, R. A.; Boekelheide, V. *J. Am. Chem. Soc.* **1974**, *96*, 1565.
(141) Matsuda, K.; Nakamura, N.; Takahashi, K.; Inoue, K.; Koga, N.; Iwamura, H. *J. Am. Chem. Soc.* **1995**, *117*, 5550.
(142) Collings, J. C.; Poon, S.-Y.; Le Droumaguet, C.; Charlot, M.; Katan, C.; Pålsson, L.-O.; Beeby, A.; Mosely, J. A.; Kaiser, H. M.; Kaufmann, D.; Wong, W.-Y.; Blanchard-Desce, M.; Marder, T. B. *Chem. Eur. J.* **2009**, *15*, 198.
(143) Plater, M. J.; Jackson, T. *Tetrahedron* **2003**, *59*, 4687.
(144) Wang, D.; Niu, Y.; Wang, Y.; Han, J.; Feng, S. *J. Organomet. Chem.* **2010**, *695*, 2329.
(145) Fisher, C. H.; Walling, C. T. *J. Am. Chem. Soc.* **1935**, *57*, 1700.
(146) Sundberg, R. J.; Sloan, K. B. *J. Org. Chem.* **1973**, *38*, 2052.
(147) Yen, W.-C.; Pal, B.; Yang, J.-S.; Hung, Y.-C.; Lin, S.-T.; Chao, C.-Y.; Su, W.-F. *J. Polym. Sci., Part A: Polym. Chem.* **2009**, *47*, 5044.
(148) Chen, C.-H.; Hsu, Y.-C.; Chou, H.-H.; Thomas, K. R. J.; Lin, J. T.; Hsu, C.-P. *Chem. Eur. J.* **2010**, *16*, 3184.
(149) Chotana, G. A.; Rak, M. A.; Smith, M. R. *J. Am. Chem. Soc.* **2005**, *127*, 10539.
(150) Pachfule, P.; Chen, Y.; Sahoo, S. C.; Jiang, J.; Banerjee, R. *Chem. Mater.* **2011**, *23*, 2908.
(151) Yang, L.; Gong, Z.; Nie, D.; Lou, B.; Bian, Z.; Guan, M.; Huang, C.; Lee, H. J.; Baik, W. P. *New J. Chem.* **2006**, *30*, 791.
(152) Kawano, T.; Yoshizumi, T.; Hirano, K.; Satoh, T.; Miura, M. *Org. Lett.* **2009**, *11*, 3072.